Dissertation

An Advanced Transient Concrete Model for the Determination of Restraint in Concrete Structures Subjected to Fire and the Fire Resistance of Concrete Tunnel Sections

A Dissertation Presented to the Faculty of Civil Engineering
Vienna University of Technology

In Partial Fulfilment of the Requirements for the degree
"Doktor der technischen Wissenschaften"

Presented by
Martin Schneider

Munich, September 2010

First Supervisor: Prof. Dr. Dr. h.c. Ulrich Schneider
Institute for Building Design and Technology,
Vienna University of Technology

Second Supervisor: Prof. Dr. Jean-Marc Franssen
Département ArGEnCo,
University of Liege

Author's coordinates:

Dipl.-Ing. Martin Schneider
Vienna University of Technology
Institute for Building Design and Technology
Karlsplatz 13/2061
1040 Wien
Austria
e0527948@student.tuwien.ac.at

Supervisor's coordinates:

Prof. Dr. Dr. h.c. Ulrich Schneider
Vienna University of Technology
Institute for Building Design and Technology
Karlsplatz 13/206
1040 Wien
Austria
ulrich.schneider+e206@tuwien.ac.at

Prof. Dr. Jean-Marc Franssen
University of Liege
Département ArGEnCo
1, Ch. des Chevreuils
4000 Liège
Belgium
JM.Franssen@ulg.ac.be

Acknowledgements

The author of the present work would like to thank all colleagues of the University of Liege and the Vienna University of Technology for the comprehensive scientific support in the field of thermal behaviour of materials and fire safety engineering. He is especially grateful to the two supervisors for their tremendous efforts and scientific inputs during their supervision of this work.

Prof. Ulrich Schneider inspired this work. He provided the basic information about mechanical behaviour of concrete under transient temperature conditions and its modelling in case of concrete structure subjected to fire. Much thanks for the helpful discussions during the realization of the concrete model and the support during the preparation of several international publications in this field.

Prof. Jean-Marc Franssen supports the realization of the advanced transient concrete model in the FE Software SAFIR, which was developed on University of Liege. During the visits in Liege the in-depth discussions of different concrete models for the calculation of fire behaviour of reinforced concrete members was an inspiring exercise in this field.

Declaration of Own Work

This work was initiated by Prof. Ulrich Schneider and supervised by Prof. Jean-Marc Franssen. The acknowledgements of the supervisors are included by consideration in the results of this work and under the topic of discussion.

The realization of all the presented theories, material models and calculations was made by the author according to the mentioned references and the computer code SAFIR being used.

Dipl.-Ing. Martin Schneider

Symbols and Abbreviations

All symbols and abbreviations are explained in the text. The symbols are explained directly after each equation. Abbreviations are explained directly after its first appearance.

Abstract

The new advanced transient concrete model (ATC-model) was developed for the prediction of the load bearing capacity and behaviour of structures subjected to fire, using new material equations for the most important material properties of ordinary concrete under transient temperatures. This model was developed with the aim of extending and generalizing the existing concrete models of EC2 with respect to thermal strain, transient thermal creep and the effect of load history.

It is possible to consider the load history in all phases of thermal exposure with this new model. With this complex model, one can calculate total strain taking into account a wide range of variations of load history and transient temperatures up to 1,000°C. Different parts of deformations are approximated with analytic equations interacting in the new concrete model. This technique is usable for a realistic calculation of behaviour of structures including cases of total restraint. By considering the load history during heating-up in several cases as compared to other concrete models, an increase of load bearing capacity due to a higher solidity of concrete may be obtained.

With this model it is possible to consider the thermal-physical behaviour of material properties for the calculation of reinforced concrete structures under transient temperatures, e.g. fire, with high accuracy. The results of the simulation of loaded concrete structures subjected to fire depend significantly on the material model being used. The results of displacement calculations using the ATC-model are much closer to the measured data than the results derived from the EC2-model for ordinary concrete. The EC2-model does not consider the transient creep of concrete. It has been observed that the ATC-model provides, in some cases, smaller reserve than the EC2-model with respect to the time of failure. On the other hand it clearly indicates the high creep potential of the material under fire and its favourable fire behaviour.

The results of the calculation using the ATC-model for ordinary concrete led to comparatively good approximations to measured data for smaller test specimen and small test columns. The tests of columns with micro silica concrete indicated shorter fire duration compared to the calculation results of EC2-model and ATC-model. Generally a brittle failure was observed. For concretes with higher Young's modulus which generally lead to an earlier failure under fire it was shown that the ATC-model worked impressively well and it seems that it is possible to adapt the model easily for applications in the field of high strength concrete (HSC and HPC).

With this respect the calculation of concrete structures with the ATC-model showed great potential for optimizing concrete structures more than that of the EC2-model. The model of EC2 is unable to determine the total strains with high accuracy and should not be used in the field of HSC or HPC without further calibrations under standard fire conditions. For natural fire curve, more general material models like the ATC-model are to be applied.

During the calculation of a tunnel cross section, a single bay frame was investigated and presented above. Lower deformations were calculated compared to the EC2-mdel in all parts of the structures using the new advanced transient concrete model (ATC-model). Due to this lowered deformation, lower axial forces during heating and a longer fire resistance time occur. The model can also be used with different design fires or calculated temperature curves. In this case the simulation of natural fires in the field of CFD-model or zone-model simulations, an adapted calculation model for structural behaviour is of general relevance.

Contents

List of Figures

List of Tables

1 Introduction

When concrete is exposed to high temperatures, extremely complex phenomena occur, including heat conduction and convection, dehydration, thermal expansion, micro-cracking, pressure driven vapour flow, vapour diffusion, evaporation and condensation, and serious changes in strength, stiffness, fracture energy, thermal conductivity, permeability, porosity and the mechanical stress field may take place [L1].

Under such conditions, the failure of concrete and reinforced concrete elements is often due to an interaction of different types of damage. Apart from the mechanical loads, reinforced concrete structures are also subjected to environmental physical (thermal) and chemical (damage) loads [L2].

Currently, various material models for concrete and steel are available. A critical review was given in literature [L3, L4, L5, and L6]. Based on these models and experimental data, a stress-strain-temperature model is proposed that incorporates the effect of transient strain implicitly.

During the course of the fire the strength of the materials and their stiffness change, thus influencing the fire resistance due to geometrical second order effects and/or due to the development of restraint forces.

The fire resistance of concrete structures relies on the slow conduction of heat within the structural members brought about by the relatively low thermal conductivity of the material. The rebar cover is expected to undergo very steep temperature gradients and a preliminary thermal analysis is generally required in order to determine the material weakening at each point in the member cross section [L7].

The fire resistance of concrete members may be determined by calculations or fire tests. During the design of load bearing reinforced concrete structures the fire rating of the structure must be defined with respect to the general suitability and stability of the structural design. Based on the proven reinforced state and concrete quality the standard fire duration may be calculated according to Eurocode 2 as an “accidental effect”.

Tabulated data as well as simple and general calculation methods can be used for the calculation of reinforced concrete structures subjected to fire [L8]. Calculations using tabulated data are based on fire exposure test results in accordance to the temperature-time curve ISO 834.

In order to determine the temperature-time curves in the cross section of the concrete members, the Fourier equation is solved including the heat transfer from the fire to the concrete surface by a thermal analysis [L9]. Mass transports can also be included because during fire exposure many phase transitions of the cement stone matrix and aggregate appear [L10, L11]. These thermally conditioned physico-chemical variables may influence the mechanical model [L12, L13, L14]. The mechanical analysis in this work is based on a practical interpretation of those results. There are numerous models available for the determination of ordinary concrete behavior at high temperatures [L15, L16, L17]. In regards to this, there is also a high dependency on the type of concrete used for high performance and ultra high performance concrete as studies have shown [L18, L19].

It has been proven many times that tabulated data and simplified arithmetic procedures yield only very rough estimates of fire behavior of concrete and that does not leave much room for innovations in designing concrete structures.

This is the reason why there are many activities done to verify analytical results in the extraordinary case of fire using approximated hand calculation methods [L20]. The approximation method after [L20] does not reduce the load bearing part of the concrete cross section which is done in other simple calculation. Nevertheless, it has been observed that those calculations may overestimate the residual strength of concrete after fire exposure.

For the calculation of deformation and load bearing capacity of structures at high temperatures, the material laws depend on the permanent loads and transient temperatures. Both effects are interactive and have to be included in the calculation of deformation elements and load bearing capacity for the material. Analysis at high temperature revealed that restrained parts of the structure show a relative increase of stiffness compared to unrestrained components [L21].

Thermal strain by definition does not depend on load, but the mechanical strain depends on both temperatures and loads [L22]. This behaviour is referred to as „load history“ as we assume both: transient temperatures and loads, i.e. the temperature and loads are functions of time.

The load bearing capacity of concrete structures can be optimized with models representing a transient material behaviour. Models that are approximated by the use of transient data are most realistic. The following investigation describes the potential of using a new transient concrete model. This model considers the thermal induced strains and transient external loads during heating up. For this model, a realisation of all components of concrete strain depending on temperature and time is needed, i.e. the concrete behaviour is influenced by transient temperature and load history.

2 Motivation and Aim of the Work

According to fire tests and realistic fires in concrete structures i.e. skyscrapers, tunnels and bridges, it has been known that the simultaneous influence of mechanical and thermal load may lead to a completely different load bearing capacity compared to ambient temperatures. The predicted results after fire often comprise of displacements, load bearing capacity and residual load bearing capacity respectively.

In small scale tests and large scale tests it was shown that the simultaneous exposure to high temperatures i.e. during natural fires and high loads, lead to a complete change of the load bearing behaviour in reinforced concrete members. The calculation of load bearing capacity of concrete structures under fire, i.e. a full period of heating and cooling must be considered.

The combination of high temperature effects and the influence of loads to the structure may have a positive effect on the structural stiffness. The compressive strength and the Young's modulus increase during heating. Micro-cracks that occur during heating because of thermal stresses are limited by stress distributions. This behaviour is well known. It is necessary to consider this change of load level during heating-up for the calculation of fire resistance of complex structures. A FE material model describing the behaviour of a transient fire exposure is advantageous in this case.

New material models that are better adapted to measured data are able to determine a realistic load bearing capacity for a long period of temperature exposure. The results may be used for optimization of reinforced concrete members. The amount of steel or the axial dimensions can be adapted.

In the new nonlinear temperature dependent material model, the load bearing capacity should be calculated with a FE structural code. The material behaviour should also be described for cooling, thus the residual material properties need to be induced too the load bearing capacity after fire and after cooling down may be calculated. This is necessary for the design of repair of structures after fire.

The new model is generally designed for all kinds of aggregates for reinforced concrete members and structures. In this PhD-thesis, the model has been implemented as a specific part of the structural code SAFIR and the calculation of a fire exposed tunnel cross section built. A cut and cover method as a single bay frame was performed as to show the applicability of the model as an example for a complex structure under fire attack.

The tunnel structure indicated high stresses during the fire attack and the deformity of the concrete were affected. During heating, the construction shows different thermal stresses, shrinkages, transient creep, change of Young's modulus and compressive strength change after each step.

The aim of the work was to develop and validate a new Advanced Transient Concrete Model (ATC-model) that should be able to consider all these effects in a FE code.

The new model is called "Advanced Transient Concrete Model" (ATC-model) and transient conditions during the whole calculation routine are taken into account. Parts of this model were presented for the first time in [L23]. The transient load and the real temperature development are

considered. The ATC-model comprises a lot of capabilities, especially that it considers the irreversible effects of temperature on several material properties at high temperatures. Generally, the ATC-model can be used to represent the results of specimens of every type of concrete. The presented model is based on ordinary concrete with siliceous aggregate because a complete set of high temperature data is available for the type of ordinary concrete that covers the classes C20/25 up to C47/55.

The non-linear model comprises thermal strain, elastic strain, plastic strain and transient temperature strains as well as load history. That means as a consequence, the modelling of restrained concrete structures subjected to fire is possible.

Calculations of various concrete members were performed using the structural code SAFIR [L24]. The new ATC-model has been incorporated in the code for the research work. Generally the code is suitable to calculate complex structures with different material models, e.g. the EC2 and EC3 material models.

The influence of high compressive stresses in concrete sections may be comparatively high due to the creep strains for transient temperature condition and which indicates a significant influence of the thermal induced transient strains.

The constitutive EC2-model does not consider this behaviour explicitly and has not been tested for natural fire conditions that include decreasing temperature conditions. It seems logical therefore to extend the Eurocode material model in respect to temperature-time curves which are outside the range of the ISO standard curve. From experimental observations it is known that:

- The Eurocode 2 concrete model is very usable and provides a high level of safety for members under bending and standard fire test conditions.
- Including the new ATC-model the structural code SAFIR was successfully applied to calculate various reinforced concrete members to show the influence of the transient effects of load induced transient strains on the behaviour of these reinforced concrete members exposed to fire.
- The reliability of the new Advanced Transient Concrete Model is high, the calculation of various reinforced concrete members prove the assumptions of the model. The calculations from small specimens to complex structure are given in [L23, L25, L26, L27]. All calculation results are compared with measured data or comparable calculation with commonly calculation methods.

In the following pages the research of the recent five years in the field of concrete modelling for calculation of reinforced concrete members is summarized.

3 Material Properties of Concrete at High Temperatures

3.1 Generals

The behaviour of concrete at high temperatures depends on different influences and effects. During temperature exposure, concrete suffers from degradation reactions that lead to changes of physical and mechanical properties. An important fact is the dependence of concrete on their mix components like aggregates, cement, water-cement ratio and additives and their reactions under fire. A lot of literatures and test results were published for different concretes since about 60 years of concrete high temperature research [L28 L29, L30, L31, L32, L33, L34, L35, L36, L37, L38].

In calculations of reinforced concrete elements the fire behaviour of concrete must taken into account.

3.2 Thermal Reactions of Concrete

During heating of concrete evaporation, dehydration crystal transformations may occur. Crystal transformations are mainly observed in the aggregates and may initiate a final breakdown of the structure and are occasionally called degradation reaction.

The main reactions in the concrete matrix are:

- Desorption of physical bounded water up to 100°C
- Water evaporation at 100°C
- Loss of gel water at about 180°C
- Breakdown of gel (first stage of Dehydration) starting at 180°C
- Decomposition of portlandite at 450°C
- Transformation of quartz at 573°C
- Decomposition of the CSH phases and formation of ß-C_2S at 650°C
- Decarbonising of limestone from 800°C onwards
- Start of melting from 1150 °C to 1200°C and above

The hardened cement paste also included aggregates thus there is also a degradation of hardened cement paste. At higher temperature the decarbonisation of carbonates occurs if the concrete contains limestone aggregate. Above 1200°C up to 1300°C the components begin to melt. During melting, some aggregates i.e. igneous rock such as basalt, show decreasing and expansion phenomena and a release of gases. Above 1300°C up to 1400°C a liquid magma is observed (see Tab. 3.1).

After melting, a glass phase develops with a total different behaviour than concrete. Small amounts of hematite may develop during cooling down near average temperature of 350°C [L39].

A loss of weight is observed during heating depending on the water content and the type of aggregates. Figure 3-1 shows the weight losses of ordinary concretes made with different types of aggregate and portland cement.

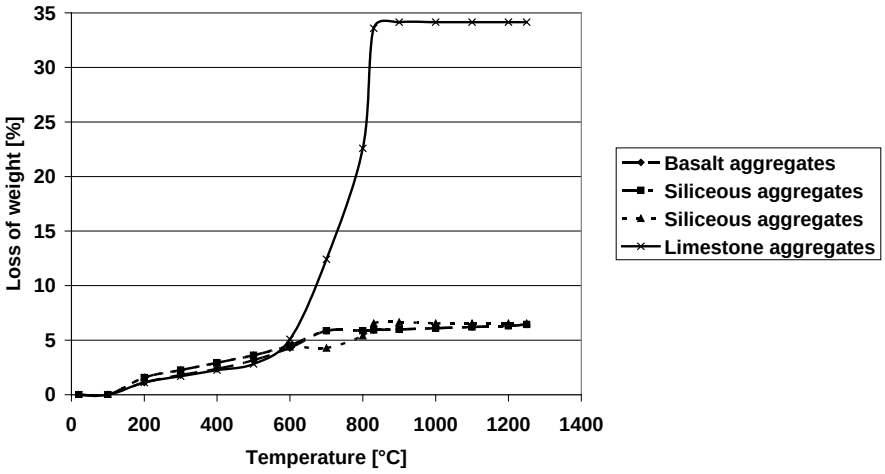

Fig. 3-1 - Thermograms of Different Concretes made with Portland Cement, according to [L40]

In Table 3-1, the transformation and decomposition reactions of quartzit and limestone concrete are shown.

Tab. 3-1 - Transformation and Decomposition Reactions of Quartzit and Limestone concrete according to [L16]

Temperature range [°C]	Transformation or decomposition reactions	Mass of reaction [kg/m³]
30-120	Desorption or evaporation of physically adsorbed water	130 (water)
120-300	Gel destruction: first stage of dehydration	< 78 (hardened cement paste)
120-600	Release of chemical adsorbed or zeolithical bonded water	60 kg (water)
450-550	Decomposition of portlandite $Ca(OH)_2$ into $CaO+H_2O$	< 40 (CaO)
570	Transformation of α- quartz into β quartz	2100 (α SiO_2)
600-700	Decomposition of CSH-phases; formation of β-C_2S	< 240 (hardened cement paste)
600-900	Dissociation of calcite (only calcite aggregates)	2100 limestone with approximately a $CaCO_3$-content of 90%
From 1100-1200	Melting of concrete, formation of glass material phases	2100 (quarzit concrete) 2100 (calcareous concrete)

3.3 Thermal Properties of Concrete

Beginning from 20°C up to melting point, the following characters of the material depending on the temperature reached:

- Density,
- Specific heat capacity,
- Thermal conductivity,
- Thermal diffusivity,
- Thermal expansion,
- Heat of evaporation,
- Heat of dehydration and
- Heat of melting.

All these properties depend on the types of aggregate, cement and water-cement ratio. Furthermore the compacting and the hydration conditions and the type of curing have an important influence on the thermal properties, as well as the geometrical features of structural components.

For the thermal conductivity and thermal diffusivity of different concretes with different aggregates, a lot of literature exists. With respect to special results in this field the following literature is cited [L40 and L41].

3.3.1 Density

For calculation of the heat transfer into the concrete, the following properties must be taken into account. Figure 3-2 shows the density during heating according to the mass loss.

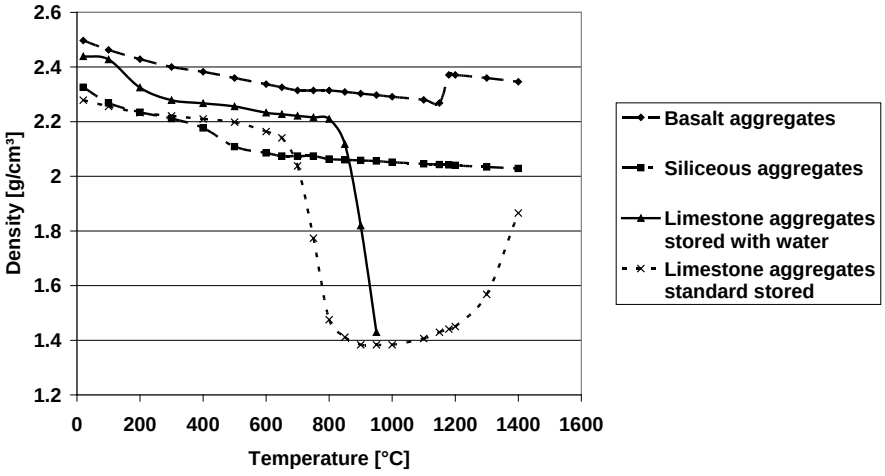

Fig. 3-2 - Density of Different Aggregates during Heating according to [L16 and L40]

Density decreases during heating of all types of concretes. Concrete with limestone aggregates has an extreme weight loss due to decarbonisation between 700°C and 900°C. Siliceous concrete and basalt concrete decrease continuously up to melting. After melting, the density in-

creases in concrete with basalt aggregates and limestone aggregates. This behaviour is not observed in siliceous concrete.

3.3.2 Thermal Expansion

For deformation and relaxation calculations the thermal expansion is very important. Figure 3-3 shows the thermal strains of concrete with different aggregates compared with the thermal strain of steel.

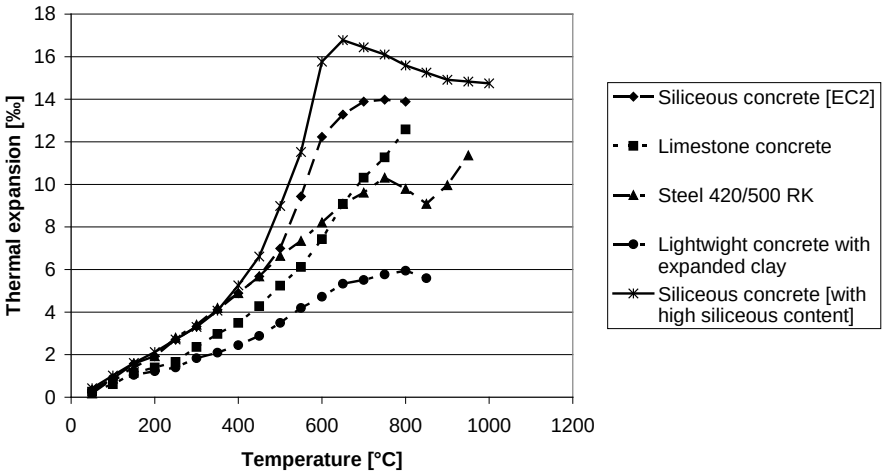

Fig. 3-3 - Thermal Expansion of Concrete with Different Aggregates compared with Steel according to [L21]

The thermal expansion depends on the type of aggregates. The highest thermal expansion at a maximum of 17% may occur in silica concrete with high siliceous aggregate content. The siliceous concrete reaches 14% as maximum as according to EC2.

In practise structural concrete may have different moisture contents. Drying may occur through capillary pores and micro cracks.

In the temperature range from 100°C to 140°C the main part of moisture evaporates easily under fire conditions (see [L52]). The heat of evaporation may be converted into a modified value for c in that range (see Fig. 3-4).

Shrinkage is accounted for by the thermal strain as this is usually determined by testing unsealed concrete specimens [L47], i.e. shrinkage occurs simultaneously to thermal expansion during heating-up of concrete members. From those measured data the expansion coefficient may be derived which depends on temperature.

3.3.3 Specific Heat Capacity

Lots of literature is available for the heat capacity with different concretes and different aggregates. From 100° to 140°C the water vapour leads to a heat loss. The influence of the c_p is also included in the Eurocode. Generally $c_{p20°C}$ is assumed with 0.8 to 1.0. In figure 3-4 the specific heat capacity is shown.

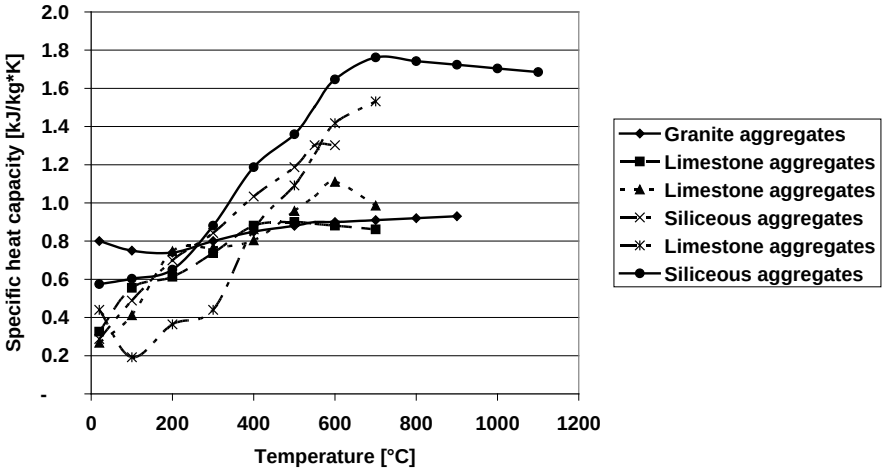

Fig. 3-4 - Main Heat Capacity of Various Concretes according to [L40, L41, L42, L43, L44, L45, L46]

The differences between various types of concretes with different aggregates are caused by water at its point of evaporation, by dehydration reactions of aggregate and by crystal conversions at high temperatures. Most of the reactions are endothermic in character and contribute to an apparent increase in specific heat [L40].

3.3.4 Thermal Conductivity

The thermal conductivity of concrete is determined between a lower and upper limit curves as a function given in Figure 3-5.

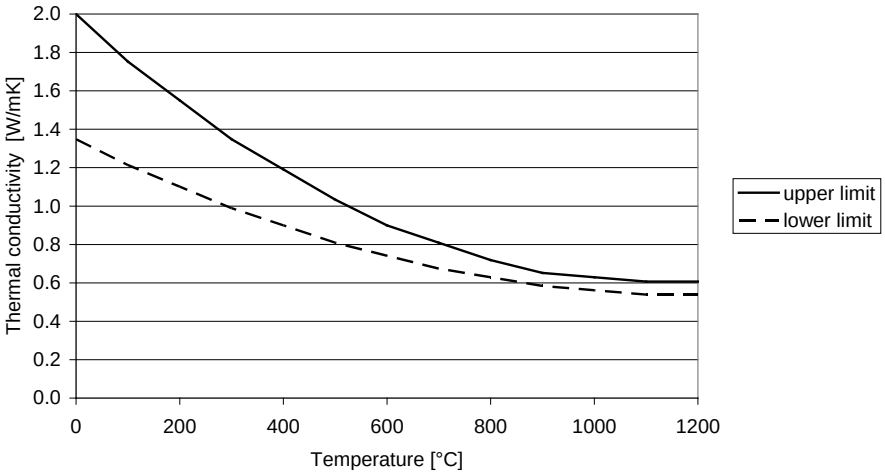

Fig. 3-5 - Thermal Conductivity of Concrete according to [L48]

The influence of aggregate is one of the main parameter. These are based and affirm measured data with pre-dried concrete which are dried at 105°C [L49, L50, L51].

The data according to Fig. 3-5 do not cover the spectrum of thermal conductivity of ordinary concrete because the important influence of aggregate on heat conduction. Fig. 3-6 shows data after [L16 and L40] which clearly indicate the wide spectrum of λ in the high temperature range.

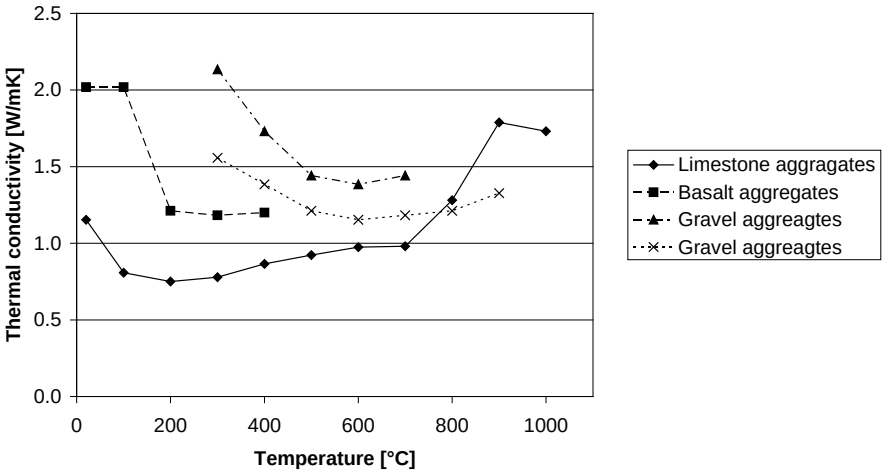

Fig. 3-6 - Thermal Conductivity of Concrete with Different Aggregate according to [L16 and L40]

For approximate calculation the following values were proposed [L52].

$\lambda_c = 1.60$ W/mK for concrete with siliceous aggregates

$\lambda_c = 1.30$ W/mK for concrete with calcareous aggregates

$\lambda_c = 0.80$ W/mK for concrete with lightweight aggregates

3.4 Material Model for Thermal Properties for FEA

3.4.1 General Description of the Input Parameters

During the calculation of the new mechanical model of concrete subjected to fire, an ordinary thermal analysis is used. In the software SAFIR, a finite element program some of the thermal material properties mentioned above is used. The calculation needs 5 input parameters:

- the water content,
- the convection coefficient on the hot surface,
- the convection coefficient on the cold surface,
- the relative emissivity and
- the type of aggregate (choice is given between calcareous and siliceous).

3.4.2 Water Content of Concrete

The water content of concrete mostly depends on the duration of hydration and the water-cement ratio. Generally the duration of hydration is a function of cement type and depends on storage conditions and on the water-cement ratio. Best input values are measured data. For an ordinary concrete the assumption of 2 to 4 % per mass is helpful for buildings and 3 to 5 % for tunnels.

3.4.3 Coefficient of Convection

The value of convection depends on the fire curve and on the situation at the surface. With respect to this behaviour the convection coefficient is considered on the hot surface and the cold surface during a calculation of fire exposure of constructions. According to [L53] the convection coefficient on the hot surface can be assumed with 25 W/m²K. Table 3-2 gives some recommended values for different situations.

Tab. 3-2 – Coefficient of Convection for Different Surface Situations according to [L54]

	α_c [W/m²K]
Unexposed side of separating elements	
Radiation considered separately	4
Radiation implicitly contained	9
Surface exposed to the fire	
Standard curve external fire curve	25
Hydrocarbon curve	50
Parametric fire, zone fire models or external members	35

During direct flame exposure on the surface the convection coefficient can increase. In [L55] a factor of 1.5 is given.

3.4.4 Relative Emissivity

Natural fires have a relative emissivity of the gas between 0.3 and 0.9. The influence of burners in fire tests may be considered in a resultant emissivity between 0.5 and 0.7 [L53]. Specific values for the surface emissivity of concrete and carbon steel are 0.9 and 0.4 of stainless steel.

3.4.5 Calculation Routine in the FEA

The calculation of the thermal conductivity takes into account the moisture content of the used materials. The stepwise calculation of the thermal conductivity is necessary for the prediction of the temperature distribution in the structure. With the parameters mentioned above, the following equations are used [L56].

The general equation for 2D transient heat conduction in an isotropic material is:

$$\left(k\frac{\partial^2 T}{\partial x^2} + k\frac{\partial^2 T}{\partial y^2} \right) + Q = \rho c \frac{\partial T}{\partial t} \qquad \text{equ. (3.4)}$$

Where:

k thermal conductivity
T temperature
Q heat source or sink in the material per unit volume
ρ density
c heat capacity
t time for the time step

There are many unsolved problems in equation 3.4 with respect to the heating of concrete. When the boundary condition is constant over a part of the boundary the following equation can be assumed with known values.

The initial temperatures are known and constant temperatures are calculated as $T = T_0$. The external heat fluxes at the surface boundaries are specified as:

$$k\frac{\partial T}{\partial n} + q = 0\,. \qquad \text{equ. (3.5)}$$

Where q is the specific heat flow and n is the outward normal vector to the boundary. When the boundary conditions are considered, the temperature specified over part of the boundary, and the heat flux specified over part of the boundary. Equation 3.5 is the transformation of this process.

$$k\left(\frac{\partial T}{\partial x}n_x + \frac{\partial T}{\partial y}n_y\right) = -q \qquad \text{equ. (3.6)}$$

The following equation considers the convective heat transfer at the boundaries.

$$k\left(\frac{\partial T}{\partial x}n_x + \frac{\partial T}{\partial y}n_y\right) = -\left(q + h\left(T - T_0\right)\right) \qquad \text{equ. (3.7)}$$

Where h is the heat transfer coefficient and T the surface temperature of the heated material.

Furthermore the values of k, ρ and c are functions of the temperature. This may be considered in a matrix formulation and an iterative solution for each time, step n may be used as shown in equation 3.8.

$$[M]\{\dot{T}\}_n + [K(\{T\}_{n-1})]\{T\}_n = \{Q\}_{n-1} + \{q\}_{n-1} \qquad \text{equ. (3.8)}$$

Using an enthalpy formulation according to the following equation the stepwise calculation of the material capacity is possible, shown in equation 3.9.

$$E(T) = \int_0^T C(u)du \qquad \text{equ. (3.9)}$$

with

$$C = \frac{E(T_\Theta) - E(T_i)}{T_\Theta - T_i} \qquad \text{equ. (3.10)}$$

T_Θ is the temperature evaluated during the iteration and T_i is the temperature within a time step increase and u is the internal energy.

3.5 Mechanical Properties

3.5.1 Compressive Strength

During heating, many mechanisms happen which influence the compressive strength in the origin. Contrary to common belief, not all the mechanisms are degradative [L57].

Table 3-3 shows the parameters determining the temperature dependence of strength of concrete and their practical importance.

Tab. 3-3 – Parameters determining the temperature dependence of strength of concrete according to [L16]

Type	Effect			Practical importance
	Strong	Medium	Weak	
Class of strength	-	-	+	great
w/c ratio	-	-	+	great
Aggregate	+++	-	-	medium
Type of cement	-	++	-	medium
Aggregate/cement ratio	-	++	-	medium
Maximum aggregate size	-	-	+	small
Load level	+++	-	-	$f < 0.3 * f_{ult}$
Heating rate	-	-	+	$\dot{T} = 4°C / \min$
Evaporation rate	+++	-	-	at T ≈ 120°C
Age of concrete	-	-	+	t>28d
Type of curing	-	++	-	medium
Sealing	+++	-	-	until T<200°C

The compressive strength of cement paste depends on the kind of used cement, is shown in Figure 3-7. It shows different types of cementitious mixes with curing under standard condition at 20°C and moisture of 65%.

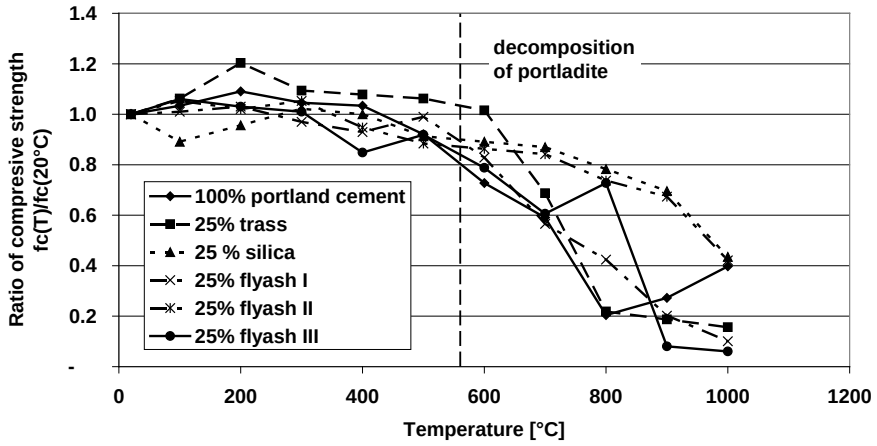

Fig. 3-6 - Comparison of compressive strength of different cementitious mixes after standard curing under 20°C/65% according to [L58]

It should be noted that the influence of binder is relatively small compared to the influence of aggregates, see Fig. 3-7 compared to Fig. 3-8. The point of decomposition of CSH-phases did not clearly recognizable.

Figure 3-8 shows a comparison between the compressive strength with different aggregates related to the compressive strength in the origin at 20°C after 28 days of 27,5 N/mm².

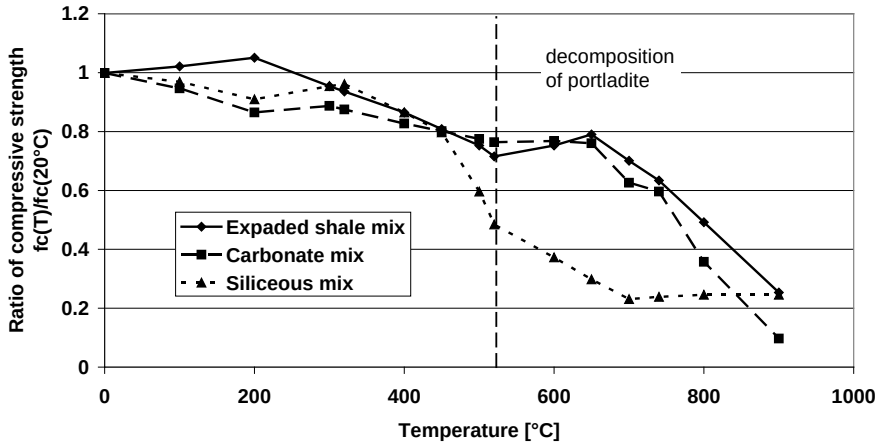

Fig. 3-7 - Compressive strength of concretes with different aggregates according to [L59]

The influence of aggregate on the temperature behaviour was reported many times. A good temperature was observed for behaviour have the expanded lightweight aggregate , basalt aggregate and the calcareous aggregate below 650°C.

3.5.2 Young's Modulus

For concrete the compressive strength depends more on the cement paste as compared to the Young's modulus which depends more on the type of aggregates. In the range of ordinary concrete from C20/25 to C50/60 the influence is shown on Fig. 3-9.

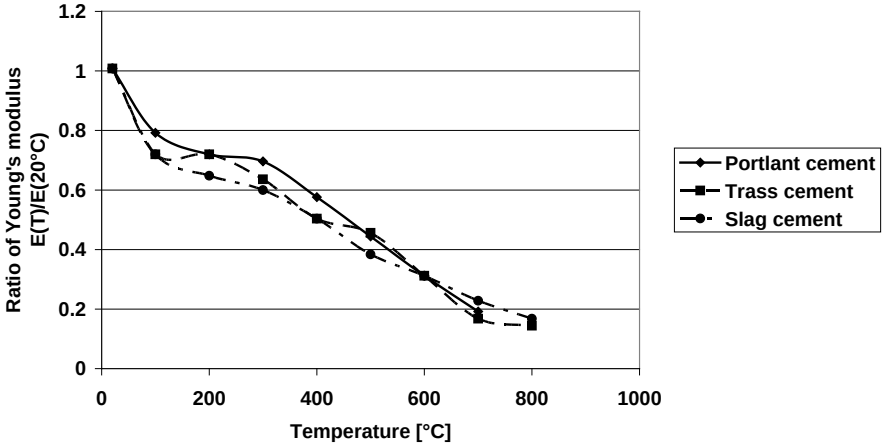

Fig. 3-8 - Influence of kind of cement on Young's modulus of ordinary concrete according to [L15]

The type of cement is not very important for the compressive strength of concrete, shown in Figure 3-9.

In Figure 3-10 the difference between concretes with various aggregates is shown.

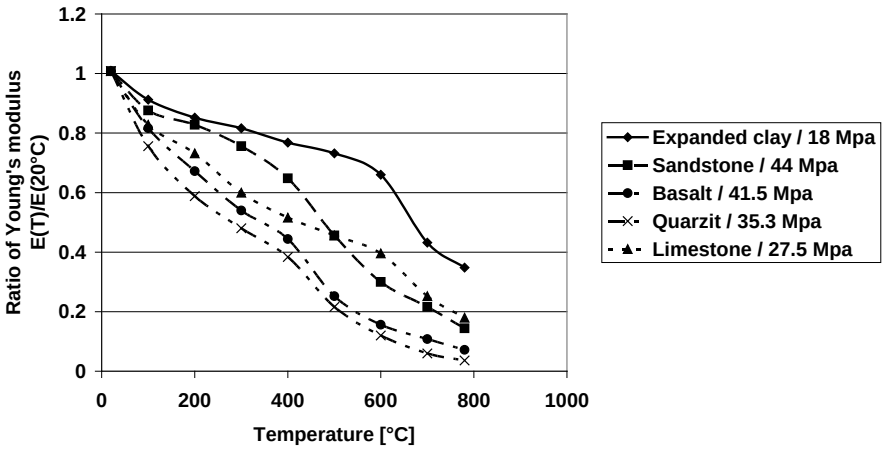

Fig. 3-9 - Young's modulus of concretes with different aggregates according to [L15 and L16]

It can be summarized that the influence of different aggregates is high on the modulus of elastic. The influence of compressive strength on the Young's modulus is relatively low.

3.5.3 Stress-strain Relationship

The mechanical behaviour of concrete during heating is calculated as a function of external loads and different types of stresses and deformations during heating up. The stress-strain relationship summarizes the different types of deformation in one temperature function. Some researches give functions with different parameters in respect to the heating rate and the load during heating [L4]. Stress-strain-curves for ordinary concrete are normalised in the Eurocode 2.

The following parameters have an observed influence to the development of the stress-strain relationship of concrete including high strength concrete [L16]:

- mix proportion
- type of cement
- type of aggregate
- fibre addition
- curing conditions
- loads during heating
- heating rate

Figures 3-11 and 3-12 show some test results of strain measurements obtained under different test conditions.

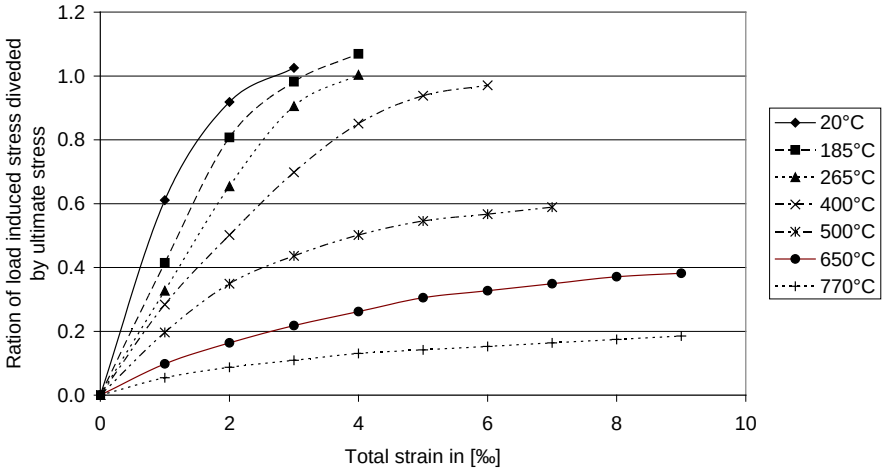

Fig. 3-10 - Stress-strain relationship of normal concrete C25/30 with quartzite aggregates in a stress rate controlled test according to [L60]

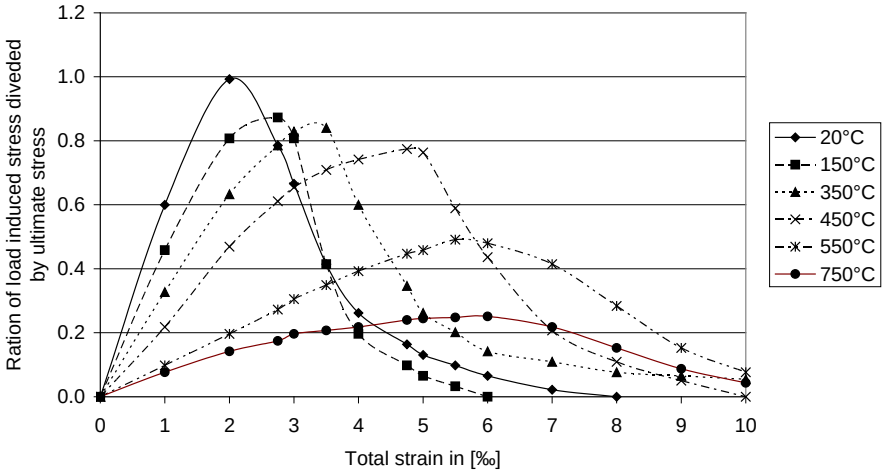

Fig. 3-11 - Stress-strain relationship of normal concrete C25/30 with basalt aggregates in a strain rate controlled test according to [L61]

It is to be seen that the stress strain relationship depends on the temperature and the type of aggregates. In the literature, there is lots of information about the parameters which influence the stress-time relationship.

The stress-strain-curve under heating is influenced by the following parameters [L16]:

- Original strength has only a little effect
- Water-Cement ration has a high effect
- Aggregate cement ration has a significant effect in concrete not so much in mortar
- Type of aggregates is a main factor and has a high effect
- Dissipation energy has influence of the crack development, this has an influence to the stress-strain curve
- Type of cement has a minor effect
- Addition of steel fibres has a significant influence
- Curing condition is important in temperature exposure under 300°C
- Test condition is an important factor, i.e. load during the test
- Ultimate strain is influenced by the temperature and this influence the stress-time relation
- Under biaxial conditions the stress-time relationship the ultimate strain is higher than in uni-axial tests, this has an effect on the stress-time relationship.

A concrete model based on a stress-time relationship has many advantages when the points mentioned above are considered in the model. In real cases, the stress-time curve change during heating according to load, chemical and physical effects.

3.5.4 Ultimate Strain

The ultimate strain is the strain in the point of a stress-strain relationship where the ultimate stress occurs. This point depends on several influences i.e. temperature and load during heating up.

Fig. 3-13 shows the general effect of temperature on the ultimate strain. The behaviour is governed by external compressive loads, crack development and the physical and chemical reactions during heating up. It is based on measurements obtained in the literature [L21]. It shows the important effect of sustained loads on the ultimate strain.

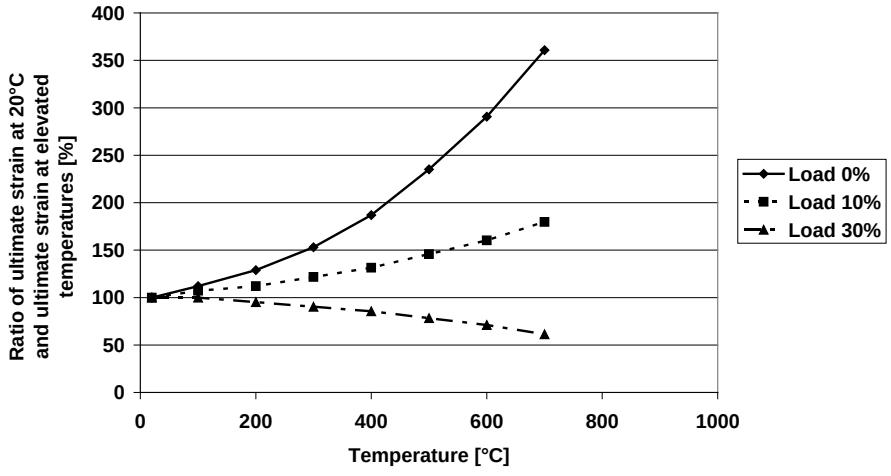

Fig. 3-12 - Ratio of ultimate strain of heated and loaded/non-loaded specimens compared to specimens tested at 20°C according to [L21]

Fig. 3-14 shows the dependence of the ultimate strain from the types of aggregates.

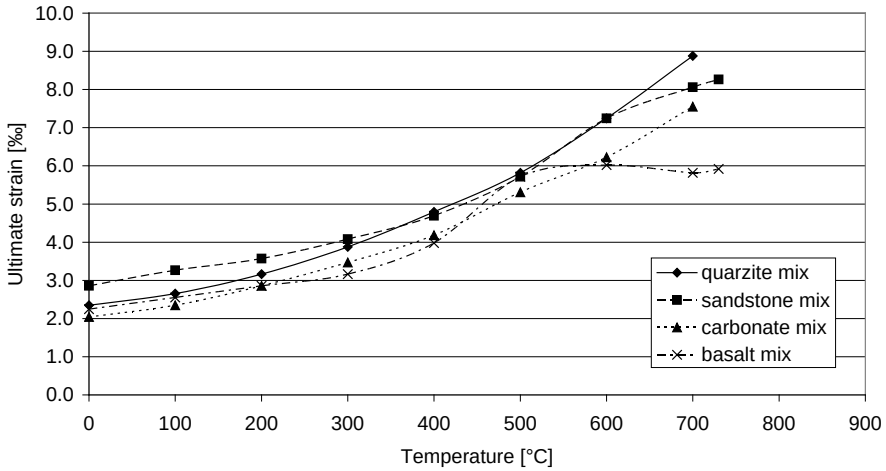

Fig. 3-13 - Ultimate strain of normal concrete with different types of aggregates according to [L61]

The influence of the type of aggregates is also at hand but less significant. The most important difference is observed above 600°C. If the types of aggregates in the concrete are known, it is basically to consider the real behaviour of ultimate strain with respect to the types of aggregates.

The chemical and physical effects are more important with respect to the overall required behaviour of concrete. Particularly, the influence of external loads is more important for the concrete behaviour as its ultimate strain has a higher influence on the stress-strain relationship.

3.5.5 Poisson Ratio

The Poisson ratio is the relation between the lateral strain and the linear strain. The Poisson ratio depends on the temperature that is seen in Figure 3-15, and is also dependent on the stress level.

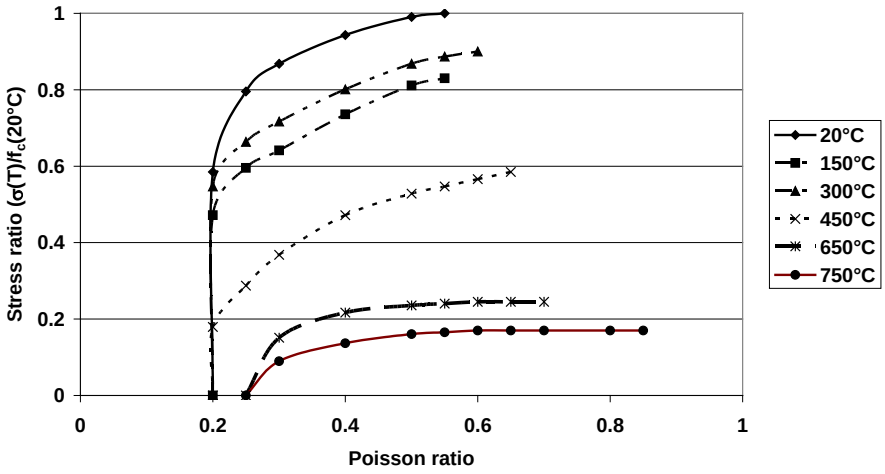

Fig. 3-14 - Poisson ratio of loaded concrete at high temperatures according to [L16]

The general assumption of μ = 0.2 is only usable for temperatures lower than 600°C. When the stress ratio increases, the Poisson ratio increases significantly.

Derived from Fig. 3-15 for calculation of complex structures, this behaviour should be included in the calculation model.

3.5.6 Tensile Strength

The experimental evidence indicates that tensile strength of concrete decreases almost linearly as the temperature increases [L59, L62]. As the temperature increases, the micro-cracks, vaporisation and decomposition of cement paste and aggregates lead to a decrease concrete tensile strength [L63].

One investigation of the transient thermal strain under tensile load concludes the effect of transient tensile creep strains during heating-up that it is not detectable or does not exist [L64].

Fig. 3-16 shows dependence from the kind of aggregates in a split cylinder tensile strength test.

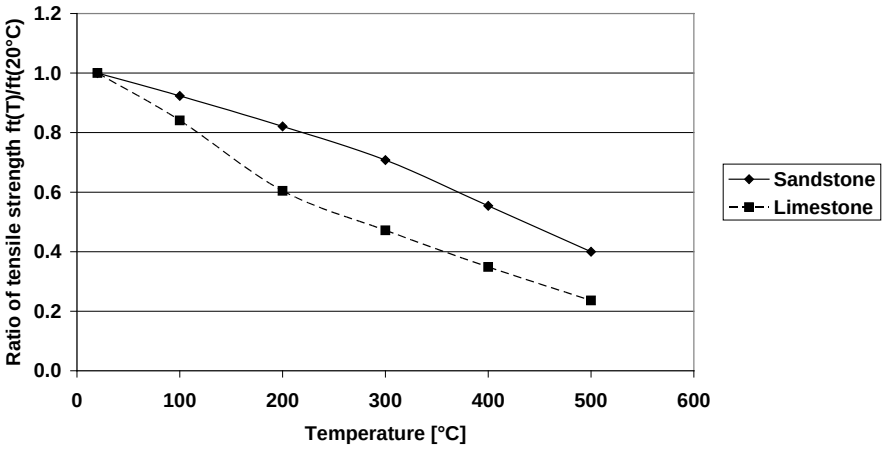

Fig. 3-15 – Split cylinder tensile strength of concrete with different aggregates after cooling according to [L16]

The limestone material indicates higher strength losses than the sandstone material.

3.5.7 Residual Behaviour

The residual behaviour of concrete after heating and cooling depends on a great number of effects. The residual compressive strength, residual tensile strength and residual Young's modulus is mainly influenced by the type of cement, water-cement ratio and the aggregate used. A non-linear behaviour with respect to the hot state of compressive strength was observed [L65].

Temperature above 450°C causes irreversible reductions of the compressive strength and other mechanical properties. The compressive strength of concrete does not recover in the cooling phase because of initial degradation and chemical decomposition of the conversion of portlandite in the cement paste [L66], see Figure 3-17 and 3-18.

The figures 3-17 and 3-18 show the influence of cooling condition. It is shown that the curves around the values are divided under slow decreasing temperatures. The residual strength is mainly influenced by the temperature during heating, the way of cooling and the time of storage after fire [L68]. The quenched specimens indicated destructive effects due to the thermal shock below 500°C.

The compressive strength before heating was 26.7 N/mm².

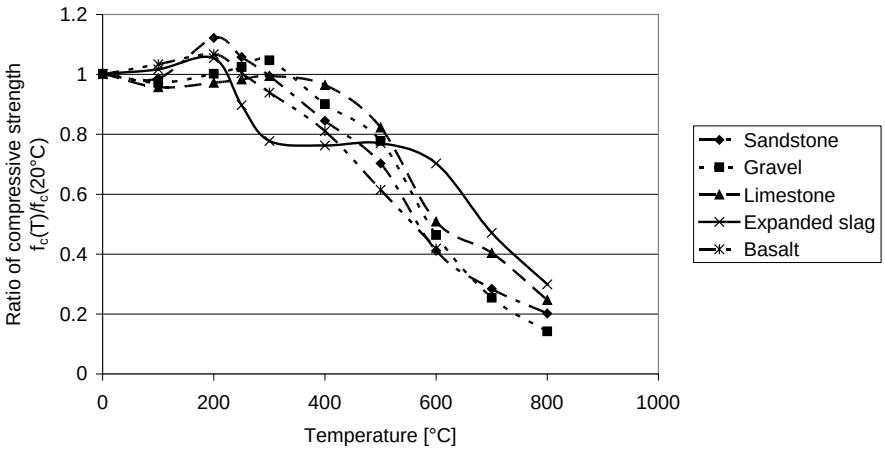

Fig. 3-16 - Residual compressive strength of concretes after slow cooling down with different aggregates according to [L59, L67]

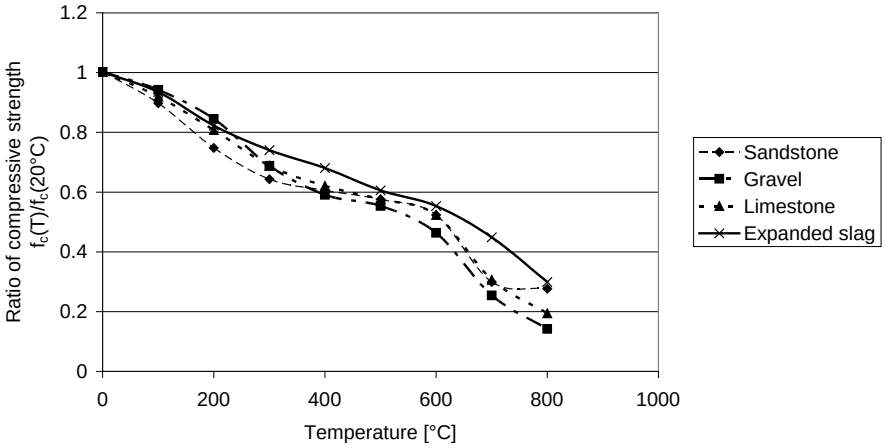

Fig. 3-17 - Residual compressive strength of concretes after quenching with different aggregates according to [L59]

Figure 3-19 shows the residual strains of concretes after heating-up to different temperatures and immediate cooling thereafter. That behaviour could be estimated as irreversible like plastic deformations.

It is clear that the residual strain measurements are very sensitive with respect to the type of aggregate being used [L6].

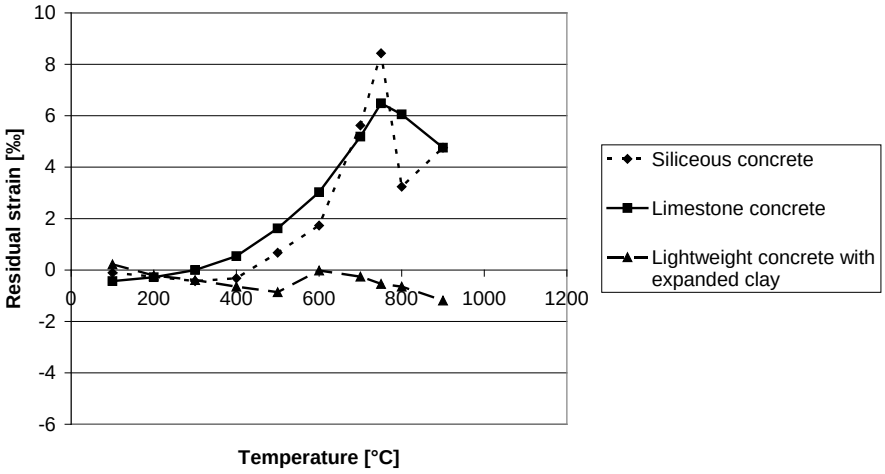

Fig. 3-18 - Residual strains after heating-up to a certain temperature T_{max} and cooling down to 20°C of different types of concretes according to [L18]

Figure 3-20 shows the residual measurements of Young's modulus of concrete with different aggregates.

A difference between the aggregates is observed, but the influence is not as important compared to the changes of the Young's modulus during heating. The influence of cracks is higher than the influence of chemical changes during heating.

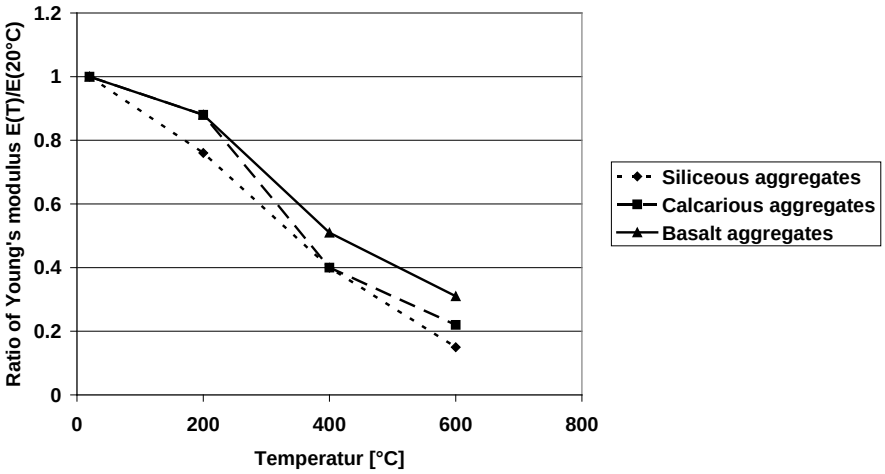

Fig. 3-19 - Residual Young's Modulus with different aggregates according to [L67]

Figure 3-21 shows the residual tensile strength of different concrete mixes with different aggregates.

Only minimal differences were observed between the three types of aggregate used. The influence of the residual strength is the result of number of cracks which develop during heating and

cooling. If aggregates suffer under high damage during heating are residual tensile strength is very small.

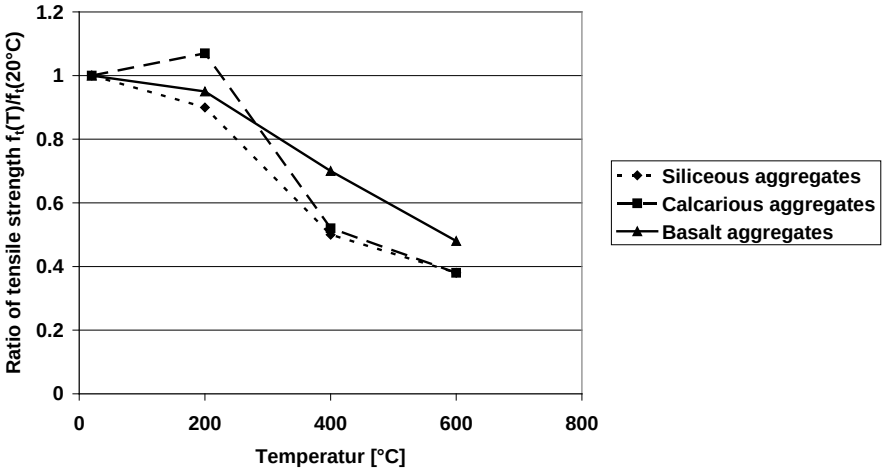

Fig. 3-20 - Residual tensile strength with different aggregates according to [L67]

3.6 Consideration of Load History

3.6.1 Stress Development without Load Effect

The dependence of the compressive strength on the temperature is well known. The influence of type of aggregates and type of cement is shown in Chapter 3.5.1. There are several models which consider this behaviour. Fig. 3-22 shows a comparison of 4 models which are used in different concrete models and countries.

Fig. 3-22 shows the difference between the four samples of concrete models. The differences given are not very important. The model of the Czech Republic works with an upper level and a lower level. The lower level is shown.

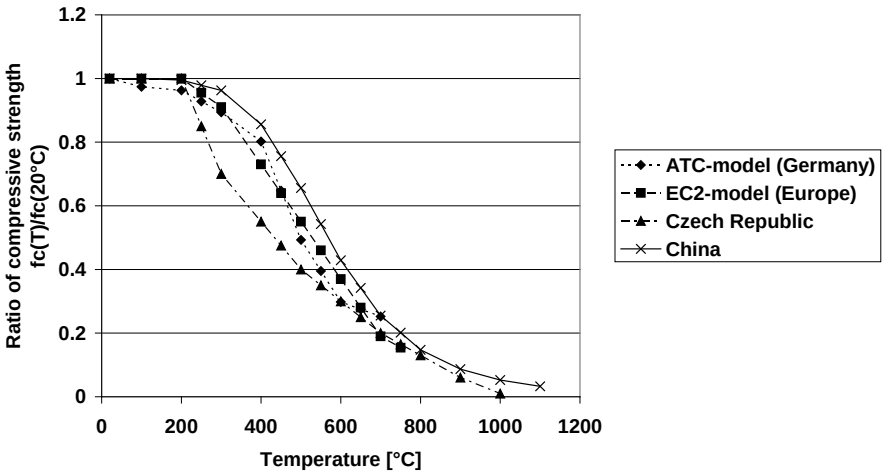

Fig. 3-21 - Comparison of temperature behaviour of compressive strength in different models according to [L16; L69 and L70]

3.6.2 Compressive Strength with Load History Effects

To calculate the mechanical strength of heated concrete members under high temperature, a load factor is introduced. This factor takes the load history during heating and cooling into account and is calculated as follows:

$$\alpha = \frac{\sigma_{hist}}{f_c(20°C)} \qquad \text{equ. (3.12)}$$

σ_{hist} is the time dependent compression stress due to external loads. In this report the load level α was kept variable during fire exposure. This factor presents the load history and is used for structures that are loaded under compression in the elastic range $\alpha \leq 0.4$ and during heating. Some researchers adopt higher load levels, e.g. $\alpha \leq 0.6$ as an upper limit for the application of this calculation method [L71].

In compression, thermal induced cracks will be closed during heating up. Therefore a relative increase of stiffness compared to unstressed concrete during first heating was observed. Even though the dehydration of cementitious binder generally leads to a decrease in stiffness and compressive strength of concrete of a compressive class of C25/30 (see Figure 3-24), but that occurs at higher temperature levels.

Figure 3-23 shows that an increase of the load factor up respectively $0 < \alpha \leq 0.6$. It indicates very clearly the relative increase of strength compared to $\alpha = 0$. A further increase of the load factor α does not increase the stiffness significantly, but an early failure of concrete at 200°C may be observed for loads > 60% of ultimate stress.

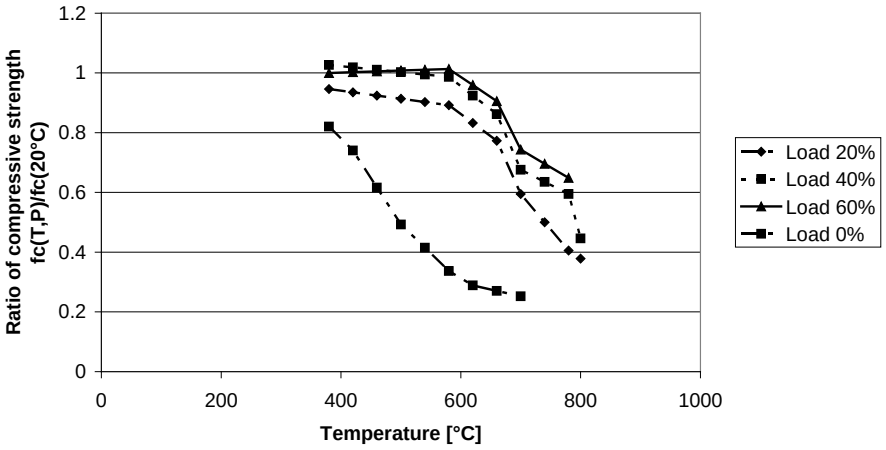

Fig. 3-22 - Comparison of concrete strength for different stress-temperature history according to [L71]

3.6.3 Development of Young's Modulus of Elasticity with Load History Effect

Due to the elastic behaviour of stress-strain relationship the Young's modulus in the range before $\alpha = 0.3$ increases continuously. After this range, a relatively constant range of the Young's modulus is observed. Then a slight decrease can be seen, i.e. the plastic deformation took place. Considering $\alpha \equiv 0.3$ is therefore acceptable if $\alpha > 0.3$. The slight decrease will be considered in the plastic part of the deformation, see Figure 3-24.

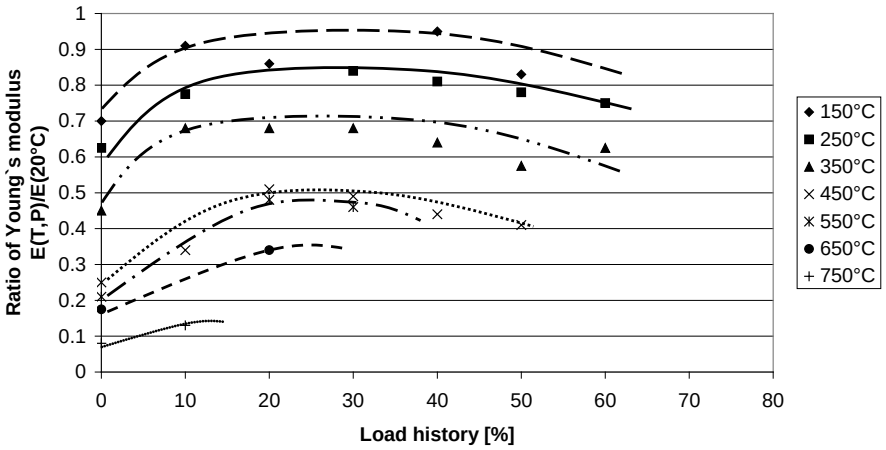

Fig. 3-23 - Young's modulus of siliceous concrete being loaded during heating up according to [L128]

4 State of the Art in Practical Applications

4.1 Behaviour of Building Elements under Fire

The behaviour of structures depends on material properties, the fire behaviour of the elements, the fire intensity and the temperature exposure. Generally the fire resistance of structures should be described by the behaviour during fire and after cooling [L72, L73, L74, L75]. The temperature and the deformation rate are recorded because the heated structures may be exposed to changes of applied loads during the heating cycle. In the calculation of slender columns, that effect may be very important in more complex structures and it may even be decisive for the fire behaviour of the total structure. Furthermore, some unintended destructive effects like explosive spalling may occur.

The spalling is the most important effect [L76]. The cross section and the heat penetration are influenced by the loss of concrete cover due to spalling. The number of publications in this field is tremendous. Particularly for that, a running research project is being discussed as an example for all the brilliant research works. For loaded structures, effects in the concrete cover may be observed [L77]. In tunnel structures spalling starts at 5 minutes after the occurrence of fire and may lead to a total destruction of the tunnel shell if the fire duration is in the order of several hours [L78]. Generally it is agreed that spalling can be minimized by addition of polypropylene fibres or a mix of steel and polypropylene fibres on the concrete mixture [L79]. It was observed that polypropylene fibres have only a small effect on creep thermal strains. For self compacting concrete the transient creep strains are smaller than those without fibres [L80].

Residual strength was often measured on structures [L81, L82, L83]. This may be included in a structural calculation model [L84], but several other material parameters must be determined if the post heating behaviour is estimated.

4.2 Tabulated Data

Tabulated data according to Eurocode 2 have wide acceptance in concrete constructions. It is a simple method with good approximated experiences. The basic assumption is a default failure of the structure. There are different types for the definition of high temperature failure of members. The failure criteria are defined as a necessary cover between axes of the rebars in reinforced concrete structures and the concrete surfaces. In this case the critical temperature of the steel is up to 500°C. This assumption is approximated by to the definition of:

$$E_{d.fi} = \gamma_s * E_d \qquad \text{equ. (4.1)}$$

with

$\gamma_s = 1.15$ (stress of the steel $\sigma_{s.fi} / f_{yk} = 0.60$) and

$E_{d.fi}$ as rated value in case of fire and E_d as rated value at ambient temperature.

The tabulated data are only usable for the standard fire curve (ISO curve) according to ISO 824. Generally, other fire curves can be determined. Using tabulated data is only possible for members not for parts of the whole structure.

All values are determined according to performance tests with concrete members, i.e. columns, walls and beams. The Eurocode 2 distinguishes between calcareous aggregate concrete and siliceous aggregate concrete. The minimum size can be reduced by 10% when calcareous aggregate concrete is used for slaps and beams. The tabulated data are based on a limited number of comparisons with test results. Some doubts were raised about the assumption that the results provided by these tables (according to Eurocode 2) were said to be conservative [L85].

Table 4-1 shows a set of data for columns with rectangular or circular cross sections.

Tab. 4-1 - Minimum size and distance of axes of columns with rectangular or circular cross sections according to [L48]

fire resistance class	minimum size [mm] width of column/ distance of axes			
	fire load on more than one surface			fire load on one surface
	$\mu_{fi} = 0.2$	$\mu_{fi} = 0.5$	$\mu_{fi} = 0.7$	$\mu_{fi} = 0.7$
1	2	3	4	5
R30	200/25	200/25	200/32 300/27	155/25
R60	200/25	200/36 300/31	250/46 350/40	155/25
R90	200/31 300/25	300/45 400/38	350/53 450/40*	155/25
R120	250/40 350/35	350/45* 450/40*	350/57* 450/51*	175/35
R180	350/45*	350/63*	450/70*	230/55
R240	350/61*	450/75*	-	295/70
* minimum 8 steels over the cross section				
Note recommended value of $\alpha_{cc} = 1.0$ is considered. α_{cc} is the reduction factor of the compressive strength of concrete.				

The buckling length $l_{0,fire}$ of the members according to table 4-1 is between $0.5 * l_0 \le l_{0,fire} \le 0.7 * l_0$ with l_0 as the length of the column at ambient temperature.

An eccentricity is considered by $0.15 * h \le e_{\max} \le 0.4 * h$ with h as minimal width of the cross section.

It is shown that the members are defined by width of column and distance of axes. Furthermore a load factor will be considered by the following equation.

$$\mu_{fi} = \frac{N_{Ed,fi}}{N_{RD}} \qquad \text{equ. (4.2)}$$

Where:

$N_{Ed,fi}$ axial force during fire load and

N_{RD} axial force during standard condition.

For other members, i.e. walls and beams, the procedure is similar to the procedure mentioned above.

The buckling is also considered by tabulated data until a slenderness of $\lambda = 80$ and standard fire curve [L48]. In this failure behaviour the tabulated data from table 4-1 changes a little. The buckling depends on the bending moment of the theory for first order and the eccentricity of the load.

The reduction of the cross section during fire due to spalling cannot be considered. That is brought about by the necessity to cover dependent distance between the rebar axis to the surface.

4.3 Simple Calculation Models

According to Eurocode 2 the reduction of the cross section method or the use of equivalent loads is allowed. The following description gives an example of equivalent loads. The material model is derived by a transformation of a layer figure of the heated cross section with temperature reactions in each layer due to fire load into an average temperature and a temperature gradient between the fire loaded side and the unloaded side [L86 and L87].

Based on the results of a "general arithmetic procedure", an approximated method can be used to calculate bending moments, axial forces and displacements as a function of time and temperature. In order to calculate thermal strength, a cross section is divided into different layers. The temperature and material qualities were determined after each time-step as a steady state in each layer [L88]. The thermal strength can be transformed into a resultant strength through the following equation [L89]:

$$\sigma_{res,i}(t) = \sigma\left(\varepsilon_{E,i}(t, T_i)\right) \qquad \text{equ. (4.3)}$$

Where:

$\sigma_{res,i}$ resulting strength in layer i,

$\sigma(\varepsilon,t)$ material law as a function of temperature of layer i at time t and

$\varepsilon_{E,i}$ the mechanical strain due to the change of Young's modulus at each time step,

T_i temperature of layer i at time t.

From the resulting strength, the Young modulus can be calculated as a function of temperature as follows:

$$\sigma_{res} = \int_{i=0}^{h} \left(E_{res,i}(T) * \alpha_T * T_i \right) dh_i \leq f_{ck}(T_i, \max)\Big|_{i=1}^{i=n} \qquad \text{equ. (4.4)}$$

σ_{res} function of the Young modulus and resulting strength at the time of temperature effect in each layer,

$f_{ck}(T_i, \max)$ maximum compressive strength at temperature T in layer I and

α_T thermal expansion coefficient of concrete equates to 10^{-5} K^{-1} (The use is approximately allowed for quartzite concrete up to a temperature of 400°C).

Figure 4-1 shows an example of the compressive strength determined by a mean temperature for each layer. At a temperature higher than 700°C, the compressive strength of layers was estimated to be zero. The cross section of the member of this example is 0.65 m x 1.00 m.

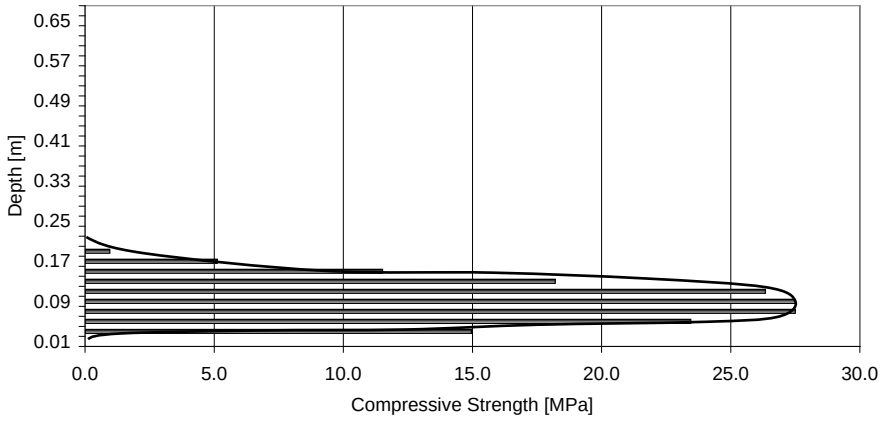

Fig. 4-1 - Example - figure of thermal strength as a function of heat penetration

The axial force as a function of temperature is nonlinear and calculated as follows:

$$N(T) = \sum_{1}^{n} \sigma_{res,i} * h_i \qquad \text{equ. (4.5)}$$

The related bending moment equates as:

$$M(T) = N(T) * h_y \qquad \text{equ. (4.6)}$$

where:

h_i is the high of layer i and

h_y is the distance from the center of the cross section to center of the figure of thermal strength (see Figure 4-1).

Constant temperatures can be assumed to be unvarying in each layer. From these thermal loads, the load bearing capacity of the structure is obtained by calculation.

$$T_m = \frac{N(T)}{E(T) * h} * \alpha_T \qquad \text{equ. (4.7)}$$

and

$$T_u - T_o = \frac{M(T) * h}{E(T) * I * \alpha_T} \qquad \text{equ. (4.8)}$$

Where:

$$I = \frac{b * h^3}{12} \qquad \text{equ. (4.9)}$$

with I as moment of inertia.

$$\Delta T = \frac{T_u - T_o}{h} \qquad \text{equ. (4.10)}$$

With h as high of the cross section and T_u and T_o as inside and outside temperatures.

This simplification defines an equivalent load for the calculation of stress after the theory of second order. That means an eccentric load is considered and the buckling will be calculated with the modified system with respect to the equivalent loads. Spalling cannot be calculated or introduced in the model. If spalling is estimated then the integral may be changed (see Fig. 4-1) according to specific experiences.

4.4 Nonlinear Model according to Eurocode Part 1-2 and Scientific Research Models

Most of the common models are based on a coupled thermal and mechanical analysis using finite element analysis [L90, L91, L92]. Also the Eurocode 2 allows a general arithmetic method. This method is separated in a thermo analytic and a mechanical analytic [L48]. The common procedure is using the heat penetration of a good known material, i.e. ordinary concrete according to standard fire curve subjected on the surface of the calculated construction. The calculation basics are derived from fire test results. In this case the data of the cooling down period must be determined by separate tests.

In specific situations it might be necessary to model concrete as a multiphase material with pores, water, vapour or dry air for the thermal phases of the structural calculation [L93] but nowadays those models are mostly applied for scientific purposes rather than practical for applications.

In the calculation of structural performance commonly the structural damage model is considered as representative [L94].

The analysis procedure may be summarized as follows [L95, L96]:

- Define the geometry and design materials of the structure.
- The transient thermal analysis is performed by using the given fire scenario according to fixed time intervals.
- The initial static conditions at the temperature before the fire starts are to be applied.
- Calculation of structural response during heating and under fire conditions during the time of fire exposure.

The analysis of structures can be calculated in 2 or 3 dimensions. Both calculations lead to good agreements between fire test results and calculation for several structures [L97].

A 2-D calculation model for the thermal calculation and the structural calculation of members was applied. This model works with fibre element in each element across a longitudinal part of the structure which seems usable, see Figure 4-2.

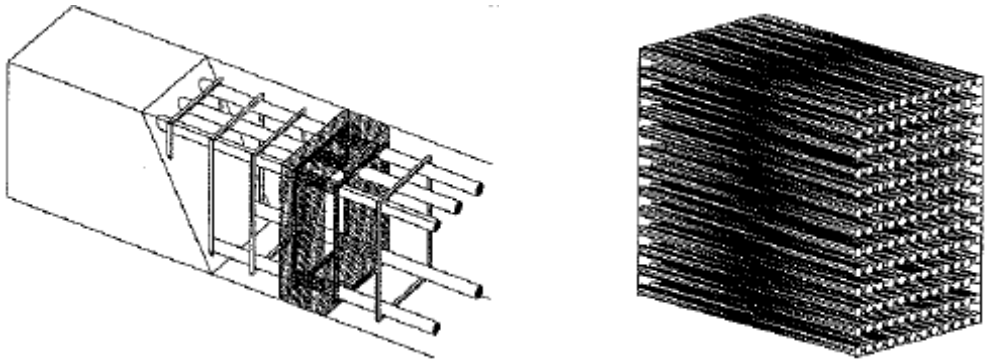

Fig. 4-2 - Application of a fibre element according to [L95]

The basis of the finite element model (FEM) used in this study is a division of the composite system into a binary system comprising “fibre elements” which account for mechanical properties such as axial effects, shear and transverse stiffness and Poisson’s effect [L98]. In general, a stress-strain curve characterizing a short-fibre composite material, when strained in stresses parallel to a fibre direction, consists of four stages. These stages are [L99]:

(1) elastic deformation of fibres and the matrix;
(2) plastic deformation of the matrix whilst the fibres deform elastically;
(3) plastic deformation of fibres and the matrix and
(4) fracture of fibres followed by fracture of the composite material.

This is a finite idealisation of a unidirectional composite. The fibre elements are two node line elements and an effective medium element which can be considered homogeneous and isotropic [L100].

The structural calculations are bases on the theory of the second order with respect to eccentric loads for the whole construction system. The buckling will be considered. Spalling can be roughly considered with a time dependent reducing of the cross sections. In this case all material laws are 0 if a maximum of temperature is reached. A detailed description of the model is given in the following chapters.

5 Presentation of the Advanced Transient Concrete Model

5.1 General Definition

This material model is developed for calculation reinforced concrete structures. The new model is an extension of the former Transient-Creep-Model and was originally given in [L18] and later extended in [L23] and is generally called the Advanced Transient Concrete Model (ATC-model). Transient conditions during the whole calculation routine are taken into account. The transient load (load history) and the real temperature development are considered. Generally, an ATC-model can be used for all types of concrete; only some parameters have to be changed. This examination is based on ordinary concrete with siliceous aggregates.

5.2 Thermal Aspects of Physical Material Models

The ATC-model is an open construction model. The model based on nonlinear thermal and mechanical material laws for ordinary quartzite aggregate.

The thermal analysis bases according to the following material parameters.

The thermal conductivity depends on moisture content of concrete and must be considered in a concrete model. Figure 5-1 shows the used thermal conductivity for siliceous concrete compared to the values of EC2.

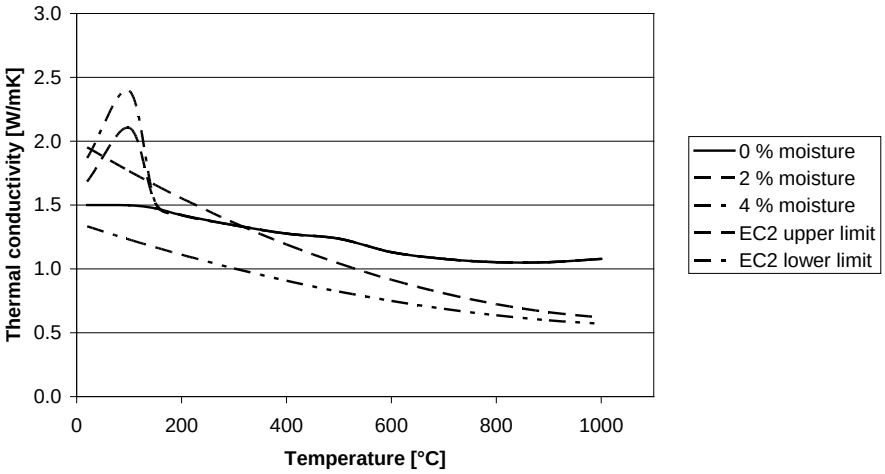

Fig. 5-1 - Thermal conductivity of siliceous concrete with different moisture contents according to [L52]

The following equations based on the functions of Fig. 5-1.

T > 100°C: $\lambda_c = 1.7455 + 0.1163 * w + 0.0001628 * (T - 20) * w$ equ. (3.1)

100°C ≤ T ≤ 700°C: $\lambda_c = 1.7455 - 0.000872 * (T - 100)$ equ. (3.2)

T > 700°C: $\lambda_c = 1{,}23$ equ. (3.3)

Where:

$\lambda_c \rightarrow$ thermal conductivity in W/mK,
T $\rightarrow$ temperature in °C and
w $\rightarrow$ humidity in % by weight.

The density of ordinary concrete depends generally on the water and moisture content. The physically bound water is vaporized at temperatures between 100°C and 140°C. 180°C vaporized the gel water and at 800°C the chemical bound water. Fig. 5-2 shows this effect for an ordinary concrete with an oven-dry density of 2.3 kg/dm³. The comparison to EC2 is included.

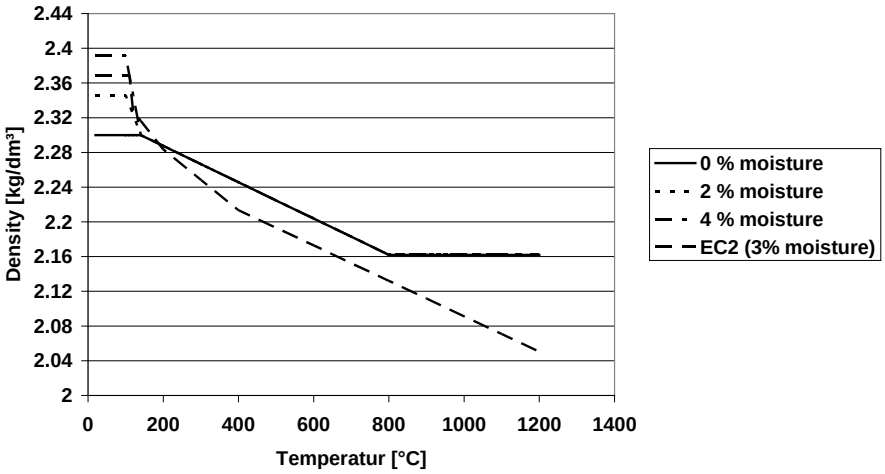

Fig. 5-2 - Density of concrete subjected to fire with different moisture contents

The following equations are given for $\rho(T,w)$:

20°C ≤ T ≤ 100°C: $\rho = \rho_{tr} + w$ equ. (5.4)

100°C ≤ T ≤ 140°C: $\rho = \rho_{tr} + w * (3.5 - 0.025 * T)$ equ. (5.5)

140°C ≤ T ≤ 700°C: $\rho = \rho_{tr} * (1.012727 - 9.0909 * 10^{-5} * T)$ equ. (5.6)

700°C ≤ T ≤ 1200°C: $\rho = 0.94 * \rho_{tr}$ equ. (5.7)

Where:

$\rho_{tr} \rightarrow$ oven-dry density in kg/m³,
T $\rightarrow$ temperature in °C and
w $\rightarrow$ humidity in kg/m³.

The specific heat capacity of siliceous concrete with different humidity is shown in Fig. 5-3 compared with EC2.

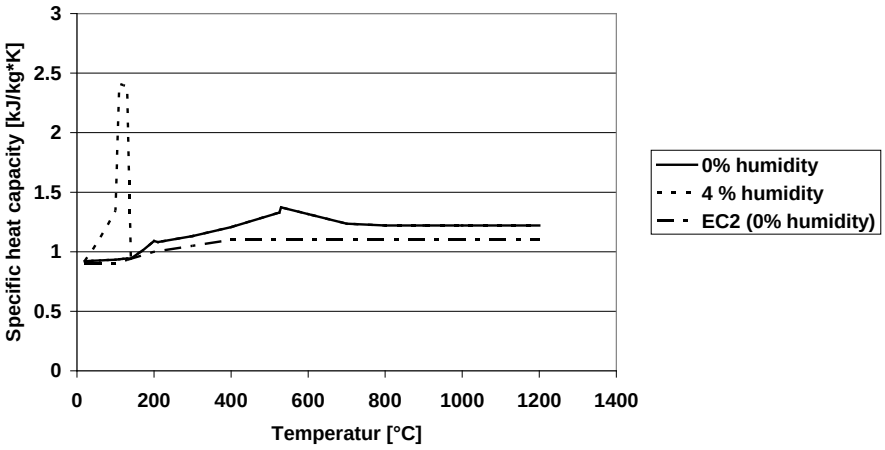

Fig. 5-3 - Specific heat capacity of siliceous concrete according to [L15]

The equations for different range of temperatures are given in the following equations for humidity of 4%:

20°C ≤ T ≤ 100°C: $c = 0.8346 + 0.0041 * T + 1 * 10^{-5} * T^2$ equ. (5.8)

100°C ≤ T ≤ 140°C: $c = 2.542 - 0.0012 * T$ equ. (5.9)

140°C ≤ T ≤ 200°C: $c = 0.7976 + 6 * 10^{-5} * T + 7 * 10^{-6} * T^2$ equ. (5.10)

200°C ≤ T ≤ 525°C: $c = 1.0268 + 5 * 10^{-5} * T + 1 * 10^{-6} * T^2$ equ. (5.11)

525°C ≤ T ≤ 700°C: $c = 1.796 - 0.0008 * T$ equ. (5.12)

700°C ≤ T ≤ 1200°C: $c = 1.22$ equ. (5.13)

Where:

$c \rightarrow$ specific heat capacity in kJ/kgK and
T $\rightarrow$ temperature in °C.

It should be notes that the temperature and moisture dependence of λ, ρ and c are important for an exact determination of temperature fields in concrete members under fire exposure. The moisture dependence of λ and c are especially important factors in the calculation of real temperatures in concrete under fire exposure.

5.3 Constitutive Aspects of Transient High Temperature Material Models

5.3.1 Most Important Available Models

At first a little overview through the history of modelling structural behaviour during fire is given. Before 1970, the calculation of thermal resistance of concrete structures comprises only the temperature dependent reduction of compressive strength and Young's modulus [L31, L35]. First research works starts to describe the behaviour of load before heating [L37]. Harada re-

ported in [L34] about a research work where the thermal expansion of concrete was examined. In the year 1973 and 1976, Anderberg published some research work in total deformation of loaded and unloaded concrete members subjected to fire [L60 and L101]. This model is a “Transient Constitutive Model”. From 1975 to 1983, Schneider developed a concrete model with respect to the creep during fire [L18, L102, L21 and L103]. In 1979, a model was developed which already considered the effects of transient creep and restraint [L18]. This model can be called “Analytic Transient Concrete Model”. 1978, the Eurocode model established with a modified stress-strain relationship according to the approach of Haksever [L104].

In the current version of Eurocode 2 the EC2-model is separated into three parts which are dependent on the peak stress strain of the stress-strain relationship (in the following this peak stress strain is called PSS). These three models can be called “EC2-Model with minimum peak strain stress”, “EC2-model with recommended peak strain stress” and “EC2-Model with maximum peak strain stress”. 1986, Khoury establish a concrete model which is called the “Load Induced Strain Model” using thermally induced strain [L105 and L106] which is a modification of the older models of [L60 and L18]. In the years 2008 to 2010, the “Advanced Transient Concrete Model” is developed by Schneider et. al.[L107].

In the following section, a short overview about some concrete models under high temperatures is given. Anderberg uses transient equations based on creep strain and a transient strain based on thermal strain using a constant temperature factor. Khoury, with transient equations based on LITS equation, adapted on measured data and Schneider with transient equation based on a creep based factor which is a function of temperature and induced separately plastic strain [L4]. All these models are dependent on temperature and load history. The ATC-model is an all inclusive model that calculates the transient reactions of structures by means of the irreversible and reversible behaviour of the material without considering a special factor for temperature. It is a most general material model for concrete. The work inside the thesis concentrates on siliceous concrete but it is indisputable that the material model of the ATC-model could also be used for other concrete materials, for instance, lightweight concrete, calcareous concrete and for siliceous concrete with other mix design and different aggregates and cements [L27].

The EC2-model works with a much simpler constitutive model based on stress-strain curves which are governed by peak stresses and strains for ultimate strain. Figure 5-4 shows the different peak stress strain values according to EC 2 [L108].

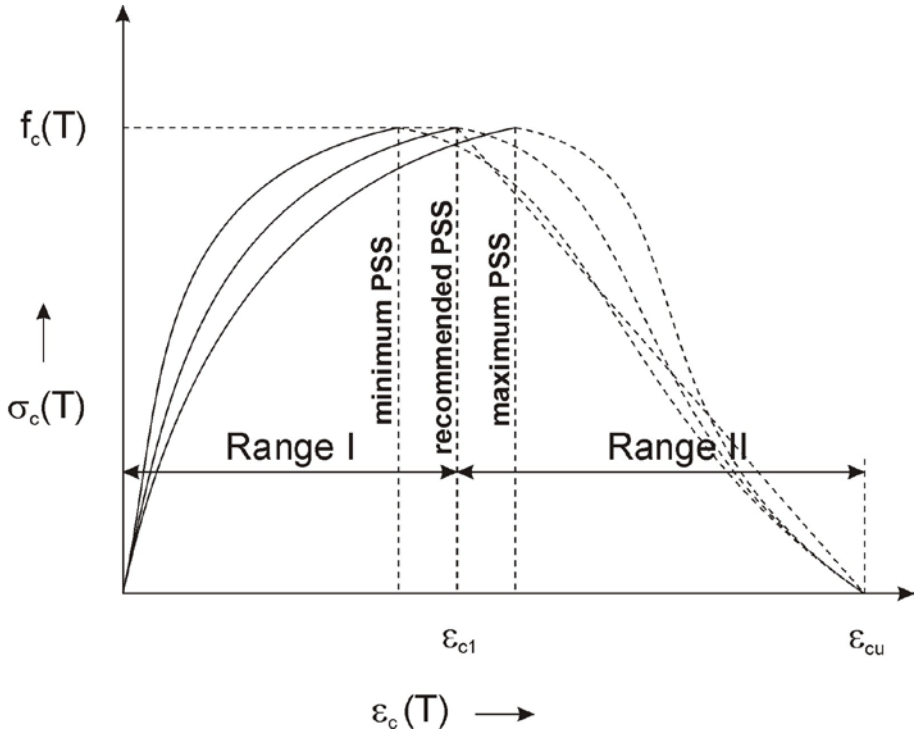

Fig. 5-4 - Stress strain relationship subjected to fire according to EC2 [L108]

For range I the following equation is given:

$$\sigma_c(T) = f_c(T) * \left[\frac{\varepsilon_c(T)}{\varepsilon_{c1}(T)} * \frac{3}{2 + \left(\frac{\varepsilon_c(T)}{\varepsilon_{c1}(T)} \right)^3} \right] \qquad \text{equ. (5.14)}$$

$f_c(T)$ and ε_{c1} are dependent on temperature according to the EC2.

The derivation of $\varepsilon_c(T)$ at $\varepsilon_c = 0$ is given by equ. (5.24 ff):

$$\left. \frac{d\sigma}{d\varepsilon_c} \right|_{\varepsilon_c = 0} = E_0(T) \qquad \text{equ. (5.15)}$$

The Young's modulus before loaded $E_0(T)$ is given in the following equation.

$$E_0(T) = 1{,}5 * \frac{f_c(T)}{\varepsilon_{c1}(T)} \qquad \text{equ. (5.16)}$$

Table 5-1 shows the parameter ε_{c1} according to the Eurocode 2. ε_{c1} is called ultimate strain or peak stress strain, and is noted in the following as peak stress strain (PSS). This parameter of

the equation mentioned above is mostly important for the calculation of structures under fire. The EC2 permits a range of minimum to maximum with a recommended value.

Tab. 5-1 - Parameters for the peak stress strain value according to EC2 [L108]

temperature [°C]	ε_{c1} (T) * 10^{-3}		ε_{cu} (T) * 10^{-3}
	range	recommended value	recommended value
20	2.5	2.5	20.0
100	2.5 – 4.0	3.5	22.5
200	3.0 – 5.5	4.5	25.0
300	4.0 – 7.0	6.0	27.5
400	4.5 – 10.0	7.5	30.0
500	5.5 – 15.0	9.5	32.5
600	6.5 – 25.0	12.5	35.0
700	7.5 – 25.0	14.0	37.5
800	8.5 – 25.0	14.5	40.0
900	10.0 – 25.0	15.0	42.5
1,000	10.0 – 25.0	15.0	45.0
1,100	10.0 – 25.0	15.0	47.5
1,200	-	-	-

The concrete behaviour shows different Young's modulus during heating, the larger the PSS the lower the Young's modulus is. The practical relationship according to measured data after equ. (5.15) is not shown in the Eurocode 2. Furthermore the stress-strain relationship in the Eurocode 2 is used for a normative temperature condition according to ISO 824 (ISO fire curve).

Constitutive models for high temperature calculations are available and are compared in several publications [L4, L109, L110]. Generally in these models, the transient strains are summarizes that the thermal strains and mechanical strains under the assumption that this approach covers all influences of creep, shrinkage, elastic and plastic strain under load. The basic creep is quickly activated during heating [L111]. With respect to the transient creep strains as a part of mechanical strain this is defined as transient thermal creep. The transient creep describes the fast reaction without the part of plastic strain but including a very small part of elastic strain. This is due to the fact that the elastic strain is a little influenced by the load history and the strain increments of this effect are hidden in the transient creep strain measurements as compared to hidden plastic strains which may occur in transient test with higher load levels.

The position of any point of the stress-strain curve for the transient strain path will change as soon as the temperature increases. The dynamic position will describe a family of stress strain curves with different loads [L71].

Figure 5-5 shows the evolution of the total strain for specimens under different constant loads during heating-up based on the calculation using the concrete model presented in this thesis. The high influence of load during transient heating-up can be seen. The elastic strain is very small at temperature T = 20°C compared to the high deformation at high temperatures. The concrete tested is specified as follows:

Cement CEM I 32.5 R	240 kg
Water	192 kg
Aggregates	Quartzite
Curing	Standard
Density (28d)	2,350 kg/m³
Test	560 d

and the following properties:

Compressive strength	30 N/mm²
Modulus of Elasticity	≈ 28,000 N/mm²

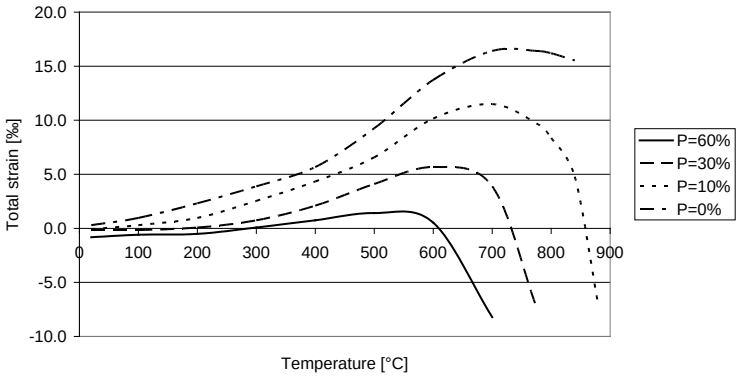

Fig. 5-5 - Total strain at high temperatures as a function of load history according to [L21]

In [L112] the following, general results are summarized:

- The dimensions of the axial force (load ratio α) and the type of aggregate are significant factors affecting fire resistance.
- When the dimension of the cross section of the structure is small and the temperature penetrates deeper in a short time period and the fire resistance is lower.
- When the load ratio increases the fire resistance also decreases and opposite. If carbonate aggregate concrete is used instead of siliceous aggregate concrete, the fire resistance is increased.

A good description of the effects in a constitutive model is given in [L113]. The thermal and hygral strain tensors leads to deviant effects in addition to the traditional thermal swelling and hygral shrinkage response of linear strain-stress-temperature-humidity relationships. That is why the simple calculation using a small curve as a constitutive model is not always correct. In this case, one parameter is not sufficient to be used as a constitutive model and the calculation is different from discrete calculations.

In accordance to different concretes we can summarize that in the case of constitutive curves high performance concrete (HPC) behave very similar to those derived from normal strength concrete at high temperature and it behaves only marginally worse during cooling down. HPC has higher temperature sensitivity. In the case of normal strength/high performance light-weight concrete the behaviour is better because of the lower thermal diffusivity of these materials [L114]. Fig. 5-6 and 5-7 show a comprehension of curves for stress-strain relationships for HPC with and without steel fibres as example.

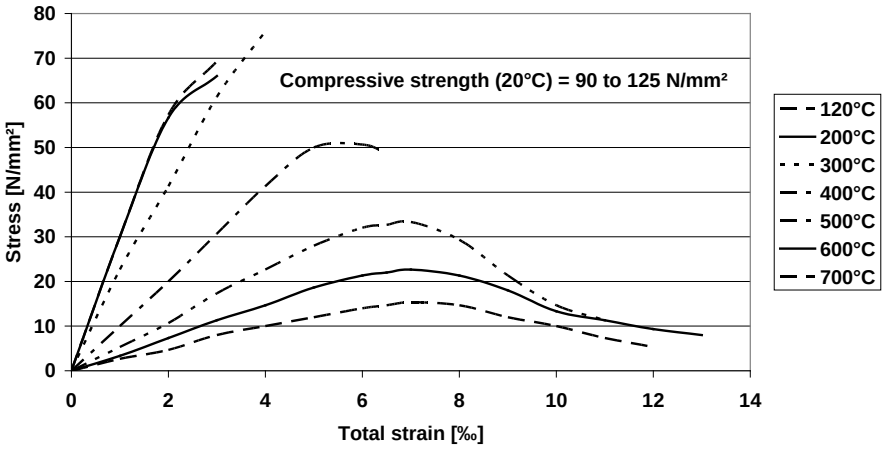

Fig. 5-6 - Stress-time relationship of high strength concrete with steel fibres according to [L115]

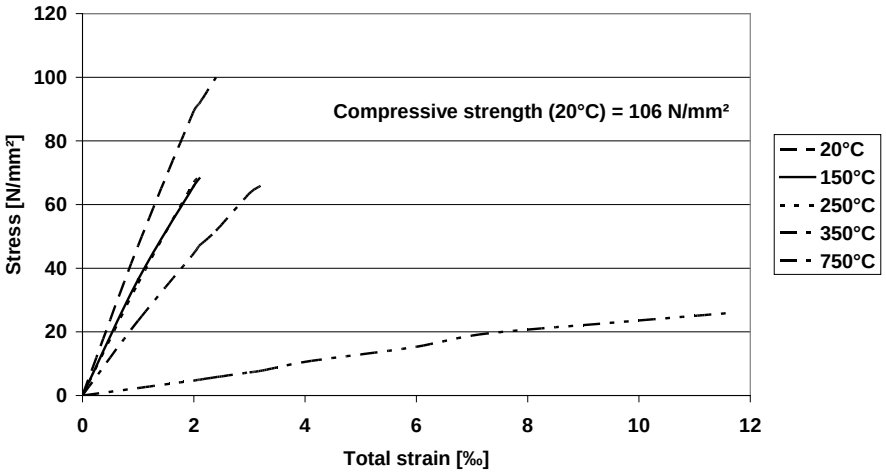

Fig. 5-7 - Stress-time relationship of high strength concrete with siliceous aggregates without steel fibres according to [L116]

In a concrete structure, thermal stresses usually change in a wide range during heating and cooling. A high compressive strength may be reduced and follow an ascending branch and finally it may turn into tensile stresses and cracking [L117].

Residual strains of loaded specimens were predicted from the sum of residual strains of the unloaded specimens, load induced transient creep strain, constant temperature creep and any expansion during cooling down [L118]. The principal sketch in Figure 5-8 shows this effect.

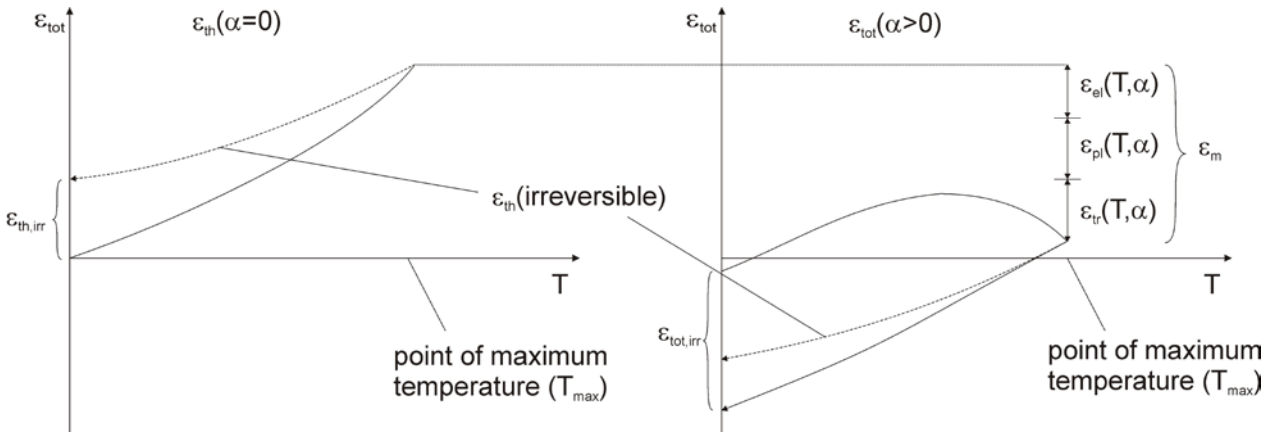

Fig. 5-8 - Residual strains of loaded specimens during heating and cooling down

The constitutive models, i.e. the EC2-model, does not consider the transient material behaviour at all, although the creep tests show significant differences between the steady state and the transient conditions [L119]. In simple calculation methods, the steady state condition is to be preferred. In finite element analysis, generally the steady state condition should not be used furthermore. The transient development of the deformation may be used in each time step and depends on temperature and, at most, the load during the time intervals of the calculation. The steady state of the load history before fire is started will be changed in the new ATC-model into a transient load history of the whole cross section.

In steady state tests the specimen are slowly heated to the desired temperature. At this temperature the load is applied. In a transient test the temperature increases according to a desired heating rate. The load is applied before heating.

5.3.2 Elastic and Plastic Strain

Two parts of the stress induced strains at high temperatures i.e. elastic and plastic strains are defined as follows:

$$\varepsilon_{el}(T,\alpha) = \frac{\sigma(t)}{E(T,\alpha)} \qquad \text{equ. (5.17)}$$

$$\varepsilon_{pl}(T,\alpha) = \kappa * \frac{\sigma(t)}{E(T,\alpha)} \qquad \text{equ. (5.18)}$$

The pure mechanical strain is a result from:

$$\varepsilon_s(\sigma(t)) = \varepsilon_{el}(T,\alpha) + \varepsilon_{pl}(T,\alpha) \qquad \text{equ. (5.19)}$$

$$\varepsilon_s(\sigma(t)) = \frac{\sigma(t)}{E(T,\alpha)} + \kappa * \frac{\sigma(t)}{E(T,\alpha)} \qquad \text{equ. (5.20)}$$

The function κ is determined according to the numerical approximation of the curve in Fig. 5-9.

For compression a stress-strain constitutive curve including the load history for ordinary concrete is given in Figure 5-9.

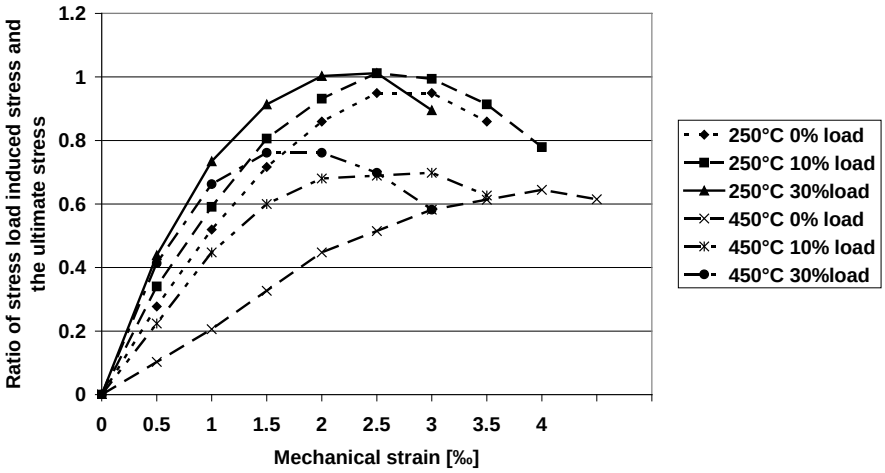

Fig. 5-9 - Stress-time relationship of ordinary concrete according to [L16]

Both strains can be included in a stress-strain relationship according to the following equations:

$$\sigma(t) = f_c(T,\alpha) * \frac{\varepsilon(\sigma(t))}{\varepsilon_u(T,\alpha)} * \frac{n}{(n-1)+\left(\frac{\varepsilon(\sigma(t))}{\varepsilon_u(T,\alpha)}\right)^n} \qquad \text{equ. (5.21)}$$

where: n=3 for ordinary concrete
n=2.5 lightweight aggregate concrete

The equation was originally proposed in [L18].

$$\sigma(t) = f_c(T,\alpha) * \frac{\varepsilon_s(T,\alpha)}{\varepsilon_u(T,\alpha)} * \frac{n}{(n-1)+\left(\frac{\varepsilon_s(T,\alpha)}{\varepsilon_u(T,\alpha)}\right)^n} \qquad \text{equ. (5.22)}$$

The derivation of this equation at $\varepsilon_u = 0$ determines the Young's modulus. The following derivations generally describe the calculation.

$$\left.\frac{d\sigma(t)}{d\varepsilon(\sigma(t))}\right|_{\varepsilon=0}^{\infty} \qquad \text{equ. (5.23)}$$

The first step is the separation of ε_u in the equation equ. (5.21) for $\sigma(t)$:

$$\sigma(t) = f_c(T,\alpha) * \frac{\varepsilon_s(T,\alpha)}{\varepsilon_u(T,\alpha)} * \frac{n}{n-1+\left(\frac{\varepsilon_s(T,\alpha)}{\varepsilon_u(T,\alpha)}\right)^n} \qquad \text{equ. (5.24a)}$$

$$\sigma(t) = \frac{n * f_c(T,\alpha) * \varepsilon_s(T,\alpha)}{\varepsilon_u(T,\alpha) * \left(n-1+\left(\frac{\varepsilon_s(T,\alpha)}{\varepsilon_u(T,\alpha)}\right)^n\right)} \qquad \text{equ. (5.24b)}$$

$$\sigma(t) = \frac{n * f_c(T,\alpha) * \varepsilon_s(T,\alpha)}{(n-1) * \varepsilon_u(T,\alpha) + \varepsilon_u(T,\alpha) * \frac{\varepsilon_s(T,\alpha)^n}{\varepsilon_u(T,\alpha)^n}} \qquad \text{equ. (5.24c)}$$

$$\sigma(t) = \frac{n * f_c(T,\alpha) * \varepsilon_s(T,\alpha)}{(n-1) * \varepsilon_u(T,\alpha) + \frac{\varepsilon_s(T,\alpha)^n}{\varepsilon_u(T,\alpha)^{n-1}}} \qquad \text{equ. (5.24d)}$$

The first derivation due to the quotient rule.

$$f'(\varepsilon_s(T,\alpha)) = \frac{v * u' - u * v'}{v^2} \qquad \text{equ. (5.24e)}$$

with:

$u = f(\varepsilon_s(T,\alpha))$ and
$v = f(\varepsilon_s(T,\alpha))$

where:

$$u = n * f_c(T,\alpha) * \varepsilon_s(T,\alpha)$$

$$v = (n-1) * \varepsilon_u(T,\alpha) + \frac{\varepsilon_s(T,\alpha)^n}{\varepsilon_u(T,\alpha)^{n-1}}$$

$$u' = n * f_c(T,\alpha)$$

$$v' = n\frac{\varepsilon_s(T,\alpha)^{n-1}}{\varepsilon_u(T,\alpha)^{n-1}}$$

From the derivations above, the calculation of Young's modulus may be derived as follows.

$$E(T,\alpha) = f'(\varepsilon_s(T,\alpha))$$

$$= \frac{\left((n-1)*\varepsilon_u(T,\alpha) + \frac{\varepsilon_s(T,\alpha)^n}{\varepsilon_u(T,\alpha)^{n-1}}\right) * n * f_c(T,\alpha) - n * f_c(T,\alpha) * \varepsilon_s(T,\alpha) * n \frac{\varepsilon_s(T,\alpha)^{n-1}}{\varepsilon_u(T,\alpha)^{n-1}}}{\left((n-1)*\varepsilon_u(T,\alpha) + \frac{\varepsilon_s(T,\alpha)^n}{\varepsilon_u(T,\alpha)^{n-1}}\right)^2} \quad \text{equ. (5.25)}$$

For $\alpha = 0$ is $\varepsilon_s(T,\alpha) = 0$.

$$E(T) = f'(\varepsilon_s(T)) = \frac{\left((n-1)*\varepsilon_u(T,\alpha) + \frac{0^n}{\varepsilon_u(T)^{n-1}}\right) * n * f_c(T) - n * f_c(T) * 0 * n \frac{0^{n-1}}{\varepsilon_u(T)^{n-1}}}{\left((n-1)*\varepsilon_u(T) + \frac{0^n}{\varepsilon_u(T)^{n-1}}\right)^2} \quad \text{equ. (5.26)}$$

$$E(T) = \frac{n * f_c(T)}{(n-1)*\varepsilon_u(T)} \quad \text{equ. (5.27)}$$

For $\varepsilon_s(T,\alpha) = 0$ is the following equation usable.

$$E(T,\alpha) = \frac{n * f_c(T,\alpha)}{(n-1)*\varepsilon_u(T,\alpha)} \quad \text{equ. (5.28)}$$

Figure 5-10 shows the relation of the plastic part and elastic part of the total mechanical strain.

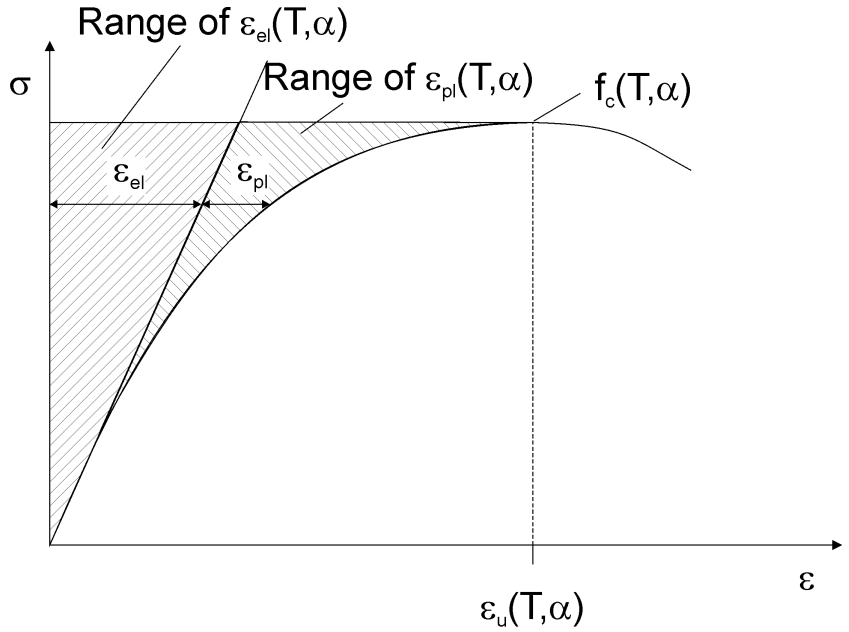

Fig. 5-10 - Range of elastic and plastic strain of a stress-strain relationship with or without a load history [L18]

The nonlinear plastic deformation starts after the linear elastic behaviour of Young's modulus and increases until the point of ultimate strain. The elastic part of mechanical strain always exists as a linear function.

5.3.3 Load Induced Transient Creep Strain

As the concrete under heating-up suffers an accelerated drying process and the observed creep deformation in [L18] were mainly attributed to a drying creep phenomenon similar to experiences known from ambient temperatures. During an isothermal creep test the following types of deformation occur, see Figure 5-11.

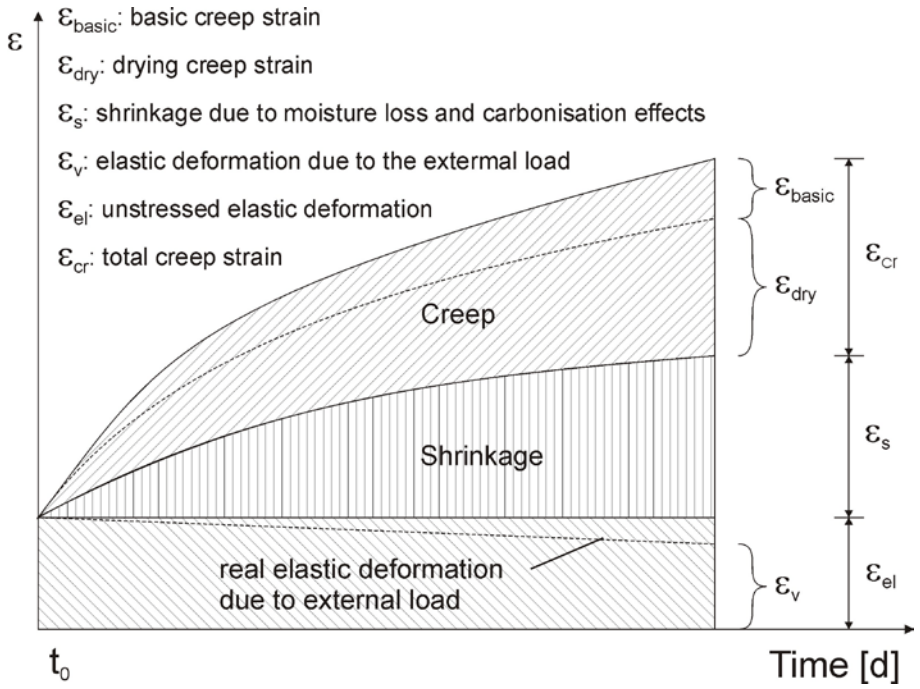

Fig. 5-11 - Deformations of concrete at ambient temperatures subjected to a constant compressive load according to [L15]

This mechanically induced deformation occurs also in cases of fire. According to [L15], in this case the term ε_m is called „load inducted thermal strain“. It consists of transient creep (transitional thermal creep and drying creep), basic creep and elastic strains. In the case of high temperatures the transient creep strains comprise the largest part of the strain.

Basically the total deformation included creep at ambient temperature based on the following equation:

$$\varepsilon_k = \frac{\sigma}{E}(1+\varphi) \qquad \text{equ. (5.29)}$$

Derived from equation (5.29) the creep strain at 20°C is generally defined as:

$$\varepsilon_{cr} = \frac{\varphi * \sigma(t)}{E} \qquad \text{equ. (5.30)}$$

The load induced transient strain due to creep reactions is relatively independent compared to dependence of Young's modulus on load history [L18] and the term $\varepsilon_{tr,cr}$ is defined as transient creep in literature [L18 and L122]. The following equation was derived from equ. (5.30) by introducing a temperature dependent Young's modulus.

$$\varepsilon_{tr,cr} = \frac{\varphi * \sigma(t)}{E(T)} \qquad \text{equ. (5.31)}$$

The φ-function for "transient creep" according to [L120 and L18] is calculated in the next equation. It utilizes new parameters as shown in Table 5-2 which were obtained by older [L18] and recent scientific results [L121, L48] and is based on the ongoing research.

$$\varphi = C_1 * \tanh \gamma_w * (T - 20) + C_2 * \tanh \gamma_0 * (T - T_g) + C_3 \qquad \text{equ. (5.32)}$$

Tab. 5-2 - Parameters for transient creep functions of structural concretes according to [L52]

Parameter	Dimension	Quarzit concrete	Limestone concrete	Lightweight concrete
C_1	1	2.50	2.50	2.50
C_2	1	0.70	1.40	3.00
C_3	1	0.70	1.40	2.90
γ_0	$°C^{-1}$	$7.5*10^{-3}$	$7.5*10^{-3}$	$7.5*10^{-3}$
T_g	°C	800	700	600

The moisture content of concrete is taken into account using equation (5.33).

$$\gamma_w = 0.3*10^{-3} * w^{0.5} + 2.2*10^{-3} \qquad \text{equ. (5.33)}$$

$\gamma_w \leq 2.8*10^{-3}$ is chosen for OPC with a moisture content w in % by weight whereby 1% < w < 4.5% [L52].

As the concrete under heating-up suffers an accelerated drying process the observed creep deformation in [L18] were mainly attributed to a drying creep phenomena similar to experiments known from ambient temperatures.

Actually the term comprises elastic, plastic and (pure) transient creep strains as shown below and were published in [L61]. Figure 5-12 shows the phi-function of concretes with different aggregates.

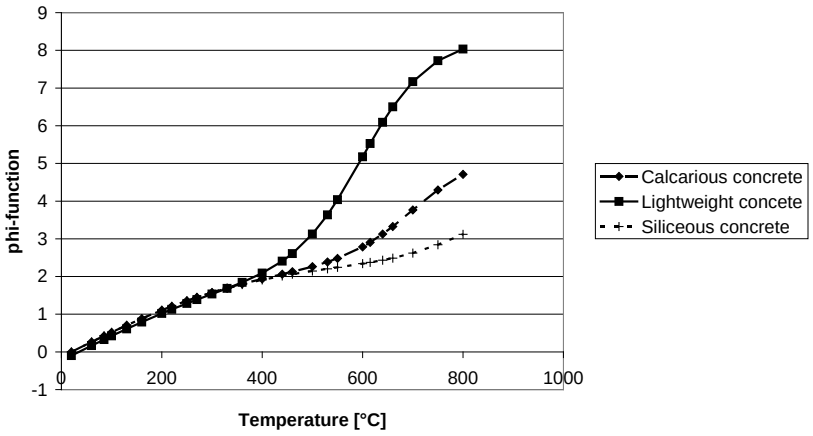

Fig. 5-12 - Transient creep function for concretes with different aggregates according to [L18]

5.4 Basic View

It is generally agreed that the total strain ε_{tot} comprises the following parts [L120]:

$$\varepsilon_{tot} = \varepsilon_{el} + \varepsilon_{pl} + \varepsilon_{tr} + \varepsilon_{th} \qquad \text{equ. (5.34)}$$

Where ε_{tot} total strain, ε_{el} elastic strain, ε_{pl} plastic strain, ε_{tr} total transient creep strain and ε_{th} thermal expansion.

It is therefore possible to derive the pure mechanical strain as follows ε_m:

$$\varepsilon_m = \varepsilon_{el} + \varepsilon_{pl} + \varepsilon_{tr} = \varepsilon_{tot} - \varepsilon_{th} \qquad \text{equ. (5.35)}$$

where ε_m is the total mechanical strain.

The temperature is referred as T and the maximum observed temperature as T_{max} at any time.

5.5 Thermal Strain

Figure 5-13 shows the thermal strains of concrete with different siliceous aggregates according to the Eurocode 2 and measured data of concrete with high siliceous content.

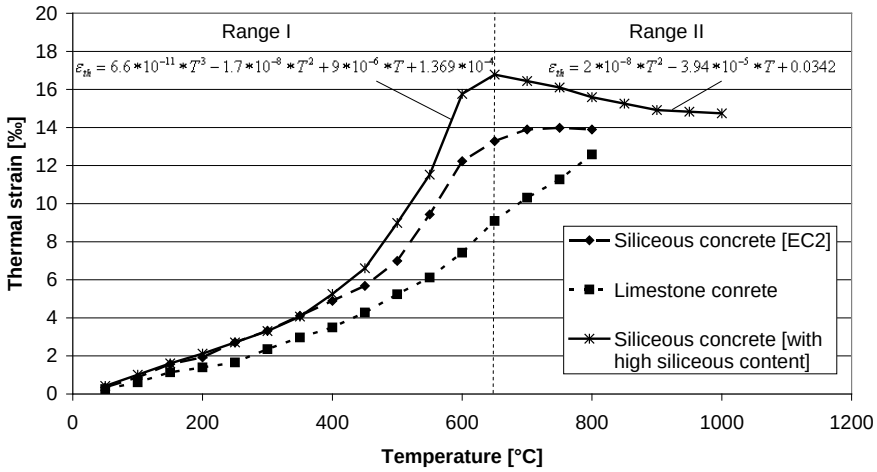

Fig. 5-13 - Thermal strain of concrete with siliceous aggregates compared to calcareous concrete according to [L21]

According to Figure 5-12, the line of siliceous concrete with a high siliceous content is calculated according to a regression function as follows:

For T ≤ 650°C equation (5.36) is valid:

$$\varepsilon_{th} = 6.6*10^{-11}*T^3 - 1.7*10^{-8}*T^2 + 9*10^{-6}*T + 1.369*10^{-4} \qquad \text{equ. (5.36)}$$

For T > 650°C equation (5.37) is valid:

$$\varepsilon_{th} = 2*10^{-8}*T^2 - 3.94*10^{-5}*T + 0.0342 \qquad \text{equ. (5.37)}$$

It should be mentioned that thermal strain of concrete is mainly determined by the type of aggregate used, i.e. in general the equations (5.36) and (5.37) do not represent the behaviour of ordinary concrete which is practically used in the Eurocode 2.

5.6 Calculation of Mechanical Strain under High Transient Temperatures

5.6.1 Compressive Strength

Figure 5-14 shows the reduction of compressive strength of concrete as a function of temperature for different load histories compared to measurements [L21]. $f_c(20°C)$ is an experimental result for ordinary concrete tested and cured under RILEM conditions [L120].

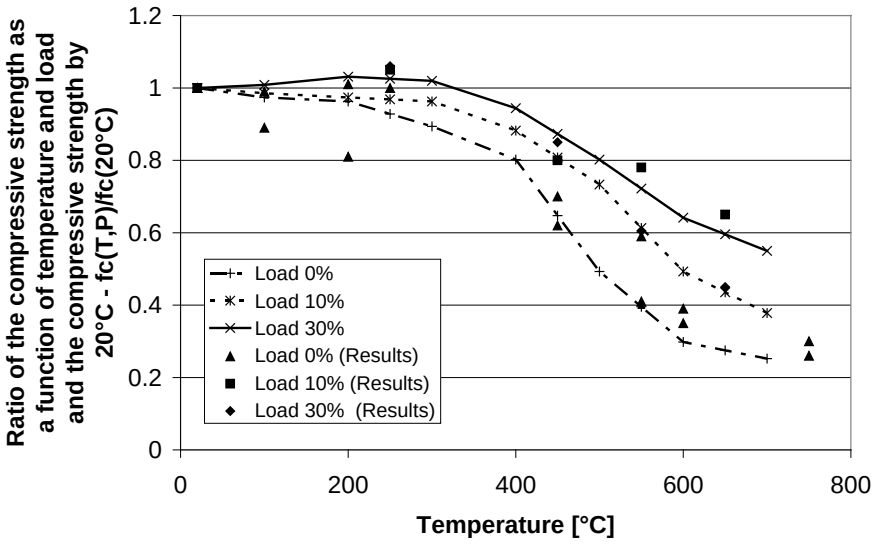

Fig. 5-14 - High temperature compressive strength of siliceous concrete being loaded or not loaded during heating-up – experimental and calculated results according to [L21]

The following equations according to Figure 5-14 are based on experimental results. Without load history the behaviour of compressive strength as a function of temperature is given according to [L15].

For T ≤ 250°C, the following is given:

$$f_c(T,\alpha=0) = f_c(20°C) \qquad \text{equ. (5.38)}$$

For 250°C <T ≤ 750°C, the following is given:

$$f_c(T,\alpha=0) = f_c(20°C) * [1 - 0.0018 * (T - 250)] \qquad \text{equ. (5.39)}$$

For 750°C< T ≤ 1,000°C, the following is given:

$$f_c(T,\alpha=0) = f_c(20°C) * [0.1 - 0.0004 * (T - 750)] \qquad \text{equ. (5.40)}$$

For 1100°C > T, the following is given whereby a linear decreasing from 1,000°C is assumed:

$$f_c(T,\alpha=0) = 0 \qquad \text{equ. (5.41)}$$

With load history the compressive strength is calculated as follows:

For T ≤ 750°C, the following is given:

$$f_c(T,\alpha=0.1) = f_c(20°C) * [-2 * 10^{-6} * T^2 + 4.7 * 10^{-4} * T + 0.977] \qquad \text{equ. (5.42)}$$

$$f_c(T,\alpha=0.3) = f_c(20°C) * \left[-2*10^{-6}*T^2 + 6.8*10^{-4}*T + 0.9875\right] \quad \text{equ. (5.43)}$$

For 750°C< T ≤ 1,000°C, the following is essential:

$$f_c(T,\alpha=0.1) = f_c(20°C) * \left[0.25 - 0.001*(T-750)\right] \quad \text{equ. (5.44)}$$

$$f_c(T,\alpha=0.3) = f_c(20°C) * \left[0.38 - 0.00152*(T-750)\right] \quad \text{equ. (5.45)}$$

For 1100°C > T, the following is essential whereby a linear decreasing from 1,000°C is assumed:

$$f_c(T,\alpha=0.1) = 0 \quad \text{equ. (5.46)}$$

$$f_c(T,\alpha=0.3) = 0 \quad \text{equ. (5.47)}$$

For values in between two given values an interpolation is allowed.

5.6.2 Young's Modulus and Elastic Strain

The Young's modulus as a function of load history and temperature $E(T,\alpha)$ should be measured according to RILEM [L122] or National Codes with respect to the geometry of specimens being used in the high temperature range. See Figure 5-15.

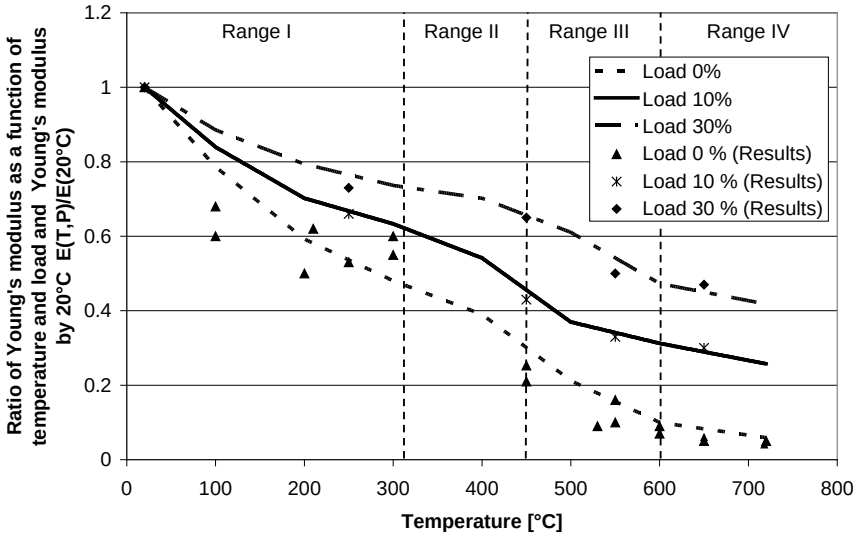

Fig. 5-15 - Influence of high temperature on the Young's modulus of siliceous concrete - experimental and calculated results according to [L21]

The following equation can be used with $\alpha = 0$, $\alpha = 0.1$ and $\alpha = 0.3$ to calculate the Young's modulus at high temperature, based on measurements of $E(T,\alpha)$ according to Figure 5-15 [L61].

Range I (T ≤ 320°C):

$$E(T,\alpha=0) = E(20°C) * \left[100 - 3*10^{-3} * (T-20) + 4.085*10^{-6} * (T-20)^2\right] \quad \text{equ. (5.48)}$$

$$E(T,\alpha=0.1) = E(20°C) * \left[3*10^{-6} * T^2 - 2.311*10^{-3} * T + 1.04505\right] \quad \text{equ. (5.49)}$$

$$E(T,\alpha=0.3) = E(20°C) * \left[2*10^{-6} * T^2 - 1.57*10^{-3} * T + 1.0306\right] \quad \text{equ. (5.50)}$$

Range II (320°C <T ≤ 450°C):

$$E(T,\alpha=0) = E(20°C) * \begin{bmatrix} 0.89406 - 3.2445*10^{-3} * T + 1.0081*10^{-5} \\ -1.2801*10^{-8} * T^3 \end{bmatrix} \quad \text{equ. (5.51)}$$

$$E(T,\alpha=0.1) = E(20°C) * \left[-5.1*10^{-6} * T^2 + 2.73*10^{-3} * T + 0.262\right] \quad \text{equ. (5.52)}$$

$$E(T,\alpha=0.3) = E(20°C) * \left[-4*10^{-6} * T^2 + 2.5*10^{-3} * T + 0.342\right] \quad \text{equ. (5.53)}$$

Range III (450°C <T ≤ 600°C):

$$E(T,\alpha=0) = E(20°C) * \left[0.45 * e^{-7.52*10^{-3}*(T-400)}\right] \quad \text{equ. (5.54)}$$

$$E(T,\alpha=0.1) = E(20°C) * \left[-6*10^{-8} * T^3 + 1*10^{-4} * T^2 - 0.056 * T + 10.874\right] \quad \text{equ. (5.55)}$$

$$E(T,\alpha=0.3) = E(20°C) * \left[1.767 * e^{-0.0022*T}\right] \quad \text{equ. (5.56)}$$

Range IV (T > 600°C):

$$E(T,\alpha=0) = E(20°C) * \left[e^{-4*10^{-3}*(T-20)}\right] \quad \text{equ. (5.57)}$$

$$E(T,\alpha=0.1) = E(20°C) * \left[0.82554 * e^{-0.0016*T}\right] \quad \text{equ. (5.58)}$$

$$E(T,\alpha=0.3) = E(20°C) * \left[0.86 * e^{-0.001*T}\right] \quad \text{equ. (5.59)}$$

For 1100°C > T, the following is essential whereby a linear decreasing from 1,000°C is assumed, according to the compressive strength:

$$E(T,\alpha) = 0 \quad \text{equ. (5.60)}$$

The reference concrete data are given below:

Mix:	quartzite concrete
Curing:	standard curing
Compressive strength after 28 d:	58.6 N/mm²
Compressive strength after 1,176 d:	53.0 N/mm²
Modulus of elasticity after 1,176 d:	23,000 N/mm²

The elastic behaviour due to the Young's modulus is represented by the elastic strains. The temperature and load dependent elastic strain is:

$$\varepsilon_{el}(T,\alpha) = \frac{\sigma(t)}{E(T,\alpha)} \qquad \text{equ. (5.61)}$$

Where $\sigma(t)$ is the stress at time *t* and $E(T,\alpha)$ is Young's modulus as a function of load history and temperature, according to equation (5.48) to (5.60).

In the measured mechanical data, there are the elastic parts of the deformation, the plastic part and the transient creep part included. A stress rate controlled test leads to a constitutive curve, a stress-strain relationship and a total deformation test leads to transient creep strains, plastic strains and elastic strains. Fig. 5-16 shows the influence of load to the constitutive behaviour of ordinary siliceous concrete, according to [L15].

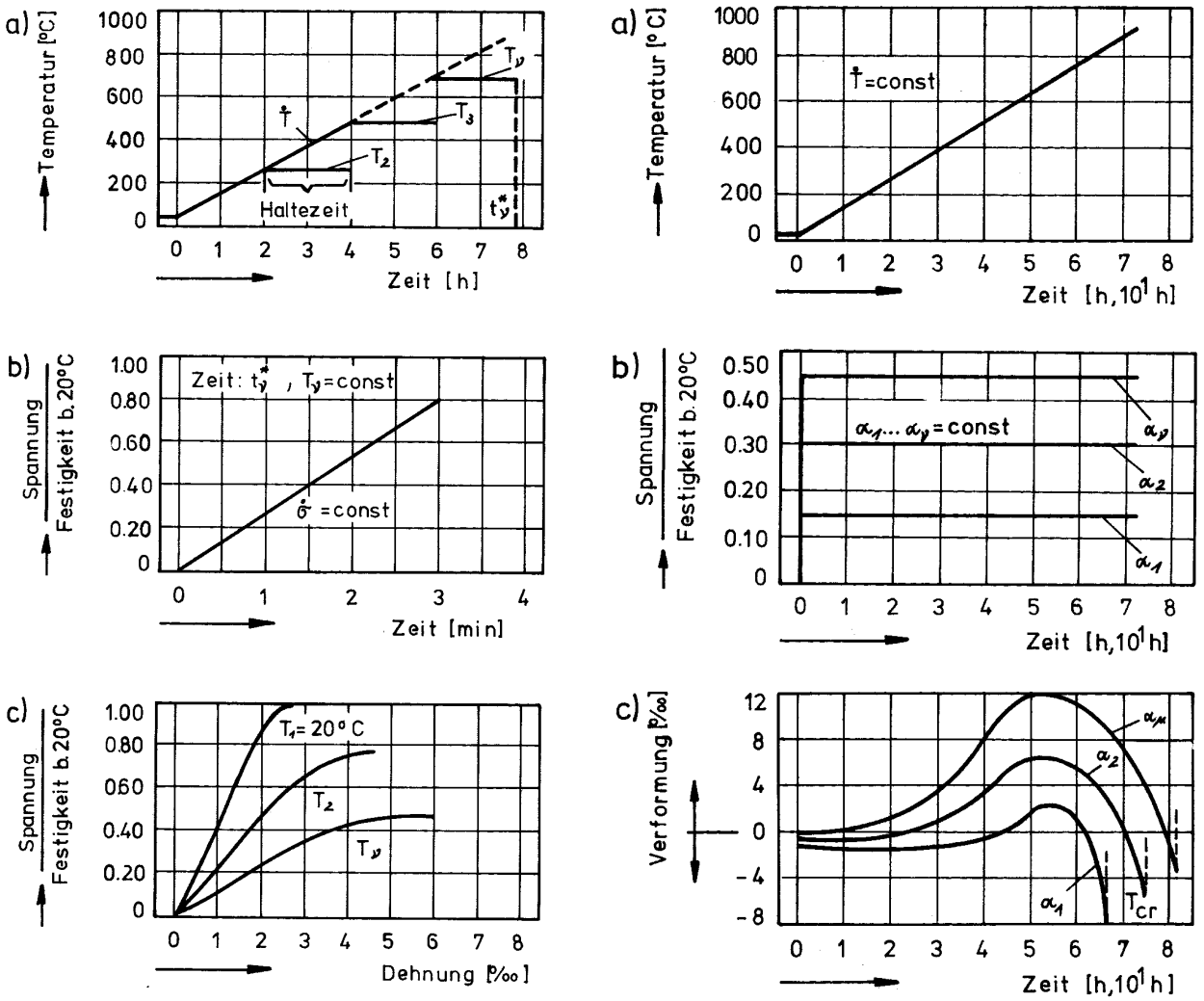

Steady state stress rate controlled test

Nonsteady transient creep test

Fig. 5-16 - Stress-strain relationship taken from RILEM [L15]

In Fig. 5-17 the influence of the transient heating to the ultimate strain is given. The concrete is defined by the following mix, material and test parameters:

Cement CEM I 32.5 R	240 kg
Water	192 kg
Aggregates	Quartzite

and the following properties:

Compressive strength	27 N/mm²
Density	2350 kg/m³

Test conditions:

Heating rate	2 K/min
Constant temperature time	2 h
Load increase	30 s

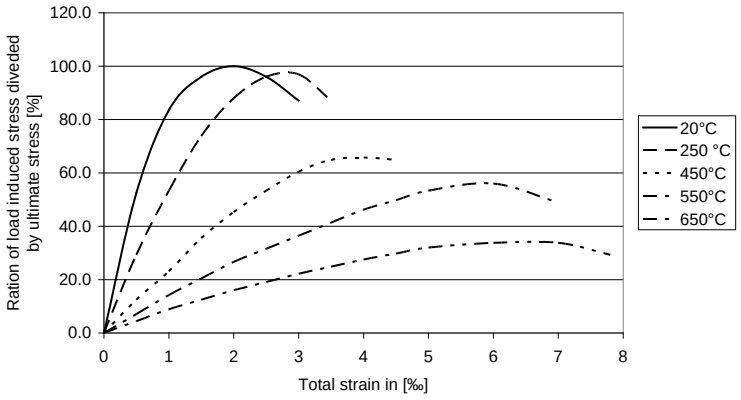

Fig. 5-17 - Stress-time relationship of normal concrete under different temperatures according to [L15]

The ultimate strain is the point of the stress-strain relationship where the stress due to the external load reaches the compressive strength. That point depends on load history and temperature, seen in Fig. 5-16 and Fig. 5-17. At the temperature of 20°C the ultimate strain is 2 ‰. The value is the calculation assumption for the general arithmetic procedure during establishing the load bearing capacity, according to the Eurocode 2 Part 1-1 [L108].

5.6.3 Ultimate Strain for Siliceous Concrete

The material behaviour of a siliceous concrete is a function of $f(\alpha)$, $\Delta\varepsilon_u(T)$ and $\varepsilon_u(T = 20°C)$ [L123].

$\varepsilon_u(T,\alpha)$ is calculated as follows:

$$\varepsilon_u(T,\alpha) = \varepsilon_u(20°C) + \Delta\varepsilon_u(T) * f(\alpha) \qquad \text{equ. (5.62)}$$

This equation is for $20°C \le T \le 700°C$ (temperature above this boundary can be extrapolated)

with $\varepsilon_u(T,\alpha) \le 7.8 * 10^{-3}$ as an upper limit for all cases (α=0).

where:

$$\varepsilon_u(20°C) = 2.2 * 10^{-3} \text{ and} \qquad \text{equ. (5.63)}$$

$$\Delta\varepsilon_u(T) = (T - 20) * \left[4.2 * 10^{-6} + (T - 20) * 5.4 * 10^{-9}\right]. \qquad \text{equ. (5.64)}$$

$f(\alpha)$ is a function of load history. A linear interpolation is applied for a given value of the load factor α:

$f(\alpha) = 1$ (α = 0),
$f(\alpha) = 0.227$ (α = 0.1),
$f(\alpha) = 0.066$ (α = 0.2),
$f(\alpha) = -0.095$ ($\alpha \geq 0.3$)

5.6.4 Plastic Strain

The plastic strains are derived from the measured stress-strain relationship. The plastic strains are defined as:

$$\varepsilon_{pl}(T,\alpha) = \varepsilon\{\sigma(t), \varepsilon_u(T,\alpha), T, \alpha\} - \varepsilon_{el}\{\sigma(t), T, \alpha\} \qquad \text{equ. (5.65)}$$

The plastic strain is also calculated using a shorter notation as follows:

$$\varepsilon_{pl}(T,\alpha) = \varepsilon\{\sigma(t), \varepsilon_u(T,\alpha), T\} - \varepsilon_{el}\{\sigma(t), T, \alpha\} \qquad \text{equ. (5.66)}$$

Whereby $\varepsilon_{pl} \equiv 0$ if $\varepsilon_{el} > \varepsilon_{pl}$ after Equation (5.65) and (5.66).

A numerical approximation for the ascending branch of the stress-strain relationship is:

$$\varepsilon_{pl}(T,\alpha) = \kappa * \frac{\sigma(T)}{E(T,\alpha)} \qquad \text{equ. (5.67)}$$

The function κ given in [L121] is as follows:

$$\kappa = \frac{1}{2} * \left[1 - \sqrt{1 - \left(\frac{\sigma(T)}{f_c(T,\alpha)}\right)^4}\right] \qquad \text{equ. (5.68)}$$

Whereby the following parameters are used:

α: load factor,
ε_u: ultimate strain according to equ (5-68),
T: temperature in °C and
f_c: compressive strength at 20 °C in N/mm².

5.6.5 Total Mechanical Strain

The total strain after chapter 5.4 minus thermal strain is given in the following equation:

$$\varepsilon_m = \varepsilon_{el} + \varepsilon_{pl} + \varepsilon_{tr} = \varepsilon_{tot} - \varepsilon_{th} \qquad \text{equ. (5.69)}$$

$$\varepsilon_m(T) = \frac{\sigma(t)}{E(T)} * (1 + \varphi) \qquad \text{equ. (5.70)}$$

The transient creep strain after equ. (5-70) turned out to be slightly dependent on load history [L18] and the same holds for the term $\varepsilon_{tr,cr} = \frac{\varphi * \sigma(t)}{E(T)}$ defined as transient creep in the literature [L122]. Actually the term comprises elastic, plastic and (pure) transient creep strains as shown below [L61]. The elastic strain is calculated according to the following equation:

$$\varepsilon_{el}(T, \alpha) = \varepsilon_{el}(T) - \Delta\varepsilon_{el}(T, \alpha) \qquad \text{equ. (5.71)}$$

The φ-function for “transient creep” strain according to [L120 and L18] is calculated according to the equation 5.16 mentioned above, i.e. the term $\Delta\varepsilon_{el}(T, \alpha)$ was neglected. This is true if the modulus of elasticity does not depend on the load history.

In Chapter 5.3.3 Fig. 5-11 shows the φ-function for siliceous concrete. The equation (5.16) is similar to the equation for creep strain at ambient temperatures. That is why the φ-function is called „transient creep function“ in RILEM literature [L120], although it was known that φ contains additional small parts of plastic and elastic strains [L18].

The same effect therefore, was also called “thermal induced strain“ according to [L106], whereby in [L106] plastic strains are not included in the mechanical material equation. The pure transient creep will not be calculated numerically within the proposed calculation procedure described below but the exact relationship is given in equation (5.71) and extended to the final relationship equation (5.72).

Fig. 5-18 shows the φ-function for siliceous concrete at transient temperatures.

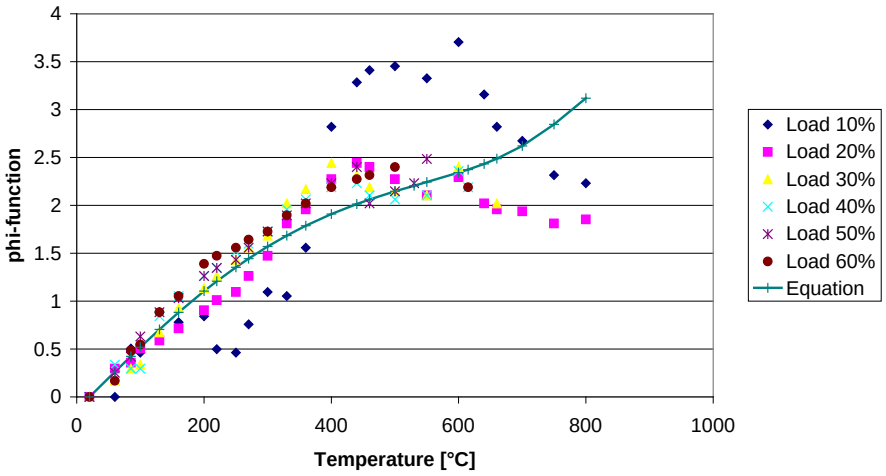

Fig. 5-18 - Transient creep function for siliceous concrete according to [L52]

It is seen that the transient creep function (φ-function) is relatively independent from load until 400 °C. In the range higher than 400 °C a greater influence of load history is observed. That is why an asymptomatic assumption is chosen. According to Fig. 5-18 a maximum value of φ = 3.5 can be assumed for the phi-function at 900°C.

After calculation of plastic strains and elastic strains the pure transient creep strain should be calculated as follows:

$$\varepsilon_{tr}(T,\alpha) = \varepsilon_{m}(T) - \varepsilon_{el}(T,\alpha) - \varepsilon_{pl}(T,\alpha) \qquad \text{equ. (5.72)}$$

Fig. 5-19 shows the results of different calculations according to equ. (5.72) with respect to equ. (5.48) to equ. (5.60).

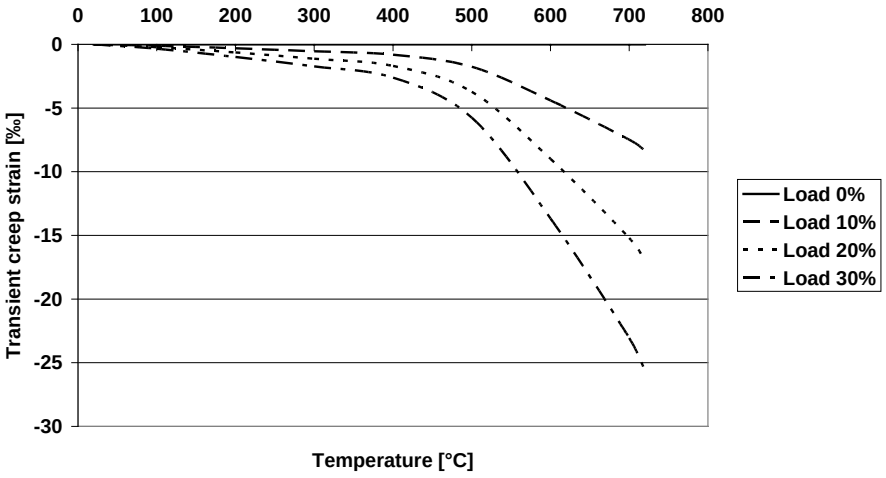

Fig. 5-19 - Transient strain due to thermal creep

According to ambient temperatures the creep strain is higher when the load increases. Above temperatures of 500°C the transient creep strain increases rapidly up to a maximum value of 25 ‰. Note that the load history is considered as steady state during the transient heating. It is obvious that the material is completely destroyed before making this value.

5.7 Determination of Strain Components of Concrete in Compression at High Temperatures under Transient Temperatures

5.7.1 Thermal Strain during Heating and Cooling

The thermal strain increases in any case by heating-up to 650°C. Above that point thermal strain slightly decreases and gradually fashion until the final strain 14.8 ‰ is reached at a temperature of 1,000°C. At each time step there is a final strain according to the reached temperature $T_{\max}$. It is essential to define the maximum thermal strain during heating and cooling according to real measurements:

$$\varepsilon_{th}{}^{n} = \varepsilon_{th}\left(T_{\max}\right) \qquad \text{equ. (5.73)}$$

Suffix n is for every time step.

The behaviour of concrete in the phase of cooling down depends only slightly on load history. Figure 5-20 shows the total strain for siliceous concrete. The cooling strain curve of loaded specimen closely follow the same function if the start point is shifted to zero at 600°C.

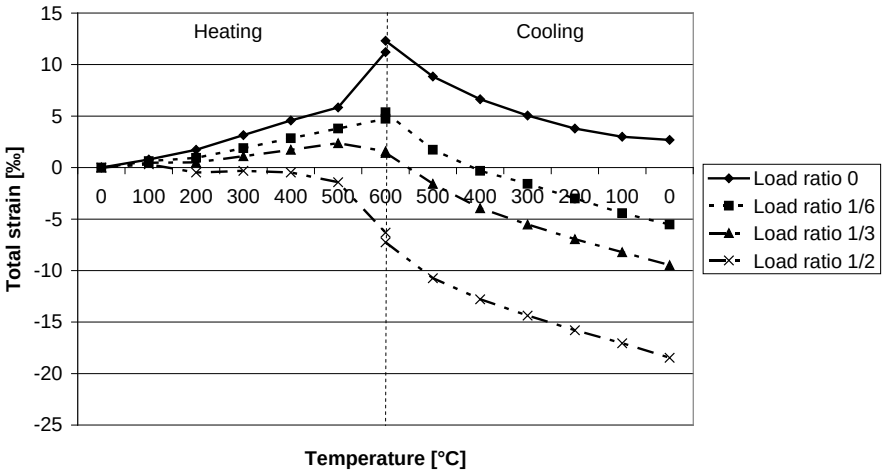

Fig. 5-20 - Total deformation of siliceous concrete under constant load during a complete heating-cooling-cycle according to [L60]

Data were obtained for the heating/cooling rates between 0.5 to 10 K/min [L101]. The residual strain according to lines in Figure 5-20 in the range 600°C ≤ T_{max} ≤ 20 °C, as follows:

For α = 0 the total strain is identical thermal strain $\varepsilon_{th}{}^{cool}\left(T, T_{\max} = 600°C\right)$ according to Fig. 5-20:

$$\varepsilon_{th}{}^{cool}\left(T, T_{\max} = 600°C\right) = \varepsilon_{th}\left(600°C\right) - \Delta\varepsilon_{th,T_{\max}=600°C} \qquad \text{equ. (5.74)}$$

whereby according to Fig. 5-19, 5-20 and 5-21:

$$\Delta\varepsilon_{th,T_{\max}=600°C} = 1.32 * 10^{-2} - 1.445 * 10^{-3} * e^{3.4*10^{-3}*T(n)} \qquad \text{equ. (5.75)}$$

with $T(n)$ as temperature at each time step n and $\Delta\varepsilon_{th,T_{\max}=600°C}$ as decreasing function of the gradient during cooling.

The following equations are also affected by cracks during heating-up to a maximum temperature in the range 600°C ≤ T_{max} ≤ 20 °C that is why it presents an empirical behaviour of concrete during cooling down.

For $\alpha > 0$ the total strain $\varepsilon_{tot}{}^{cool}\left(T, T_{\max} = 600°C, \alpha\right)$ is according to Fig. 5-20:

$$\varepsilon_{tot}{}^{cool}\left(T, T_{\max} = 600°C, \alpha\right) = \varepsilon_{tot}\left(600°C, \alpha\right) - \Delta\varepsilon_{\alpha,T_{\max}=600°C} \qquad \text{equ. (5.76)}$$

whereby according to Fig. 5-20:

$$\Delta\varepsilon_{\alpha,T_{\max}=600°C} = 1.2 * 10^{-2} - \left[1.9 * 10^{-8} * T(n)^2 + 8 * 10^{-6} * T(n) + 3.2 * 10^{-4}\right] \qquad \text{equ. (5.77)}$$

With $T(n)$ as temperature at each time step n and $\Delta\varepsilon_{\alpha,T_{\max}=600°C}$ as decreasing function of the gradient during cooling.

Astonishingly, the function $\varepsilon_{tot}{}^{cool}\left(T, T_{\max} = 600°C, \alpha\right)$ is nearly identical in all load factors.

Thermal strain of ordinary concrete is normally irreversible. Figure 5-21 shows the residual strains of concretes after heating-up to different temperatures and immediate cooling thereafter. This behaviour could be estimated as irreversible like plastic deformations.

That is because during heating-up to the maximum temperature, a three dimensional crack system develops. These cracks do not close completely during cooling down which leads to residual thermal strains during cooling [L21]. It is important to take the residual thermal crack strains into account if the residual load bearing capacity of concrete structures after a fire should be determined.

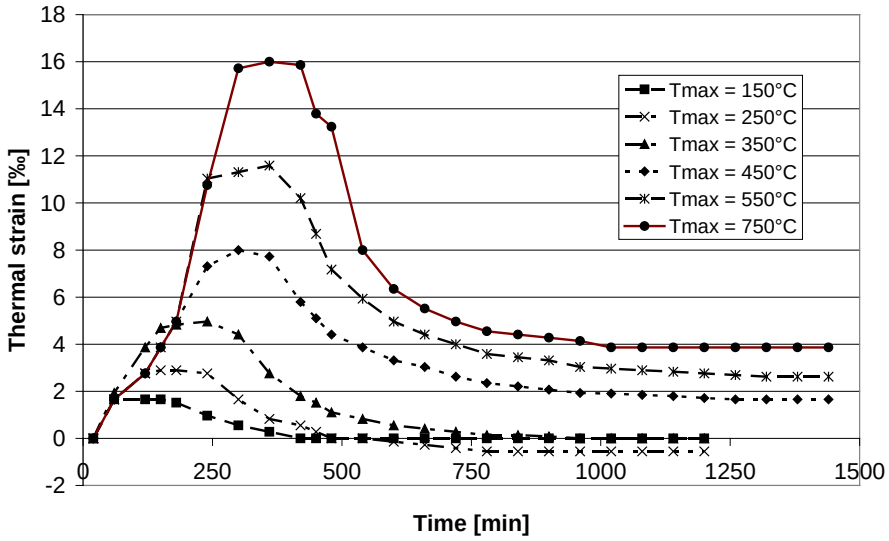

Fig. 5-21 – Thermal strain after heating and cooling for siliceous concrete (cooling rate: 2K/min) according to [L124]

The thermal strain after cooling is different related to the maximum temperature. During temperatures of up to 350°C the thermal strain is near the original value, the thermal strain above 350°C after cooling is clearly higher than the original. The curve should be considered in a concrete model, but the influences of mechanical strain are not clearly definable. That is why the concrete model works with total deformation during cooling.

It is to assume that the behaviour of concrete during cooling depends on load history and the maximum temperature. Fig. 5-22 shows some test results of a heating-cooling relationship of concretes at different heating and load conditions.

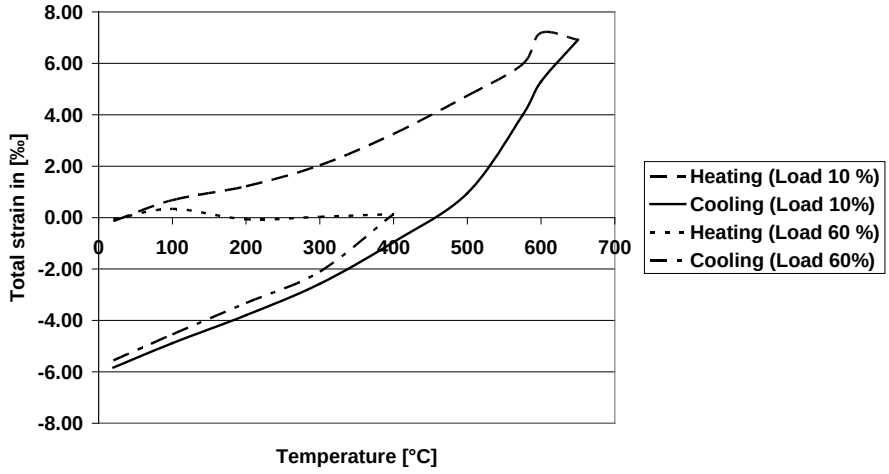

Fig. 5-22 - Irreversible deformation during cooling down at different conditions according to [56]

The following step is necessary to describe the irreversible deformations during cooling down. For the pure thermal strain, i.e. the case where the load equals 0, the description is very easy.

Fig. 5-21 shows a time dependent behaviour with a cooling rate of 2 K/min. All cooling curves are exponential functions below the thermal strain at maximum temperature. The curvature is nearly identical to the original temperature. The approach of thermal strain during cooling after equ. (5.77) can be transferred one by one. A small variation exists at temperatures of more than 600°C, but the character of the exponential function leads is very usable data for this case.

For general cooling at different temperatures the following equations for the thermal strain $\varepsilon_{th}^{\ cool}(T)$ are given:

$$\varepsilon_{th}^{\ cool}(T) = \varepsilon_{tot}(T_{\max}) - \Delta\varepsilon_{th} \qquad \text{equ. (5.78)}$$

whereby according to Fig. 5-20:

$$\Delta\varepsilon_{th} = 1.445 * 10^{-3} e^{3.4*10^{-3}*T_{\max}} - 1.445 * 10^{-3} * e^{3.4*10^{-3}*T(n)} \qquad \text{equ. (5.79)}$$

with $T(n)$ as temperature at each time step n and $\Delta\varepsilon_{th}$ is a decreasing function for the gradient during cooling.

According to Fig. 5-22 the gradient of the decreasing branch of the total deformation is relatively identical. It seems that the deformation during cooling down depends more on the absolute value of total deformation when the cooling is started. The same behaviour was observed in Fig. 5-21. The general equation of the irreversible deformation due to cooling down depending on the load is derived as follows:

$$\varepsilon_{tot}^{\ cool}(T,\alpha) = \varepsilon_{tot}(T_{\max},\alpha) - \Delta\varepsilon_{\alpha} \qquad \text{equ. (5.80)}$$

whereby according to Fig. 5-20 and 5-21:

$$\begin{aligned}\Delta\varepsilon_{\alpha} = &\left[1.9 * 10^{-8} * {T_{\max}}^{2} + 8 * 10^{-6} * T_{\max} + 3.2 * 10^{-4}\right] \\ &- \left[1.9 * 10^{-8} * T(n)^{2} + 8 * 10^{-6} * T(n) + 3.2 * 10^{-4}\right]\end{aligned} \qquad \text{equ. (5.81)}$$

with $T(n)$ as temperature at each time step n and $\Delta\varepsilon_{\alpha}$ as decreasing function of the gradient during cooling.

According to the Fig. 5-20 to Fig. 5-22 the strains for cooling curves are relatively good. For each maximum temperature, there is a cooling function that depends on the load history. In numerous research projects we observed that those mentioned above, equations are available for maximum temperature from 150°C to 750°C [L21, L18, L124]. The equations are relatively identical due to the fact that during cooling, no creep occurs. See Fig. 5-23.

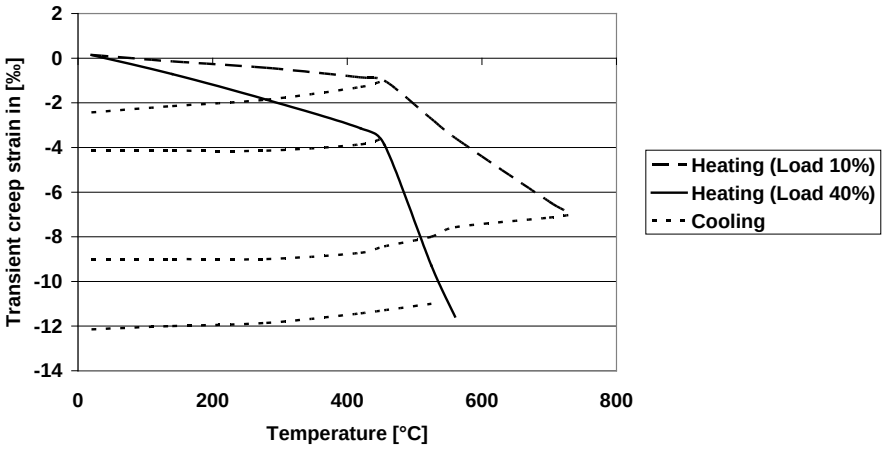

Fig. 5-23 - Transient creep during cooling down at different load level and different temperatures according to [L124]

The type of cement and of concrete i.e. self compacting concrete also has an influence on the cooling down behaviour of the deformations, see [L125].

If the Young's modulus does not change, the irreversible deformations during cooling depend only on thermal effects.

The irreversibility part of the cooling down strain curve is caused by residual crack opening because cracks do not close completely during cooling down.

5.7.2 Elastic and Plastic Strain during Heating and Cooling including Load History

At any time in the ascending branch the elastic strain is:

$$\varepsilon_{el}{}^{n} = \varepsilon_{el}(T, \alpha) \qquad \text{equ. (5.82)}$$

During cooling down, the elastic strain is reversible. The deformation energy may be released after heating-up, assuming that further cracking takes places during cooling however this is not always the case.

Plastic strain is irreversible and cannot decrease. Subsequently by different behaviour in the ascending and descending branches of the stress-strain relationship must be taken into account. The plastic strains are calculated as described before including the load history in the stress-strain relationship. If temperature or load history decreases the plastic strain, then the deformation is taken as constant at that point.

$$\varepsilon_{pl}{}^{n} = \varepsilon_{pl}(T_{\max}, \alpha) \qquad \text{equ. (5.83)}$$

During cooling down the plastic deformations are generally assumed as constant. This must be taken into account in the nonlinear FEA-model. In the range of $\varepsilon_{pl} + \varepsilon_{el} \geq \varepsilon_u$, the deformation may be calculated according to the linear model of EC2 [L48] given in Table 5-3.

Tab. 5-3 - Ultimate strain and stress induced strain in ascending and descending branches of the stress-strain relationship according to [L48]

Concrete Temperature	20 … 1100 °C
$\varepsilon_u(T,\alpha)$ see chapter 5.6.3	$\varepsilon_u(T,\alpha) = \varepsilon_u(20°C) + \Delta\varepsilon_u(T) * f(\alpha)$ and $\varepsilon_u(T,\alpha) \leq 7.8 * 10^{-3}$
$\varepsilon_{u,1}(T)$	$\varepsilon_{u,1}(T) = 3 * 10^{-5} * T - 0.0199$

Where:

$\varepsilon_u(T,\alpha)$ = ultimate strain in the ascending branch and

$\varepsilon_{u,1}(T,\alpha)$ = maximum strain of the descending branch of stress-strain relationship, according to [L48].

The Figures 5-24, 5-25 and 5-26 show the stress strain behaviour separated in the elastic plus plastic strain and separated in transient stresses.

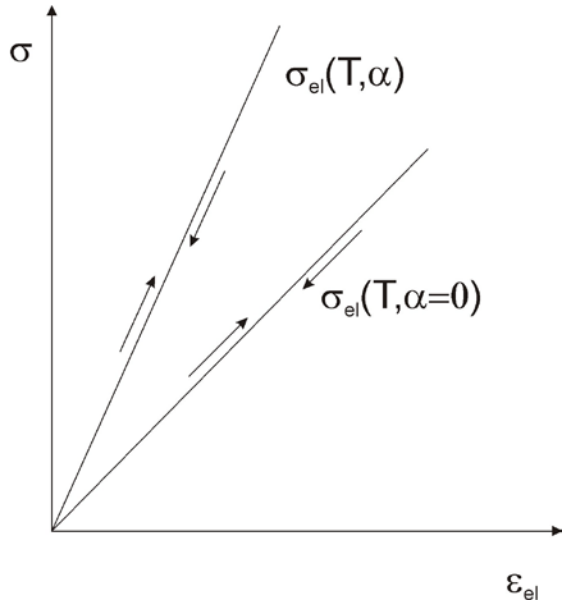

Fig. 5-24 - Elastic part of the stress-strain relationship with constant loads or without load

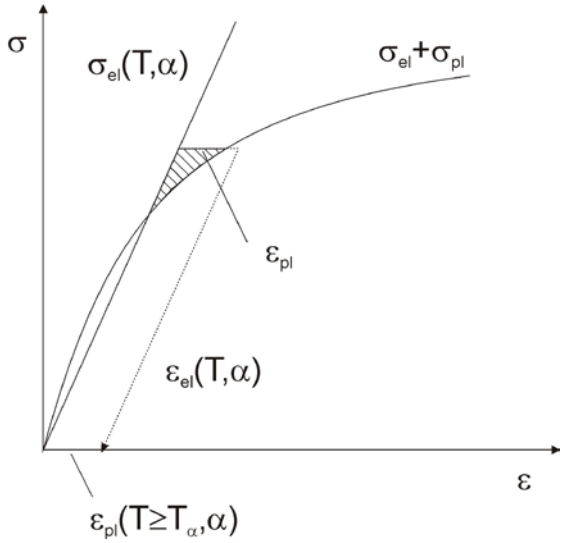

Fig. 5-25 - Plastic part of the stress-strain relationship with constant loads or without load

The Figures should show the irreversibility of the stress-strain relationship during heating. Fig. 5-24 shows the elastic strain. The elastic strain is full reversible. Fig. 5-25 shows the irreversibility of the plastic strain.

Fig. 5-26 shows the stresses during transient heating. For each temperature a separate stress-strain relationship exists. In a stepwise finite element analysis the reaction of the concrete during each time step and for any temperature change the stress distribution at any point of the cross section is considered.

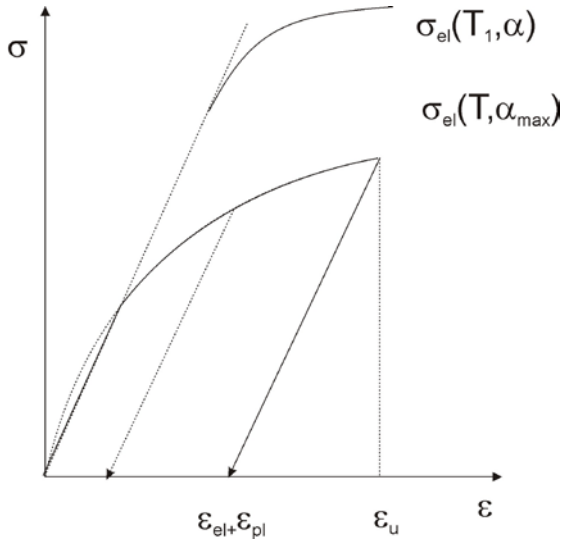

Fig. 5-26 - Stresses during transient heating

5.7.3 Transient Creep during Heating-up and Load History

The strain component of the transient creep-function is irreversible. The consideration is discrete in temperature scale during heating up. For each time step, there exists a point of the creep function that belongs to the thermal transient strain and the main part of it belongs to transient creep strain that depends on load history and temperature [L126, L127].

Fig. 5-27 shows two transient creep functions at different constant load factors.

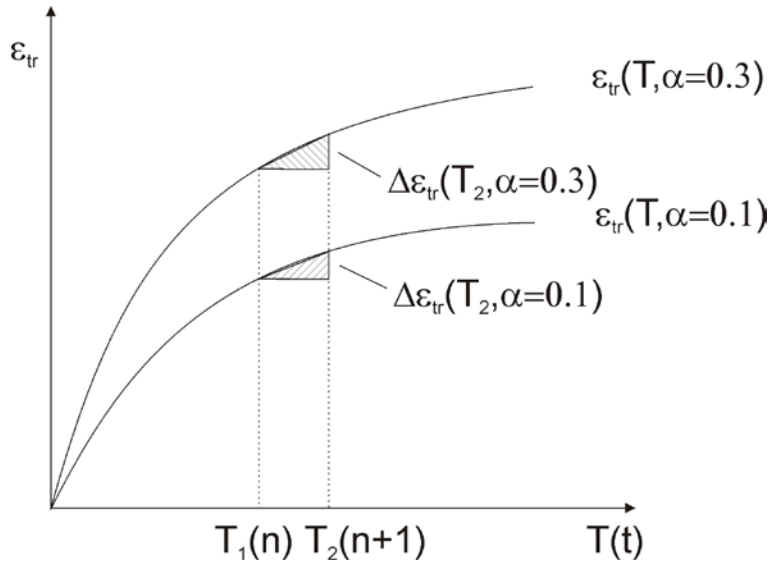

Fig. 5-27 - Examples of transient creep functions

Only the term $\Delta\varepsilon_{tr}(T,\alpha)$ is taken into account during a calculation process.

Fig 5-28 shows the calculation process of the function $\varepsilon_{tr}{}^{n}$ respectively $\varepsilon_{tr}(T(t),\alpha(t))$.

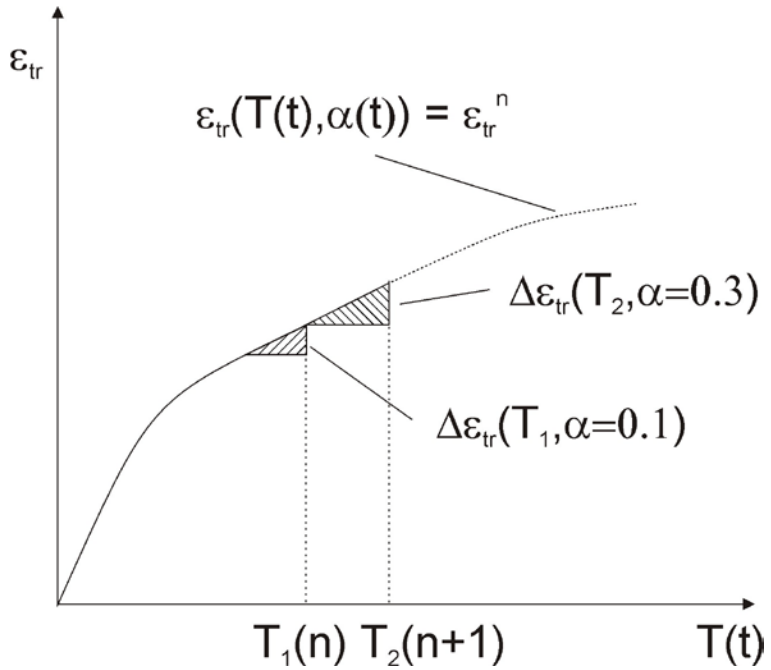

Fig. 5-28 - Transient creep function depends on temperature and time step during the calculation process

It can be seen that there is a fictitious transient function, which is added using the term $\Delta\varepsilon_{tr}(T,\alpha)$ in each time step. The size of the time step depends on the calculation software and the calculation time. In the following research, the time step is 2 seconds whereby during an iteration step the time step will be reduced. The temperature step depends on time. According to the chosen temperature exposition, the temperature step is variable according to the time. In elements near the concrete surface, the temperature step is higher than in elements inside the structure.

In the case of increasing temperatures and changes of load, the parts of plastic and transient creep parts are irreversible. The part of elastic strain $\Delta\varepsilon_{el}$ is reversible. The stepwise calculation of strain is based on the total strain approach illustrated as follows:

$$\varepsilon_{tr}{}^{n} = \varepsilon_{tr}{}^{n-1} + \Delta\varepsilon_{tr}(T,\alpha) \qquad \text{equ. (5.84)}$$

where superscript n indicates the new time step with $T = T(n)$ and n-1 the old time step with

$\varepsilon_{tr}{}^{n} \geq \varepsilon_{tr}{}^{n-1}$ (temperature increases and stress = constant or increases)

$$\Delta\varepsilon_{tr}(T,\alpha) = \varepsilon_{tr}{}^{n} - \varepsilon_{tr}{}^{n-1} \quad \text{equ. (5.85)}$$

with $\varepsilon_{tr}{}^{n} < \varepsilon_{tr}{}^{n-1}$ (temperature increases and stress decreases)

$$\Delta\varepsilon_{tr}(T,\alpha) = \max \varepsilon_{tr}{}^{n} - \Delta\varepsilon_{el}{}^{n}(T,\alpha) \quad \text{equ. (5.86)}$$

Whereas $\Delta\varepsilon_{el}$ is:

$$\Delta\varepsilon_{el}(T,\alpha) = \varepsilon_{el}(T,\alpha) - \varepsilon_{el}(T) \quad \text{equ. (5.87)}$$

From the basic equations we obtain:

$$\varepsilon_{m}(T) = \varepsilon_{el}(T,\alpha) + \varepsilon_{pl}(T,\alpha) + \varepsilon_{tr}(T,\alpha) \quad \text{equ. (5.88)}$$

$$\varepsilon_{m}(T) = \frac{\sigma(t)}{E(T)} * (1+\varphi) \quad \text{equ. (5.89)}$$

$$\varepsilon_{el}(T) = \frac{\sigma(t)}{E(T)} \quad \text{equ. (5.90)}$$

$$\frac{\varphi * \sigma(t)}{E(T)} = \varepsilon_{pl}(T,\alpha) + \Delta\varepsilon_{el}(T,\alpha) + \varepsilon_{tr}(T,\alpha) \quad \text{equ. (5.91)}$$

For the pure transient creep, from equation (5.91), we finally obtain:

$$\varepsilon_{tr}(T,\alpha) = \frac{\varphi * \sigma(t)}{E(T)} - \varepsilon_{pl}(T,\alpha) - \Delta\varepsilon_{el}(T,\alpha) \quad \text{equ. (5.92)}$$

It is astonishing to observe that the influence of load history originates from plasticity effects and only to a very small extent on the load effect on the modulus of elasticity. The pure transient function according to equation (5.92) is obviously of high complexity and up to now it cannot be quantitatively determined for ordinary concrete (OPC). The possible data for determining such information is given in the equation cited above and are used in the ATC-model.

5.8 Strain Model in Tension

The concrete model for tensile stress is assumed as one tenth of the stress-strain curve for compression, excluding load history and transient creep [L108]. Figure 5-29 indicates a nearly identical behaviour between compression and tensile strength at high temperatures according to split cylinder tensile tests results.

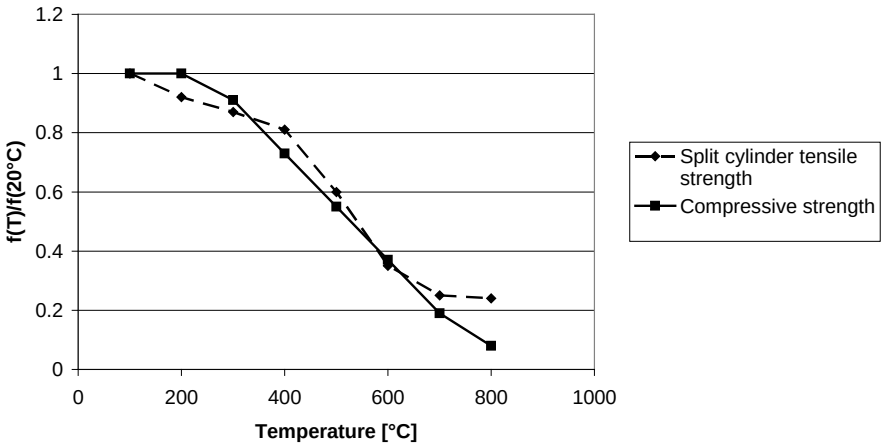

Fig. 5-29 - Ratio of split cylinder tensile strength and compressive strength of OPC at high temperatures according to [L128]

Therefore, tensile strength at high temperatures $f_T(T, \alpha = 0)$ is calculated as one tenth of the data according to equation (5) to (9).

Compared with the concrete model in compression, the plastic deformation in tension could decrease because of the relocation of loads into compression; open cracks could close again and change the prefix of stress. The concrete model in tensile is:

$$\varepsilon_{tot,t} = \varepsilon_{el,t} + \varepsilon_{pl,t} + \varepsilon_{th} \qquad \text{equ. (5.93)}$$

Where subscript t means tension.

A tensile creep at ambient temperatures exists. A creep factor φ of unsealed specimens of 3.4 is observed [L129]. As discussed in Chapter 5.6.5, it is also assumed that a tensile creep exists during fire. The value of tensile creep at ambient temperatures is relatively small compared to transient thermal creep. Because of this behaviour, tensile creep is not to be considered in the concrete ATC-model.

5.9 Failure Model at High Temperature

For the determination of failure of specimens in a concrete model by finite element analysis, an appropriate failure model must be developed. In the case of high temperature or fire exposure the following procedure is proposed in the calculation.

The failure of plain concrete usually starts due to development of crack under compression, i.e. if

$$\frac{\sigma(t)}{f_c(T)} > 0 .$$

On the other hand, the failure of concrete may occur due to pure tensile stresses. In reality, the whole stresses are transferred to the reinforcement steel; hence, the specimens will not fail due to tensile failure of concrete. Without reinforcement, the whole concrete structure fails under

tension in this case. As long as we consider concrete as basic material, the cracking is a dominant factor.

Cracks start directly due to the release of tensile strain and plastic deformation energy that exceed the surface crack energy. In practise, the failure may be estimated by the following criteria [L124]:

- $T_{\max} \geq T_{critical}(\alpha)$ Permissible critical temperatures are locally exceeded.
- $v(\dot{\varepsilon}_{tot}) \geq v(\dot{\varepsilon}_{critical})$ Permissible critical strain rates are locally exceeded.
- $\varepsilon_{tot} \geq \varepsilon_{critical}$ Permissible maximum load deformations are exceeded.

In the case of high temperatures, concrete under different constant compressive load fails during heating up, as shown in Figure 5-30. The heating rates range from 4 to 0.5 K/min.

Note that the maximum of critical concrete temperature is in the range of 850°C to 950°C for loaded structures. The upper level of fatigue load at this temperature range is α = 0.1. This means that if you heat up the concrete specimen continuously with a load factor of α = 0.1, the specimen fails ultimately at about 900°C.

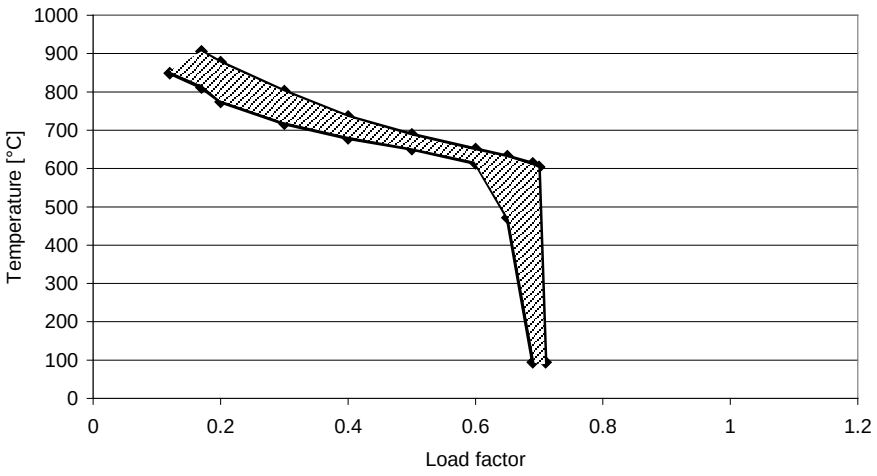

Fig. 5-30 - Critical concrete temperatures of siliceous concrete with constant load under compression during heating up according to [L130 and L103]

From the test results for the total deformation strain ε_{tot}, one may conclude that the deformation rate $v(\dot{\varepsilon}_{tot})$ plays a dominant role during the simulation of transient load history. If the maximum deformation rate is exceeded, the concrete fails according to test results given in Figure 5-30, after [L18]). This means that in this case, the ratio $\frac{\sigma(t)}{E(T,\alpha)}$ during heating cannot be larger than the results of the deformation rate per second. The observed deformation rates are shown in Figure 5-31. The limit of the failure curve in Figure 5-31 presents the failure of concrete, if the deformation rate in ‰/s is larger than the limit failure curve based on the range of failure accord-

ing to Fig. 5-31 [L18]. The observed failure rates $v(\dot{\varepsilon}_{tot})$ range from $5*10^{-4}$ ‰/s to $35*10^{-4}$ ‰/s depending on the load level and the test temperature. The failure rates are due to the crack development in concrete cross section.

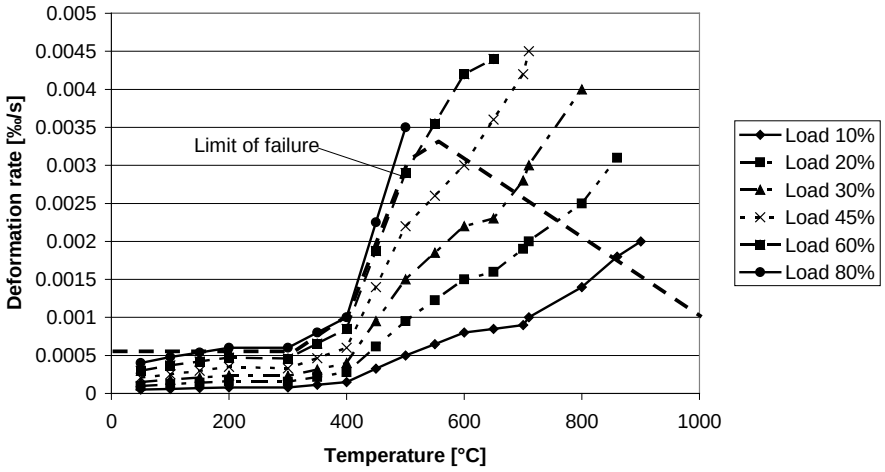

Fig. 5-31 - Deformation rate of concrete under different load factors during heating-up with 2 K/min according to [L18]

Under 400°C, the failure occurs due to the cold compressive strength of 80 to 100 %. This is why the deformation rate is relatively independent on load history. During temperatures of 500°C and higher, the short time compressive strength is less than 60 % of the cold compressive strength. The deformation rate increases exponentially according to Fig. 5-31. A lightly decrease of the deformation rate is observed at the temperature of 600°C. Thermal incompatibility and parasitic stresses normally relaxed by transient creep ends here.

At high temperatures, the concrete cracks are developed by physical-chemical conversions, thermal destruction of CSH phases and by crystalline conversion of aggregates respectively. These phenomena are considered to be the main reason for the decrease of compressive strength and critical temperatures. Furthermore, cracks are influenced by the kinetic parameters such as activation energy, reaction rate of dehydration products and reaction rate of concrete aggregates which may lead to the time and temperature dependent loss of strength [L131]. The drying of concrete at high temperatures is another factor that is responsible for crack development [L132].

In the ATC-model, the shrinkage strain during heating is included in the transient thermal strain part that depends on the type of concrete [L133]. The ultimate strain of ordinary concrete is considered as a function of load factor α and temperature T(t). It was observed that relating the ultimate strain of loaded specimens at high temperatures just to the ultimate strain at 20°C is not sufficient approach for a failure concept. A great part of the larger deformations is compensated by transient creep. The ability of concrete for plasticizing at higher loads is depleted this is why the ultimate strain is unexpectedly low [L15], whereas the total strains under failure conditions are very high. Fig. 5-32 shows the deformation condition at high temperatures near the point of sudden failure.

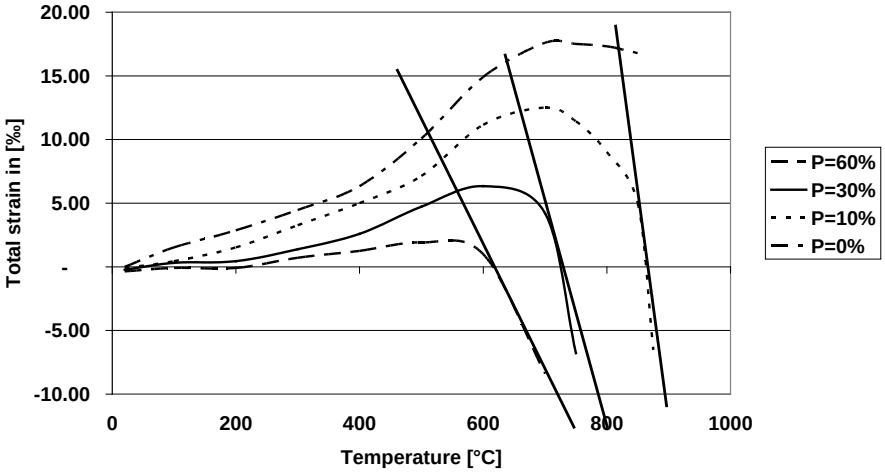

Fig. 5-32 - Strain condition during failure at high temperatures

If the first derivation of total strain over temperature $\frac{\varepsilon(T)}{T}dT$ approaches, infinity failure occurs.

5.10 Residual Properties

During a temperature cycling, many different failure mechanisms may arise. They are governed by the load bearing strength and the residual strength after cooling down. Thermal damages that might occur during cycling and cooling are:

- Chemical dehydration reactions of cement mortar and aggregates,
- Physical conversions and
- Crack development, increase of crack growth, crack numbers, length and width, increasing of pores content

The low residual strength after cooling down of concrete at high temperatures is shown in Figure 5-33. It is also determined as a function of load history. The relative decrease of compressive strength around 150°C by lower load factors depend on the activation and flow of moisture in the structure and are not due to thermal reactions inside of the concrete. It is also determined as a function of load history. This effect is essentially an experimental effect due to vaporisation of the capillary water and the gel bounded water above 100°C because the surface energy reduces

by moisture layers. If the test runs more than 2 days, the concrete is dry and the strength loss vanishes.

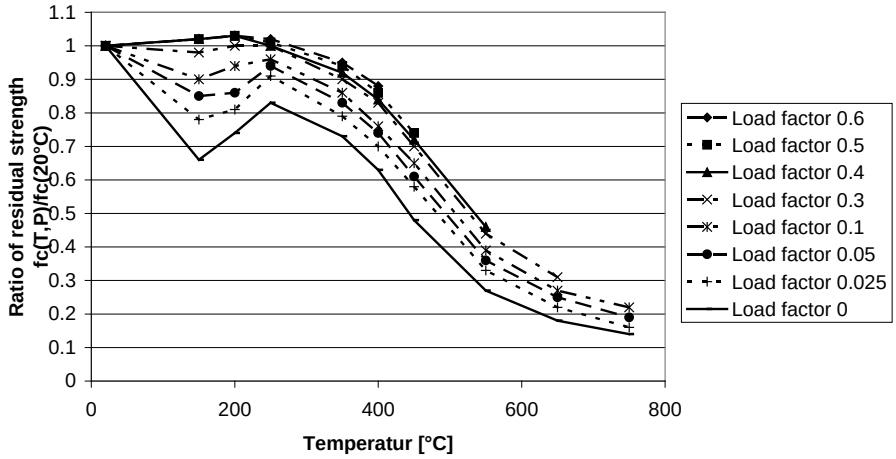

Fig. 5-33 - Residual strength of siliceous concrete under different sustained loads during heating up according to [L16]

The residual strain can be calculated approximately according to Section 5.9. In relation to the reduction of Young's modulus at elevated temperature, the results from Figure 5-33 may be used.

Figure 5-34 shows the ratio of Young's modulus after heating-up to a maximum temperature T_{max} and testing after cooling down to 20°C $E_{residual(Tmax)}$ divided by Young's modulus at 20°C $E_{(20°C)}$. It seems that the relation between Young's modulus at elevated temperatures and Young's modulus at 20°C is similar for ordinary concrete and high-performance concrete [L21, L134]. The residual Young's modulus is greater or equal to the minimum value of Young's modulus during heating that may be calculated according to Figure 5-34.

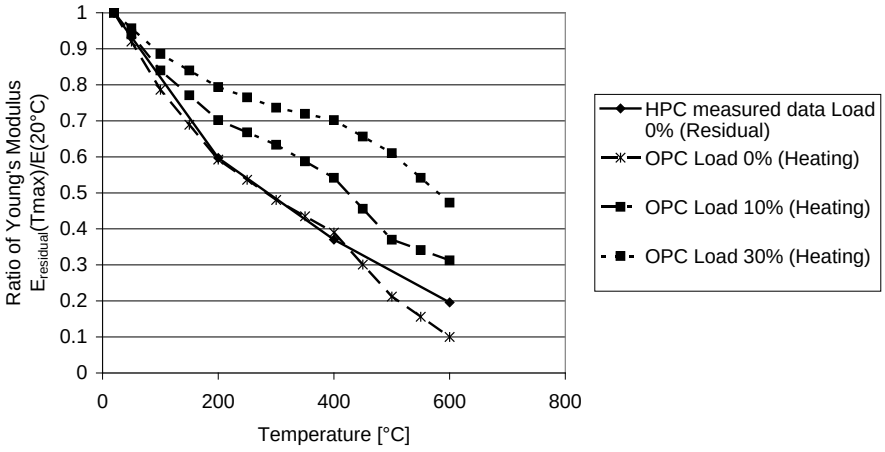

Fig. 5-34 – Reduction of Young's modulus at elevated temperature (Residual test) of high strength concrete according to [L134]

Due to limited information about Young's modulus after cooling, the comparison of HPC and OPC without load is essential. The curves are approximately good. According to [L147], the following equation is used for the calculation of the Young's modulus in relation to the compressive strength:

$$E_{HPC} = \left(0.8 + 0.2 * \frac{f_{c,HPC}}{88}\right) * 9500 * \left(f_{c,HPC} + 8\right)^{\frac{1}{3}} \qquad \text{equ. (5.94)}$$

A cooling down calculation of 2 different concrete models, namely the EC2-model and the ATC-model both used siliceous aggregate in the calculated concrete. This is illustrated in the next figures. Fig. 5-35 shows the used temperature-time curve and should only show the differences which are observed.

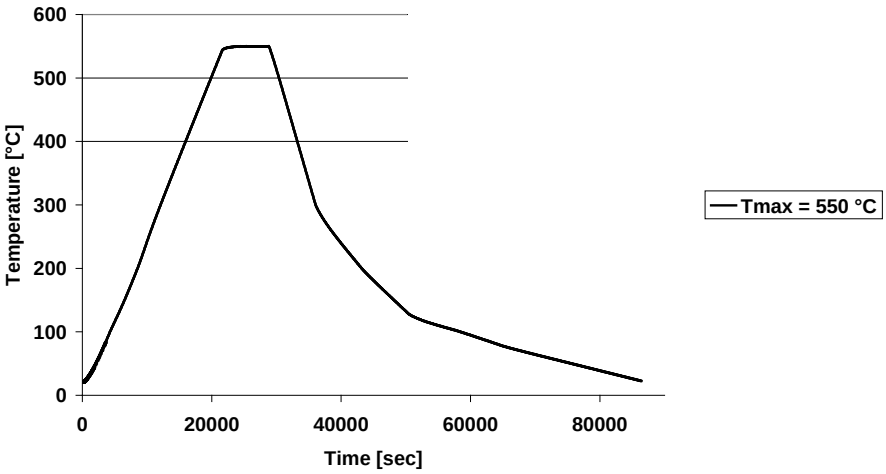

Fig. 5-35 - Temperature-time curve with cooling down

The temperature increase up to 550°C in 21600 seconds and is constant for 7200 seconds. Afterward, the temperature decreases till the ambient temperature after 86400 seconds. The temperature of 550°C is chosen because the failure is near this point with a load of 30% for siliceous OPC. Also, this temperature is below the quartz conversion temperature.

Fig. 3-36 and 3-37 show the results of the simulation of the total deformation during heating and cooling down with different concrete loading history during these procedures.

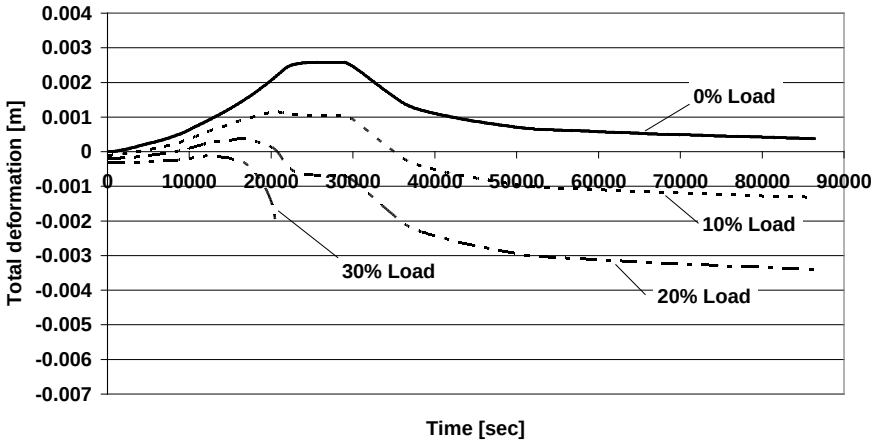

Fig. 5-36 - Simulation of the deformation of siliceous concrete according to EC2 during heating-up to 550°C and cooling down with different load levels

The simulation with the EC2-model shows a failure with 30% load at 20,000 seconds. The maximum of the deformation is due to thermal strain without load. Due to the different calculation models the absolute deformation due to heating is different, as seen in Fig. 5-36.

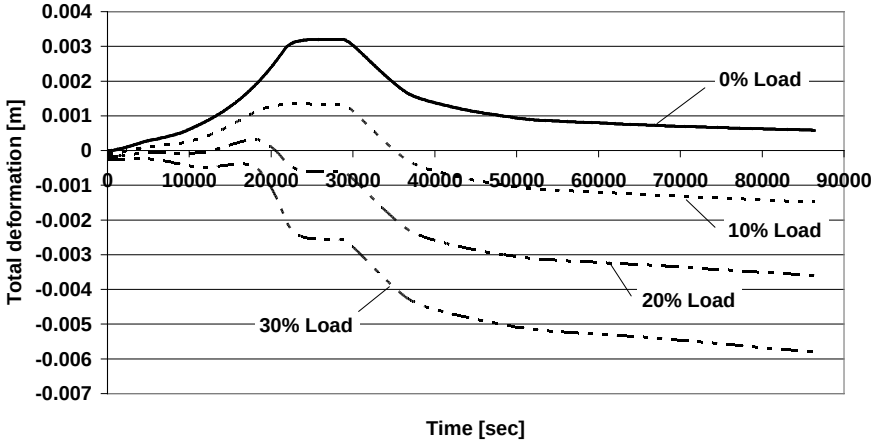

Fig. 5-37 - Simulation of the deformation of siliceous concrete according to ATCM during heating-up to 550°C and cooling down with different load levels.

The failure with 30% load does not occur during the simulation with the ATC-model. The model is softer. It is possible that the model does not reach the failure criteria before it starts cooling down. The decreasing curves are almost the same for EC2- and ATC-model. In the EC2-model, the residual compressive strength was used. In the ATC-model, the decreasing during cooling down was simulated with the equations (5.78) to (5.81) for the calculation of cooling down.

5.11 Transient Creep of High Performance Concrete

5.11.1 General Task for Transient Creep of HPC

Transient creep also occurs in a high performance concrete. The following chapter shows the differences between the transient creeps of ordinary concrete and high performance concrete.

This examination based on measured data given in [L134 and L116] show the derivation of HPC to a phi-function.

5.11.2 Deformation Tests of HPC

In [L116], excellent research results were presented on the behaviour of high performance concrete under high temperatures.

Fig. 5-38 shows the measured total deformation curves of unloaded and loaded high performance concrete with siliceous aggregates during temperature exposure.

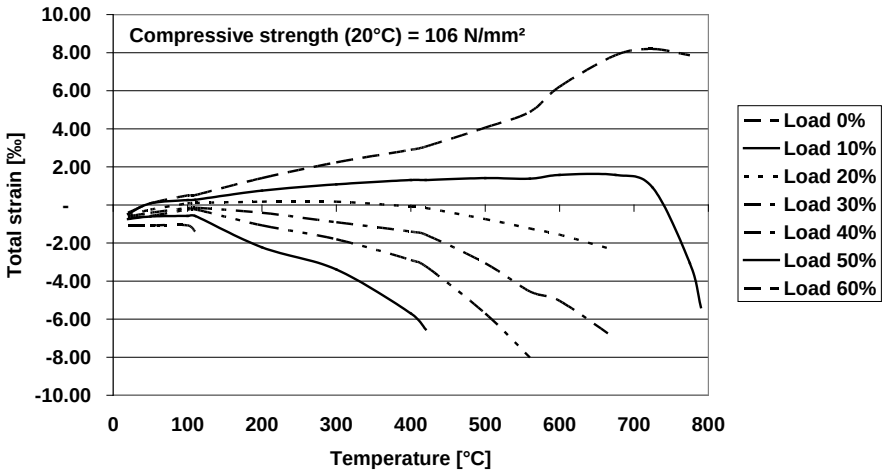

Fig. 5-38 - Total deformation of loaded of high performance concrete according to [L116]

In [L116], measured data are given in the Young's modulus of siliceous high performance concrete. Fig. 5-39 shows these results.

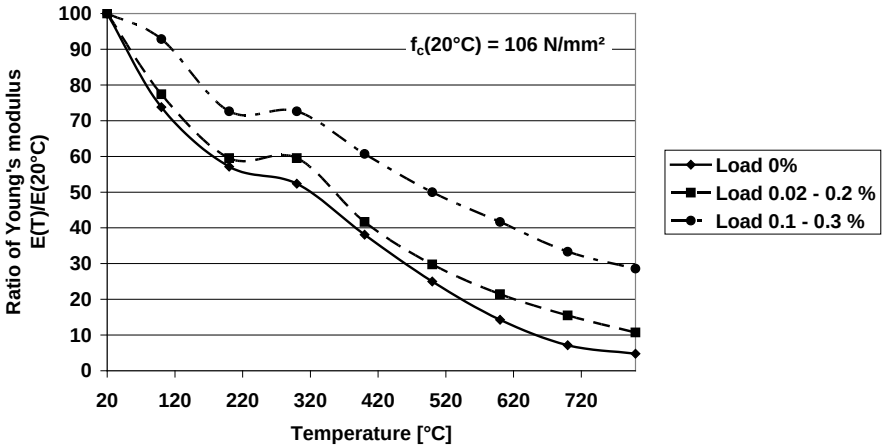

Fig. 5-39 – Young's modulus of unloaded and loaded of high performance concrete according to [L116]

According to ordinary siliceous concrete, the high performance concrete with siliceous aggregate also depends on load. This fact is being considered in the types of mechanical strains.

Fig. 5-40 shows the transient strain of high performance concrete with siliceous aggregates from test results.

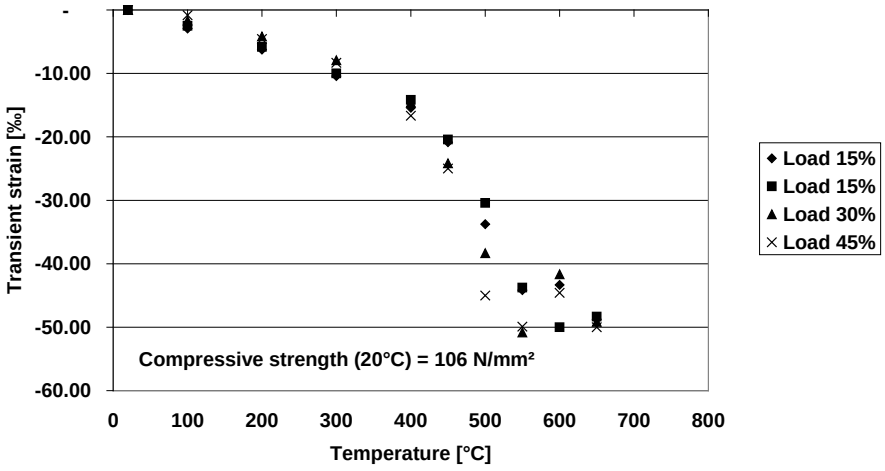

Fig. 5-40 - Transient creep of loaded high performance concrete according to [L116]

5.11.3 Derivation of the phi-function of HPC

According to Fig. 5-38 to Fig. 5-40, it may be possible to calculate a φ-function of high performance concrete after equation (5.92). The Young's modulus used is 67600 MPa, according to

measured data taken from [L116]. The temperature dependence was simulated according to the equations (5.48) to (5.60).The results are shown in Fig. 5-41.

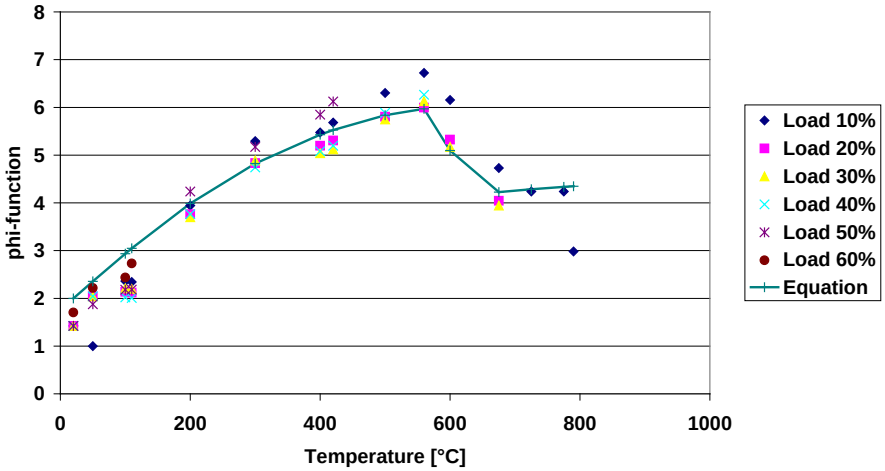

Fig. 5-41 - phi-function of high performance concrete

The equation (3.32) cannot be used in this case. A decrease of φ are obtained at 600 °C. With respect to this behaviour, the second term of the equation is negative. Otherwise the parameters of the Table 5-4 must be changed. The result of the transformation of the equation is the following equation (6.1).

$$\varphi = C_1 * \tanh \gamma_w * (T - 20) - C_2 * \tanh \gamma_0 * (T - T_g) + C_3 \qquad \text{equ. (5.95)}$$

Tab. 5-4 - Parameters for transient creep functions of high performance concrete

Parameter	Dimension	Siliceous aggregates
C_1	1	4.5
C_2	1	1.0
C_3	1	1.0
γ_w [1)]	$°C^{-1}$	$2.6*10^{-2}$
γ_0	$°C^{-1}$	$5*10^{-2}$
T_g	°C	600

The moisture content of concrete is taken into account in the γ_w-function according to equation (5.33). The given value [1)] holds for an assumed moisture content of 2% by weight.

Generally the φ-function is higher according to the φ-function of ordinary concrete. An identical behaviour is observed according to ordinary concrete for the load factor. The φ-function is relatively independent from the load. According to Fig. 5-41 a maximum value of φ can be assumed with 7.0.

6 The Finite Element Calculation of Structures Subjected to Fire

6.1 General Description of Finite Element Calculation

The calculation of finite elements (FE) particularly the finite element analysis (FEA) or finite element method (FEM) is a general accepted method to predict material and structural behaviour of simple or complex structures. In FE calculations, linear and nonlinear material equations are used. The nonlinear aspect is for calculations of structures for the following aspects if these are taken into account [L135]:

- complex geometry or kinematic,
- nonlinear material properties,
- complex thermal boundary conditions and
- load history.

The nonlinear problem is usually solved by an iterative or step wise calculation of each increment. Generally the FEA is defined as an equation of a stress vector, material matrix (stiffness matrix) and a deformation vector. The following equation shows the general 3D mathematical equation.

$$\{\sigma\} = [K]\{\varepsilon\} \qquad \text{equ. (6.1)}$$

with

$\{\sigma\}$ - stress vector given as $\begin{Bmatrix} \sigma_x \\ \sigma_y \\ \sigma_{zx} \\ \tau_{xy} \\ \tau_{yz} \\ \tau_{zx} \end{Bmatrix}$

$[K]$ - stiffness matrix as $\frac{E(1-\nu)}{(1+\nu)(1-2\nu)} \begin{bmatrix} 1 & \frac{\nu}{1-\nu} & \frac{\nu}{1-\nu} & 0 & 0 & 0 \\ \frac{\nu}{1-\nu} & 1 & \frac{\nu}{1-\nu} & 0 & 0 & 0 \\ \frac{\nu}{1-\nu} & \frac{\nu}{1-\nu} & 1 & 0 & 0 & 0 \\ 0 & 0 & 0 & \frac{1-2\nu}{2(1-\nu)} & 0 & 0 \\ 0 & 0 & 0 & 0 & \frac{1-2\nu}{2(1-\nu)} & 0 \\ 0 & 0 & 0 & 0 & 0 & \frac{1-2\nu}{2(1-\nu)} \end{bmatrix}$

with ν - Poisson ratio

$\{\varepsilon\}$ - deformation vector given as $\begin{Bmatrix} \varepsilon_x \\ \varepsilon_y \\ \varepsilon_z \\ \gamma_{xy} \\ \gamma_{yz} \\ \gamma_{zx} \end{Bmatrix}$

The FEA may be applied for 3D analysis. The 3D analysis is not even optimal. In view of a usable models for the application of FEA, the determinations can be reduced to a 2 dimensional model or a 2 ½ dimensional model respectively [L136].

In the same manner, an application of thermal FE calculation of temperature fields is possible. This is usable for predicting the following behaviour of the material [L135]:

- Evaluation of operating or catastrophic temperatures,
- Evaluation of heat flows and energy flows and
- Examination of influence of temperatures on fatigue or failure.

The thermal stress is the determining factor of the mechanical behaviour of the structure. Therefore the temperature field must be known in each time step [L137].

The general equation of the FE calculation for temperature fields is given by [L135]:

$$\{q\} = [K_t]\{T\} \qquad \text{equ. (6.2)}$$

with

$\{q\}$ - Heat flow vector given as $\begin{Bmatrix} q_x \\ q_y \\ q_z \end{Bmatrix}$

$[K_t]$ - Heat conduction matrix given as $-\begin{bmatrix} \lambda_x & 0 & 0 \\ 0 & \lambda_y & 0 \\ 0 & 0 & \lambda_z \end{bmatrix}$ with λ - heat conduction

$\{T\}$ - Temperature vector given as $\begin{Bmatrix} \partial T / \partial x \\ \partial T / \partial y \\ \partial T / \partial z \end{Bmatrix}$

An important factor in the structural analysis is the structure of meshes of the FE calculation. All material properties, loads and temperatures influence mentioned above are defined for one node or one element in a mesh of the structure. It defines the stepwise transfer of heat flow from one node to the other or the stress field from node to node. The geometry of the elements of the mesh depends on the structure or the cross section which is investigated. Areas that are ex-

posed to high temperatures and local areas that are especially designed for the structure (i.e. edges or hollows) do usually need finer meshes than areas with lower temperature gradients for instance inside of the structure [L138, L139].

Mesh generation and the algebraic solver are also two important aspects of the finite element methodology. Additionally, compositions of different geometry and different grids allow to simulate slightly more complex situations whereby either the grid generation is done with a combination of several different strategies or the solution behaviour changes dramatically from one part of the domain to another part of domain [L140]. Figure 6-1 shows an example of a mesh with different local areas of interest.

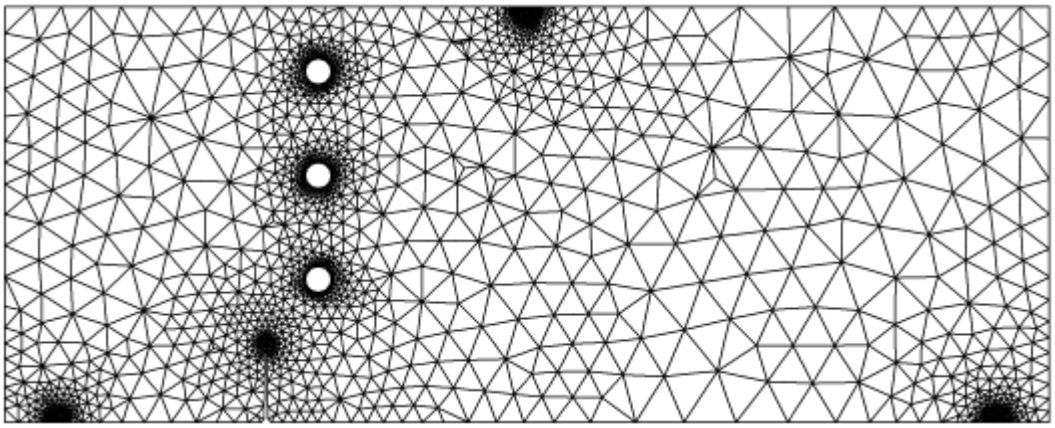

Fig. 6-1 - Example for a finite element mesh for thermal calculations according to [L141]

In order to reach convergence and stable solutions, a tolerance value has to be specified in the program. SAFIR uses an iterative procedure to converge on the correct solution for each increment. The precision given in the data file is a small value that must be reached at different times in SAFIR calculations in order to obtain convergence. A good precision value depends on the type of structure that is being analyzed and information from preliminary runs. After the first run, an examination in the output of the out-of-balance forces and increments of displacement during subsequent iterations can help to modify the corresponding precision value to obtain acceptable solutions [L56]. Figure 6-2 shows the theory of convergence iterations as example for the determination of internal forces.

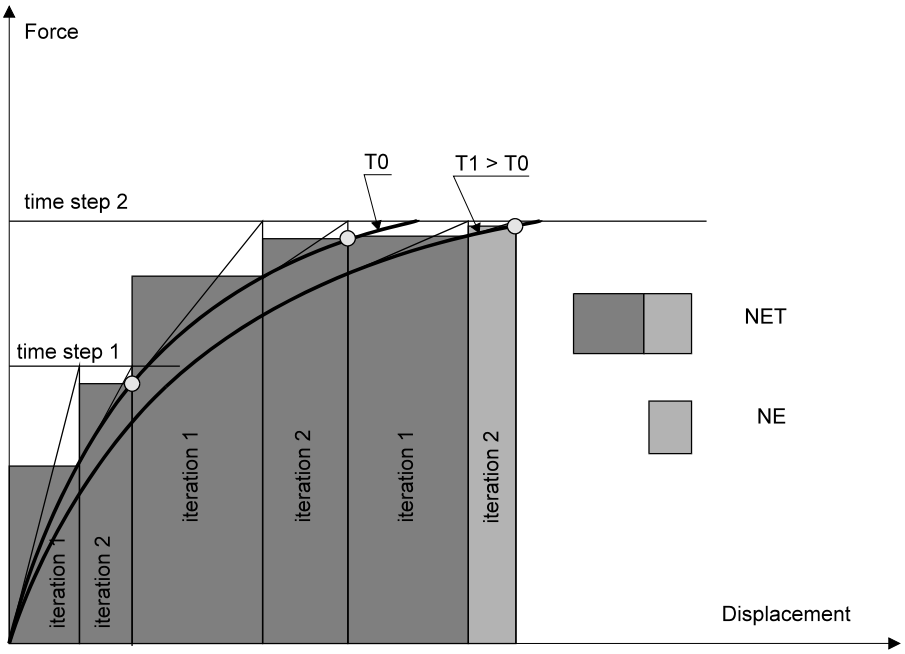

Fig. 6-2 - Convergence iterations for internal forces according to [L56]

The Equation at each iteration of each time step follows equation (7.3)

$$NE = \sum_{k=1}^{NDOF} \left| du_k^{i,j} F\,\mathrm{int}_k \right| \qquad \text{equ. (6.3)}$$

Where:

$F\,\mathrm{int}_k$	Internal forces. Those forces are calculated at the nodes as the result of the internal forces coming from the elements: axial forces, bending forces.
du_k^{ij}	Incremental displacement at time step i and iteration j.
NDOF	Number of degrees of Freedom of the structure.
NE	Norm (vector) of the energy, calculated at each iteration.
NET	Norm (vector) of the total energy, calculated as the summation of all the previous NE.
PRECISION	A number, chosen by the user, supposed to be small.

At the starts of the program the variable NET equals 0.

NE is not exactly the energy because a force associated to a negative displacement should be counted as a negative energy, whereas it is counted as positive in equation (6.3). Each component of equation (6.3) is counted as positive because, if not, the negative components would tend to reduce the energy NE, and if by chance the sum of the negative components is exactly equal to the sum of the positive components, this would give NE = 0, whereas the iteration under consideration has produced a lot of incremental movements. Even if all displacements and forces are positive, NET is not exactly the energy, as can be seen on the Figure 6-2, drawn for a

system with 1 degree of freedom, a load applied in two time steps under constant temperature T0, and then the temperature changing from T0 to T1 in one time step [L56].

6.2 Implementation of the ATC-model in FEA Software SAFIR

SAFIR is a special purpose computer program for the analysis of structures under ambient and elevated temperature conditions. The program, that is based on the Finite Element Method, can be used to study the behaviour of two and three-dimensional structures. The program SAFIR software was developed at the University of Liège, Belgium [L142].

As a finite element program, SAFIR accommodates various elements for different idealizations, calculation procedures and various material models for incorporating stress-strain behaviour.

For the implementation of the ATC-model into the SAFIR software, the program itself and the input file were enhanced with the parameters Young's modulus in the origin and the water content of the concrete. According to the chapter 3.4.5 the thermal calculation of the FE calculation with SAFIR uses the following input parameters:

- Water content of the concrete,
- Convection coefficient at hot surface,
- Convection coefficient at cold surface,
- Emissivity of concrete and
- Type of aggregate.

The mechanical calculation uses the following input parameters at 20°C:

- Young's modulus at the origin,
- Poisson's ratio,
- Compressive strength,
- Tensile Strength,
- Water content of the concrete and
- Type of aggregate.

The compressive strength at high temperature will be calculated according to the equations in Chapter 5.6.1 and Young's modulus at high temperature bases on the Young's modulus at the origin. The equations are given in Chapter 5.6.2.

The Poisson's ratio is given as a constant value. According to Chapter 3.5.5 the Poisson ratio depends on load and temperature, which is not taken into account.

The tensile strength is considered according to Chapter 3.5.6.

The water content in the mechanical calculation is only necessary for the calculation of the thermal creep according to Chapter 5.3.3.

All the other parameters of the material model presented before were implemented using the full equations for the material properties in a couple of separate subroutines in SAFIR which are employed using a specific input file for concrete. The calculation with SAFIR is based on different material models. The ATC-model was adapted based on the EC2-model with a stress-strain-

constitutive calculation of ultimate strain. Considering the transient strains according to the creep function which depends on the φ-factor for siliceous concretes. The mechanical strain is a conglomerate of elastic, plastic and transient strain according to the load induced transient strain and the thermal strain.

The calculation is possible from a temperature of not less than 20°C up to a temperature according to each chosen temperature time curve. The maximum temperature used was 1300°C together with a HC-increased fire curve .

Most of the increments are functions inside the software code of SAFIR,, hence, the parameters of Chapter 3 can be included with a small cost of time. The siliceous concrete was fixed for the following calculations. The SAFIR 2004 base code with the model of Eurocode, is a relatively simple and powerful tool that provides results which are usually slightly on the safety side [L143].

In the first step, the cold parameters were transferred in hot parameters according to the known equations. This depends on the current temperatures or the maximum temperatures which were reached in the whole simulation. This is important because some calculated values are irreversible.

In the program, the following equation determines the mechanical strain. Where ε_{res} is the residual strain from the last iteration.

$$\varepsilon_{mec} = \varepsilon_{tot} - \varepsilon_{th} - \varepsilon_{res} \qquad \text{equ. (6.4)}$$

The calculation of ε_{th} and ε_{mec} is mentioned above. The calculation does not use a constitutive model according the Eurocode 2. For each time step, all the hot values of the input parameters were taken into account.

The whole calculation separates in tension based calculation and compression based calculation. The full program code for the ATC-model is attached in the appendix.

7 Applications of the ATC-model for Concrete Specimens and Structures

7.1 Introduction

In the following chapters, the performance of the new model will be shown for different examples and calculations. In the first example the behaviour of small specimens made by siliceous concrete and time dependent external loads is investigated. The results were derived by a non finite element analysis with the ATC-model, which just calculates the mechanical strains considering the whole specimen (cylinders with 80 mm diameter and 300 mm height) as homogenous in temperature and compressive stresses. The calculation results are compared with measured results according to [L23].

In a second example, the total strain of the same specimens under the same conditions will be calculated with the non-finite element analysis and the FE method. In a first step the calculation runs with the ATC-model. The FE method considers different material behaviour which is why all results with the ATC-model will be compared with the results of the calculation with the Eurocode 2 model that is used commonly in Europe.

The EC2-model does not consider the transient creep of concrete. This is why before the calculation starts, the engineer must choose a realistic value of the peak stress strain which is the strain of the maximum compressive strength. In the first comparison, the EC2-model will be calculated with the recommended value (EC2(a)-model) and in the second comparison the maximum value of the peak stress strain (EC2(b)-model) was used.

After the calculation of simple specimens, the calculation of structures will be done. It starts with a calculation of small columns (cross section 150 x 150 mm and a high of 90 cm) with a small amount of steel reinforcement.

The next calculation was a calculation of an ordinary column (cross section 400 x 400 mm and a high of 600 cm).

In the last calculation, a comparison of the EC2-model and the ATC-model during a simulation of a tunnel cross section will be shown.

With these examples, the usability of the new ATC-model should be tested. Most of the calculations are compared with test results or the EC2-model.

Note that the results of ε_{tot} are also influenced by different thermal strain models according to the ATC-model and EC2-model, see Fig. 3-3.

7.2 Calculation of Mechanical Strains using Analytical Analyses

7.2.1 General Task for Calculations of Concrete Specimens

The new ATC-model is taken for calculation of the mechanical strain of different specimens under different load and heating conditions. It shows the effect of load history for mechanical strain if concrete is heated up until 700°C. The results are compared to measured data taken from [L18].

7.2.2 Model Parameters

The specimens are concrete cylinders with 80 mm diameter and 300 mm height. Heating rate is 2 K/min. The compressive strength of the siliceous concrete at 20°C is 38 N/mm². The moisture content is 2 % per mass. The results are obtained from heated specimens under different stress-time relationships were published in [L18].

7.2.3 Applied Stress-time Relations and Calculated Strain Results – example 1

The applied stress-time relation during heating-up with 2K/min is given in Fig. 7-1.

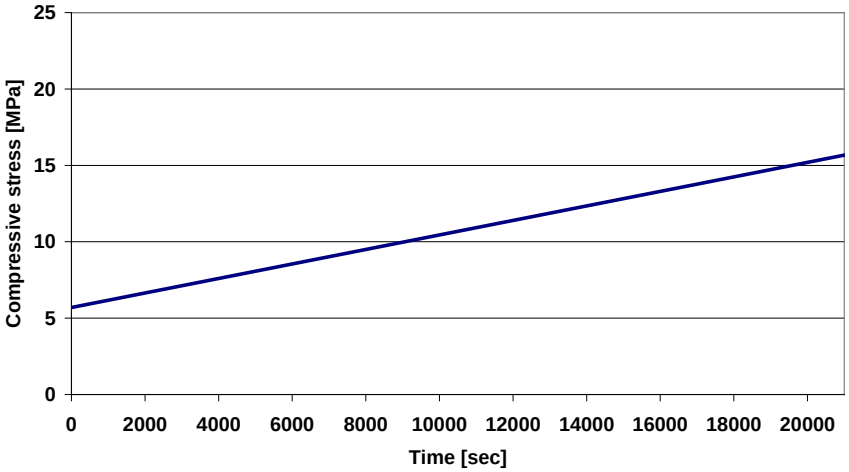

Fig. 7-1 - Stress-time relationship with constant increasing load

The application of the linear increase of stress according to Fig. 7-1 should simulate a homogeneous increase of the load factor. After 6 hours the stress reaches the maximum of 16 N/mm². This represents a load factor of 0.42.

The calculation of the time dependent results of mechanical strains, considering unsteady temperatures and loads according to the material laws given in Chapter 5, are shown in Figure 7-2.

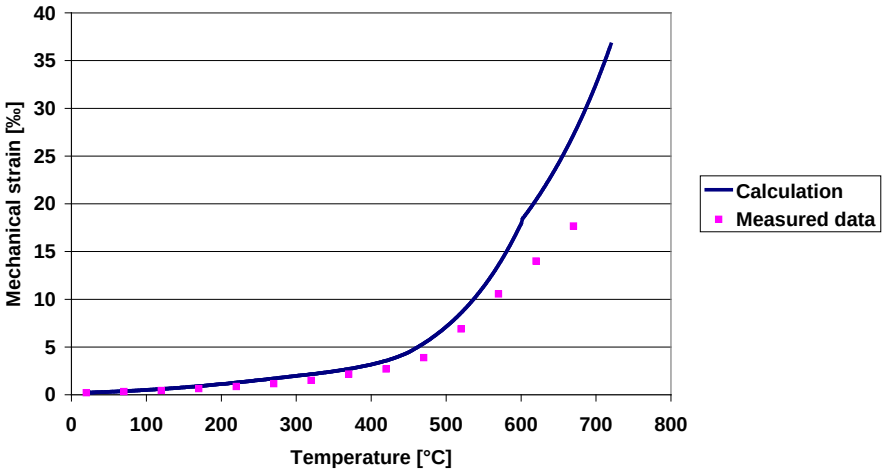

Fig. 7-2 - Comparison between calculated results and experimental results according to [L18] with the load function according to Figure 7-1

The results of the calculation are overestimated compared to the measured results. From temperatures above 600°C the mechanical deformations are higher than the measured data. At this point, the influence of the plastic part of the mechanical stress and the creep at high temperature greatly increases. The non-finite element calculation does not take into account the aspect of failure. The calculation is only a simulation of the material behaviour. It could be possible that there are areas which failed but in reality it still show a finite value for deformations. This is taken into account and the results at high temperature are higher than the measured data.

7.2.4 Applied Stress-time Relations and Calculated Strain Results – example 2

Fig. 7-3 shows the stress-time relationship of the second calculation which uses a continuous increasing load until 750 °C which is followed by a continuous decrease of load after reaching 750°C and above 15,000 seconds.

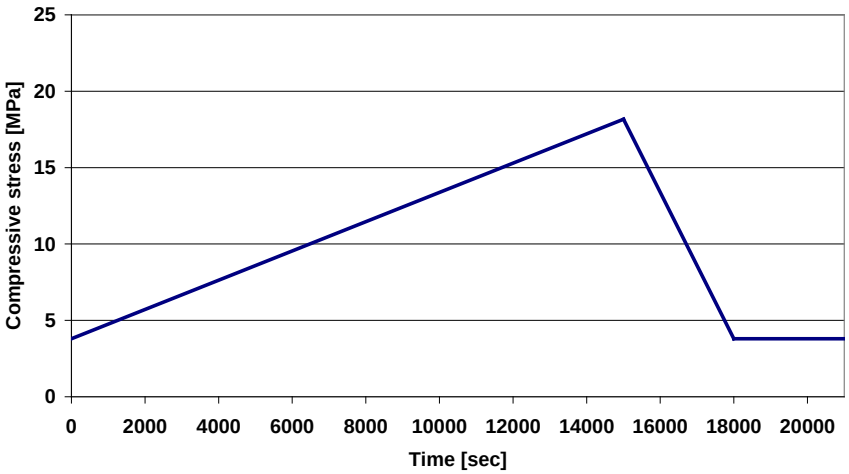

Fig. 7-3 - Stress-time relationship with continuously increasing load with continuous decreasing above 15,000 seconds

The application of the linear increase and decrease of stresses according to Fig. 7-3 should lead to the model behaviour during decrease of stresses. The maximal stress reaches a load factor of 0.46.

Fig. 7-4 shows the results of the simulation with the stress-time curve according to Fig. 7-3.

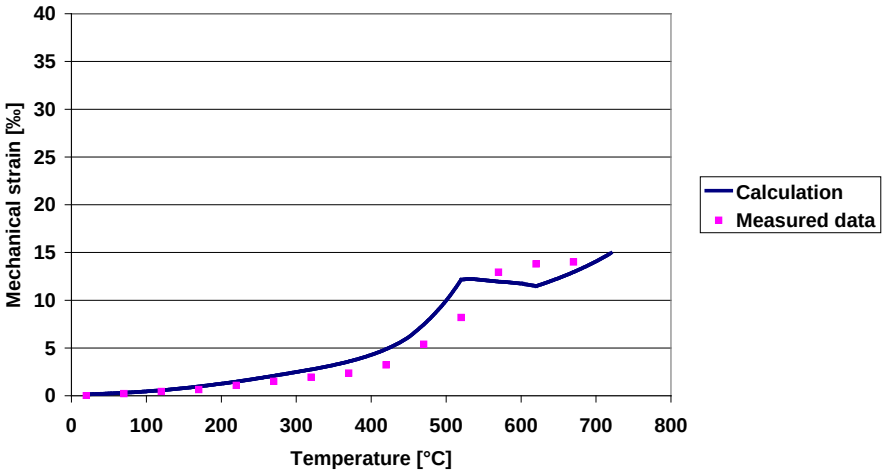

Fig. 7-4 - Comparison between calculated results and experimental results according to [L18] with the load function according to Figure 7-3

Figure 7-4 indicates a comparatively good agreement between the results of the analytical calculation and the measured data. Specifically, the load decrease was perfectly met in the simulation model. A slight overestimation of the linear increase of stress occurs above 500°C. The calculation shows that at the temperature of 550°C, there is a discrete change of the continuity of the curve. This behaviour considers only the decrease of the stress at this temperature and not a possible increase of stresses due to strain hardening.

7.2.5 Applied Stress-time Relations and Calculated Strain Results – example 3

Fig. 7-5 shows the stress-time relationship of the third example which is used as a step increase of load from 30 % up to 60 % of the compressive strength at ambient temperature. The first step occurs at 210°C. The step decrease of load starts at 420°C.

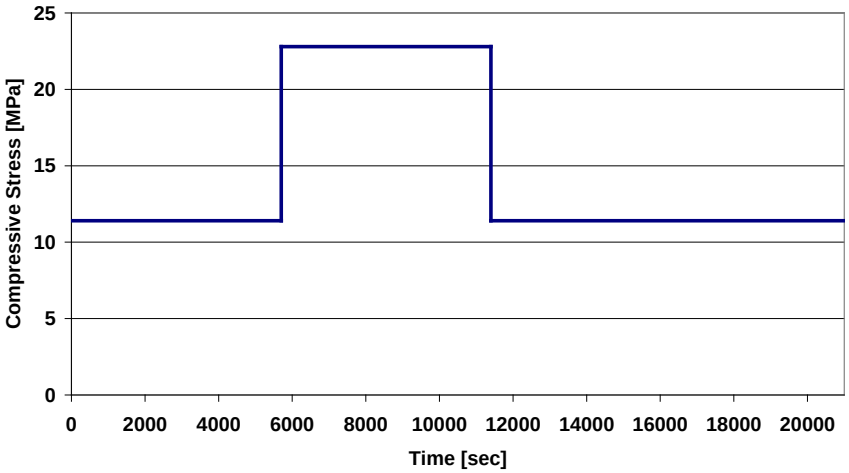

Fig. 7-5 - Stress-Time relationship with a step increase and a step decrease of load until the original stress level

Fig. 7-6 shows the results of the simulation with the stress-time curve according to Fig. 7-5.

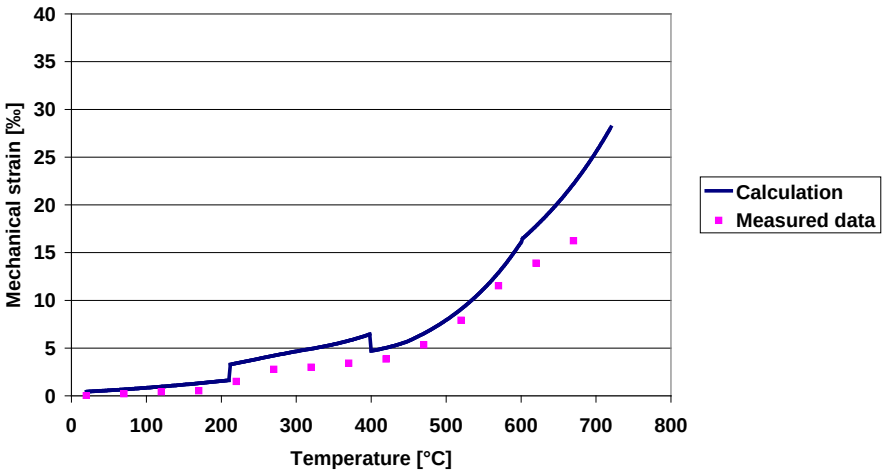

Fig. 7-6 - Comparison between calculated results and experimental results according to [L18] with the load function according to Figure 7-5

Generally, the curve approximation is good. The very high load of 60% between 210°C and 420°C indicates a slightly higher deformation than the measured data show, but this is accept-

able. Beyond the temperature of 600°C an identical behaviour occurs that is similar to the observation in example 1.

7.2.6 Applied Stress-time Relations and Calculated Strain Results – example 4

Fig. 7-7 shows a stress time relationship with 3 increasing and 3 decreasing steps. At the first step, the load increases from 16% up to 32 % at a temperature of 220°C. After 45 minutes the load increases to 17 N/mm² which is 45% of the compressive strength at ambient temperature. The temperature is 200°C. After further 45 minutes with constant load, the next step to the maximum load level starts. The load level is 60%. The temperature at this point is 300°C. The decreasing steps of load follow the same rules. Every 45 minutes the next step is followed. The maximum temperature reaches 720°C.

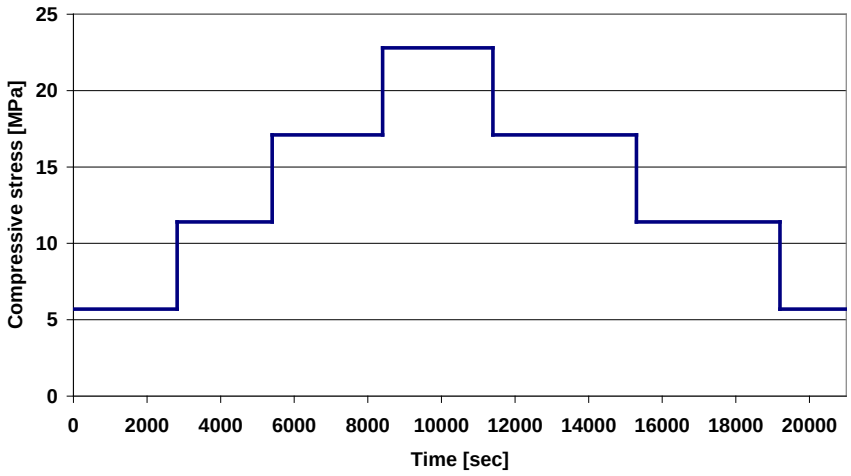

Fig. 7-7 - Stress-Time relationship with 3 steps with an increase level in load and 3 steps with a decrease in load until the original level

Fig. 7-8 shows the results of the analytical calculation with the stress-time relationship taken from Fig. 7-7.

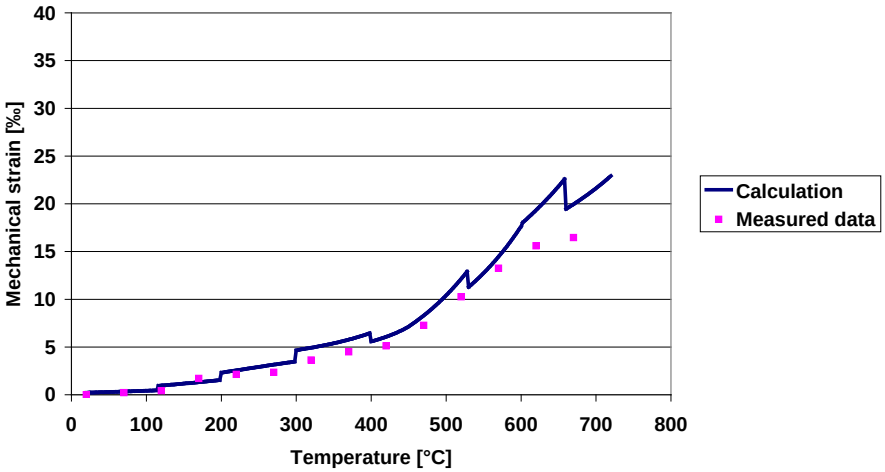

Fig. 7-8 - Comparison between calculated results and experimental results according to [L18] with the load function according to Figure 7-7

There is a rather good agreement between measured and calculated results in the fourth example. The results are calculated with consideration of material laws depending on transient temperatures and load history as discussed before. Beyond the temperature of 600°C the same behaviour is observed similar to examples 1 and 3. In conclusion, the calculated results show a good approximation in accordance to the measured data. The usability of the new ATC-model is proven.

7.3 Calculation of Total Strains with the Finite Element Model Compared to Measured Data

7.3.1 Model Parameters and Content of the Results

According to Chapter 8.2, the analytic method according to [L18] allows the calculation of the total strain of test specimen under transient temperature and load conditions. The calculation results are in good agreement with the experimental data.

In the following chapter, these measured data are compared to results of different finite element calculations with different material models. These material models are the EC2-model and the ACT-model.

The calculation was done with different load functions during heating which were already shown and described in Chapter 8.2. The ATC-model method is also approximately good for the mechanical strain in accordance to measured data according to [L18].

The specimens and tests to be investigated are the same concrete cylinders according to Chapter 8.2 as well as for the heating rate and compressive strength.

In the advanced transient concrete model (ATC-model), the total strain model after chapter 5 is used. The FEA uses material models taken from the Eurocode 2 with a stress-strain constitutive model with a minimum, recommended and the maximum value of the peak stress strain. The minimum value of the peak stress strain is nevertheless not considered in this investigation be-

cause the results obtained with this assumption gave an unreliable data compared to the other models.

The ATC-model considers all new material features from the model described in Chapter 5.

7.3.2 Finite Element Analysis with Different Material Parameters – example 1

The load function as stress-time relationship of a constant increasing load is given in Fig 7-1. The comparison between the ATC-model method and the EC2 calculation with the recommended values of peak stress strain (EC2(a)-model) and the EC2-model calculation with the maximum values of peak stress strain (EC2(b)-model) after table 5-1 are given in Figure 7-9.

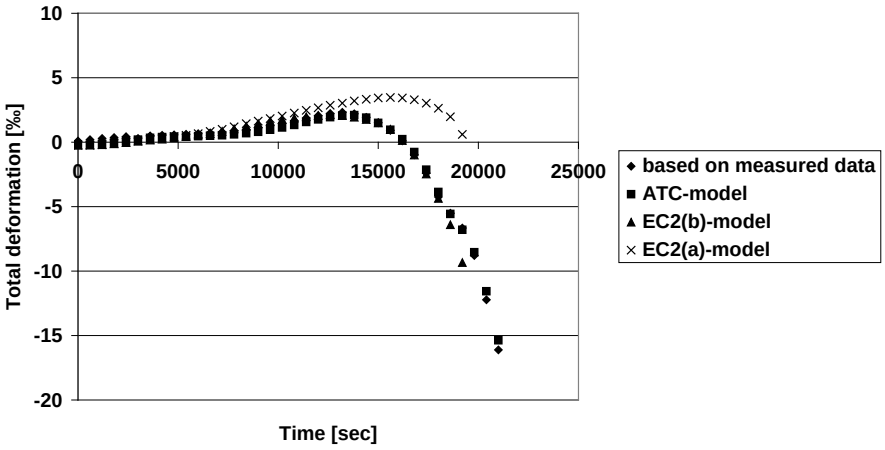

Fig. 7-9 - Comparison of measured and calculated total strains under an applied load function according to Figure 7-1

The ATC-model with the transient strain model is approximately very good compared to the measured based data. The result of the calculation with EC2(b)-model is generally as good as the approximation by the ATC-model. The calculation with the recommended value of PSS in the EC2(a)-model is totally different after 3.5 h of heating. The maximum temperature is 720°C. This is why a failure was observed at the end of simulation time for the EC2(a)-model.

7.3.3 Finite Element Analysis with Different Material Parameters – example 2

In Figure 7-3 the evolution of stress as a function of time with respect to temperature which has with a linear increase until 15,000 seconds and a linear decrease thereafter is given. Figure 7-10 shows the results of the comparison.

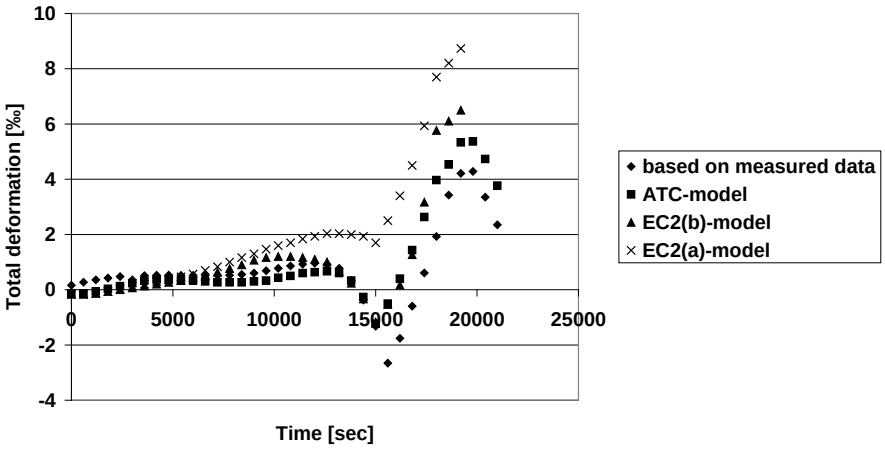

Fig. 7-10 - Comparison of measured and calculated total strains under an applied load function according to Figure 7-3

The results of the EC2(b)-model and the finite element simulation with the ATC-model are in good agreement with the measured data. The calculation with EC2(a)-model indicates a generally higher deformations compared to the measurements and the other calculations, hence, it is not applicable in this case.

7.3.4 Finite Element Analysis with Different Material Parameters – example 3

The load function as stress-time relationship with a stepwise application of load and a stepwise unloading is given in Figure 7-5. The comparison between the different models is shown in Figure 7-11.

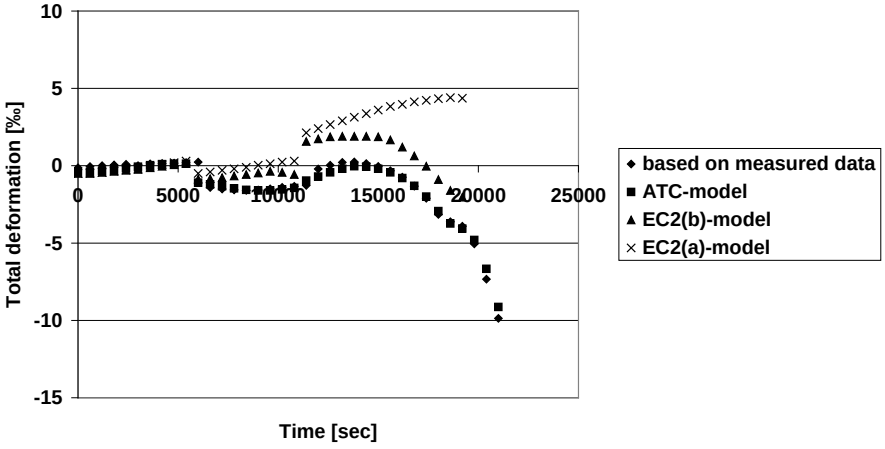

Fig. 7-11 - Comparison of measured and calculated total strains under an applied load function according to Figure 7-5

After the start of the test, i.e. until 5,000 seconds the comparison between the two calculation methods with the ATC-model is comparatively good. With increasing time (temperatures), higher differences between the total strains calculated with the ATC-model and the EC2(b)-model are observed. The result of the calculation with the EC2(a)-model is significantly different from calculations with the ATC-model and from the test results, hence, this model is not applicable in this case.

7.3.5 Finite Element Analysis with Different Material Parameters – example 4

Figure 7-7 shows the load function as a stress-time relationship with 3 steps of increase and 3 steps of decrease in load. Figure 7-12 shows the comparison between the different calculation models.

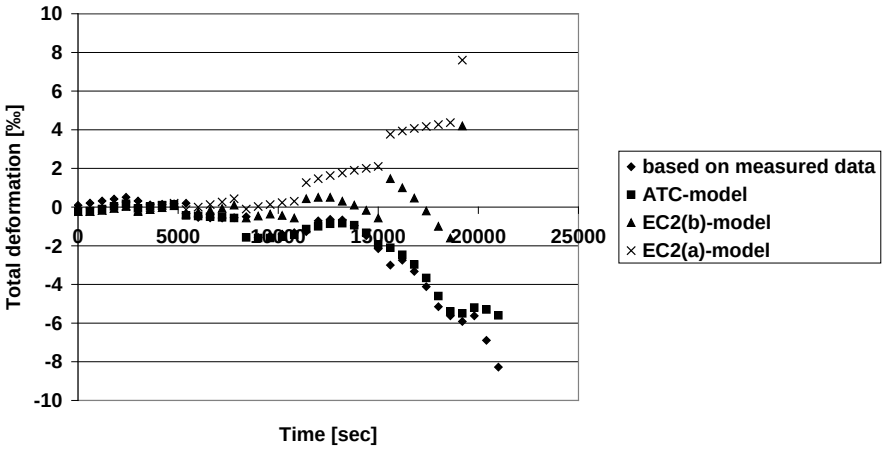

Fig. 7-12 - Comparison of measured and calculated total strains under an applied load function according to Figure 7-6

The test results are generally very good particularly the approximated calculations using the ATC-model. With increasing numbers of load steps, a general increase of differences between the calculations with EC2-model and ATC-model occurs. The EC2-model, in whatever chosen value of PSS ,does not allow calculating the total deformations under a load function with a complex stress-time relationship. For this type of calculations at the time being, only the ATC-model simulation allows to simulate realistic total deformations of the concrete and transient temperature conditions.

7.4 Calculation of Transient Restraint Axial Forces for Concrete Cylinders under Heating-up and Zero Axial Strains

7.4.1 Model Parameters and Content of the Results

The calculation of forces due to restraint is very important in complex structures i.e. frames where the bending moment in the corner is often the most loaded point of the structure. During heating-up under a catastrophic fire, the bending moment meets the maximum value. At this point full restraint occurs during the thermal expansion.

The objective of the investigation is the calculation of restraint forces of fully restraint concrete cylinders under 100% restraint (ε_{tot} = 0) during heating-up to the temperature of 700°C at maximum.

The specimens are calculated with the ATC-model under an axial load. The load at t = 0 is given by a mechanical compressive strain of 30% of the compressive strength. The results are compared with measured data.

The measured data are a perfect basis for the comparison of existing high temperature material models for the calculation of the deformations and relaxation of concrete members subjected to fire. The calculations by FEA were done using the structural code SAFIR.

The specimens are cylinders with 80 mm diameter and 300 mm height. Heating rate is 2 K/min. The compressive strength of the siliceous concrete at 20°C is 27.9 MPa. The moisture content is 1.5 % per mass [L18]. The curing reached from storage under water until standard climate condition (20°C/50% r.h.):

- Curing under water,
- Pre-dried with 105°C and
- Standard curing.

7.4.2 Results of Restraint Cylinders Calculation

In the following figures the results of the calculation with the ATC-model are compared with measured data. Figure 7-13 shows the measured transient restraint axial forces during heating with an initial load factor of 0.3. The measured data are based on different storage conditions during curing.

In the following, the results of the calculation with the ATC-model are compared according to measured data taken from [L18].

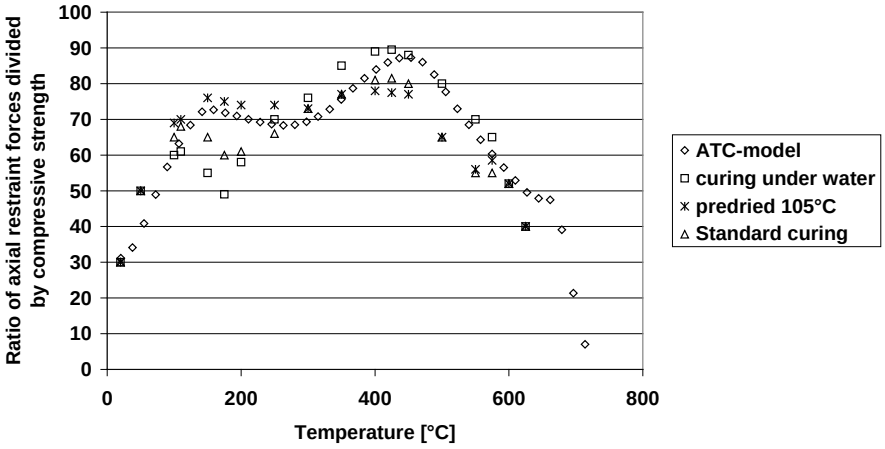

Fig. 7-13 – Transient restraint axial force during heating-up of a specimen in initial load of 30% of reference strength compared to measured results

The curve of the ATC-model is below the data of 105°C dried concrete specimen until 300°C and near the standard cured concrete (w = 1-4 %). Above the temperature of 300°C the curve of the ATC-model is close to the curve of water stored specimen. The curve of ATC-model lies in the confidence interval of all three experimental curves.

Figure 7-14 shows the ratio of restraint axial force divided by compressive strength for a comparison of transient restraint axial forces by different load conditions. The EC2-model is a stress-strain constitutive model without considering a load factor, i.e. it does not give a good simulation result for restraint. The EC2(a)-restraint and the EC2(b)-restraint forces are much lower compared to the experimental values.

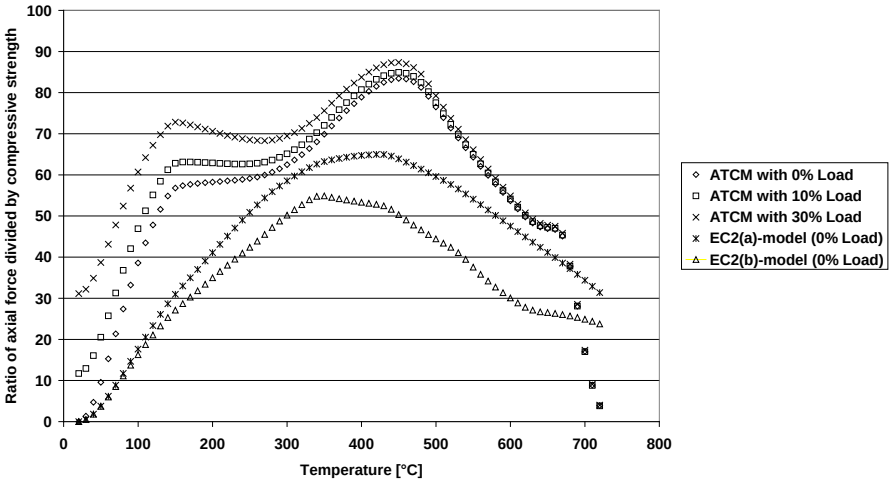

Fig. 7-14 - Comparison of restraint forces for different load factors according to [L18]

The lines of the calculation with the EC2(a)- and EC2(b)-model neither give a good approximation to the results of the ATC-model nor to the measured values after Fig. 7-14. From the experimental result of Figure 7-13 we come to the conclusion that the EC2(a)- and EC2(b)-model simulations do not meet the measured values. The restraint axial forces are significantly lower than the measured data.

With respect to practical applications, it is concluded, that restraint calculations after the EC2(a)- and EC2(b) material models lead generally to significant lower restraint forces than those of experimental observations, i.e. an underestimation of the height of restraint forces up to 100% in the range of 100 to 150°C is possible (see Fig. 7-14).

At a temperature of less than 420°C, the different load conditions indicate different restraint axial forces. At above 420°C the curves are nearly identical around a level of 80% of the reference strength at ambient temperature. The higher the load level the higher are the restraint axial forces.

Since the axial stress has a significant effect on the fire resistance of building elements according to [L144], a realistic simulation of restraint effects are important for loaded structures.

It seems that the calculation with the Eurocode models lead to a significant difference between the real measured data and the calculation results. The EC2(a)- and EC2(b)-model are not suit-

able for the determination of restraint during a fire incidence. The EC2(a)-model is stiffer in the stress-strain relationship and has a faster increase in the ascending branch of the PSS. This is why the restraint calculation may be higher than the softer material model of EC2(b)-model.

7.5 Small Scale Tests with Reinforced Columns

7.5.1 Principally Calculations and Experimental Set-up

Centric loaded columns were investigated with SAFIR using the new ATC-model too. Measured data were taken from [L145]. A comparison of the measured strains over the total length of the centrically loaded columns was performed. The model does not consider the accidental eccentricity of the load as recommended by EC2 for calculation of columns. However, it is better to show the effect of calculations using the EC2 material model and the new ATC-model [L146]. The results were obtained using the test equipment shown in Figure 7-15.

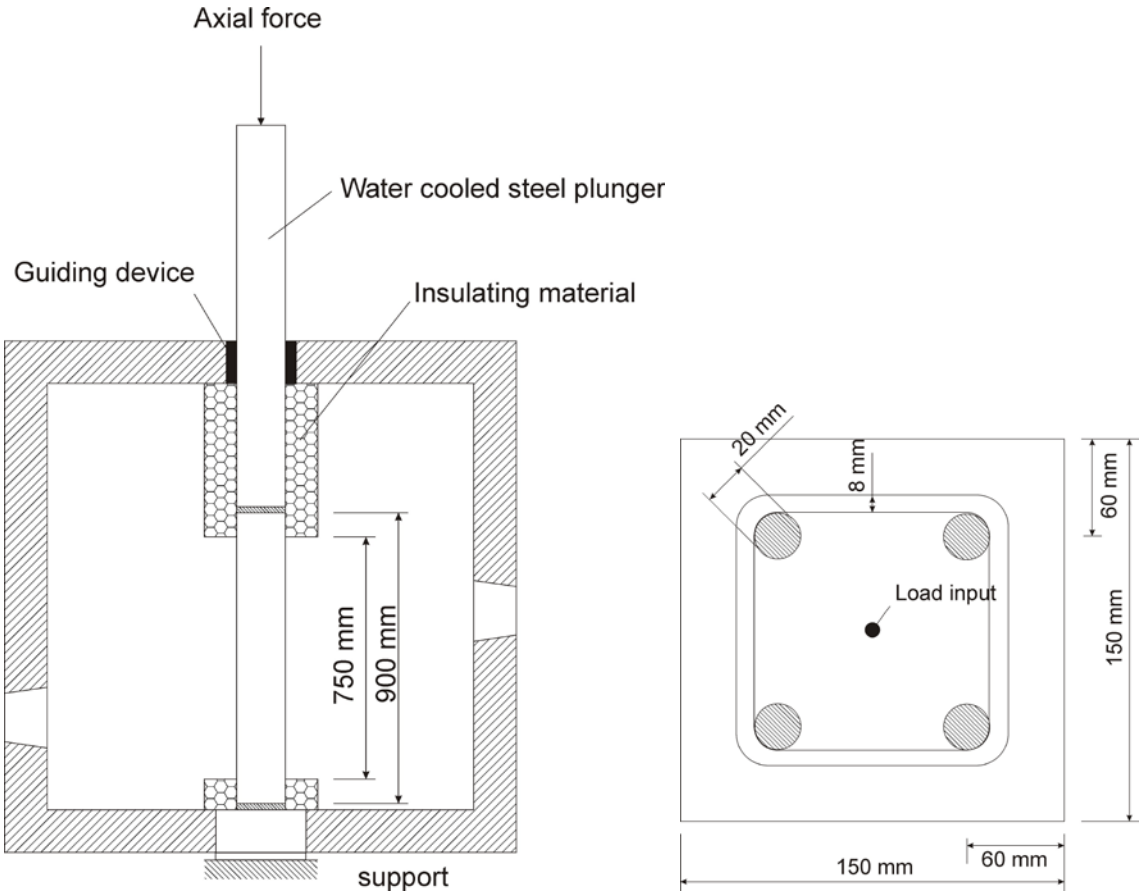

Fig. 7-15 – Principle sketch of test equipment and cross section of specimens

In these examples, the calculations are based on fire exposure test in accordance to the time-temperature curve according to ISO 834**,** as shown in Figure 7-16.

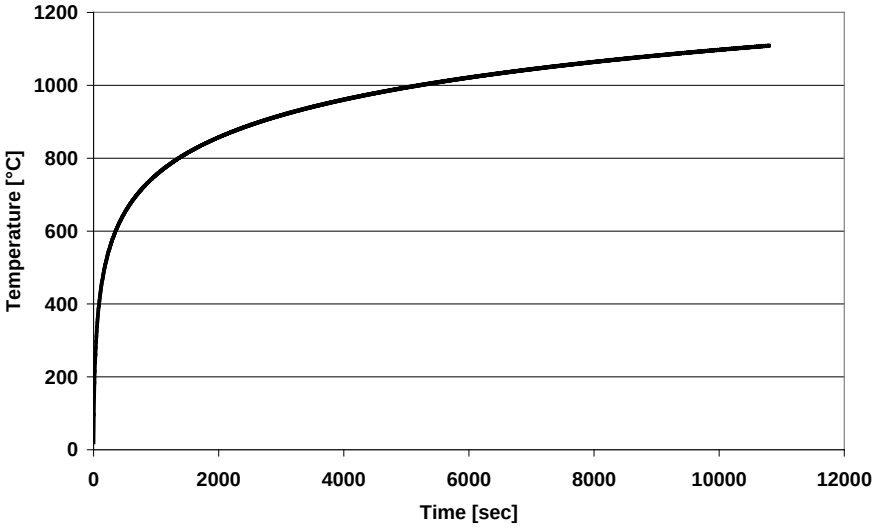

Fig. 7-16 - Fire curve according to ISO 834 after [L48]

The measured data of thermo couples across the cross section showed reasonable results with respect to the applied fire curve. The surface of the specimens showed a temperature of 1,000°C after 60 minutes that means practically that the fire curve at testing exceeded the standard fire curve. In the centre of the column, the temperature reached 350°C as a maximum. The results of the thermal analysis of the specimens using the SAFIR model compared to measured data are presented in Fig 7-17.

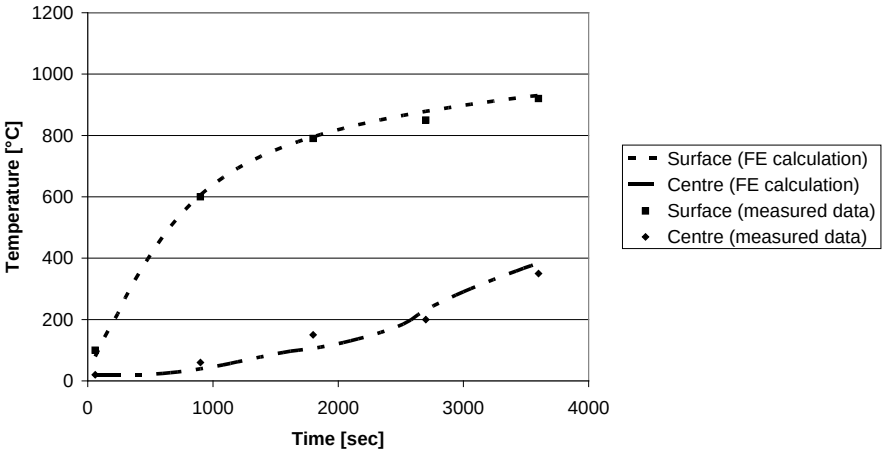

Fig. 7-17 – Measured and calculated temperatures at the surface and in the centre of the specimen

Five different specimens were tested using siliceous concrete mixtures with the following material properties: (Reinforcement: 4 bars ∅ 20 mm, yield strength = 500 MPa, stirrups ∅8 mm, cover 20 mm). In Table 7-1 the mixture parameters are shown in kg/m³. Table 7-2 shows the material properties and the test parameter of the load.

Tab. 7-1 - Mixture parameters of concrete for the mixtures 1 to 5

	Mixture 1	Mixture 2	Mixture 3	Mixture 4	Mixture 5
Cement content	320	320	320	320	320
Sand 0-2 mm	480	480	480	480	480
Gravel 2-8 mm	480	480	480	480	480
Gravel 7-16 mm	960	960	960	960	960
Plasticizer	10	10	14.2	10	10
Water	170	170	170	170	170
Dispersed silica	10	10	10	-	10
Dispersed micro silica	-	1.0	2.0	2.0	2.0

Tab. 7-2 - Material properties and load during heating of the mixtures 1 to 5

	Material properties						Test parameter
Mixture	Density [g/cm³]	$f_{c,cube,dry}$ [MPa]	f_{ck} [MPa]	E_{c0m} [MPa]	E_{cm} [MPa]	Moisture [% by mass]	Load [kN]
1	2.377	66	50	36762	34251	3.6	609.2
2	2.357	60	45	35776	32963	3.7	599.4
3	2.355	59	45	35606	32745	4.1	628.6
4	2.352	46	35	33234	29821	3.2	451.9
5	2.344	55	42	34910	31865	4.0	540.8

The tangent modulus (the modulus at zero strain) was calculated after [L147]

$$E_{c0m} = 9500 * \left(f_{ck} + 8 \right)^{\frac{1}{3}} \qquad \text{equ. (7.1)}$$

and for Young's modulus is used:

$$E_{cm} = \left(0.8 + 0.2 * \frac{f_{ck} + 8}{88} \right) * E_{c0m} \text{ with } E_{cm} \le E_{c0m} \qquad \text{equ. (7.2)}$$

The concrete mixtures 1 to 5 were altered using different amounts of dispersed silica and fine dispersed micro silica in the mix. It should be noted that the ATC-model used in this investigation was developed for ordinary concrete without any modifications by addition of small amounts of dispersed silica. But as the concrete strength of all specimen tested was below 66 N/mm² it is assumed that the material model is still applicable.

7.5.2 Results of Small Column Calculation

In the investigation, the results obtained by the ATC-model were compared with the results of calculations using the two EC2(a)- and EC2(b)-models (ENV with recommended and maximum value of the peak stress strain), see table 5-1. The measured data were taken from [L48]. The comparisons show the four transient longitudinal strains ε_{tot} of the specimens. Between the results of the three calculation models significant differences were observed. The EC2-model uses

the curve of siliceous concrete and the new ATC-model uses the curve of siliceous concrete [with high siliceous content]. The ATC-model considers the influence of external load during heating on the stress-strain relationship of concrete and the transient creep effect. Due to the ATC-model, the concrete indicates a wide range of compressive strains at failure, whereas the EC2-model shows a more or less brittle type of failure. Fig. 7-18 shows the comparison between the results of the ATC-model with mixture 1 (the mixture highest Young's modulus of 34,250 N/mm²).

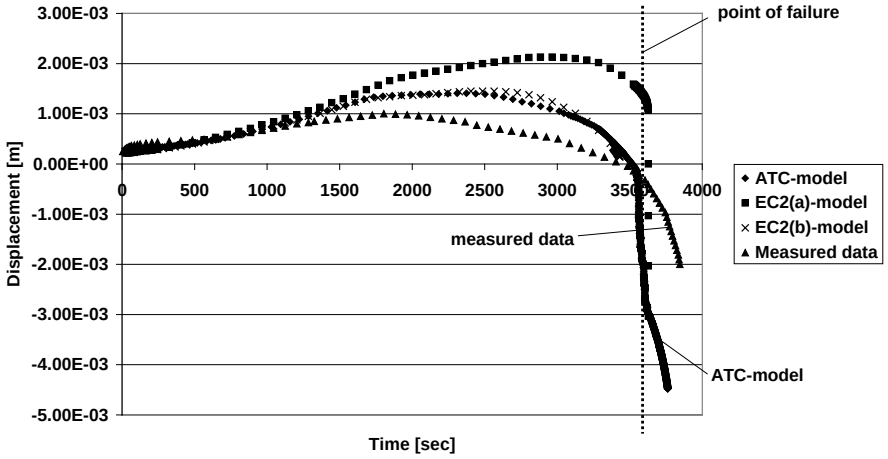

Fig. 7-18 - Calculation results compared to measured data - mixture 1

The results of the ATC-model and the EC2(b)-model with the maximum PSS are nearly identical. Only small differences between the calculation results and the measured data are observed. The failure behaviour is identical compared to the measured data. The results of the EC2(a)-model with the recommended value of PSS are different, but the point of failure is below the measured data.

Fig. 7-19 shows the examination with mixture 2.

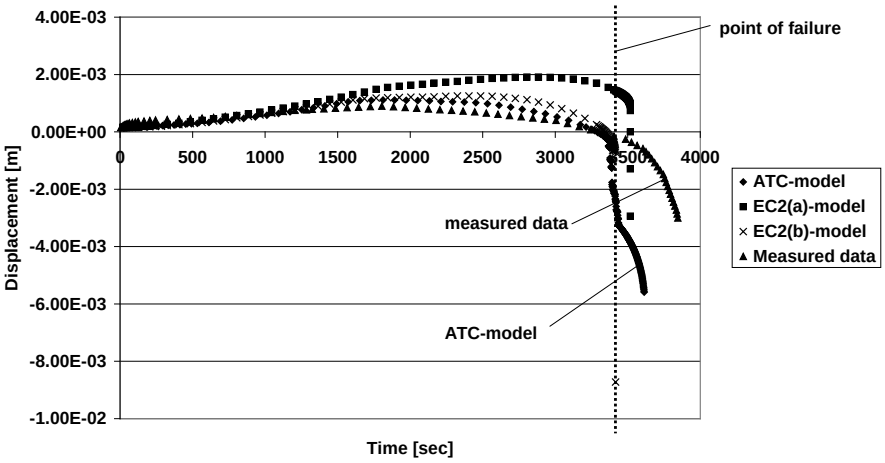

Fig. 7-19 - Calculation results compared to measured data - mixture 2

The curves of the ATC-model and the EC2(b)-model are very close. Both curves are in good agreement with the measure data. In this investigation, the Young's modulus was 33,000 N/mm². The EC2(a)-model did not meet the curve of measured data.

Fig. 7-20 shows the results with mixture 3. The Young's modulus is very close to the value of mixture 2.

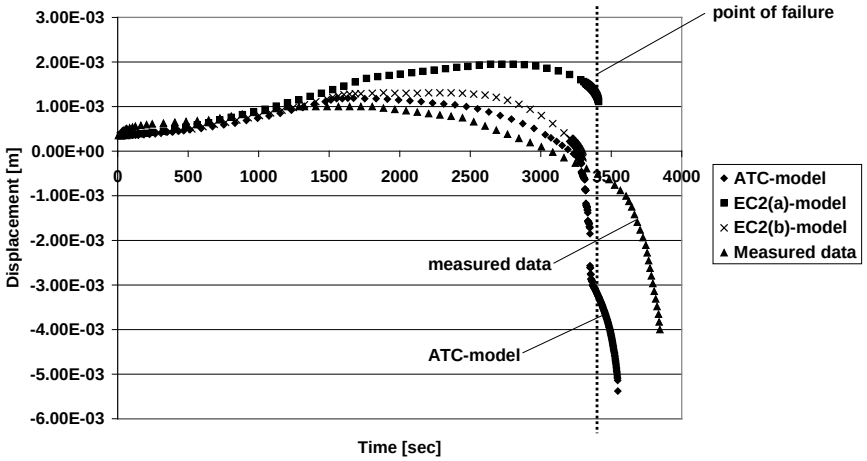

Fig. 7-20 - Calculation results compared to measured data - mixture 3

The results of the ATC-model are more approximated to the measured data than the results of the calculation with the EC2(b)-model. It can also be seen that the recommended value of the EC2(a)-model does not meet the test results.

Fig. 7-21 shows the results of the mixture 4. The Young's modulus is 30,000 MPa.

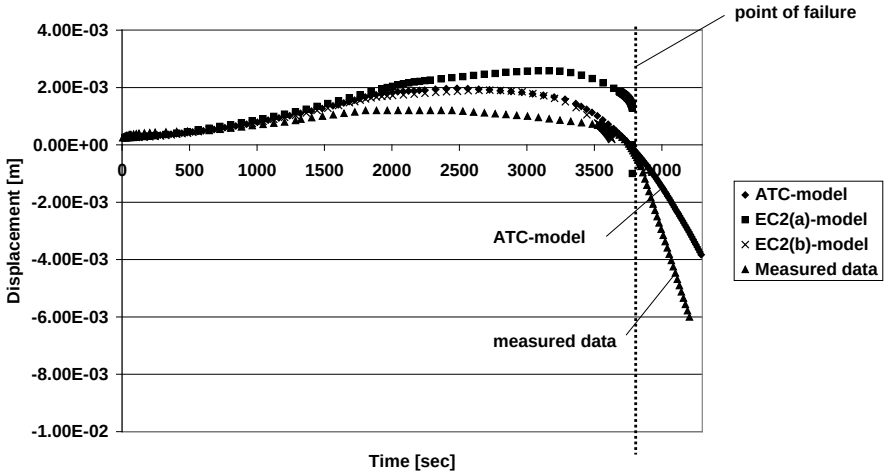

Fig. 7-21 - Calculation results compared to measured data - mixture 4 (without dispersed silica)

In this figure, one can see that the curve of the EC2(a)-model is evidently not in agreement with the curve of the measured data. A difference between the two other simulations is also observed. The ATC-model has comparatively met the failure time and displacements.

Fig. 7-22 shows the results of mixture 5 with a Young's modulus of 31,000 N/mm² and the highest content of micro silica.

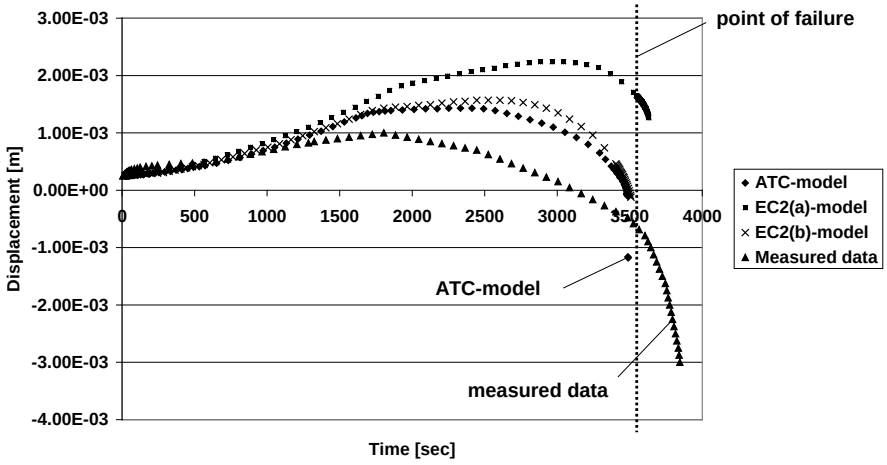

Fig. 7-22 - Calculation results compared to measured data - mixture 5

All displacement curves are not in good agreement compared to the measured data. It is also evident that the recommended value of PSS in the EC2(a)-model did not meet the curve of measured data. The curves of the EC2(b)-model and the ATC-model are very close, but the time of failure is underestimated by five minutes.

Generally, the measurements started after loading the columns and the calculated results were adapted to the level of deformation at that time. The result of mixture 2 to 4 gave the best approximation with respect to the measured data. On one of these tests specimen, no micro silica was used and the Young's modulus is less than 31,000 N/mm². The specimen with silica indicated a Young's modulus higher than 32,000 N/mm², i.e. the modulus is higher than for ordinary concrete. Generally there is a good agreement between measured and calculated results in long time behaviour of the columns.

It was found that for mixtures with higher Young's modulus, the failure in the calculation starts at a time of about 50 minutes. The simulation with the ATC-model that considers the creep part of the deformation is very good up to this time. It should be noted that the model of concrete was originally developed for ordinary concrete with a Young's modulus of less than 30,000 N/mm². With higher Young's modulus, the results of the calculation met the measured strains very well up to the time of 50 minutes, but the failure of the specimen is more brittle and started still earlier than the deformations from our material model. The current model does not consider the specific reduction of the compression strength of high performance concrete and uses a φ-function for the transient thermal creep strain according to ordinary concrete. Nevertheless, we have also obtained a very high accuracy in our calculations with the ATC-model for ordinary concrete compared to existing structural tests of concrete with a higher Young's modulus.

The calculations with the average value of ultimate strain according to Eurocode 2 predicted much higher strains of concrete columns compared to the measured data, but the time of failure is agreeably calibrated to the ISO curve. The failure behaviour of concrete with Young's modulus higher than 32,000 N/mm² is close to the EC2(b)-model. The failure point and ultimate strain of mixture 4 is nearly identical to the calculation with the ATC-model. Generally, one can state that the strain prediction of the EC2 is less accurate than the calculated data using the ATC-model. For natural fire curves, the EC2-model is not calibrated and therefore may not be used for strain or restraint calculations at high temperatures.

7.6 Calculation of Structures

7.6.1 Principal Calculations and Experimental Set-ups for Columns

In this chapter, the calculations of a column under fire using the ATC-model compared to the EC2(b)-model with the maximum value of peak stress strain are shown. An eccentrically loaded column with a cross section of 30 x 40 cm was calculated with three different material models.

The column was prepared using a siliceous concrete mixtures with the following material properties (Concrete: compression strength 35 MPa, Reinforcement: 6 bars ∅ 25 mm, yield strength = 500 N/mm², cover 37.5 mm).

The constant loads of the column are:

- Dead weight of the reinforcement concrete by 3 kN/m,
- Assumed horizontal load by 10 kN,
- Assumed eccentric vertical load on top of the column by 200 kN.

The variable (see Eurocode 2) loads of the column are:

- Assumed horizontal load by 5 kN,

- Assumed beam load by 2,4 kN/m (wind load),
- Assumed eccentric vertical load on top of the column by 100 kN (variable load).

The combination factors according to EN 1991-1-2 [L48] for permanent loads are:

- ψ_1 = 0.2 for wind load and
- ψ_1 = 0.5 for traffic load.

For quasi permanent load the combination factors according to [L108] are:

- ψ_2 = 0.0 for wind load and
- ψ_2 = 0.3 for traffic load.

The fire curve is taken according to the standard ISO 834, see Fig.7-16.

In this model, the accidental eccentricity of the load as recommended by EC2 for the calculation of columns was taken into account. The geometry of the structure in the calculation model is shown in Figure 7-23.

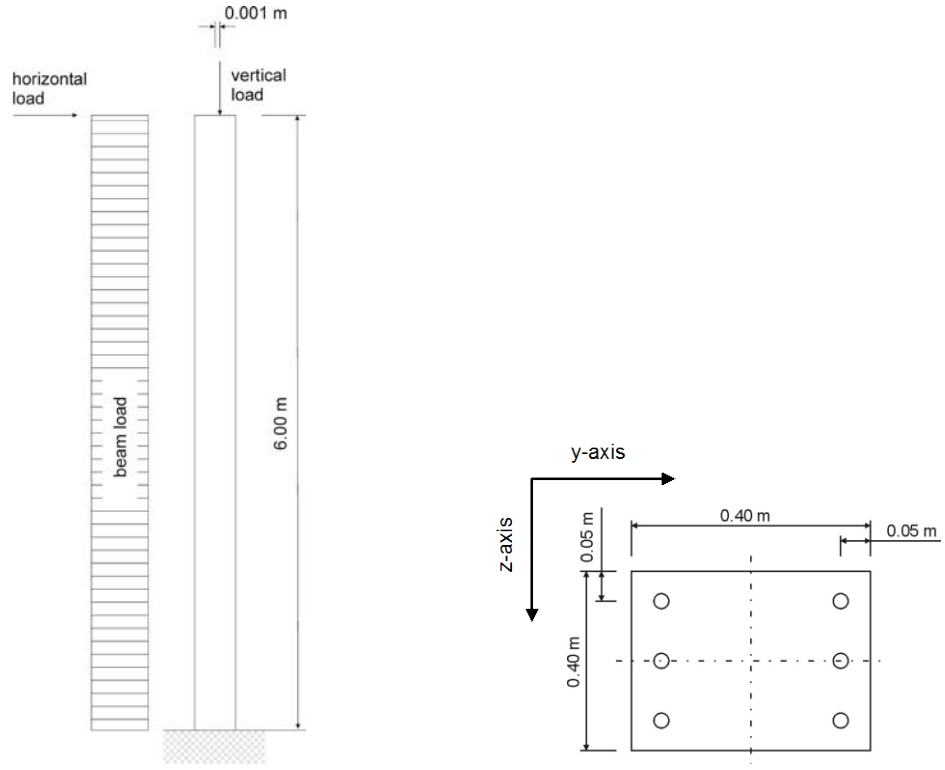

Fig. 7-23 – Length, cross section and load of the investigated column

7.6.2 Results of the Calculation of Column

In the following figures, a comparison is made between the calculation results obtained by the ATC-model and the EC2-model (ENV with recommended (EC2(a)-model) and maximum (EC2(b).model) value of the peak stress strain) taken from [L52].

The following Figures show the stress distribution across the cross section at different times of the calculation. The calculations use the EC2(b)-model with the maximum value of PSS and the ATC-model. Fig. 7-24 shows the results before the fire starts.

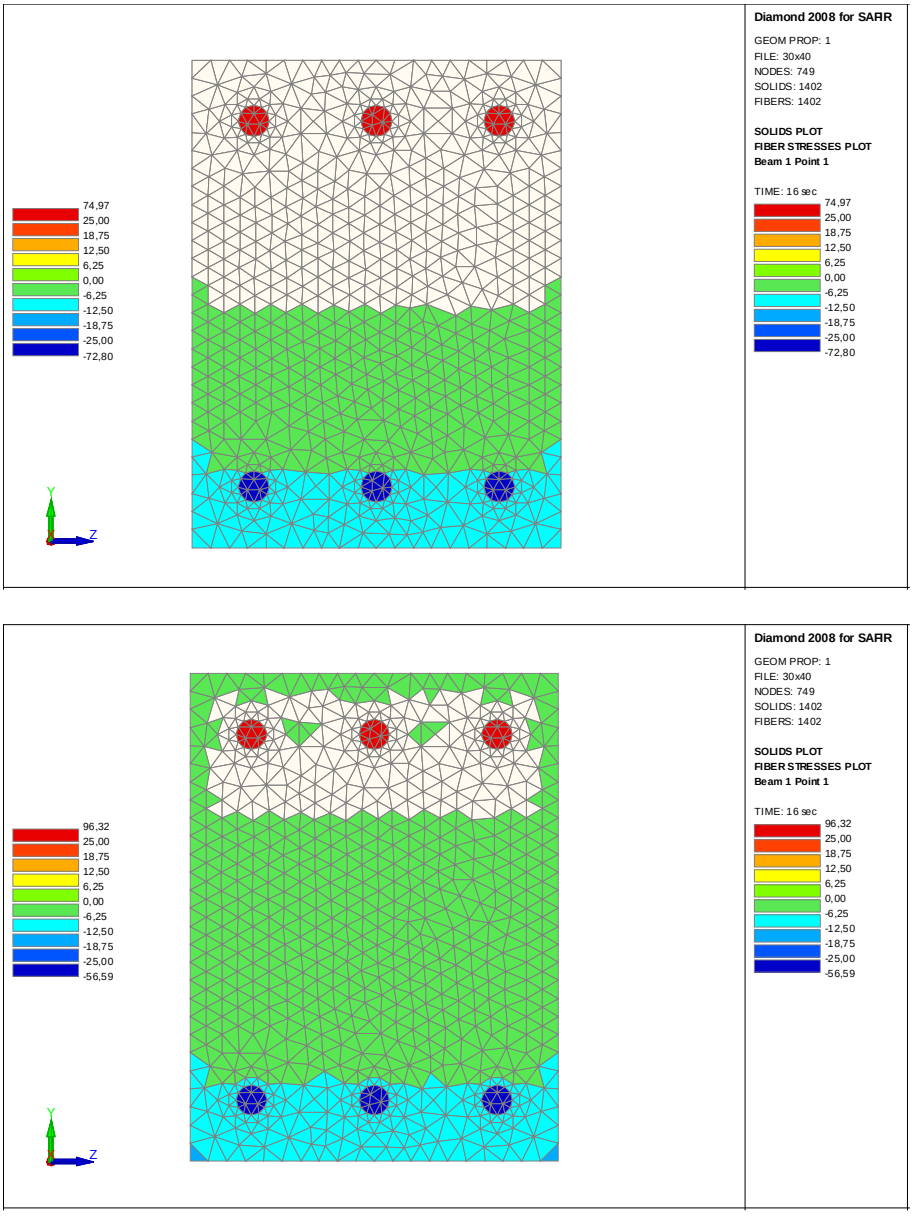

Fig. 7-24 - Stress in each finite element across the cross section before fire exposure (top EC2(b)-model, bottom ATC-model)

The band of stress distribution across the cross section in the calculations with the EC2(b)-model with the maximum value of PSS is significantly smaller than that of the ATC-model. The stress in the rebars is identical between the two models. The differences of the stress distribution inside of the cross sections are very small. The different colours show a very small range of less than 0.25 N/mm². In the ATC-model, the tensile strength was activated at 10% of the compressive strength and this is why Fig. 7-24 to 7-32 shows a different range of tensile stress inside the column with the ATC-model. In the EC2(b)-model, the tensile strength was not activated because this is the default value for the concrete model. Generally this is irrelevant for the conclusions of this examination.

Fig. 7-25 shows the results of the thermal calculation after 1200 seconds after the fire starts for both material models.

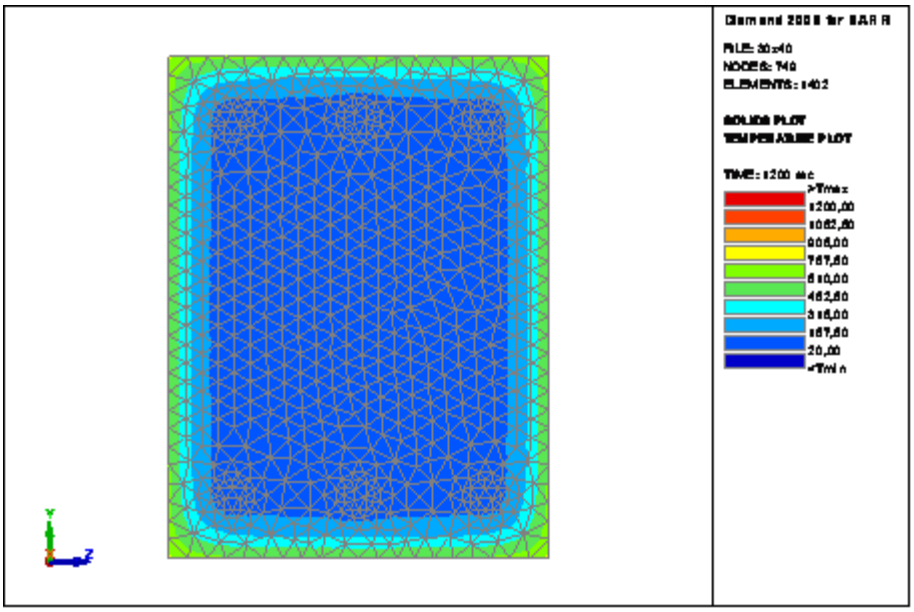

Fig. 7-25 – Temperature distribution across the cross section after 1200 seconds after fire exposure for both material models

The temperature of the surface is 780°C. The centre of the column is constant at 20°C. The heat penetration is about 50 mm as maximum.

Fig. 7-26 shows the results of the stress distribution after 1200 seconds after the fire starts.

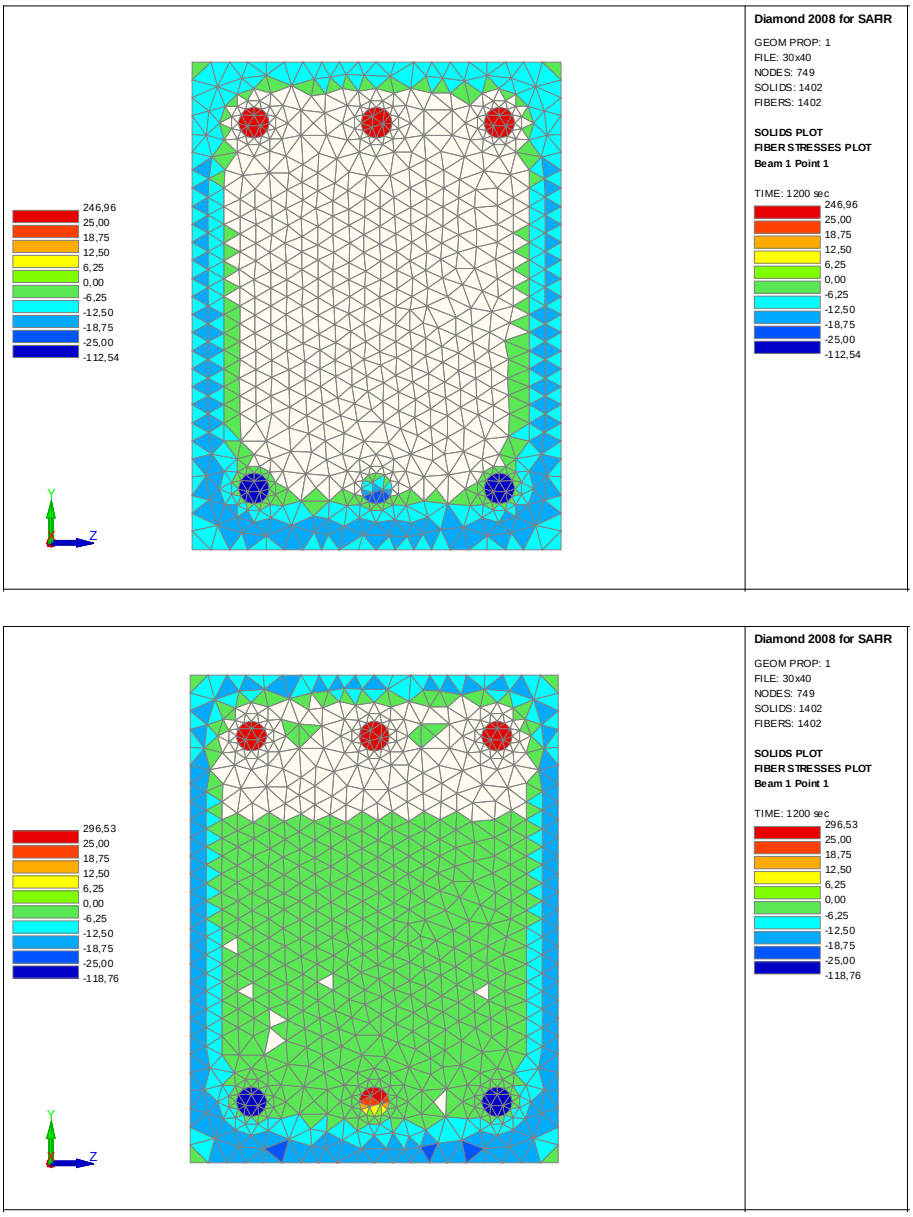

Fig. 7-26 - Stress in each finite element across the cross section after 1200 seconds after fire exposure (top EC2(b)-model, bottom ATC-model)

Irrespective of the stress distribution at the beginning, the stress distribution in the ATC-model is less pronounced than in the EC2(b)-model. A different stress distribution is observed in the central rebar at the side with the eccentric load. The stress is higher in this rebar for the ATC model.

Fig. 7-27 shows the results of the thermal calculation after 2400 seconds after the fire starts for both material models.

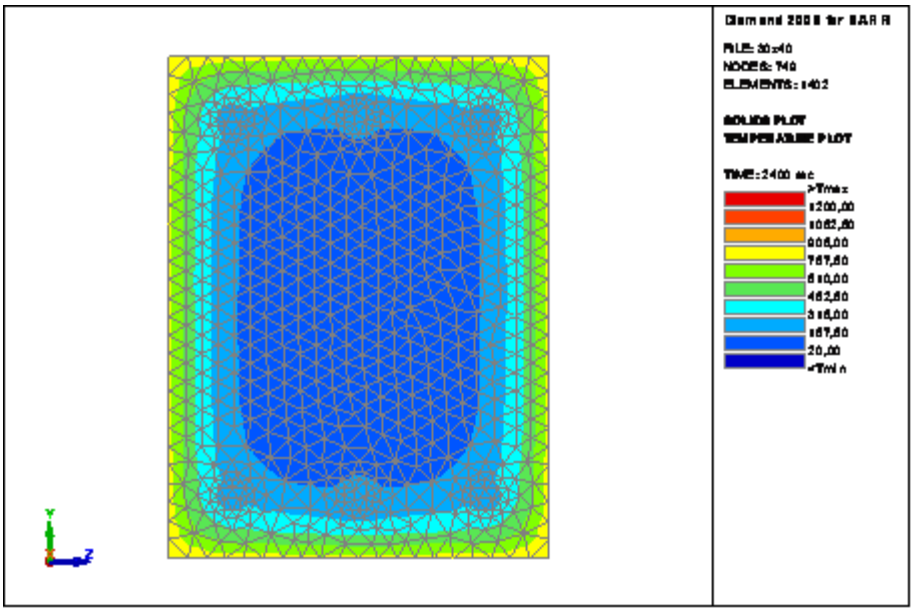

Fig. 7-27 – Temperature distribution across the cross section after 2400 seconds after fire exposure for both material models

The temperature of the surface is 885°C. The centre of the column is constant at 20°C. The heat penetration is about 80 mm as maximum.

Fig. 7-28 shows the results of the stress distribution after 1200 seconds after the fire starts.

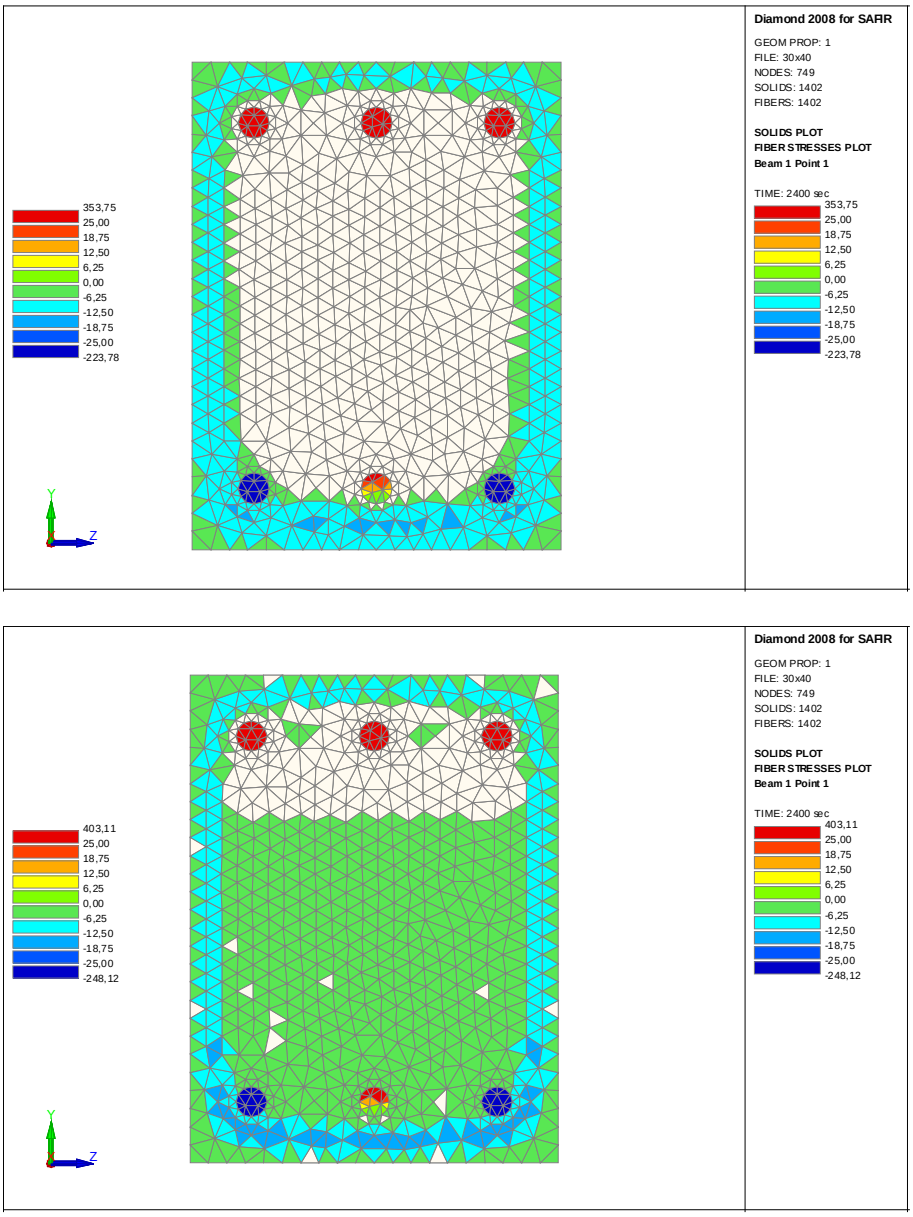

Fig. 7-28 - Stress in each finite element across the cross section after 2400 second after fire exposure (top EC2(b)-model, bottom ATC-model)

The stress distribution is relatively constant compared to the results at 1200 seconds. The stress in the mentioned rebar increases in the EC2(b)-model. Finally, the stresses are relatively identical in the rebar. The stress in the ATC-model at the eccentric loaded side is slightly lower than in the EC2(b)-model.

Fig. 7-29 shows the results of the thermal calculation after 3600 seconds after the fire starts for both material models.

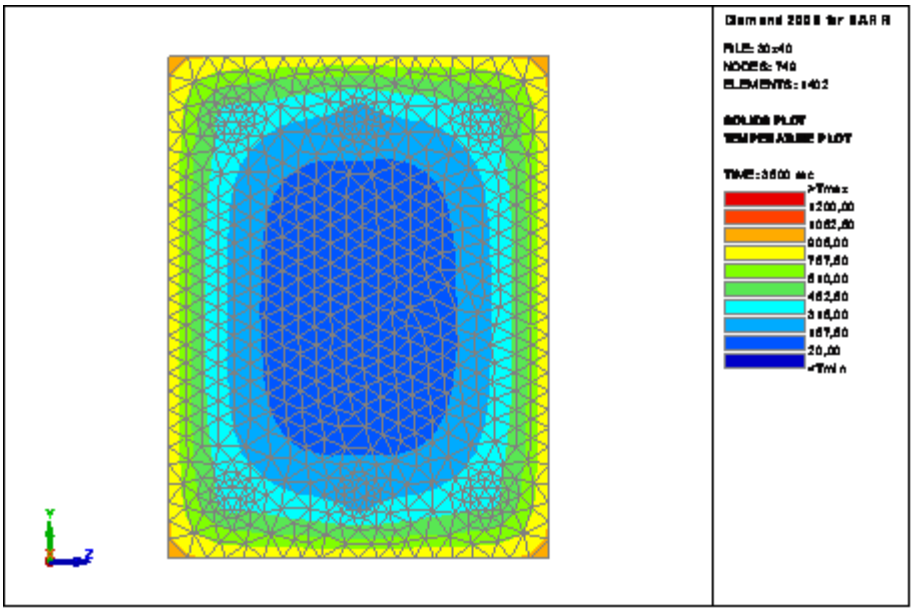

Fig. 7-29 – Temperature distribution across the cross section after 3600 second after fire exposure for both material models

The temperature of the surface is 940°C. The centre of the column is constant at 20°C. The heat penetration is about 120 mm as maximum.

Fig. 7-30 shows the results of the stress distribution after 3600 seconds after the fire starts.

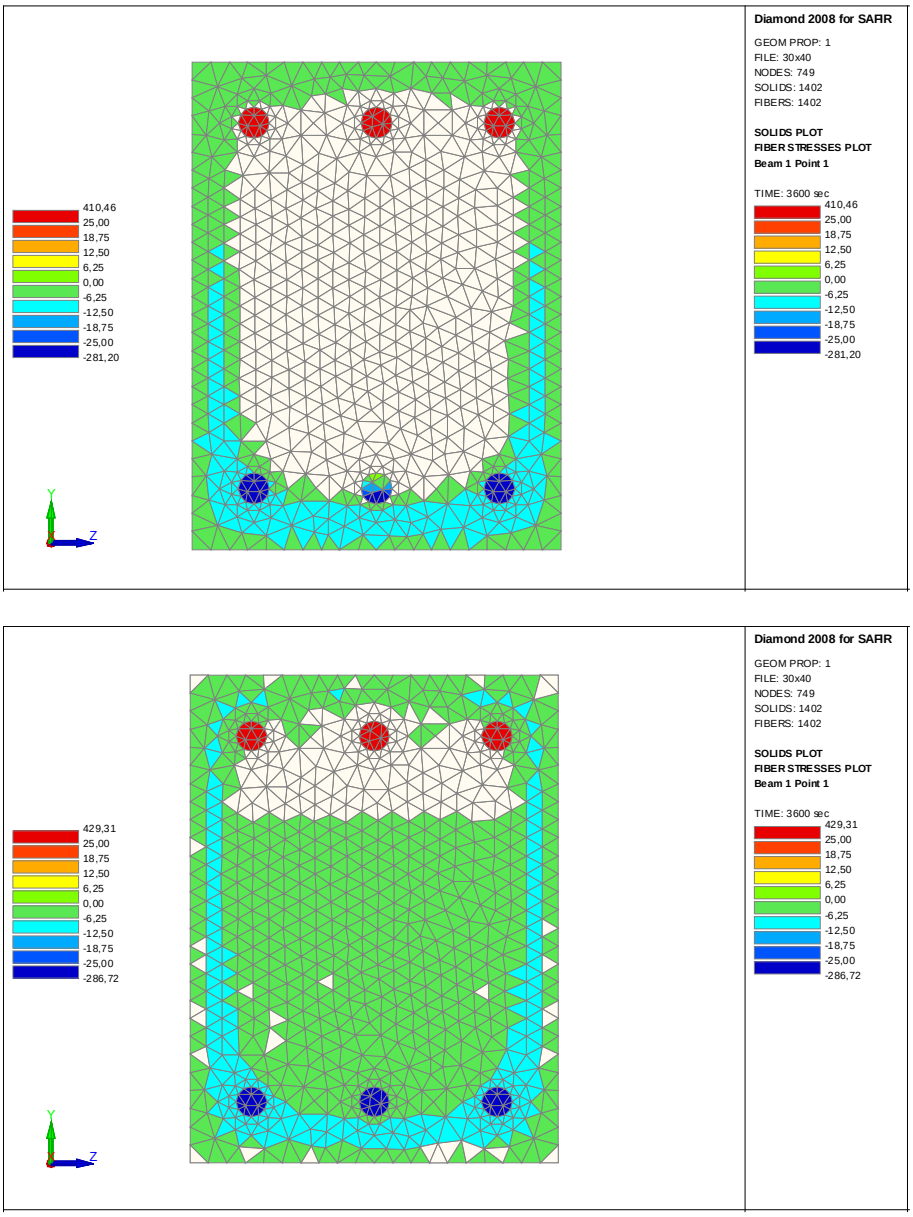

Fig. 7-30 - Stress in each finite element across the cross section after 3600 second after fire exposure (top EC2(b)-model, bottom ATC-model)

The compressive stresses increase in the boundary areas. The stress in the rebar in the middle of the eccentric loaded side decreases. The stresses are solely in the eccentric loaded side of the cross section.

Fig. 7-31 shows the results the thermal calculation after 4800 seconds after the fire starts for both material models.

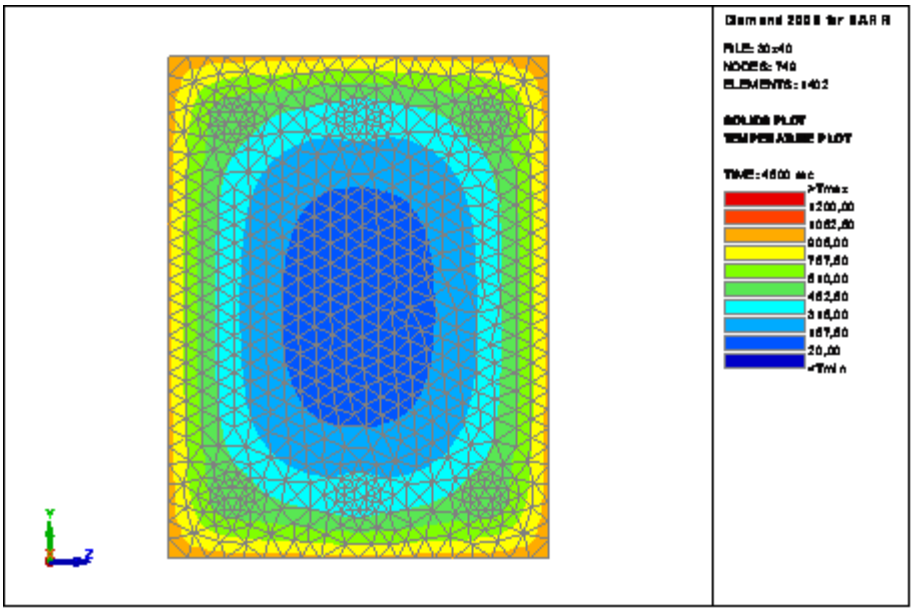

Fig. 7-31 – Temperature distribution across the cross section after 4800 second after fire exposure for both material models

The temperature of the surface is 990°C. The centre of the column is constant at 20°C. The heat penetration is about 150 mm as maximum. The column collapses after this time in the simulation.

Fig. 7-32 shows the results of the stress distribution after 4800 seconds after the fire starts.

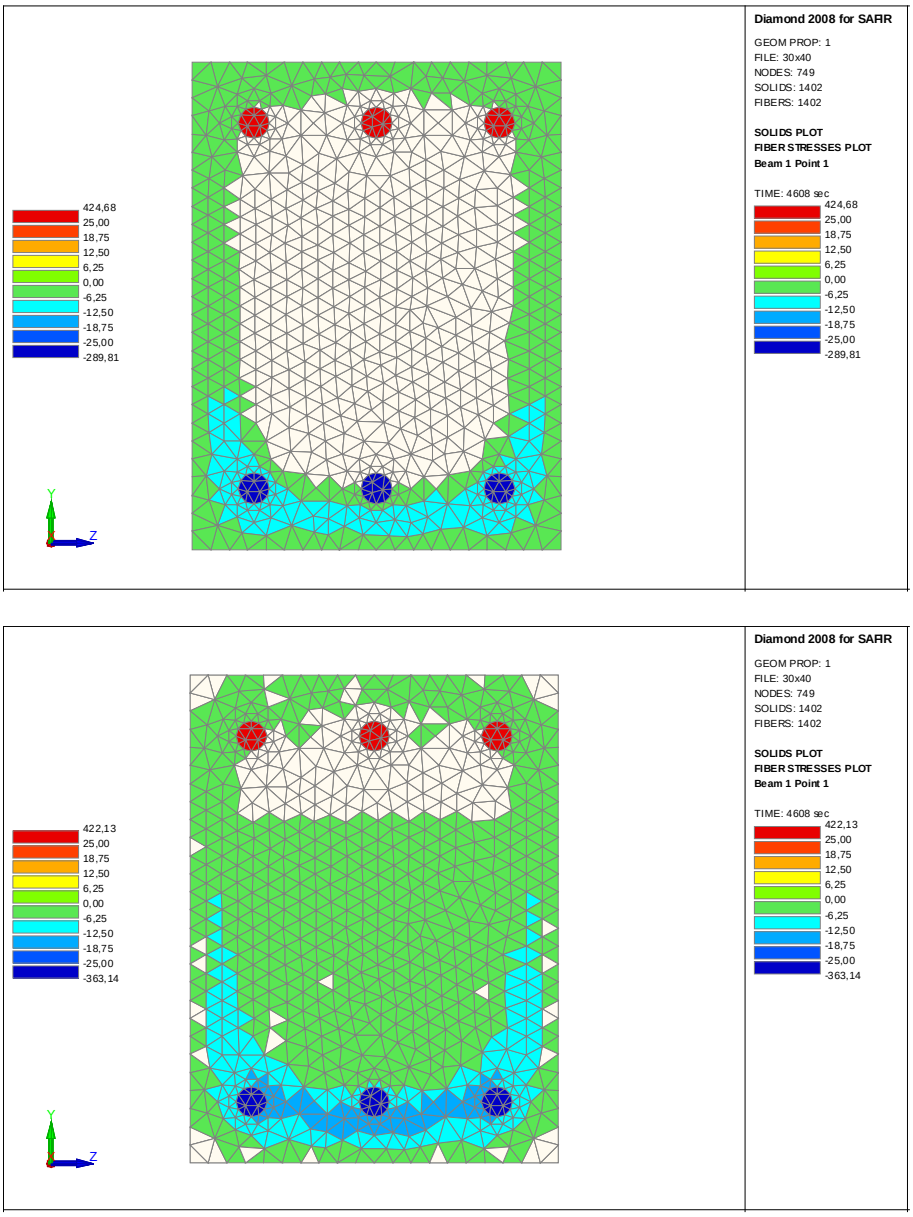

Fig. 7-32 - Stress in each finite element across the cross section after 4800 second after fire exposure (top EC2(b)-model, bottom ATC-model)

Before the column collapses, the stresses concentrate on the eccentric loaded side in both models. The concrete stresses in the ATC-model are slightly higher than in the EC2(b)-model. The failure starts earlier for the ATC-model.

The most part of the compressive loads is covered by the steel bars. This is why the stresses are concentrated in a zone around the steel bars and not over main parts of the concrete part of the cross section.

It was shown that the difference between the ATC-model and the EC2(a)- and EC2(b)-models is significant for the stresses across the cross section. In the following, the results of the displacements on top of the column in x-axis and y-axis are shown.

Figure 7-34 shows the vertical displacements of the x-axis of the calculated column.

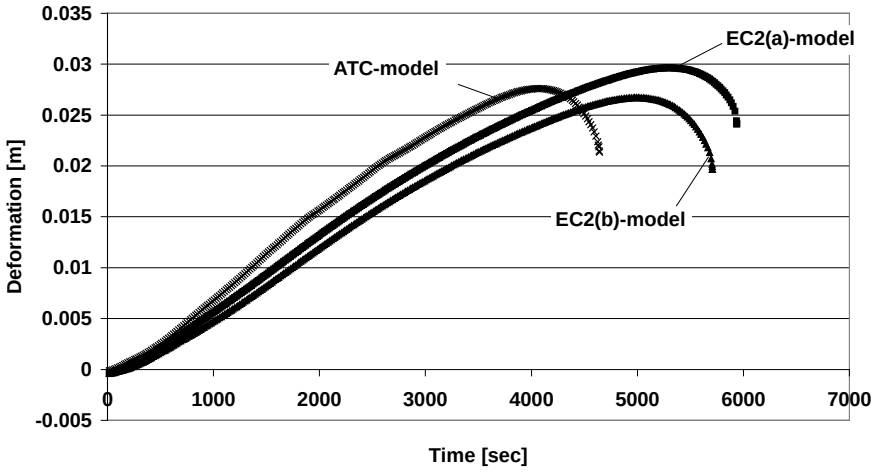

Fig. 7-33 - Vertical deformations of the examined column subjected to ISO fire curve

After a small reduction in length due to the vertical load at the start of the calculation, an increase of the vertical displacements is indicated immediately. In the ATC-model with the softer behaviour of the concrete, the failure time is shorter compared to the results of the EC2(a)- and EC2(b)-models. The absolute results of the ATC-model are close to the results of the EC2(b)-model with the maximum value of the PSS.

Figure 7-34 shows the horizontal displacement of the y-axis on the top of the investigated column.

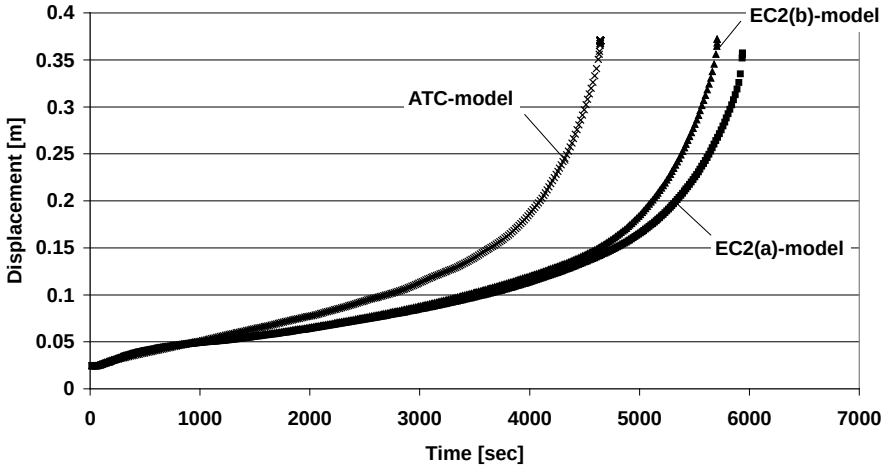

Fig. 7-34 - Horizontal displacements of the examined column subjected to ISO fire curve

The absolute values of the horizontal displacements are identical in all used models. The result of the EC2(a)-model with the recommended value of the PSS has the highest deformation at the top of the free end of the column.

The examination shows a different behaviour of the three concrete models at high temperature calculation of a structure.

The difference between the ATC-model and the EC2(a)- and EC2(b)-models can be explained as follows:

- The ATC-model does not work with a constitutive stress-strain relationship. At each time step, the strain components were summarized. This leads to a better agreement of the pure concrete material behaviour. This behaviour is sufficiently described in chapters 8.3 to 8.5.
- The ATC-model uses a more realistic thermal expansion for siliceous concrete than the standard thermal expansion for siliceous concrete of the EC2(a)- and EC2(b)-models.
- The ATC-model uses the effect of thermal induced transient creep strain.
- The ATC-model calculates higher restraint across the cross section.

In a structure calculation, the calculation of the fire resistance depends from the used material models for steel and concrete. The steel is a relatively homogeneous material with relatively constant parameters. The concrete material is completely different. In calculating the parameters, it should be measured first as it was shown and mentioned above.

It was shown that the different concrete models have an influence on the fire resistance. In the material models, different strain parts are used, i.e. different thermal expansion and the transient thermal creep strain. Both have good observed effects to the fire resistance on the examined column.

Some researchers prefer constitutive models without a softening branch in the material model for concrete on fire resistance calculations. The classic limit-analysis based on strain limitations is not applicable if stress-strain diagrams with softening branches are used [L148]. Thus, the ATC-model uses a failure model based on the limitation of the deformation rate. The limit rate should not exceed the maximum level shown in the Chapter 5.

7.6.3 Results of Column Calculation with Cooling

In the following consideration, the same column of the Chapter 8.6.3 with a design fire curve including a cooling period will be investigated. Figure 7-35 shows the design fire curve. In this case, only the ATC-model and the EC2(b)-model with the maximum value of PSS led to comparable results.

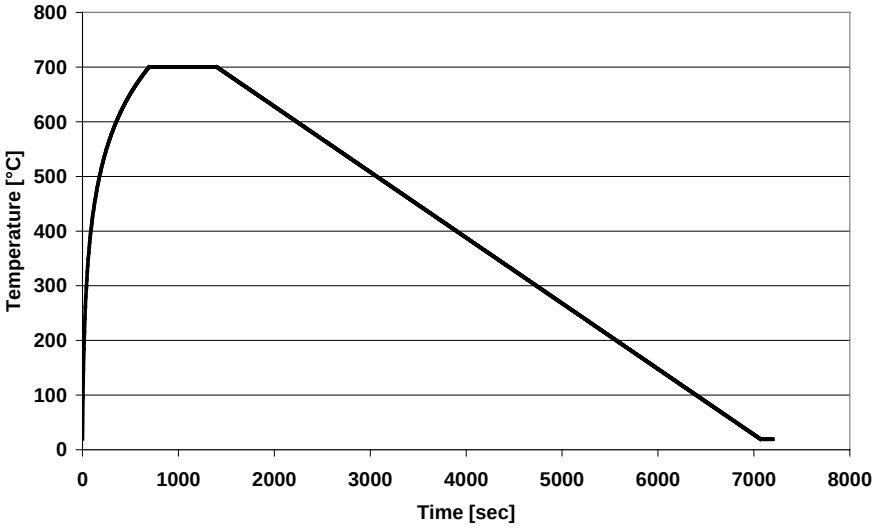

Fig. 7-35 - Design fire curve with cooling

The design fire starts with a heating curve according to the ISO 834 curve until 700°C; the temperature is constant for 700 seconds. After the hold time the temperature decreases with 7K/min.

During heating of the column, the ATC-model shows a slightly higher deformation than the EC2(b)-model. The ATC-model contains a high siliceous content. This kind of concrete has a higher thermal expansion than ordinary concrete according to EC2(b)-model. The design fire curve has no effect of the load bearing capacity of the cross section. It seems therefore that most of the forces are transferred to the steel bars. The softening behaviour of the ATC-model could not be activated in this case. Figures 7-36 shows the vertical displacement at the free end of the column.

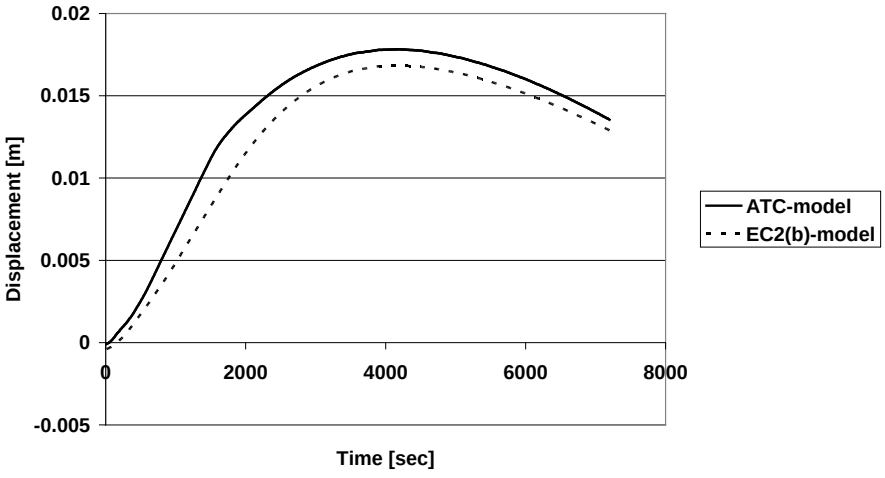

Fig. 7-36 - Vertical displacements of the examined column subjected to design fire curve

Generally, there is an observed decreasing of the vertical deformations after fire. The re-deformation of the ATC-model is a slightly higher than the EC2(b)-model. The two models used different material laws during cooling. The ATC-model uses cooling down curves according to measured data with different load levels. The EC2-Model uses the residual behaviour of compression strength and a decreasing part of the thermal strain. Astonishingly, both models indicate very similar behaviour in this case.

Figures 7-37 shows the calculated horizontal displacement at the free end of the column.

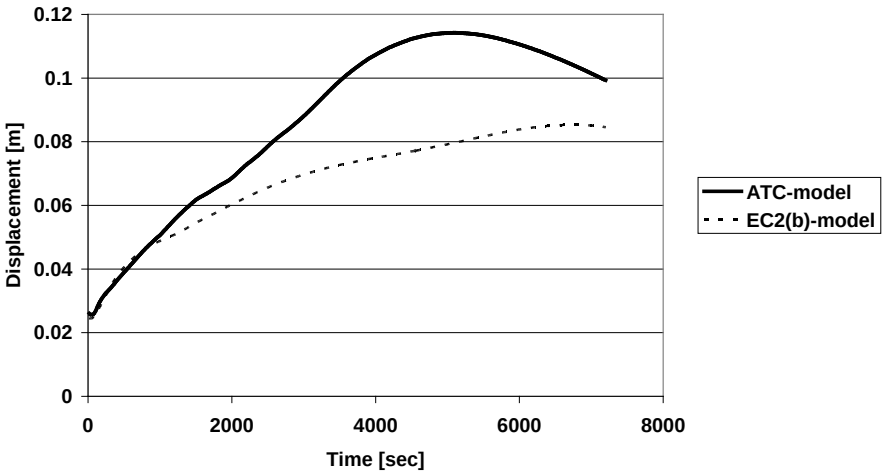

Fig. 7-37 - Horizontal displacements of the examined column subjected to design fire curve

The total deformation in horizontal direction after the ATC-model is significantly higher than the deformations after the EC2(b)-model. Most of the strain parts are irreversible, i.e. plastic strain and a smaller part of the transient strains. Also the thermal strain is not fully reversible. The ATC-model considers the irreversibility of these strains. The EC2(b)-model calculates mostly reversible according to the stress-strain relationship [L48]. This behaviour is reflected in the results after Fig. 8.37, i.e. the EC2(b)-model shows no reduction of displacements during cooling which is the case in praxis and was observed in many fire tests.

7.6.4 Results of Column Calculation with Restraint

The last part of the investigation shows restraint stresses in the column for the case where the length of the column is completely fixed in the calculation model during fire exposure. The heating rate according to ISO 834 is shown in Fig. 7-16. The principle sketch is given in Fig. 7-38.

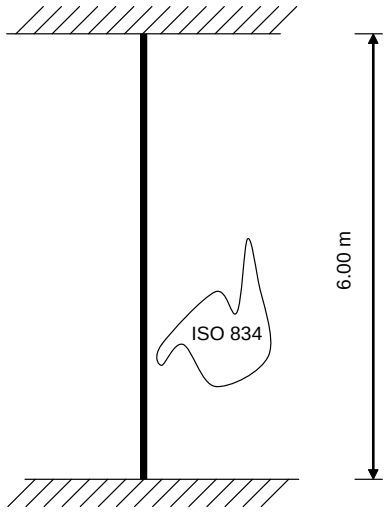

Fig. 7-38 – Principle sketch of the test set-up of the investigated column

Figure 7-39 shows the axial forces of the ATC-model and the EC2(b)-model with the maximum value of PSS.

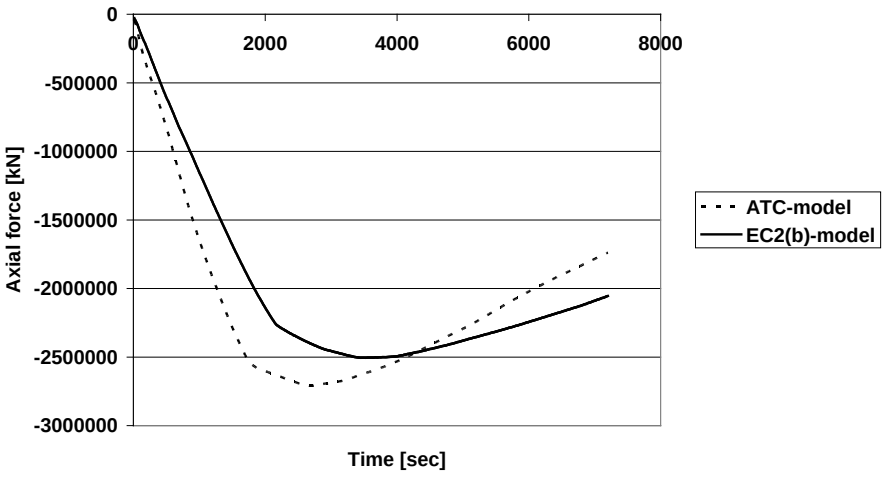

Fig. 7-39 - Restraint axial force of the investigated column

According to Chapter 8.4.2, calculations with the ATC-model leads to higher restraint axial forces than the EC2(b)-model. The restraint stresses exceed the compressive strength of the concrete near the heated surface and after about 3,000 seconds (ATC-model) and 4,000 seconds (EC2(b)-model) a decrease of the axial forces is observed until 7000 seconds. In this examination, the ATC-model also indicates a faster decrease of axial forces than the EC2-model.

The higher restraint axial forces during the first period of heating for about 2,000 seconds leads to higher damage of the concrete column compared to the EC2(b)-model calculation. As the EC2(b)-model does not allow calculation of the cooling period after heating, it was not possible to prove that column is able to withstand the loads during cooling down. The calculations with the ATC-model in this case indicated that no failure occurs during cooling down.

7.6.5 Conclusion of Structural Behaviour with the ATC-model and the EC2-model

In this chapter, the structural behaviour of a column will be analysed. The different possibilities of the new ATC-model and the EC2(a)- and EC2(b)-models in the Eurocode 2 for columns were investigated. A comparison shows some differences due to two general effects. On one hand, the thermal deformation is based on different equations and on the other hand, the irreversible behaviour of the concrete in the ATC-model is not considered.

The ATC-model has the irreversibility in the parts of the thermal strain, plastic strain and the transient thermal strain, see chapter 5.7.1 and 5.7.2. Only the part of elastic strain in the transient thermal strain and the elastic strain due to Young's modulus are reversible in the ATC-model. The reversibility depends on the thermal behaviour of the Young's modulus and the residual properties in the ATC-model (see Chapter 4).

The constitutive model of EC2 works with different stress-strain relationships which build up a different material behaviour for fire exposure after ISO standard fire with a minimum peak stress strain, a recommended peak stress strain and a maximum peak stress strain. In the Eurocode, this is considered only as a lumped parameter in the decreasing branch of the stress strain and in the plastic strain. In the Eurocode, only the elastic stain is reversible.

The most comparable behaviour between EC2 and the ACT-model was obtained by using the maximum peak stress strain relation given in Eurocode 2. Evidently, the Eurocode respects here are of a softer material model. The second EC2-model with the maximum PSS should, in many cases, not be applied under fire conditions.

For building elements where the steel has an important influence on the deformation in a structure and to the whole structural behaviour, the different models activate nearly the steel forces with little differences in the concrete behaviour, i.e. the different material models of the concrete have only minor influence on the total structural behaviour. The most important fact is the thermal strain and, in general, the irreversible behaviour of strains mentioned above.

7.7 Calculation of a Tunnel Cross-section for a Road Tunnel

7.7.1 Model Parameters and Content of the Results

For the investigations, it was concluded that the irreversible character of the several material properties must be incorporated in a calculation model for high temperatures as to ensure a realistic calculation of the behavior of concrete. This conduction is the main outcome of the results of examinations of Chapter 8.6.

The good adaptations of the ATC-model to measured data leads automatically to calculation results of the whole structure. The tunnel structure investigated is a cut and cover rectangular-shaped reinforced concrete tunnel. In the following example, a single-bay frame is calculated. It is a model of a tunnel taken from a research project, shown in Figure 7-40 [L151].

In general, the calculation methods have two separate arithmetic steps: a thermal and a mechanical analysis. For further information, see the references [L52, L149, L150].

The calculation model is divided into the following parts of the structure:

- ground plate	BEAM 01 = symmetric axis of the cross section at node 1
	BEAM 12 = mid-point between BEAM 01 and BEAM 20 at node 20
	BEAM 20 = corner between ground plate and wall at node 41
- wall	BEAM 23 = corner between wall and ground plate at node 41
	BEAM 36 = point of maximum bending moment at node 75
	BEAM 49 = corner between ceiling and wall at node 97
- ceiling	BEAM 49 = corner between wall and ceiling at node 97
	BEAM 60 = mid-point between BEAM 49 and BEAM 71 at node 120
	BEAM 71 = symmetric axis of the cross section at node 143

In the calculation, the structure is divided in several beams with a node at each end of the beam with 2 degrees of freedom. The ground plate has 20 beams with 41 nodes. The wall has 26 beams with 56 nodes and the ceiling has 22 beams with 46 nodes. Each beam has an own temperature exposure and an own structure definition.

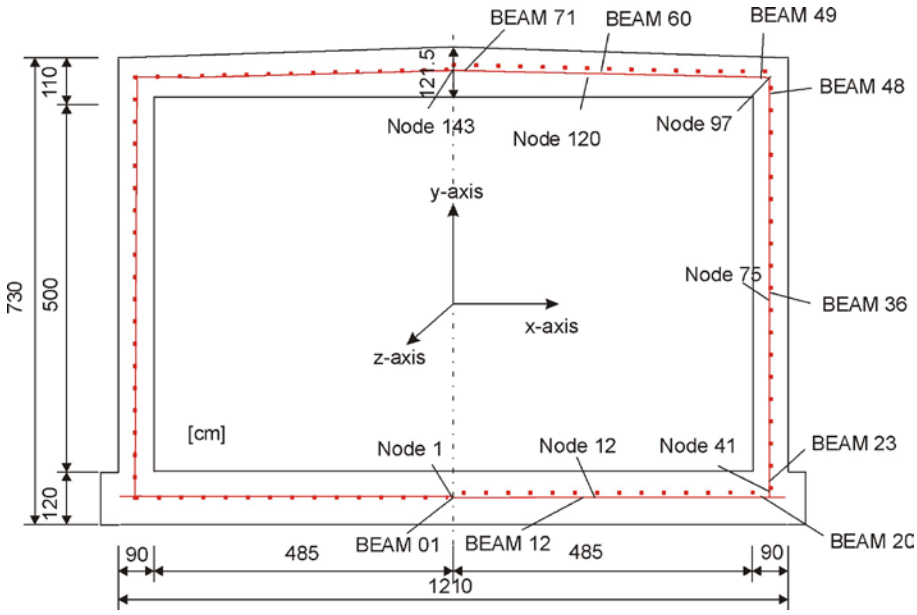

Fig. 7-40 - Principle sketch of the road tunnel according to [L151]

In the simulation of the tunnel cross section, a fire exposure according to the HC-increased fire curve (HC_{incr}) was investigated; possible explosive spallings of concrete under this condition were ignored [L152]. Only at the wall and the ceiling were exposed to the HC_{incr}-curve. The ground plate temperature is assumed to be constant during the calculation at ambient temperature.

Derived from the hydrocarbon fire, the maximum temperature of the HC_{incr}-curve is 1300ºC instead of the 1100ºC for the standard HC curve. However, the temperature gradient in the first five minutes of the fire is as severe as all Hydrocarbon fires like RWS, HCM, HC, possibly causing a temperature shock to the surrounding concrete structure and concrete spalling. This may be one of its results. The temperature development of the Hydrocarbon Increased (HC_{incr}) fire curve is described by the following equation:

$$T = 20 + 1280 * \left(1 - 0.325 * e^{-0.167*t} - 0.675 * e^{-2.5*t}\right) \qquad \text{equ. (7.3)}$$

With: T – temperature in °C

t – time in minutes

Such fires may be caused by accidents, i.e. liquid fires in a tunnel lead to this type of exposure [L55, L153]. Figure 7-41 shows the time-temperature relationship.

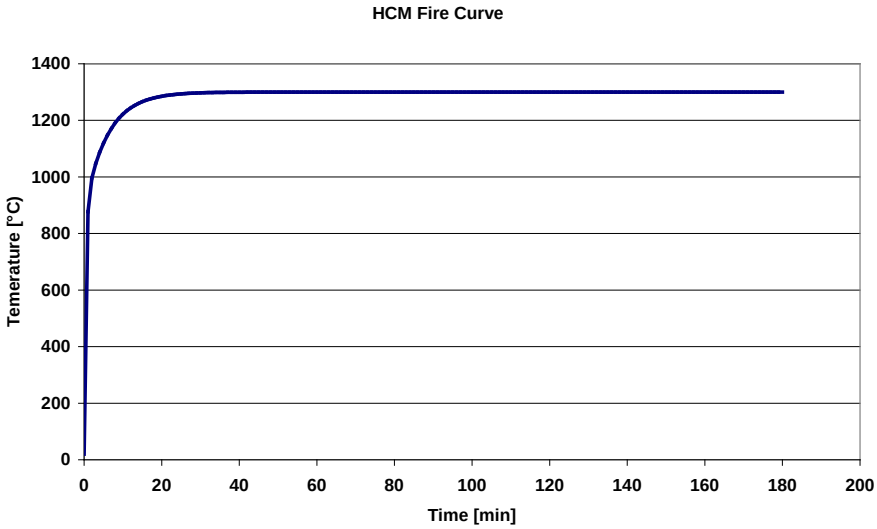

Fig. 7-41 – Hydro-Carbon-Increased fire curve according to [L55]

The geometric tunnel model is based on a vertical cut with a width of 1 meter, see Fig. 7-42.

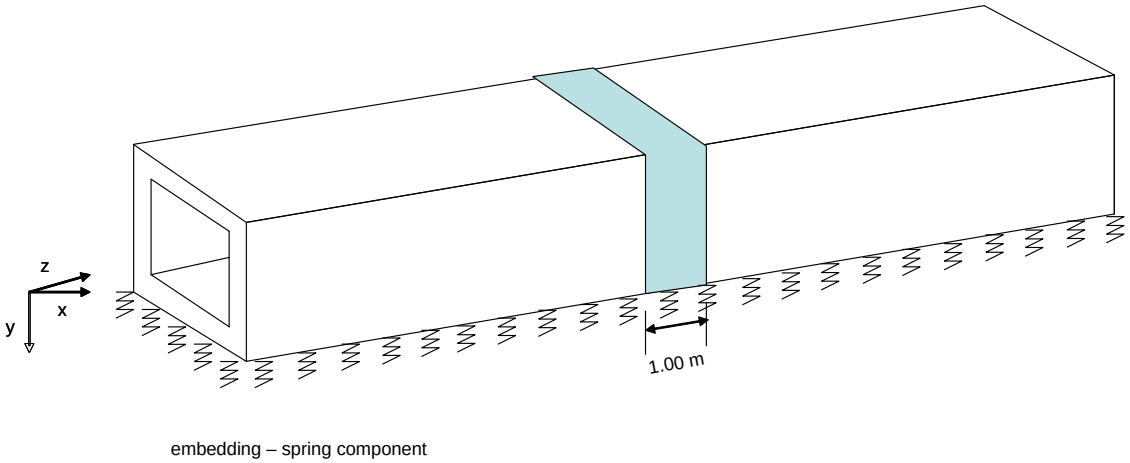

Fig. 7-42 – Geometric tunnel model according to [L154]

For treatment of an idealized frame, the following conditions must be adhered when using the approximation method after [L155]:

- External loads and their functions of time and temperature are known at every time step.
- The cross sections are preserved during the fire until failure.

- The displacements of the section axes are very small compared to the dimensions of the cross sections. All forces, displacements and the general stiffness are related to the undeformed section axis.
- Local stability failure is not taken into consideration.
- Distortion as a result of strength is neglected.
- Torsion does not appear.

General calculations utilize the semi-probabilistic concept of the Eurocode 1 [L156]. Figure 7-43 shows the principle loads of the tunnel cross section.

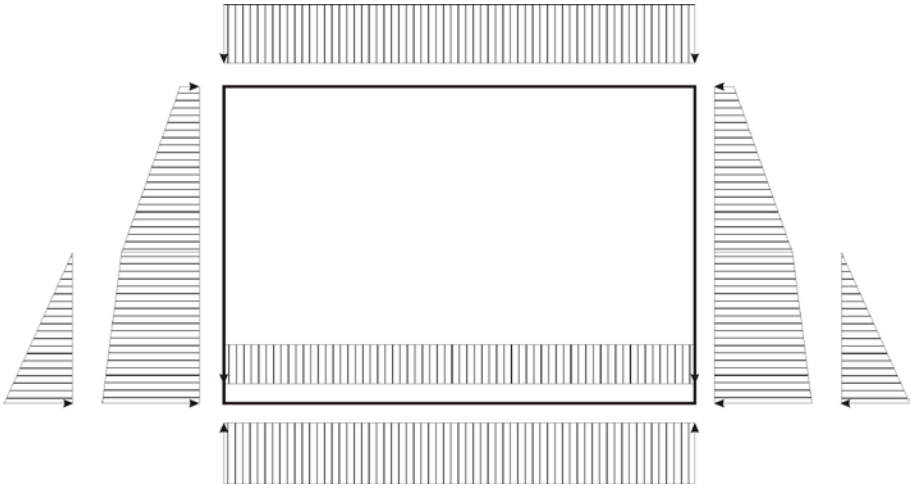

Fig. 7-43 - Principle load of the tunnel

Consequently, these results in the following load factors using the combination coefficient from the safety concept for tunnels subjected to fire, according to [L154]:

Weight of reinforced concrete	γ=1.0
Earth pressure gravel-sand	γ=1.0 dry
	γ'=1.0 in ground-water
Hydraulic pressure	γ=1.0
Variable load	γ=0.5
Variable load on top of the structure	γ=0.5

The embedding is considered with the help of a spring component under every beam element of the ground plate [L157]. The used structural materials are ordinary siliceous concrete C25/30 and steel BSt500.

The heating is calculated for transient heating according to the HC_{incr}-curve. During cooling down, the heating stops at 180 minutes and cooling down period starts from 360 minutes until 20°C. A coefficient of convection of α_c = 50 W/m²K was used during the calculation of the heat flow to the hot surface.

Before the structure is subjected to fire, the amount of reinforcement must be calculated at ambient temperature which is to be used for the fire exposure. It is assumed that no spalling occurs during the fire. The cover was chosen as 80 mm, according to [L154].

The following results based on a study comprise the comparison of the calculation models during heating-up to the collapse of the structure which occurs due to defined failure conditions given in the calculation routine, see Chapter 5.9.

Furthermore, a simulation was started with heating up to 180 minutes and a period of cooling down until a constant level of deformation by nearly 85 hours. Whereby the results are focused to the deformation at two nodes where the maximum value of deformation occurs in x-axis and y-axis, according to the first study.

In the final simulation, the regular EC2(b)-model is compared with an EC2(b)-model that considers the thermal strain of the ATC-model and the ATC-model to observe the influence of the thermal strain on the structural behavior.

7.7.2 Deformations of the Tunnel Structure for Heating up to the Point of Failure

In the following diagrams, the results for the calculation of heating-up until collapse of the structure occurs are shown. On one hand are the different failure criteria where investigated criteria was failure and on the other hand, the displacements during heating are shown.

The Figure 7-44 shows at first the results of the deformation using the EC2(b)-model with the maximum value of PSS (left) and the ATC-model (right) at various nodes in x–axis.

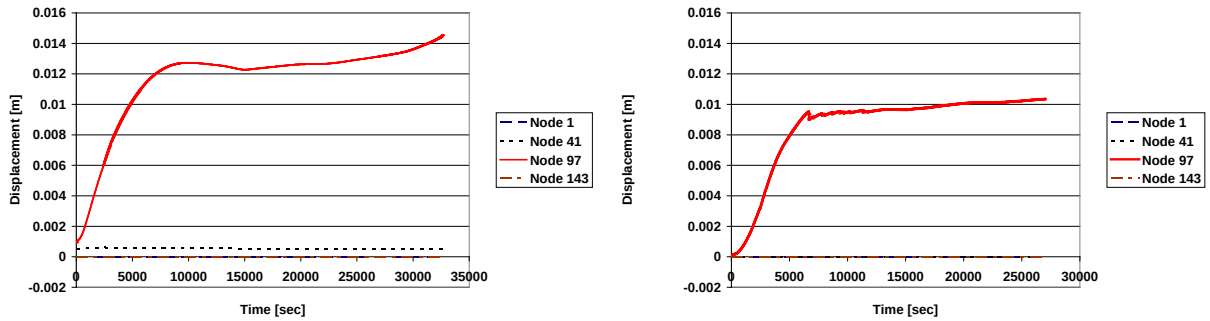

Fig. 7-44 - Displacement in x - axis in various nodes

The most important node for the deformation in the x-axis is node 97. This node is in the two upper corners of the single bay frame. The deformation with the ATC-model is lower than the deformation with the EC2(b)-model even though the thermal strains are significantly higher than in the commonly used EC2(b)-model, see chapter 3.3.2. After 7200 seconds for the ATC-model, a decrease of deformation is observed. From this level, the deformation is nearly constant to its collapse for the ATC-model. The collapse of the structure with the EC2(b)-model starts after 27,000 seconds and shows an increase of deformations. Generally, the calculation with the EC2(b)-model stops at 31,000 seconds while the calculation with the ATC-model stops at 27,000 seconds. The convergence criteria of the software were reached differently.

At 7200 seconds, the calculation after ATC-model shows discontinuity behaviour. It seems that according to the calculation, a plastic failure of the structure occurs after calculation, i.e. due to the maximum temperature in the finite elements near the hot surface. Due to the irreversible approach of the ATC-model, the concrete behaviour is softer than the EC2(b) model. This can be observed at this point.

In Figure 7-45 the deformation in y-axis is shown (left the EC2(b)-model and right the ATC-model).

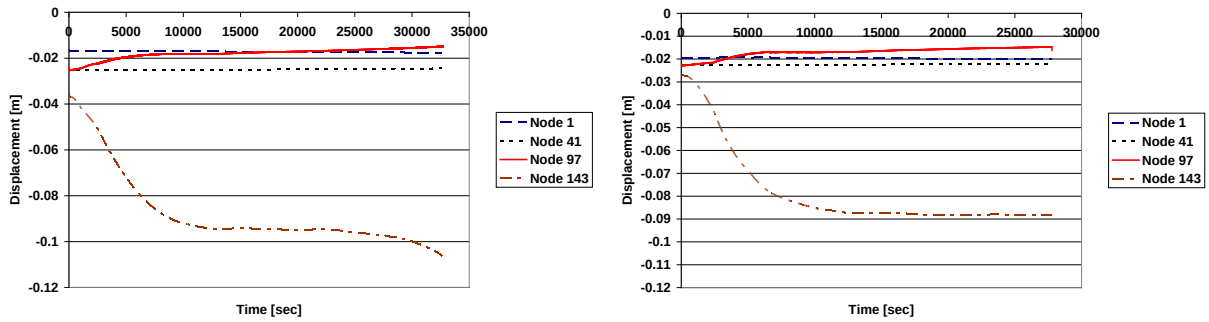

Fig. 7-45 - Displacement in y - axis in various nodes

At node 143, the most important deformation is observed. This node is in the centre of the ceiling at the point of the maximum bending moment. The deformations of the ATC-model are lower than those of the EC2(b)-model. Contradictory to Fig. 7-43, discontinuous behaviour of the EC2(b)-model could not be observed at 7200 seconds. The softer behaviour of the ATC-model is responsible for a lower deformation because the strains of the ceiling in x-axis are lower in the ATC-model than in the EC2(b)-model. These results are due to the higher load utilisation across the cross section in the new model. Without considering the load history, the influence of the load under temperature exposure is not sufficiently reflected in the calculation of deformation of the structure.

The various displacements demonstrate the whole structure responds during heating. The stiffness of the system is changing as a function of time [L158, L159].

In the next figures, different displacements of the calculations with both material models in various nodes are compared. A direct comparison is given between the two models. Generally, the same information is given according to Fig. 7-44 and 7-45. Node 1 is in the centre of the ground

plate wherein it gives a deformation only in the y-direction. Node 41 is in the lower corner of the frame. Node 97 is in the upper corner of the frame and node 143 is in the centre of the ceiling.

Fig. 7-46 shows a direct comparison of the deformation in y-axis in node 1. A deformation in x-direction could not be considered because fixed load support was simulated.

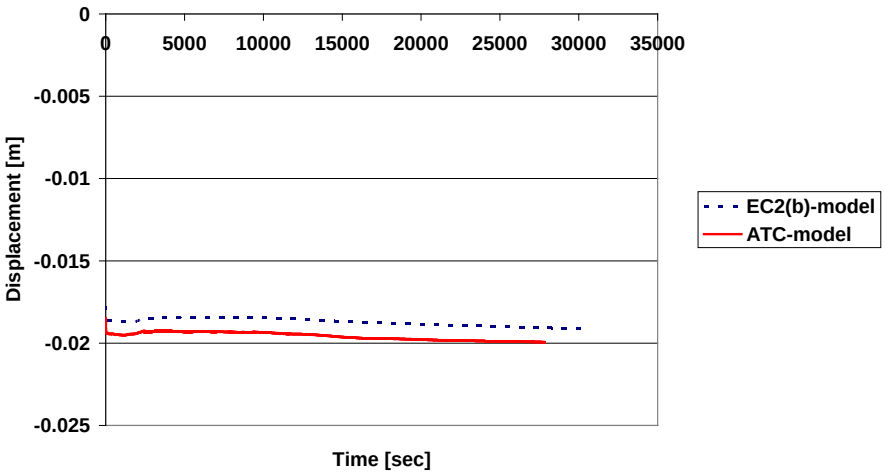

Fig. 7-46 - Displacement in y - axis in node 1 (centre of the ground plate)

The deformation in y-axis at node 1 is relatively low. The ATC-model calculates lower results. The reason is discussed under Fig. 7-43 and 7-44. A significant difference could not be observed, this is why the results cannot be considered any further. The temperature at the surface was chosen at ambient temperature. The reaction is only due to the restraint and deformation of the whole structure.

Fig. 7-46 shows the comparison of the two models in node 41 in x-axis.

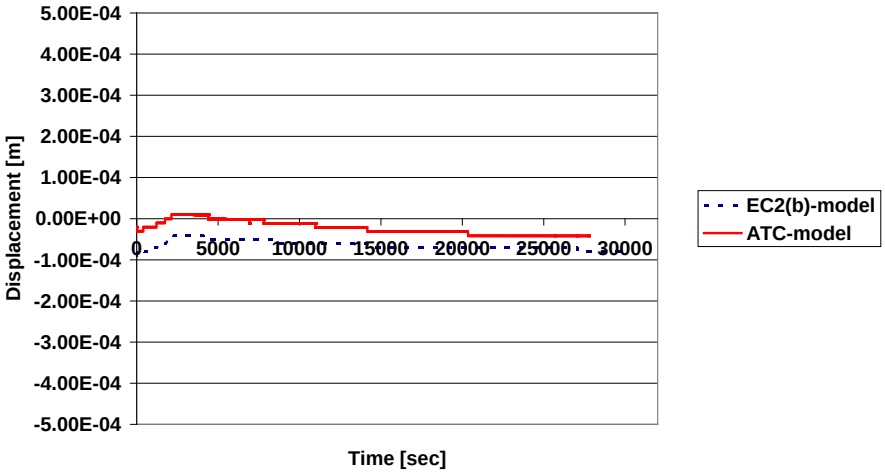

Fig. 7-47 - Displacement in x - axis in node 41 (right bottom corner of the structure)

The deformations are relatively low in both cases. With the ATC-model, a significant reaction could not be observed. The temperature influence is relatively low. In this corner the HC_{incr}-curve starts at the surface of the wall.

Fig. 7-48 shows the deformation in y-axis at node 41.

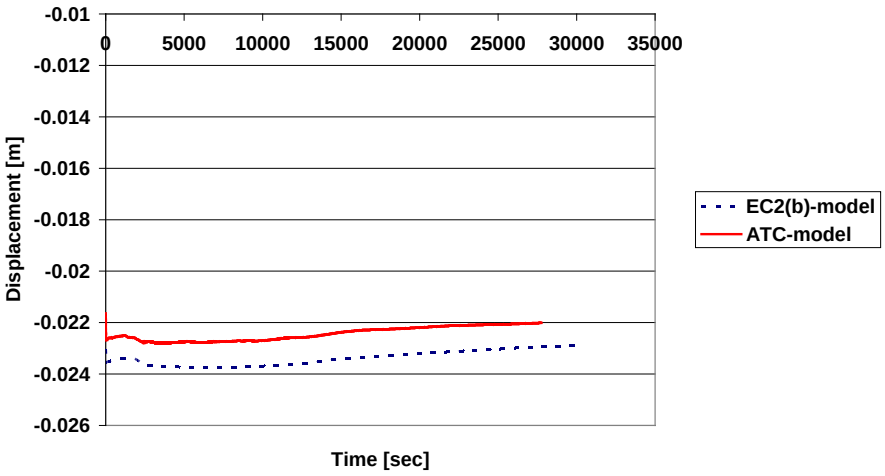

Fig. 7-48 - Displacement in y - axis in node 41 (right bottom corner of the structure)

The deformation in the lower corner of the single bay frame is slightly higher than in the middle of the ground plate. The temperature influence is higher because the HC_{incr}-curve starts here. The deformation with the ATC-model is a little lower than in the EC2(b)-model. The curves are continuous and do not show a critical behaviour of the structure in this node.

Fig. 7-49 shows the deformation in node 97.

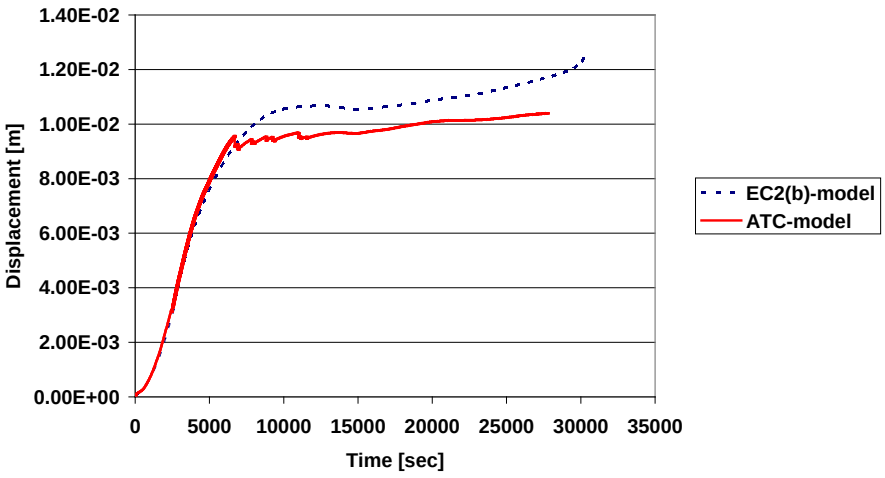

Fig. 7-49 - Displacement in x - axis in node 97 (upper right corner of the structure)

A critical behaviour of the structure can be observed in both cases. The results with the ATC-model are lower than in the EC2(b)-model. The reason is already discussed under Fig. 7-44 and Fig. 7-45. In this case, the ATC-model shows higher displacements of the structure.

Fig. 7-50 shows the displacement in node 97 in y-axis.

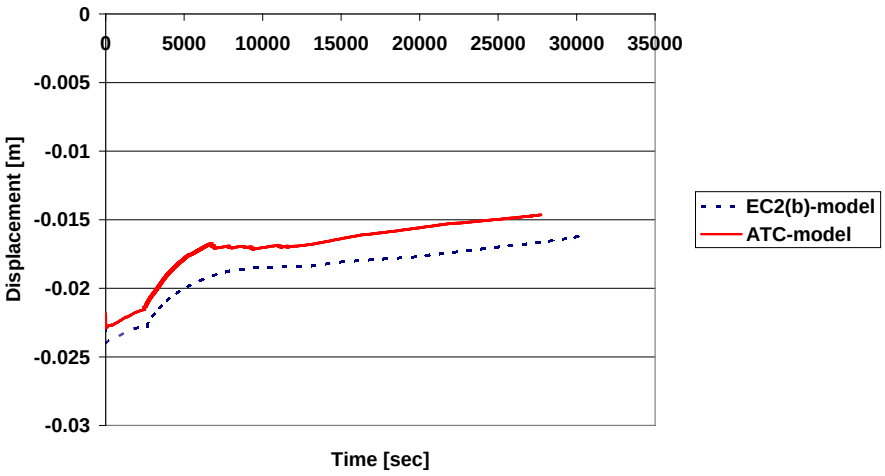

Fig. 7-50 - Displacement in y - axis in node 97 (upper right corner of the structure)

The displacement in y-axis is relatively unimportant compared to the displacement in x-axis. No critical behaviour can be observed. The deformation with the ATC-model is slightly higher than the EC2(b)-model. In the upper corner of the frame, the maximum bending moments are in the rear of the soil side of the structure. The high temperatures are applied inside the concrete frame, therefore a softer behaviour of the ATC-model can be observed.

Fig 7-51 shows the deformations in y-axis at the centre of the ceiling at node 143. A deformation in the x-direction could not be taken into consideration because a fixed load support was simulated for the ground plate.

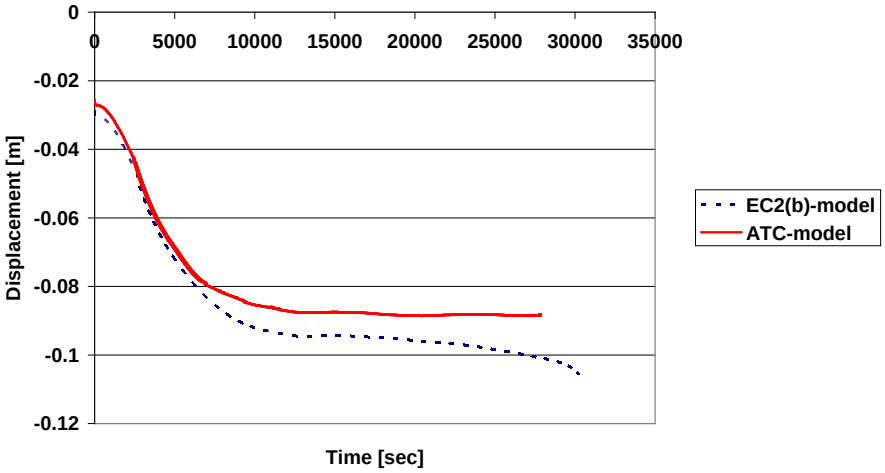

Fig. 7-51 - Displacement in y - axis in node 143 (centre of the ceiling)

The deformation with the ATC-model is lower than in the EC2(b)-model. As discussed above, the reason is given under Fig. 7-434 and 7-45. After EC2(b)-model, one can see a start of collapse after 27,000 seconds. At this point, the deformation increases with the EC2(b)-model, whereas the ATC-model indicates a constant displacements which may be due to a new load distribution in the tunnel frame.

Most parts of the tunnel structure show lower deformations with the ATC-model under fire exposure compared to the EC2(b)-model. Only in node 97 is where the deformation in x-axis is larger with the ATC-model than with the EC2(b)-model. This behaviour is generally also observed in the y-axis. Whereas at node 1, a slightly higher deformations with the ATC-model can be observed.

7.7.3 Axial Forces of a Tunnel Structure under Heating to the Point of Failure

During the heating, the initial axial forces change due to increase in temperature. The following overview gives the results of the axial forces in several beam elements. The beam elements are chosen in each corner of the load support and one in the middle of the construction segment. Beam element 20 is in the corner of this member.

Fig. 7-51 shows the axial forces in the ground plate. The left diagram shows the results of the EC2(b)-model and the right diagram shows the results of the ATC-model. Beam 1 is at the load support, beam element 12 is in the middle between the load support and the lower corner of the single bay frame, see Fig. 7-40.

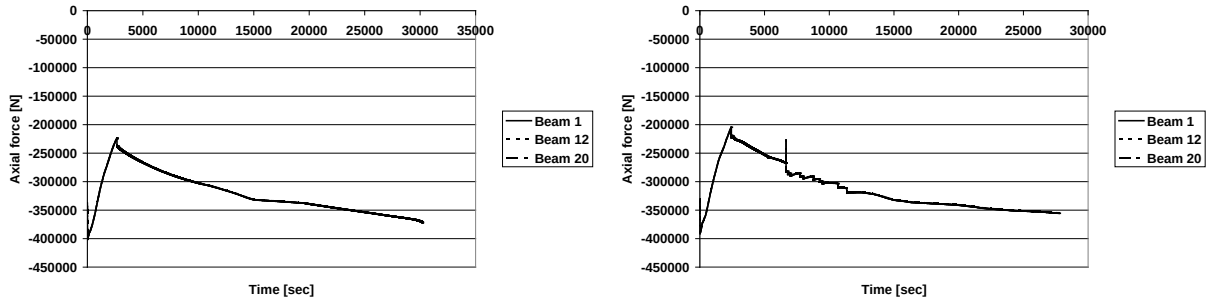

Fig. 7-52 - Axial forces in the beam elements of the ground plate

In all beam elements, the axial force is constant. The axial force decreases from 400 kN to 230 kN in the first 4,000 seconds of the simulation with the EC2-model. In the simulation with the ATC-model, the axial force decreases from 400 kN to 200 kN. After this time, a continuous increase is observed. The calculation with the EC2(b)-model reaches at the end of the simulation at the value of 370 kN. The calculation with the ATC-model calculates 360 kN at the point of failure. It is seen that the ATC-model loads to lower axial forces during heating. This is obtained by the softer behaviour of the material model.

Fig. 7-53 shows the axial forces of the wall of the single bay frame. Beam element 23 is in the lower corner, beam element 36 is in the middle of the wall and beam element 48 is in the upper corner of the wall (EC2(b)-model is left, ATC-model is right).

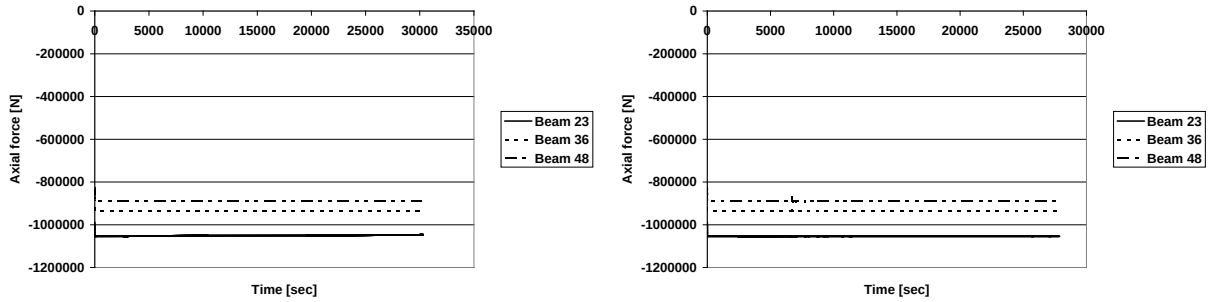

Fig. 7-53 - Axial forces in various beam elements in the wall

The axial forces are different. If the beam element is higher in the upper corner, the axial force decreases. There is no observed difference between the EC2(b)-model and the ATC-model. The axial forces are constant over the whole heating period of 3,000 seconds.

Fig. 7-54 shows the axial forces in the ceiling between the upper corners of the single bay frame and the fixed load support. Beam element 49 is directly at the corner, beam element 60 in the middle of the considered segment and beam element 71 is at the fixed load support. The EC2(b)-model is shown in left the diagram and the ATC-model is shown in the right diagram.

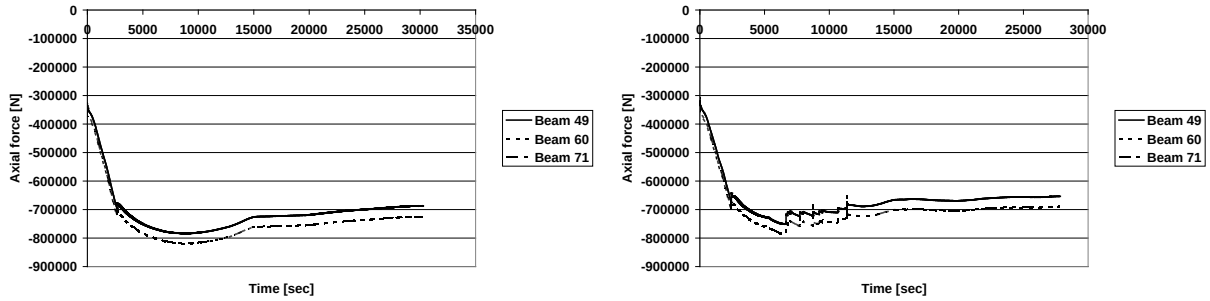

Fig. 7-54 - Axial forces in various beam elements in the ceiling

The axial forces are different in the different beam elements. In the EC2(b)-model, the axial forces are generally higher than in the ATC-model. The axial force increases from 350 kN to 810 kN as maximum in beam element 71 with the EC2(b)-model in 8,000 seconds. After this time the axial force decreases continuously to a minimum of 690 kN in beam element 49.

The results with the ATC-model start from the same axial force and increases to a maximum of 800 kN after 7,000 seconds in beam element 71. After this point, the axial forces decrease to a minimum of 650 kN at beam element 49.

The axial forces of the ground plate, the wall and the ceiling are generally higher according to simulations with the EC2(b)-model compared to the ATC-model. Due to the lower strains in the ATC-model, lower axial forces occur. It is obvious that the lower strains result from transient creep under compression and a stress relieve by this effect.

7.7.4 Bending Moments of the Structure under Heating to the Point of Failure

The bending moments in points of interest are discussed in this chapter. The results are separated into the ground plate, wall and ceiling.

Fig. 7-55 shows the bending moments in the ground plate. Beam element 1 is at the load support, beam element 12 is in the middle of the load support and the lower corner of the single bay frame. Beam element 20 is in the corner of this member (EC2(b)-model is left, ATC-model is right).

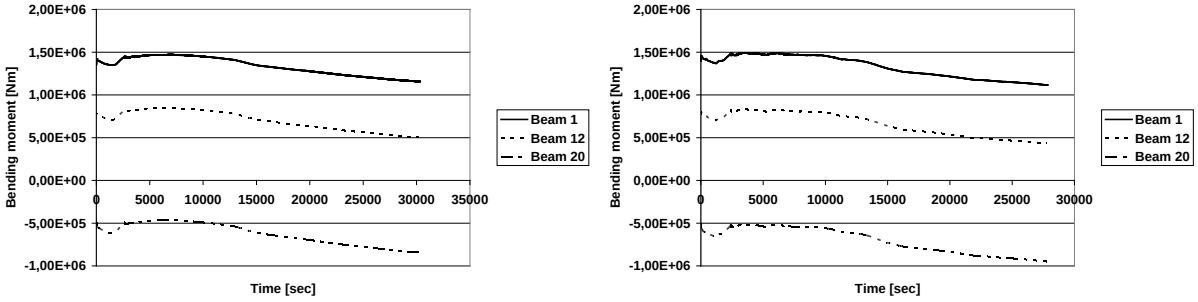

Fig. 7-55 - Bending moments in various beam elements in the ground plate

Beam element 1 has the highest bending moment and beam element 20 has the lowest. During heating, the bending moments decrease constantly which can be expected to be between 1,000 and 2,000 seconds of heating. A significant difference cannot be observed between the two observed concrete models. Nevertheless, a very small difference can be observed wherein the ATC-model has slightly lower bending moments. Compared to the displacements, the bending moments do not show important differences between the two models.

Fig. 7-56 shows the bending moment of the wall of the single bay frame. Beam element 23 is in the lower corner, beam element 36 is in the middle of the wall and beam element 48 is in the upper corner of the wall. The left diagram shows the EC2(b)-model and the right diagram shows the ATC-model.

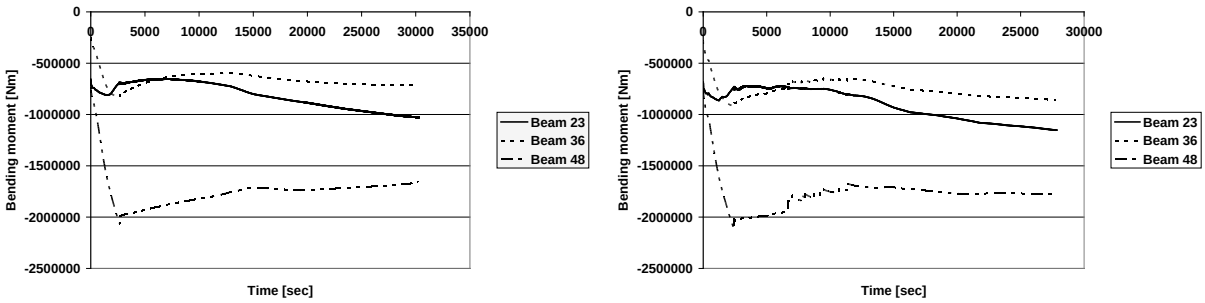

Fig. 7-56 - Bending moments of three beam elements in the wall

The most important information is given by beam element 48. This is the upper corner of the beam element. During the first 3,000 seconds the bending moment increases quickly to a maximum of 2,000 kNm. After this time the bending moment decreases to 1,600 kNm after 2,700 seconds. This behaviour shows that the fire exposure at the start of the fire is very important to the reaction of the structure. The wall the bending moments of the beam elements are slightly higher for the ATC-model than for the EC2(b)-model. This is in agreement with the other observations with the ATC-model.

Fig. 7-57 shows the bending moments of the ceiling. Beam element 49 is directly at the corner, beam element 60 in the middle of the considered segment and beam element 71 is at the fixed load support. On the left hand, the EC2(b)-model is shown and on the right hand, the ATC-model is shown.

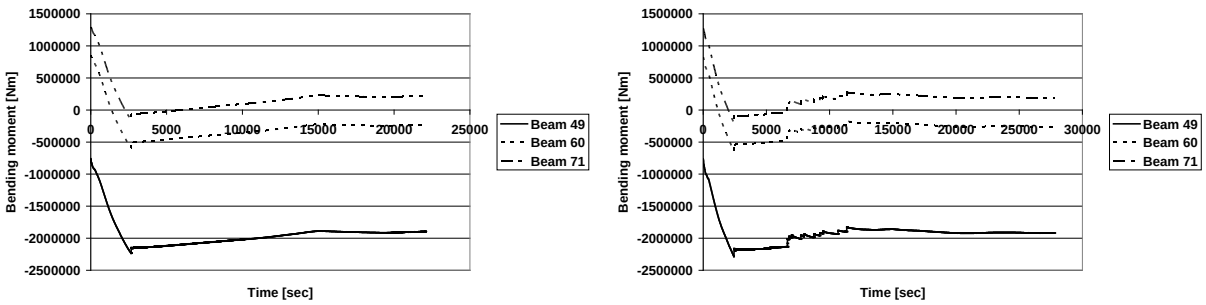

Fig. 7-57 - Bending moments of three beam elements in the ceiling

In the ceiling, the bending moments are nearly identical in the two concrete models. At the beginning of the heating, the bending moments increase to a maximum of 2,200 kNm after 3,000 seconds. The same was observed in all beam elements of the ceiling.

Generally, an insignificant difference between the two models may be seen in the calculation of the bending moment. The positive bending moments are lower with the ATC-model than with the EC2(b)-model. The negative bending moments are higher with the ATC-model than with the EC2(b)-model.

The differences in the result can be explained by two reasons. The material model of the ATC-model is softer than the material model of the EC2(b)-model. This was established in the previous chapters where the examples of pure concrete specimens were given. The softer behaviour due to the transient creep strain and the higher restraint due to thermal strain of siliceous concrete with high siliceous content lead to a higher negative bending moment and a lower positive bending moment. This is because the axial forces were taken into account during the calculation steps. At this point, the model influenced the results of the calculation because the respect of the step wise consideration of load history and the consideration of the reversible and irreversible parts of the total strain during an iteration.

7.7.5 General Remarks on of the Calculation Results of a Tunnel Fire in a Single Bay Frame Model

It was shown that the recommended model of EC2 does not calculate realistic values of deformations of concrete structures under high temperature if one compares the results of the advanced transient concrete model (ATC-model) which is based on individual derived and measured data with the proposed EC2 concrete model based on data for an “average European concrete”. A maximum value of peak stress strain in the EC2-model is necessary for describing a relatively realistic behaviour of the structure. For calculations of tunnels made of concrete with siliceous aggregates, the EC2-model should be taken into account with the maximum value of the peak stress strain and a thermal strain model for concrete individual derived. For calculations bearing members with high loads, the ATC-model should be applied. It should be noted that if one uses all the equations of the ATC-model, the full concrete behaviour is realistically in a structure under fire. This kind of effort is respected.

The reliability of the load bearing capacity is higher with the ATC-model because the deformations are lower than with the EC2-model. The calculated axial forces with the ATC-model are close to the EC2-model.

The comparison was made with the same temperatures in the cross section where it should be a principally examined for large building structure made of special aggregate concrete and where EC2 data are to be applied for high temperatures.

The main differences in the two models are the stiffness of the concrete material during heating, the difference in thermal strain and the influence of transient strain in the ATC-model. One way or reason is the difference of material laws e.g. the thermal strain of a concrete with high content of siliceous aggregates. The EC2 gives an average of different concretes with and without siliceous aggregates. Practically, the simulation must be adapted at least on measured data of the input parameters thermal strain, compressive strength, Young’s modulus and transient creep strain. In addition, the Poisson ratio may also be derived from measured data. The thermal strain is a very important factor in the concept of the total strain determination. If sufficient data are available, the factor may be adopted in the program code of SAFIR easily. This is possible through the EC2-model and the ATC-model. Considering the transient effects, their implementation is only possible in the ATC-model.

7.7.6 Eurocode 2 with a Thermal Strain Model after of the ATC-model

In the following chapters, the high influence of the thermal strain in the framework of total deformation will be discussed. The Eurocode 2 is adjusted with the thermal strain to a concrete with high silica aggregate content, thus, the same thermal strain equations are used just like in the ATC-model.

Fig. 7-58 shows the comparison between the 3 models. The results are obtained for the most interesting point of the single bay frame in x-axis. This is node 97 in the upper corner of the wall.

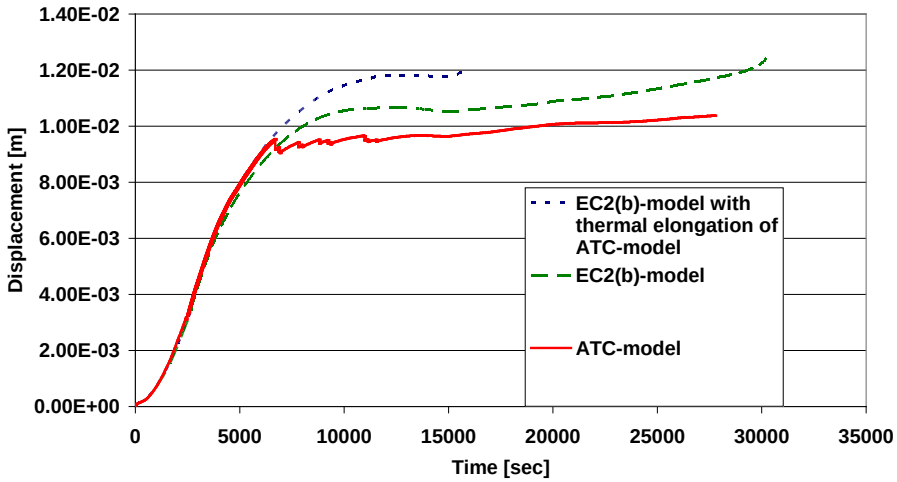

Fig. 7-58 - Displacement in x - axis at node 97

The effect of the higher thermal strain in the modified EC2(b)-model leads to a higher total deformation at node 97 in x-axis compared with the EC2(b)-model. It is astonishing to note the early failure of the structure after 15,000 seconds. The absolute maximum deformation reaches nearly the same value like the original EC2(b)-model. After reaching the maximum, the simulation stops because the iteration shows no convergence in the FE calculation.

Fig. 7-59 shows the simulation of the total deformation in y-axis at node 143. This is the centre of the ceiling in the load support of the single bay frame when the maximum bending moment occurs.

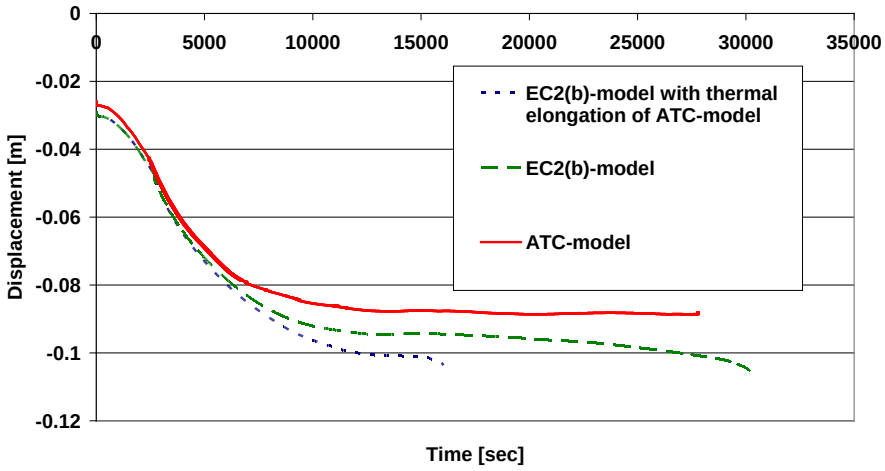

Fig. 7-59 - Displacement in y - axis at node 143

The deformation with the modified EC2(b)-model is higher than with the original EC2(b)-model from the origin. The calculation of the modified EC2(b)-model finishes at 15000 seconds due to absence of convergence during the FE calculation. The same maximum value of displacement is reached after 15000 seconds as it was already shown before.

Generally, the higher deformation of the total strain due to the higher thermal strain of concrete leads to maximum deformations where the simulation automatically stops. The load bearing capacity could not be completely described. The investigation shows that the simple adaption of the thermal strain of a tunnel concrete with a high siliceous content may lead to problems with the constitutive model of EC2(b). The ATC-model allow the use of a higher thermal strain of the concrete and even any other measured material parameter without difficulties in the fire design.

7.7.7 Cooling Down after Fire in the Tunnel

In the last chapter of this topic, the simulation with the ATC-model and the EC2(b)-model was adjusted to the fully cooling down period of the structure. The full cooling down was reached after 90 hours. The results are given at the two important nodes: node 97 in the upper corner of the single bay frame in x-axis and node 143 at the fixed load support in y-axis.

In Fig. 7-60 the results at node 97 are given.

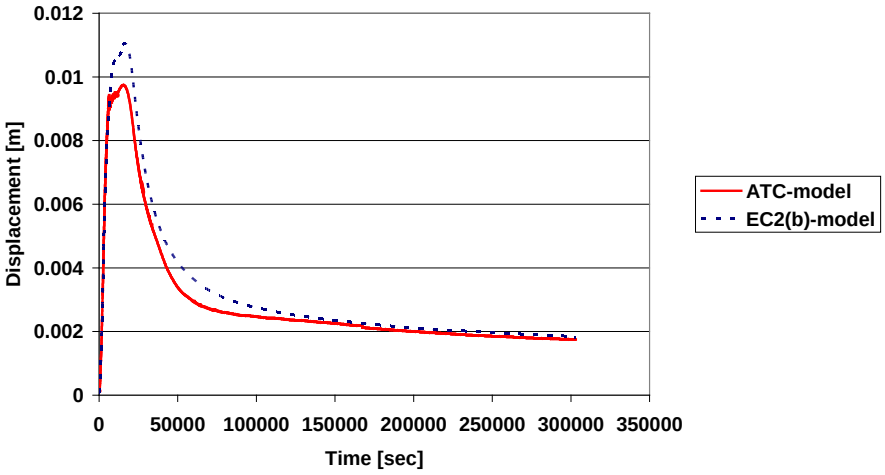

Fig. 7-60 - Displacement in x - axis at node 97

A higher maximum deformation is observed with the EC2(b)-model. The cooling down is slightly faster with the ATC-model than with the EC2(b)-model. The residual value is identical for both models. A different behaviour in cooling down is observed. The ATC-model is cooling faster according to the equations in Chapter 5. This is the only effect that can be observed. This effect is probably not relevant. It should be mentioned that the influence of thermal strain during cooling is determined by the duration of a fire and the maximum temperature reached. After the duration of a long fire, most concretes show large irreversible strain effects during cooling down.

Fig. 7-61 shows the displacement in y-direction at node 143. This is the centre of the ceiling.

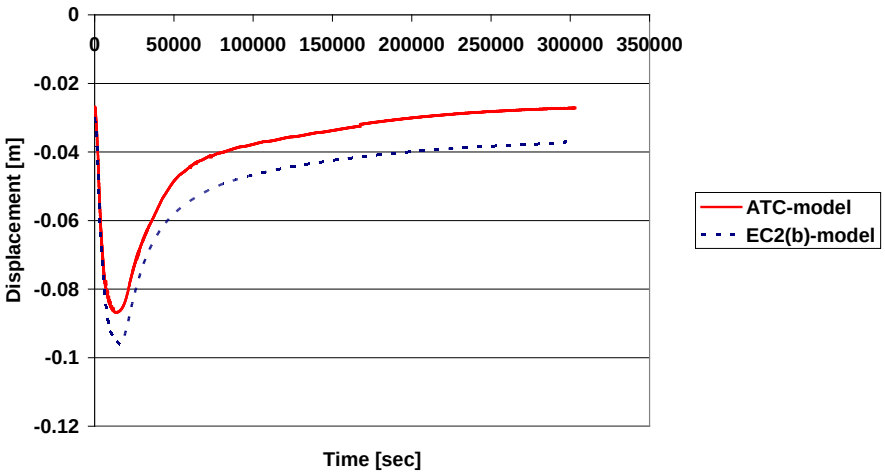

Fig. 7-61 - Displacement in y - axis at node 143

The total deformation is higher with the EC2(b)-model. The deformation during cooling down is identical between the two models. This is because at the end of the simulation, a difference between the EC2(b)-model and the ATC-model is observed. The absolute value of deformation during cooling down is nearly identical and the decreasing curves are nearly parallel.

This simulation should lead to special information on the behaviour of the two concrete models during cooling down. The test results are plausible. The higher deformation of EC2(b)-model leads to a higher residual strain than the ATC-model. The cooling down curve is parallel in y-axis. The cooling down behaviour in x-axis is different compared to the cooling down behaviour in y-axis. The higher effect of restraint is supposed to be responsible for this behaviour. The restraint is calculated in different ways for the two models. In x-axis direction, the restraint has the highest influence on the axial displacements.

8 Conclusions

A new thermal concrete model (ATC-model) was developed for the prediction of the load bearing capacity and behaviour of structures subjected to fire. This is done by using new material equations for the most important material properties of ordinary concrete under transient temperatures [L23, L26]. This model was developed with the aim to extend and generalize the existing concrete models of EC2 with respect to thermal strain, transient thermal creep and the effect of load history.

It is possible for this new model to consider the load history in all phases of thermal exposure. With this complex model, one can calculate total strain taking into account a wide range of variations of load history and transient temperatures up to 1,000°C. Different parts of deformations are approximated with analytical equations interacting with the new concrete model. This technique is usable for a realistically calculation of behaviour of structures according to [L160, L161, L162], including cases of total restraint.

By considering the load history during heating-up in several cases and comparing to other concrete models, an increase of load bearing capacity due to a higher stiffness of concrete may be obtained.

With this model, it is also possible to consider the thermal-physical behaviour of material properties for the calculation of reinforced concrete structures under transient temperatures, e.g. fire, with high accuracy. The results of the simulation of loaded concrete structures subjected to fire depend significantly to the material model being used. The results of displacement calculations using the ATC-model are much closer to measured data than the results derived by the EC2-model for ordinary concrete. The EC2-model does not consider the transient creep of concrete. It was observed that the ATC-model provides, in some cases, smaller reserve than the EC2-model with respect to the time of failure. On the other hand, it clearly indicates the high creep potential of the material under fire and its favourable fire behaviour.

The results of the calculation using the ATC-model for ordinary concrete led to comparatively good approximations to measured data for smaller test specimen and small test columns. The tests of columns with micro silica concrete indicated shorter fire duration compared to the calculation results of EC2-model and ATC-model. Generally, a brittle failure was observed in the test. For concretes with higher Young's modulus which generally leads to an earlier failure under fire, it was shown that the ATC-model worked astonishingly good and it seems that it is possible to adapt the model easily for applications in the field of high strength concrete (HSC and HPC).

With this respect, the calculation of concrete structures with the ATC-model showed the high potential for optimizing concrete structures more than the EC2-model [L159]. The model of EC2(b) was not able to determine the total strains with high accuracy and should not be used in the field of HSC or HPC without further calibrations under standard fire conditions. For natural fire curve, more general material models like the ATC-model are to be applied.

During the calculation of a tunnel cross section, a single bay frame was investigated and presented above. Lower deformations were calculated compared to the EC2-model in all parts of the structures using the new advanced transient concrete model (ATC-model). Due to this lower deformation lower axial forces during heating and a longer fire resistance time occur.

The results of calculations of bending moments show lower moments at the internal surface of the tunnel and higher bending moment at the outside surface. If one compares the results of ATC-model with those of EC2-model calculations, it was noted that the differences for both types of calculations in this case are very small. We did not observe a significant difference in the structural behaviour according to the results of the different concrete models.

Constitutive models for structures should be able to describe continuously the behaviour and load in reality. If a discontinuous behaviour is observed which may be due to sudden changes in stiffness. In this case, one needs a calculation model which takes care of such reactions. One needs a separate definition of several paths of the reaction inside of the structure, inside of the material and between different materials (concrete/steel). In the ATC-model, the reversible and irreversible parts of strains are calculated separately. Therefore, one can directly observe the occurrence of sudden reactions of the material in case of fire.

In the ATC-model, a transient creep reaction is separately included which is based on transient behaviour of the concrete material. The advantage of this is the possibility to account for the material reaction after every time step; this means that in cases of ongoing cooling down of fire, changes of load history and residual effects in the material, the effects may be directly taken into account by ATC simulation model. Only calculations which consider all reversible and irreversible effects at each time step can predict the real structural behaviour. This work can be shown by comparing generally accepted models, especially the Eurocode model EC2, and the differences which may occur in reality if one use a more sophisticated concrete model like the ATC-model. We observed slight differences and some advantages especially by the ATC-model in instances such as the better approximation to measured data of many types of tests.

There are various types of material models for calculation of concrete members that are available. They were usually developed by calculation of structures during fire. All models are generally usable for certain fire cases because the material equations are all based on measured data mostly derived in standard fire furnace tests. The most usable Eurocode model is one with an approximation of all data with a standardized fire curve. The most important advantage of the ATC-model is the possibility for calculating real fire curves particularly model fires because the material model considers the transient effects of temperature with respect to strains and loads.

The implementation of this model in the structural calculation software SAFIR leads to a good tool for calculation structures on the basis of real fires. All calculations showed a good approximation with measured data derived from small specimen and simple structures. Likewise, we compared these results with the good adapted calculation model of the Eurocode for standard fires. This model is generally accepted for an average concrete and standard fire conditions. The new ATC-model is able to include completely the behaviour of all concrete materials and the behaviour under (non-standard) transient fire conditions.

The ATC-model works in general with finite element analysis of SAFIR. The choice for the right calculation model tabulated data, simple calculation method or finite element analysis depends on the complexity of the structure. Simple calculation methods in most cases are only used for the determination of simple structural elements under standard fire conditions. Likewise, more complex structures have more complex reactions and one needs calculations with finite element methods including nonlinear high temperature. Mostly, the continuously exposed structures calculations with simple constitutive models are used. For example, the EC2-model shows good results compared to measured data of building elements under standard fire conditions. But, if there exist a complex structure and a complex material behaviour to be considered, the behav-

iour of these structures should be estimated by the use of an advanced transient concrete model. The calculation using the ATC-model has a high potential for optimizing concrete structures including natural fire curve.

9 Outlook

In the future, there is a great potential for more detailed calculations of complex structures. In the concept of the design of structures, it may be possible to use lower safety factors, i.e. lower excess charges may be used in the design, if the calculation method is based on sophisticated material and structural models.

The results of the calculation using the advanced transient concrete model (ATC-model) for ordinary concrete lead to a comparatively good approximation to measured data for structure under natural and standard fire conditions.

The application of this model, in addition to the existing calculation system of EC2, will lead to a better evaluation of the safety level for special structures under all types of fire curves. This opens the way to optimizing reinforced concrete structures and material design under fire exposure.

The reliability of the new Advanced Transient Concrete Model is high with the validation of calculations of various reinforced concrete members and which were tested under different temperature and load conditions. The validations comprise the safety calculation of the structures during fire exposure and after cooling down. The model includes residual behaviour, transient effects depending on strains, load and temperature, cooling behaviour and a model in tension. With all these conditions, the structure can be optimized in several ways, such as the adaption of reinforced content or examination of structural behaviour with different kinds of concretes.

Likewise, the model can be used with different fire designs or calculated temperature curves. In this case, the simulation of natural fires in the field of CFD-model or zone-model simulations as an adapted calculation model for structural behaviour is of general relevance [L163].

The load bearing capacity is better approached with more realistic and accurate material models. The safety requirements of a calculation using the new ATC-model could be the same as the generally used in the country-specific codes. This will lead to a very usable structure with a very high security level. If the safety requirements are connected to the new realistic material models, the optimization of the structure could also have positive financial effects. The material behaviour of the used concrete can be involved directly in a finite element structural code or in the ATC-model. All aspects of fire behaviour in heating, cooling and residual values after cooling are described and can be calculated. Such calculated structures have regional adaption and safe material resources.

10 References

[L1] Colin, D.T.; Zhang, H.; Pearce, C.J.; Bicanic, N.: Computational Modelling of Concrete Exposed to Fire: The Effects of Coupled Hygro-Thermal-Mechanical Behaviour on the Development of Spalling in Concrete Structures, Proceedings of the Fifth International Conference – Structures in Fire SIF 08, pp. 357-368, Singapore 2008

[L2] Peterson, L.: Einfluss baustofflicher Schädigungsprozesse auf das Tragverhalten von Stahlbetonbauteilen, Berichte aus dem Institut für Baustoffe, Heft 3, Universität Hannover 2003

[L3] Chung, K.; Park, S.; Choi, S.: Material effect for predicting the fire resistance of concrete-filled square steel tube column under constant axial load, Journal of Construction Steel Research, Elsevier Ltd. 2008

[L4] Li, L.; Purkiss, J.: Stress-strain constitutive equations of concrete material at elevated temperatures, Fire Safety Journal (40) 2005

[L5] Anderberg, Y.: The impact of various material models on structural fire behaviour prediction, Proceedings of the Fifth International Conference – Structures in Fire SIF 08, pp. 253-265, Singapore 2008

[L6] Khoury, G.A.: Fire and Concrete: From Materials Behaviour to Application, Proceedings of International Workshop – fire design of concrete structures – from materials modelling to structural performance, , 8th and 9th November, Coimbra 2007

[L7] Felicetti, R.: Assessment of the Equivalent Thermal Diffusivity for Fire Analysis of Concrete Structures, Proceedings of International Workshop – fire design of concrete structures – from materials modelling to structural performance, , 8th and 9th November, Coimbra 2007

[L8] Kordina, K.; Meyer-Ottens, C.: Beton Brandschutz Handbuch, Verlag Bau-Technik, 2. Auflage Düsseldorf 1999

[L9] Pesaveto, F. et al: Finite – Element Modelling of Concrete subjected to high Temperature, Proceedings of the International Workshop - Fire Design of Concrete Structures: What now? What next?, Milano 2004

[L10] Lang, E.: Feuerbeton, Schriftenreihe Spezialbetone Band 4, Verlag Bau + Technik 2001

[L11] Wolf, G.: Untersuchung über das Temperaturverhalten eines Tunnelbetons mit spezieller Gesteinskörnung, Diplomarbeit, Technische Universität Wien, 2004

[L11] Florian, A.: Schädigung von Beton bei Tunnelbränden, Diplomarbeit, Universität Innsbruck, 2002

[L13] Wickström, U.: Heat Transfer and Temperature calculations Based on Plate Thermometer Measurements, Proceedings of the 11th International Conference and Exhibition, FIRE AND MATERIALS 2009, 26-28 January 2009, Fisherman's Wharf, San Francisco, USA

[L14] Debicki, G.; Langhcha, A.: Mass Transport trough Concrete Walls Subjected to High Temperature and Gas Pressure, Proceedings of the International Workshop - Fire Design of Concrete Structures: What now? What next?, Milano 2004

[L15] Schneider, U.: Verhalten von Betonen bei hohen Temperaturen; Deutscher Ausschuss für Stahlbeton, Verlag Wilhelm Ernst & Sohn , Berlin – München 1982

[L16] Horvath, J; Schneider, U.: Behaviour of Ordinary Concrete at High Temperatures, Institut für Baustofflehre, Bauphysik und Brandschutz, TU Wien 2003

[L17] Schneider, U.; Morita, T.; Franssen, J.-M.: A Concrete Model Considering the Load History Applied to Centrally Loaded Columns Under Fire Attack, Fire Safety Science – Proceedings of the fourth International Symposium, Ontario 1994

[L18] Schneider, U.: Ein Beitrag zur Frage des Kriechens und der Relaxation von Beton unter hohen Temperaturen, Habilitationsschrift, Institut für Baustoffe, Massivbau und Brandschutz, TU Braunschweig, Heft 42, Braunschweig, 1979

[L19] Horvath, J; Schneider, U., Diedrichs, U.: Brandverhalten von Hochleistungsbetonen, Institut für Baustofflehre, Bauphysik und Brandschutz, TU Wien 2004

[L20] Lindlbauer, W.: Innovative Brandschutzplanung und – ausführung, Vortrag Arch+Ing Akademie, Wien 2006

[L21] Schneider, U., Diederichs, U.; Weiß, R.: Hochtemperaturverhalten von Festbeton, Sonderforschungsbereich 148 – Brandverhalten von Bauteilen – TU Braunschweig, 1977

[L22] Schneider, U.; Morita, T.; Franssen, J.-M.: Influence of Stress History Function in the Schneider-Concrete-Model Under Fire Attack, Proc. 5th Int. Symp. on Fire Safety Science, Melbourne, IAFSS, pp. 1057-1068, Hasemi ed. Tsukuba, 1997

[L23] Schneider, U.; Schneider, M.; Franssen, J.-M.: Consideration of nonlinear creep strain of siliceous concrete on calculation of mechanical strain under transient temperatures as a function of load history, Proceedings of the Fifth International Conference – Structures in Fire SIF 08, pp. 463-476, Singapore 2008

[L24] Franssen J.-M.,: SAFIR. A Thermal/Structural Program Modelling Structures under Fire, Engineering Journal, A.I.S.C., Vol. 42, No. 3 (2005), 143-158

[L25] Schneider, U.; Schneider, M.; Franssen, J.-M.: Numerical Evaluation of Load Induced Thermal Strain in Restraint Structures - Calculation of a tunnel cross section subjected to fire, Proceedings of the International Conference Applications of Structural Fire Engineering in Prague, 19th-20th February 2009, Czech University of Technology, Prague, Czech Republic

[L26] Nielsen, C.V.; Pearce, C.J.; Bicanic, N.: Improved phenomenological modelling of transient thermal strains for concrete at high temperatures, Comput Concrete 1(2), 2004

[L27] Li, Y.; Wu, B.; Schneider, M.: Numerical Modelling of Restraint RC Columns in Fire, Proceedings of the International Symposium on Computational Structural Engineering, 22nd-24th June 2009, Tongji University in Shanghai, China

[L28] Lea, F.; Stradling, R.: The resistance to fire of concrete and reinforced concrete, Engineering, Vol. 114, No 2959. London 1922

[L29] Endell, H.: Über die Einwirkung hoher Temperaturen auf erhärtetem Zement, Zuschlag und Beton, Zement pp. 823-828, 1926

[L30] Dorn, J.E.: Some fundamental experiments on high temperature creep. Journal of Mechanics Phys Solids. Vol. 3, pp 85-116, 1954

[L31] Philleo, R.: Some physical properties of concrete at high temperatures, Proceedings American Concrete Institute, Vol. 54, 1958

[L32] Zoldners, N.G.: Effect of high temperatures on concrete incorporating different aggregates. ASTM Proceedings Vol. 60, 1960

[L33] England, G.L.; Ross, A.D.: Reinforced concrete under thermal gradients, Magazine of Concrete Research, Vol. 14, No. 40, pp 5-12, March 1962

[L34] Harada, T.: The thermal expansion of concrete at high temperatures. Japan. Tokyo Institute of Technology. Dissertation Pr. 1.2, Tokyo, 1962

[L35] Cruz, C.R.: Elastic properties of concrete at high temperatures. Journal of PCA, Research and Development Laboratories, Vol. 8, No. 1, pp 37-45, January 1966

[L36] Davis, H.S.: Effects of high-temperature exposure on concrete. Materials Research & Standards, Vol. 7, No. 10, October 1966

[L37] Hansen, T.C.; Erikson, L.: Temperature change effect on behaviour of cement paste, mortar and concrete under load, Journal of ACI, Vol. 63, S. 489-504, 1966

[L38] Birkimer, D.L. et al: The effects of exposure to elevated temperatures on time-dependent strains in concrete, ASME, First International Conference on Pressure Vessels Technology, Delft, Betherlands, September 29 – October 2, 1969

[L39] Bruckner, H: Beitrag zur Entwicklung eines Expertensystems zur Betonanalyse, Institut für Baustofflehre, Bauphysik und Brandschutz, TU Wien, Heft 2, 1995

[L40] Schneider, U.; Diederichs, U.: Physical properties of concrete from 20°C up to melting. Part 1 and 2, Betonwerk + Fertigteiltechnik, H. 3 u. 4, 1981

[L41] Hildenbrand, G.; Peeks, M.; Skokan, A.; Reimann, M.: Untersuchung der Wecheslwirkung von Kernschmelze und Reaktorbeton, Research Paper BMTF RS 154, May 1978, Erlangen

[L42] Bazant, Z.P.; Kaplan, M.F.: Concrete at High Temperatures: Material Properties and Mathematical Models, Longham (Addison-Wesley), London, 1996

[L43] Ödeen, K.: Fire Resistance of Prestressed Concrete T Units, National Swedish Institute of Material Testing, 1968

[L44] Schneider, U; Horvath, J: Behaviour of Ordinary Concrete at High Temperatures, RILEM Committee HTC, Vienna, Austria, December 2002

[L45] Collet, Y.; Tavernier, E.: Etude des properties du beton soumis a des temperatures elevees, Comportement du Materiaux Beton en Fonction de la Temperature, Groupe de Travial, November, Brussels 1976

[L46] Harmathy, T.Z.; Allen, L.W.: Thermal properties of selected masonry unit concretes, Journal American Concrete Institute, 70(2), pp. 132-142, 1973

[L47] Khoury, G.A.: Creep of Heated Concrete, Berichte aus der Forschung und Praxis, Festschrift, Institut für Baustofflehre, Bauphysik und Brandschutz, Technische Universität Wien, Wien 2002

[L48] Eurocode 2: Design of concrete structures – Part 1-2: General rules – Structural fire design; 2004

[L49] Wald, F. et al: Urban habitat constructions under catastrophic events, technical sheets, fire resistance, Ed. Czech Technical University in Prague, January 2009

[L50] Jansson, R.: Material properties related to fire spalling of concrete, Report TVBM-3143, Lund Institute of Technology, Lund University, Lund 2008

[L51] Jansson, R.: Measurement of Concrete Thermal Properties at High Temperature, Proceedings from the fib Task Group 4.3 workshop “Fire Design of Concrete structures: What now? What next?”, Milan, Italy, December 2-3, 2004

[L52] Schneider, U.; Franssen, J.-M.; Lebeda, C.: Baulicher Brandschutz, Bauwerk Verlag GmbH, Berlin, 2008

[L53] Schneider, U,: Ingenieurmethoden im Brandschutz, Bauphysik Kaleder 2006, Ernst & Sohn Verlag, Berlin, 2006

[L54] Franssen, J.-M.; Zaharia, R.: Design of Steel Structures subjected to Fire, Les Éditions de l’Univerité de Liège, Liège, 2005

[L55] Schneider, U.; Horvath, J.: Brandschutz – Praxis in Tunnelbauten, Bauwerk Verlag GmbH, Berlin, 2006

[L56] Franssen, J.-M.; Kodur, V.K.R.; Mason, J.: Elements of Theory for SAFIR 2002, A Computer Program for Analysis of Structures submitted to the Fire, University of Liege, 2002

[L57] Khoury, G.A.: Compressive strength of concrete at high temperatures: a reassessment, Magazine of Concrete Research, 44, No. 161, pp. 291-309, December 1992

[L58] Zürz, A.: Dissertation über die thermische Zersetzung hydratisierter Zementpasten und Betone unter Brandbedingungen, Technische Universität Clausthal, September 1988

[L59] Schneider, U.: Properties of Materials at High Temperatures Concrete, published by Gesamthochschule Kassel 1985

[L60] Anderberg, Y.; Thelanderson, S.: Stress and deformation characteristics of concrete at high temperatures, 1. General discussion and critical review of literature. Division of Structural Mechanics and Concrete Constructions, Lund, Institute of Technology, Lund, Bulletin 34, 1973

[L61] Schneider, U., Diederichs, Rosenberger, W.; U.; Weiß, R.: Hochtemperaturverhalten von Festbeton, Sonderforschungsbereich 148 – Brandverhalten von Bauteilen – TU Braunschweig, 1980

[L62] Bicanic, N.; Zhang, B.: Residual Fracture Toughness of Normal- and High-Strength Gravel Concrete after heating to 600°C; ACI Materials Journal, Vol. 99, No 3, 2002

[L63] Ozbolt, J.; Eligehausen, R.; Kozar, I.; Perisic, G.: Transient Thermal 3-D FE Analysis of the Headed Stud Anchors Exposed to Fire, Proceedings of the International Workshop - Fire Design of Concrete Structures: What now? What next?, Milano 2004

[L64] Hager, I.; Pimienta, P.: Mechanical Properties of HPC at High Temperature, Proceedings of the International Workshop - Fire Design of Concrete Structures: What now? What next?, Milano 2004

[L65] Klingsch, E.; Frangi, A.; Fontana, M.: Experimental Analysis of Concrete Strength at High Temperatures and after Cooling, Proceedings of International Conference Applications of Structural Fire Engineering, Prague, 19th-20th February 2009

[L66] Cvetkovska, M.; Cvetanovski, P.; Mihajlov, V.: Numerical and Experimental Determination of Residual Concrete Strength after Action of Fire, Proceedings of International

Conference Applications of Structural Fire Engineering, Prague, 19th-20th February 2009

[L67] Bamonte, P.; Gambarova, P.G.; Felicetti, R.; Meda, A.: Structural Behaviour and Failure Modes of R/C at High Temperature: R/C Sections and 2-D Members, Proceedings of the International Workshop - Fire Design of Concrete Structures: What now? What next?, Milano 2004

[L68] Annarel, E.; Taerwe, L.: Basic Approach for the Diagnosis of Concrete after Fire Exposure, Proceedings of International Conference Applications of Structural Fire Engineering, Prague, 19th-20th February 2009

[L69] CSN 73 1230: Navrhování Betonových Konstrukcí pro Zvýsené a Vyssí Teploty, Vydavatelství Norem Praha, 1990

[L70] Excerpt from the Chinese Normalisation Paper, transmitted by South China University of Technology, Ghouangzou, 2008

[L71] Shi, X.; Tan, T.-H.; Tan, K.-H.; Guo, Z.: Concrete Constitutive Relationships Under Different Stress-Temperature Paths, Journal of Structural Engineering, pp. 1511-1518, December 2002

[L72] Jau, W.-C.; Hunag, K.-L.: A study of reinforced concrete corner columns after fire, ELSEVIER Science Direct, Cement & Concrete Composites 30 (2008) pp. 622-638

[L73] Han, L.-H.; Hou, J.-s.: Concrete-Filled Hollow Structural Steel Columns after Exposure to ISO-834 Fire Standard, Journal of Structural Engineering, January 2003

[L74] Wu. B.; Li, Y.: An experimental Study on Behaviours of Axially Restraint NSC and HSC Columns in Fire, Work of Department of Civil Engineering, South China University of Technology, Guangzhou, China 2008

[L75] Hung, Z.; Burgess, I.W.; Plank, R.J.: Behaviour of Reinforced Concrete Structures in Fire, Proceedings of the Fourth International Workshop – Structures in Fire SIF 06, pp. 561-572, Aveiro 2006

[L76] Boström, L.; Jansson, R.: Results from two Research Programs on Spalling of Concrete, Proceedings of the Fifth International Conference – Structures in Fire SIF 08, pp. 477-487, Singapore 2008

[L77] Richter, E.: Fire Tests on single-Shell Tunnel Segments Made of a New High-Performance Fireproof concrete, Proceedings of the International Workshop - Fire Design of Concrete Structures: What now? What next?, Milano 2004

[L78] Savov, K.; Lackner, R.; Mang, H.A.: Stability assessment of shallow tunnels subjected to fire load, Fire Safety Journal, 2005

[L79] Kusterle, W. et al: Brandbeständigkeit von Faser-, Stahl- und Spannbeton, Hrsg. Bundesministerium für Verkehr, Innovation und Technologie in Zusammenarbeit mit der Eisenbahn-Hochleistungsstrecken AG, Straßenforschung Heft 544, Wien 2004

[L80] Persson, B.: Transient Thermal Strain of Self-Compacting Concrete With and Without Polypropylene Fibres, Proceedings of the Fourth International Workshop – Structures in Fire SIF 06, pp. 735-746, Aveiro 2006

[L81] Lie, T.T.; Rowe, T.J.; Lin, T.D.: Residual Strength of Fire Exposed Reinforced Concrete Columns, National Research Council Canada, NRCC 26486, Canada 1986

[L82] Yang, H.; Han, L.-H.; Wang, Y.-C.: Effects of heating and loading on post-fire cooling behaviour of concrete-filled steel tabular columns, Journal of Constructional Steel Research 64, pp. 556-570, 2008

[L83] Coccia, S.; Rinaldi, Z.: Residual Strength of R.C. Beams after Fire, Proceedings of the Fourth International Workshop – Structures in Fire SIF 06, pp. 767-777, Aveiro 2006

[L84] Franssen, J.-M.; Kodur, V.K.R.: Residual load bearing capacity of structures exposed to fire, ASCE 2004

[L85] Franssen, J.M.: Design of Concrete Columns Based on EC2 Tabulated Data – A Critical Review, Proceedings of the First International Workshop Structures in Fire", 19th and 20th June, Copenhagen 2000

[L86] Schneider, U.; Schneider, M.; Franssen, J.-M.: Comparison of an approximated method with FEA calculations for the evaluation of the fire resistance of concrete tunnel sections, Proceedings of International Workshop – fire design of concrete structures – from materials modelling to structural performance, , 8th and 9th November, Coimbra 2007

[L87] Ring, T.; Zeiml, M.; Lackner, R.: Structural Safety Assessment of Tunnels Subjected to Fire Loading, Proceedings of the International Conference Applications of Structural Fire Engineering in Prague, 19th-20th February 2009, Czech University of Technology, Prague, Czech Republic

[L88] Borgono, W.: Tragverhalten von Slim Floor Decken mit Betonhohlplatten bei Raumtemperatur und Brandeinwirkung, IBK Bericht Nr. 233, Institut für Baustatik und Konstruktion, ETH Zürich 1997

[L89] Reick, M.: Brandverhalten von Befestigungen mit großem Randabstand in Beton bei zentrischer Zugbeanspruchung, Dissertation Universität Stuttgart, Institut für Werkstoffe im Bauwesen, Stuttgart 2001

[L90] Badders, B.L.; Mehaffey, J.R.; Richardson, L.R.: Using commercial Software Packages to Model the Fire Performance of exposed Glulam Beams, Proceedings of the Fourth International Workshop – Structures in Fire SIF 06, pp. 931-937, Aveiro 2006

[L91] Kodur, V.; Dwaikat, M.; Raut, N.: Macroscopic Finite Element Model for Tracing the Response of Concrete Structures under Fire Conditions, Proceedings of International Workshop – fire design of concrete structures – from materials modelling to structural performance, 8th and 9th November, Coimbra 2007

[L92] Franssen, Jean-Marc: Plastic Analysis of Concrete Structures Subjected to Fire, Proceedings of the International Workshop - Fire Design of Concrete Structures: What now? What next?, Milano 2004

[L93] Pesavento, F.; Gawin, D.; Schrefler, B.: Finite-Element Modelling of Concrete Subjected to High Temperature, Proceedings of the International Workshop - Fire Design of Concrete Structures: What now? What next?, Milano 2004

[L94] Majorana, C.; Salomoni, V.A.; Khoury, G.A.: Micro-Structural Modelling of concrete under Fire Conditions, Proceedings of International Workshop – fire design of concrete structures – from materials modelling to structural performance, , 8th and 9th November, Coimbra 2007

[L95] Riva, P.: Nonlinear and Plastic Analysis of Reinforced-Concrete Beams, Proceedings of the International Workshop - Fire Design of Concrete Structures: What now? What next?, Milano 2004

[L96] Media, A.; Riva, P.: Behaviour of Precast R.C.: Elements Under Fire Conditions, Proceedings Fourth International Workshop “Structures in Fire” in Aveiro 2006

[L97] Quiel, S.E.; Garlock, M.E.M.: 3-D versus 2-D Modelling of a High-Rise Steel Framed Building under Fire, Proceedings of the Fifth International Conference – Structures in Fire SIF 08, pp. 277-289, Singapore 2008

[L98] Khennane, A.; Melchers, R.E.: Meso-Scale Finite Element Investigation into the Short and Long Term Strengths of Glass Fibre Reinforced Composites, Report TR-2003-04, Faculty of Engineering & Surveying University of Southern Queensland, 2003

[L99] Goh, K. L.; Aspden, R. M.; Hukins D. W. L.: Review: Finite element analysis of stress transfer in short-fibre composite materials, Composites Science and Technology 64 (2004) 1091–1100

[L100] Khennane, A.; Melchers, R.E.: A finite element approach for modelling the statical strength of a unidirectional composite, Advances in Mechanics of Structures and Materials, Proceedings of the 17th Australian Conference (ACMSM17), Queensland, Australia, 12.-14. June 2002

[L101] Anderberg, Y.; Thelanderson, S.: Stress and deformation characteristics of concrete at high temperatures, 2. Experimental investigation and material behaviour model. Division of Structural Mechanics and Concrete Constructions, Lund, Institute of Technology, Lund, Bulletin 54, 1976

[L102] Klingsch, W.; Kordina, K.; Schneider, U.; Haksever, A.: “Zur Berechnung von Stahlbetonkonstruktionen im Brandfall”; CIB – w 14 paper 90/75 (D), SFB 148, Technische Universität Braunschweig, (1975).

[L103] Schneider, U.: Zur Kinetik festigkeitsmindernder Reaktionen in Normalbeton bei hohen Temperaturen, Schriftenreihe des Sonderforschungsbereichs 148, TU Braunschweig, Heft 3, Braunschweig 1974

[L104] Haksever, A.: Zur Frage des Trag- und Verformungsverhaltens ebener Stahlbetonrahmen im Brandfall, Dissertationsschrift, Institut für Baustoffkunde und Stahlbetonbau, Heft 35, TU Braunschweig, Braunschweig, 1977

[L105] Khoury, G.A.; Grainger, B.N.; Sullivan, P.J.E.: Transient thermal strain of concrete: Literature review, conditions with specimens and behaviour of individual constituents, Magazine of Concrete Research Vol. 37 No. 132, 1985

[L106] Khoury, G.A.; Grainger, B.N.; Sullivan, P.J.E.: Strain of concrete during first heating to 600°C under load, Magazine of Concrete Research Vol. 37 No. 133, 1985

[L107] Schneider, U; Schneider, M.: An Advanced Transient Concrete Model for the Determination of Restraint in Concrete Structures Subjected to Fire, in: Journal of Advanced Concrete Technology, Vol. 7 No. 3, October 2009, Japan Concrete Institute

[L108] Eurocode 2: Design of concrete structures Part 1-1: General rules and rules for buildings; 2004

[L109] Chung, K.; Park, S.; Choi, S.: Material effect for predicting the fire resistance of concrete-filled square steel tube column under constant axial load, Journal of Construction Steel Research, Elsevier Ltd. 2008

[L110] Diederichs, U.: Modelle zur Beschreibung der Betonverformung bei instationären Temperaturen, Abschlußkolloqium Bauwerke unter Brandeinwirkung, Technische Universität Braunschweig, pp. 25-35, Braunschweig 1987

[L111] Mindeguia, J.C. et al.: Experimental Study of Transient Thermal Strain and Creep of an Ordinary Concrete at High Temperatures, Proceedings of the Fourth International Workshop – Structures in Fire SIF 06, pp. 697-708, Aveiro 2006

[L112] Cvetkovska, M.; Cvetanovski, P.; Mihajlov, V.: Fire Resistance Curves for RC Columns, Proceedings of International Conference Applications of Structural Fire Engineering, Prague, 19th-20th February 2009

[L113] Willam, K.; Xi, Y.; Basche, H.: Constitutive Aspect of High-Temperature Material Models, Proceedings of the International Workshop - Fire Design of Concrete Structures: What now? What next?, Milano 2004

[L114] Bamonte, P.; Cangiano, S; Gambarova, P.G.: Thermo-Mechanical Behaviour of Concrete Mixes Suitable for the Rehabilitation of Fire-Damaged Tunnel Liners, Proceedings of the Fourth International Workshop – Structures in Fire SIF 06, pp. 545-559, Aveiro 2006

[L115] Diederichs, U.: Hochtemperatur- und Brandverhalten von hochfestem Stahlfaserbeton, Institut für Baustoffe, Massivbau und Brandschutz, TU Braunschweig, Heft 142, Braunschweig 1999

[L116] Diederichs, U.; Jumppanen, U.-M.; Penttala, V.: Behaviour of high strength concrete at high temperatures, ESPOO, 1989, Helsinki University of Technology, Helsinki 1989

[L117] Anderberg, Y.: The effect of the Constitutive Models on the Prediction of Concrete Mechanical Behaviour and on the Design of Concrete Structures Exposed to Fire, Proceedings of the International Workshop - Fire Design of Concrete Structures: What now? What next?, Milano 2004

[L118] Khoury, G.A.; Grainger, B.N.; Sullivan, P.J.E.: Strain of concrete during first cooling from 600°C under load, Magazine of Concrete Research Vol. 37 No. 134, 1986

[L119] Schneider, U.: Behaviours of concrete under thermal steady state and no steady state conditions in: Fire Materials, 1976, pp. 103–115

[L120] RILEM TC HTC 200: Mechanical Concrete Properties at High Temperature - Recommendation Part 1: Mat.&Struct., Vol. 44, Paris, June 2007

[L121] Law, A; Gillie, M.: Load Induced Thermal Strain: Implication for Structural Behaviour, Proceedings of the Fifth International Conference – Structures in Fire SIF 08, pp. 487-496, Singapore 2008

[L122] RILEM TC 129-MHT: Test Methods for Mechanical Properties of Concrete - Recommendation: Part 7: Transient creep for service and accident conditions, Mat.&Struct., Vol. 31, Paris, June 1998

[L123] Schneider, U.: Concrete at High Temperatures – A General Review, Fire Safety Journal, 13, 1988

[L124] Diederichs, U.; Ehm, C.; Hinrichsmeyer, K.; Schneider, U.; Wydra, W.: Hochtemperaturverhalten von Festbeton, Sonderforschungsbereich 148 – Brandverhalten von Bauteilen – TU Braunschweig, 1987

[L125] Klingsch, E.; Frangi, A.; Fontana, M.: Experimental Analysis of Concrete Strength at High Temperatures and after Cooling, Acta Polytechnica Vol. 49 No. 1/2009, Czech Technical University Publishing House

[L126] Bockhold, J.; Stangenberg, F.: Modellierung des nichtlinearen Kriechens von Beton, Beton- und Stahlbetonbau 99, Heft 3, Verlag Ernst & Sohn, Berlin 2004

[L127] Larson, M.; Jonasson, J.-E.: Linear Logarithmic Model for Concrete Creep, Journal of Advanced Concrete Technology, Vol. 1, No 2, pp. 172-187, Japan, July 2008

[L128] Schneider, U.: Behaviour of Concrete at High Temperatures, Verlag Ernst & Sohn, Berlin 1982

[L129] Kordina, K.: Zug-Kriechen von Normalbeton, Institut für Baustoffe, Massivbau und Brandschutz, TU Braunschweig, Heft 142, Braunschweig 1999

[L130] Schneider, U: Ein Beitrag zur Klärung des Kriechens und der Relaxation von Beton unter instationärer Temperaturentwicklung, Forschungsbeiträge für die Baupraxis, Verlag Ernst & Sohn, Berlin, 1979

[L131] Alonso, C.: Assessment of Damage in Concrete Structures Exposed to Fire. Micro and Macrostructural Analysis, Proceedings of the Fourth International Workshop – Structures in Fire SIF 06, pp. 599-611, Aveiro 2006

[L132] Alonso, C.; Lorenzo, F.-M.: Dehydratation and Rehydratation Processes in Cementitious Materials after Fire – Correlation between Micro and Macrostructural Transformations, Proceedings of International Workshop – fire design of concrete structures – from materials modelling to structural performance, , 8th and 9th November, Coimbra 2007

[L133] Hirashima, T., Toyoda, K,; Yamashita, H.; Tokoyoda, M.; Uesugi, H.: Compression tests of High-Strength Concrete Cylinder at Elevated Temperature, Proceedings of International Workshop – fire design of concrete structures – from materials modelling to structural performance, , 8th and 9th November, Coimbra 2007

[L134] Watanabe, K.; Horiguchi, T.: Effect of elevated temperatures on flexural behaviour of hybrid reinforced high strength concrete, Proceedings of the Fifth International Conference – Structures in Fire SIF 08, pp. 430-439, Singapore 2008

[L134] Horvath, J.: Beiträge zum Brandverhalten von Hochleistungsbetonen, Technische Universität Wien 2003

[L135] Deger, Y.: Die Methode der Finiten Elemente, Grundlagen und Einsatz in der Praxis, 3. erweiterte Auflage, expert-Verlag, Renningen, 2004

[L136] Pacson, F: 2 ½ Thermal-Mechanical Model of continuous casting of steel using Finite Element Method, PHD-Thesis, University of Liege, 2003

[L137] Long, B.H.; Wang, F.: Calculation of thermal stress in reinforced concrete beam, Advances in Mechanics of Structures and Materials, Proceedings of the 17th Australian Conference (ACMSM17), Queensland, Australia, 12.-14. June 2002

[L138] Thieme, D.: Einführung in die Finite-Elemente-Methode für Bauingenieure, Verlag für Bauwesen, Berlin, 1996

[L139] Li, R.; Tang, T.; Zhang, P.: A Moving Mesh Finite Element Algorithm for Singular Problems in Two and Three Space Dimensions, Journal of Computational Physics 177, 365–393 (2002)

[L140] Du, Q.; Huang, Z.; Wang, D.: Mesh and Solver Co-adaptation in Finite Element Methods for Anisotropic Problems, published online in Wiley InterScience 4 March 2005

[L141] Souiyah, M.; Alshoaibi, A; Muchtar, A; Arffin, A.K.: Finite element model for linear-elastic mixed mode loading using adaptive mesh strategy, Journal of Zhejiang University SCIENCE A, 2008 9(1):32-37

[L142] Franssen, J.-M: SAFIR: A thermal/structural Program for Modelling Structures under Fire, Engineering Journal / 3rd Quarter / 2005

[L143] Goncalves, M.C.; Franssen, J.-M.; Abrantes, V.; Rodrigues, J.P.: Numerical Analysis of Concrete Columns in Fire – Advanced versus simplified calculation methods, Proceedings of International Conference Applications of Structural Fire Engineering, Prague, 19th-20th February 2009

[L144] Dwaikat, M.B.; Kodur, V.K.R.: Effect of fire scenario, restraint conditions, and spalling on the behaviour of RC columns, Proceedings of the Fifth International Conference – Structures in Fire SIF 08, pp. 463-476, Singapore 2008

[L145] Diederichs, U; Rostásy, F. S.: Untersuchungsbericht 5001/0013 – Herstellung von Stützenabschnitten aus 10 verschiedenen Mischungen hochfesten Betons und ihre Prüfung unter Brandbeanspruchung nach der Einheitstemperaturkurve gemäß DIN 4102 (ISO 834), IBMB TU Braunschweig, 1993

[L146] Schneider, U.; Schneider, M.; Franssen, J.-M.: Numerical evaluation of load induced thermal strain in restraint structures compared with an experimental study on reinforced concrete columns, Proceedings of the 11th International Conference and Exhibition, FIRE AND MATERIALS 2009, 26-28 January 2009, Fisherman's Wharf, San Francisco, USA

[L147] Wesche, K.: Beton für tragende Bauteile, Vieweg+Teubner Verlag, 3. Auflage, Wiesbaden, 1993

[L148] Bamonte, P.; Meda, A.: On Fire Behaviour of R/C Sections Subjected to an Eccentric Axial Force, Proceedings of the International Workshop - Fire Design of Concrete Structures: What now? What next?, Milano 2004

[L149] Franssen, J.-M.: Contributions à la Modélisation des Incendies dans les Bâtiments et leurs Effets sur les Structures, Université de Liège, Belgium 1998

[L150] Mason, J.E.: Heat Transfer Programs for the Design of Structures Exposed to Fire, University of Canterbury, Christchurch 1999

[L151] Franssen, J.-M.; Hanus, F.; Dotreppe, J.-C.: Numerical Evaluation of the Fire Behaviour of a Concrete Tunnel Integrating the Effects of Spalling, Proceedings of International Workshop – fire design of concrete structures – from materials modelling to structural performance, , 8th and 9th November, Coimbra 2007

[L152] OVBB-Sachstandsbericht: Brandeinwirkungen – Straße, Eisenbahn, U-Bahn. ÖVBB-Arbeitskreis AA1, Entwurf zum Grundstück, Verf.: Lemmerer, J. et al: Wien, Januar 2005

[L153] SFPE – The SFPE Handbook of Fire Protection Engineering 2nd edition, SFPE, Quincy, Ma, USA 1995

[L154] Wittke, W.; Wittke-Gattermann, P.: Tunnelstatik, Beton Kalender 2005: Fertigteile-Tunnelbauwerke, Verlag Ernst & Sohn, Berlin 2005

[L155] Upmeier, J.: Nachweis der Brandsicherheit von kammerbetonierten Verbundbauteilen über Grenzbrandlasten, Universität Hannover, Institut für Stahlbau, Schriftenreihe Heft 19, Hannover 2001

[L156] Eurocode 1: Actions on structures. Part 1-1: General actions. Densities, self-weight, imposed loads for buildings; EN 1991-1-1:2002

[L157] Beutinger, P.; Sawade, G.: Standsicherheit – Vorhersagemöglichkeit der Bodentragfähigkeit aus geotechnischer Sicht, Tiefbau Tagung Magdeburg 2004

[L158] Feron, Celine: The Effect of the Restrain Conditions on the Fire Resistance of Tunnel Structures, Proceedings of the International Workshop - Fire Design of Concrete Structures: What now? What next?, Milano 2004

[L159] VÖZFI: Abschlussbericht – Praxisverhalten von erhöht brandbeständigem Innenschalen-Beton, Wien, 2003

[L160] Rotter, J.M.; Usmani, A.S.: Thermal Effects, Proceedings of the First International Workshop Structures in Fire", 19th and 20th June, Copenhagen 2000

[L161] Harada, Kazunori: Actual State of the Codes on Fire Design in Japan Proceedings of the International Workshop - Fire Design of Concrete Structures: What now? What next?, Milano 2004

[L162] Bailey, Colin G.; Toh, Wee Siang: Small-scale concrete slab tests at ambient and elevated temperatures, Science Direct, Elsevier 2007

[L163] Schneider, U.: Ingenieurmethoden im Brandschutz, 2. Auflage, Werner Verlag, Köln

Appendix

11 Appendix 1 – The program code of SAFIR ATC-model

11.1 The Routine DONNEE

```
case ( 'ATCM' )

lprint = .false.

if (ltemperature) then

        read(i1,*) (paracold(npara,nm),npara=i5,i8)
        write(2,323) nm,cloc,(paracold(iloc,nm),iloc=i5,i8)
        323      format(/3X,I2,1x,A10/
        '     This material is CONCRETE, from Ordinary Concrete.'/
        '       WATER CONTENT in l/m³          :',E12.5/
        '       CONVECTION COEFF. ON HOT  SURF.  :',E12.5/
        '       CONVECTION COEFF. ON COLD SURF.  :',E12.5/
        '       RELATIVE EMISSIVITY            :',E12.5)
        else

        epsu = 2.2d-3

        read(i1,*) (paracold(npara,nm),npara=i1,i5)

        lprint = .false.
        write(2,129) nm,cloc,(paracold(iloc,nm),iloc=i1,i5)

        129      format(/3X,I2,1x,A10/
        '     This material is CONCRETE, SCHNEIDER MODEL.'/
        '       YOUNG''S MODULUS      :',E12.5/
        '       POISON''S RATIO       :',E12.5/
        '       COMPRESSIVE STRENGTH  :',E12.5/
        '       TENSION STRENGTH      :',E12.5/
        '       WATER CONTENT in l/m3  :',E12.5)

endif
```

11.2 The Routine MATER1

```
else if (cmat.eq.'ATCM') then

Rc = paracold(i3,nm)
Rt = paracold(i4,nm)
E = paracold(i1,nm)

parahot(i13,ntot) = tmax
alpha = parahot(i7,ntot)

ft0 = rkfc0_schneiders(t,tmax)
ft = rkfc_schneiders(t,tmax,alpha)
re = rkre_schneiders(t,tmax,alpha)

if (t. le. tmax) then
        parahot(i1,ntot) = ft * Rc
else

        if ( (t.lt.tmax) .and. (dabs(tmax-20.).ge.precision) ) then
                factor = re + (ft - re) * ((t - 20) / (tmax - 20))
                else
                factor = re
        endif
        parahot(i1,ntot) = factor * Rc
endif


if (t. le. tmax) then
        parahot(i2,ntot) = ft0*Rt
else
        if (tmax. le. 300) then
                re0 = 2d-5 * tmax * tmax - 0.006 * tmax + 1.1
        else
                re0 = 3.3955 * exp( - 0.0044 * tmax)
        endif
        if (t. ge. 20.d0) then
                factor = re0 + (ft0 - re0) * ((t - 20) / (tmax - 20))
        else
                factor = re0
        endif
        parahot(i2,ntot) = factor * Rc
endif

        fy0 = rkym0_schneiders(t,tmax)
        fy = rkym_schneiders(t,tmax,alpha)

        if (t. le. tmax) then
                parahot(i8,ntot) = fy * E
```

```
                else
                if ( (t.lt.tmax) .and. (dabs(tmax-20.).ge.precision) ) then
                        factor = fy0 + (fy - fy0) * ((t - 20) / (tmax - 20))
                else
                        factor = fy0
                endif
                parahot(i8,ntot) = factor * E
        endif

Ehotalpha = parahot(i8,ntot)
parahot(i9,ntot) = fy0 * E
Ehottension = parahot(i9,ntot)
parahot(idimpara-i8,ntot) = parahot(i9,ntot) / parahot(i8,ntot)
epsu = epsu_schneiders(t,tmax,alpha)

epscu = EPScu_CONCEC2(tmax)
parahot(i3,ntot) = epsu
parahot(i4,ntot) = epscu

w = paracold(i5,nm) / 23d0
gammaw = 0.3d-3 * sqrt(w) + 2.2d-3

Tg = 800.D0
RC1 = 2.5d0
RC2 = 0.7d0
RC3 = 0.7d0
gamma0 = 7.5d-3
t1 = gammaw * (tmax - 20.d0)
t2 = gamma0 * (tmax - Tg)

phi = RC1 * tanh(t1) + RC2 * tanh(t2) + RC3

parahot(i5,ntot) = phi

epsth = epsth_schneiders(t,tmax)

if ( (t.lt.tmax) .and. (dabs(tmax-20.).ge.precision) ) then
        if (parahot(i7,ntot). eq. 0.) then
                delta0 = 1.445d-3 * exp(3.4d-3 * tmax) - 1.445d-3
                * exp(3.4d-3 * t)
                epsth = epsth - delta0
                parahot(idimpara-i7,ntot) = delta0
        else
                delta1 = 1.9d-8 * tmax * tmax + 8d-6 * tmax + 3.2d-4
                delta2 = 1.9d-8 * t * t + 8d-6 * t + 3.2d-4
                deltaalpha = delta1 - delta2
                epsth = epsth - deltaalpha
        endif
endif
```

```
parahot(idimpara,ntot) = epsth

if (parahot(idimpara-i2,ntot). le. 0.) then
        alphatcritical = - parahot(idimpara-i2,ntot) / paracold(i3,nm)
        else
        alphatcritical = 0
endif

if (alphatcritical. le. 0.1) then
        tcritical = 900.d0
        elseif (alphatcritical. le. 0.2) then
                tcritical = 850.d0
        elseif (alphatcritical. le. 0.3) then
                tcritical = 800.d0
        elseif (alphatcritical. le. 0.4) then
                tcritical = 750.d0
        elseif (alphatcritical. le. 0.5) then
                tcritical = 700.d0
        elseif (alphatcritical. le. 0.6) then
                tcritical = 650.d0
else
        tcritical = 600.d0
endif

if (tmax. ge. tcritical) then
        parahot(i8,ntot) = r0
        parahot(i9,ntot) = r0
        parahot(i1,ntot) = r0
        parahot(i2,ntot) = r0
endif

if (t. le. 300) then
        vcritical = 0.0005 / 1000
        elseif (t. le. 350) then
                vcritical = 0.00075 / 1000
        elseif (t. le. 400) then
                vcritical = 0.001 / 1000
        elseif (t. le. 450) then
                vcritical = 0.002 / 1000
        elseif (t. le. 500) then
                vcritical = 0.003 / 1000
        elseif (t. le. 550) then
                vcritical = 0.00325 / 1000
        elseif (t. le. 600) then
                vcritical = 0.003 / 1000
        elseif (t. le. 700) then
                vcritical = 0.0025 / 1000
        elseif (t. le. 800) then
                vcritical = 0.002 / 1000
        elseif (t. le. 900) then
```

```
                vcritical = 0.0015 / 1000
else
        vcritical = 0.001 / 1000
endif

if (parahot(idimpara-i9,ntot). le. 0) then
        depssurdsigma = - parahot(idimpara-i9,ntot)
        else
                depssurdsigma = parahot(idimpara-i9,ntot)
endif

if (depssurdsigma. gt. vcritical) then
        parahot(i8,ntot) = r0
        parahot(i9,ntot) = r0
        parahot(i1,ntot) = r0
        parahot(i2,ntot) = r0

endif

continue
```

```
FUNCTION EPSTH_SCHNEIDERS(t,tmax)

include 'declare.inc'
include 'mycom.inc'

T1 = tmax
T2 = tmax * tmax
T3 = tmax * tmax * tmax

if (tmax.le.650.) then
        epsth = 6.6d-11 * T3 - 1.7d-8 * T2 + 9d-6 * T1 + 1.369d-4
        else if ((tmax. ge. 650.) .and. (tmax. le. 1000.)) then
                epsth = 2d-8 * T2 - 3.94d-5 * T1 + 0.0342
else
        epsth = 2d-8 * 1000 * 1000 - 3.94d-5 * 1000 + 0.0342
endif

if (tmax. eq. 20.) then
        epsth20 = 6.6d-11 * T3 - 1.7d-8 * T2 + 9d-6 * T1 + 1.369d-4
endif

if (tmax. le. 100.) then
        epsth = epsth + epsth20 * (T1-100)/80
endif

epsth_schneiders = epsth

return

end
```

```
FUNCTION RKFC_SCHNEIDERS(t,tmax,alpha)

include 'declare.inc'
include 'mycom.inc'

if (tmax. le. 100.d0) then
        fc0 = r1 - 0.05d0 * (tmax - 20.d0) / 80.d0
        else if (tmax. le. 200.d0) then
                fc0 = 0.95d0 - .0005d0 * (tmax - 100.d0)
        else if (tmax. le. 300.d0) then
                fc0 = 0.90d0 - .0005d0 * (tmax - 200.d0)
        else if (tmax. le. 400.d0) then
                fc0 = 0.85d0 - .0010d0 * (tmax - 300.d0)
        else if (tmax. le. 500.d0) then
                fc0 = 0.75d0 - .0015d0 * (tmax - 400.d0)
        else if (tmax. le. 600.d0) then
                fc0 = 0.60d0 - .0015d0 * (tmax - 500.d0)
        else if (tmax. le. 700.d0) then
                fc0 = 0.45d0 - .0015d0 * (tmax - 600.d0)
        else if (tmax. le. 800.d0) then
                fc0 = 0.30d0 - .0015d0 * (tmax - 700.d0)
        else if (tmax. le. 900.d0) then
                fc0 = 0.15d0 - .0007d0 * (tmax - 800.d0)
        else if (tmax. le. 1000.d0) then
                fc0 = 0.08d0 - .0004d0 * (tmax - 900.d0)
        else if (tmax. le. 1100.d0) then
                fc0 = 0.04d0 - .0003d0 * (tmax - 1000.d0)
else
        fc0 = max(0.01d0 - .0001d0 * (tmax - 1100.d0),0.0001)
endif

if (tmax. le. 750.d0) then
        fc01 = (- 2d-4 * tmax * tmax + 0.047 * tmax + 97.7) / 100
        else if (tmax. le. 1000.d0) then
                fc01 = 0.25 - 0.001 * (tmax - 750.d0)
else
        fc01 = 0.
endif

if (tmax. le. 750.d0) then
        fc03 = (- 2d-4 * tmax * tmax + 0.068 * tmax + 98.75) / 100
        else if (tmax. le. 1000.d0) then
                fc03 = 0.38 - 0.00152 * (tmax - 750.d0)
else
        fc03 = 0.
endif

if (alpha. le. 0.1d0) then
        fc = fc0 + ((fc01 - fc0) / (0.1 - 0.)) * (alpha - 0.)
else
```

```
        fc = fc01 + ((fc03 - fc01) / (0.3 - 0.1)) * (alpha-0.1)
endif

rkfc_schneiders = fc

return

end
```

```
FUNCTION RKFC0_SCHNEIDERS(t,tmax)

include 'declare.inc'
include 'mycom.inc'

if (tmax. le. 100.d0) then
        fc0 = r1 - 0.05d0 * (tmax - 20.d0) / 80.d0
        else if (tmax. le. 200.d0) then
                fc0 = 0.95d0 - .0005d0 * (tmax - 100.d0)
        else if (tmax. le. 300.d0) then
                fc0 = 0.90d0 - .0005d0 * (tmax - 200.d0)
        else if (tmax. le. 400.d0) then
                fc0 = 0.85d0 - .0010d0 * (tmax - 300.d0)
        else if (tmax. le. 500.d0) then
                fc0 = 0.75d0 - .0015d0 * (tmax - 400.d0)
        else if (tmax. le. 600.d0) then
                fc0 = 0.60d0 - .0015d0 * (tmax - 500.d0)
        else if (tmax. le. 700.d0) then
                fc0 = 0.45d0 - .0015d0 * (tmax - 600.d0)
        else if (tmax. le. 800.d0) then
                fc0 = 0.30d0 - .0015d0 * (tmax - 700.d0)
        else if (tmax. le. 900.d0) then
                fc0 = 0.15d0 - .0007d0 * (tmax - 800.d0)
        else if (tmax. le. 1000.d0) then
                fc0 = 0.08d0 - .0004d0 * (tmax - 900.d0)
        else if (tmax. le. 1100.d0) then
                fc0 = 0.04d0 - .0003d0 * (tmax - 1000.d0)
else
        fc0 = max(0.01d0 - .0001d0 * (tmax - 1100.d0),0.0001)
endif

rkfc0_schneiders = fc0

return

end
```

```
FUNCTION RKYM_SCHNEIDERS(t,tmax,alpha)

include 'declare.inc'
include 'mycom.inc'

T1 = tmax
T2 = tmax * tmax
T3 = tmax * tmax * tmax

if (tmax. le. 320.d0) then
        ym0 = 1 - 3d-3 * (T1 - 20.) + 4.085d-6 * (T1 - 20.) * (T1 - 20.d0)
        else if (tmax. le. 450.d0) then
                ym0 = 0.89406 - 3.2445d-3 * T1 + 1.0081d-5 * T2 - 1.2801d-8 * T3
        else if (tmax. le. 600.d0) then
                ym0 = 0.45 * exp( - 7.52d-3 * (T1 - 400.))
else
        ym0 = exp( - 4.d-3 * (T1 - 20.))
endif

if (tmax. le. 320.d0) then
        ym01 = 3.d-6 * T2 - 2.311d-3 * T1 + 1.04505
        else if (tmax. le. 450.d0) then
                ym01 = - 5.1d-6 * T2 + 2.73d-3 * T1 + 0.262
        else if (tmax. le. 600.d0) then
                ym01 = - 6.d-8 * T3 + 1d-4 * T2 - 0.056 * T1 + 10.874
        else
                ym01 = 0.82554d0 * exp( - 0.0016 * T1)
endif

if (tmax. le. 320.d0) then
        ym03 = 2.d-6 * T2 - 1.57d-3 * T1 + 1.0306
        else if (tmax. le. 450.d0) then
                ym03 = - 4.d-6 * T2 + 2.5d-3 * T1 + 0.342
        else if (tmax. le. 600.d0) then
                ym03 = 1.767d0 * exp( - 0.0022 * T1)
else
        ym03 = 0.86 * exp( - 0.001 * T1)
endif

if (alpha. le. 0.1d0) then
        ym = ym0 + ((ym01 - ym0) / (0.1 - 0.)) * (alpha - 0.)
else
                ym = ym01 + ((ym03 - ym01) / (0.3 - 0.1)) * (alpha - 0.1)
endif

rkym_schneiders = ym

return

end
```

```
FUNCTION RKYM0_SCHNEIDERS(t,tmax)

include 'declare.inc'
include 'mycom.inc'

T1 = tmax
T2 = tmax * tmax
T3 = tmax * tmax * tmax

if (tmax. le. 320.d0) then
        ym0 = 1 - 3d-3 * (T1 - 20.) + 4.085d-6 * (T1 - 20.) * (T1 - 20.d0)
        else if (tmax. le. 450.d0) then
                ym0 = 0.89406 - 3.2445d-3 * T1 + 1.0081d-5 * T2 - 1.2801d-8 * T3
        else if (tmax. le. 600.d0) then
                ym0 = 0.45 * exp( - 7.52d-3 * (T1 - 400.))
else
        ym0 = exp( - 4.d-3 * (T1 - 20.))
endif

rkym0_schneiders = ym0

return

end
```

```
FUNCTION RKRE_SCHNEIDERS(t,tmax,alpha)

include 'declare.inc'
include 'mycom.inc'

if (tmax. le. 300) then
        re0 = 2d-5 * Tmax * tmax - 0.006 * tmax + 1.1
        re01 = 5d-6 * Tmax * Tmax -0.0015 * tmax + 1.03
        re03 = 1
        if (alpha. le. 0.1) then
                re = re0 + ((re01 - re0) / (0.1 - 0.)) * (alpha - 0.)
        else
                re = re01 + ((re03 - re01) / (0.3 - 0.1)) * (alpha - 0.1)
        endif

else

        re0 = 3.3955 * exp( - 0.0044 * tmax)
        re01 = 3.1659 * exp( - 0.0037 * tmax)
        re03 = 3.5607 * exp ( - 0.0037 * tmax)

        if (alpha. le. 0.1) then
                re = re0 + ((re01 - re0) / (0.1 - 0.)) * (alpha - 0.)
        else
                re = re01 + ((re03 - re01) / (0.3 - 0.1)) * (alpha - 0.1)
        endif
endif

rkre_schneiders = re

return

end
```

```
FUNCTION epsu_SCHNEIDERS(t,tmax,alpha)

include 'declare.inc'
include 'mycom.inc'

dt = tmax - 20.d0
depsu0 = dt*(4.2d-6+dt*5.4d-9)

if (depsu0. gt. 7.8d-3) depsu0 = 7.8d-3
        if (alpha. le. 0.1d0) then
                depsus = depsu0 * (1 - 7.73d0 * alpha)
                else if (alpha. lt. 0.3d0) then
                        depsus = depsu0 * (.227d0 - 1.61d0 * (alpha - 0.1d0))
        else
                depsus = - 0.095d0 * depsu0
endif

epsu = 2.2d-3 + depsus
epsu_schneiders = epsu

return

end
```

11.3 The Routine MATER2

```
else if (cmat.eq.'ATCM') then

Et = r0
dfy = parahot(idimpara-i8,ntot)
sigma = r0

etra = parahot(i9,ntot)
Em = etra

Rc = parahot(i1,ntot)

        if (Rc. le. precision) then
                parahot(idimpara-i5,ntot) = r0
                parahot(idimpara-i2,ntot) = r0
                return
        endif

Rt = parahot(i2,ntot)

epsu = parahot(i3,ntot)
epscu = parahot(i4,ntot)

epspl = parahot(idimpara-i1,ntot)

Eo = parahot(i8,ntot)

edscb = 2d0*Rc/(epscu-epsu)

epstr = parahot(idimpara-i4,ntot)

epssig0 = epsmec - epstr

epsel = epssig0 - epspl

sigma = parahot(idimpara-i2,ntot)

sigmaphisure = parahot(i6,ntot)

phi = parahot(i5,ntot)

if (epsel. lt. r0) then
        sigma1 = sigma
        if (sigma1. ge. r0) sigma1 = r0
                epspl1 = epspl
                epstr1 = parahot(i11,ntot)
                iloc = i0
continue
```

```
iloc = iloc + i1

if (iloc. gt. 20) then
        write(2,*)' MORE THAN 20 ITER. IN MATER2. NTOT =',ntot
        write(*,*)' MORE THAN 20 ITER. IN MATER2. NTOT =',ntot
        stop
endif

if (sigma1. le. r0) then
        sigmar1 = - sigma1 / Rc
        sr2 = sigmar1 * sigmar1
        sr4 = sr2 * sr2
        if (sr4. le. r1) rcapa1 = (r1 - sqrt(r1 - sr4)) / r2
                epsel1 = sigma1 / Eo
                depsel1 = r1 / Eo
        if (sigma1. gt. -Rc) then
                epspl1 = sigma1 * rcapa1 / Eo
        else
        epspl1 = - epsu / r3 + (sigma1 + Rc) / precision
endif

if (epspl1. lt. epspl) then
        if (sigma1. gt. -Rc) then
                depspl1 = (rcapa1 + sr4 / (r1 - r2 * rcapa1)) / Eo
        else
                depspl1 = r1 / precision
        endif
else
        epspl1 = epspl
        depspl1 = r0
endif

depsel2 = epsel1 - (Sigma1/Em)

rloc = (sigma1 * phi / Em - depsel2 - epspl1)
        - sigmaphisure

depsel0 = parahot(i12,ntot)

if (parahot(idimpara-i7,ntot). ne. 0.) then
        ddepsel = depsel0 - depsel2
else
        ddepsel = 0.
endif

if (rloc. le. precision3) then
        epstr1 = epstr + rloc - ddepsel
        f = 1/dfy + 1/(dfy*phi) - 1/phi
        depstr1 = f * phi / Eo
else
```

```
        epstr1 = epstr - ddepsel
        depstr1 = r0
endif

depssurdsigma = depsel1 + depspl1 + depstr1

parahot(idimpara-i9,ntot) = depssurdsigma

epssigma1 = epsel1 + epspl1 + epstr1

sigma2 = sigma1 + (epsmec - epssigma1) / depssurdsigma

Et1 = r1 / depssurdsigma

        if (dabs((sigma2-sigma1) / sigma2). gt. precision) then

        sigma1 = sigma2
                go to 103
        endif
        else
if ((etra. ne. r0). and. (Rt. ne. r0)) then
        epssig1 = epsmec - epstr1
        epsel1  = epssig1 - epspl1
        epsut = 2d0 * Rt / Eo
        if (epsel1. le. epsut) then
                sigel1 = Em * epsel1
                sigcharge1 = sigel1 * (r1 - sigel1 / (Rt * r4))
                Echarge1 = Em * (r1 - sigel1 / (Rt * r2))
        else
                teps = epsel1 - epsut - Rt / edscb
                edsteps = edscb * teps
                if (teps. le. r0) then
                        sigcharge1 = - edsteps * (edsteps / (r2 * Rt) + r1)
                                        + Rt / r2
                        Echarge1 = - edscb * (edsteps / Rt + r1)
                        else if (teps. le. (Rt / edscb)) then
                                sigcharge1 = edsteps * (edsteps / (r2 * Rt) - r1)
                                        + Rt / r2
                                Echarge1 = edscb * (edsteps / Rt - r1)
                else
                go to 4
                endif
        endif

sigdech1 = epsel1 * etra
Edech1 = etra

                if (sigdech1. lt. sigcharge1) then
                        Et1 = Edech1
                        sigma2 = sigdech1
```

```
                else
                        Et1 = Echarge1
                        sigma2 = sigcharge1
                endif

continue

                        if (dabs((sigma2 - sigma1) / sigma2). gt. precision) then
                                sigma1 = sigma2
                                epstr1 = epstr
                                go to 103
                        endif
                else
                        sigma2 = r0
                        Et1 = r0
                endif
        endif

        Et = Et1
        sigma = sigma2
else

if ((etra. ne. r0). and. (Rt. ne. r0)) then
        epsut = 2d0 * Rt / Eo
        if (epsel. le. epsut) then
                sigel = Em * epsel
                sigcharge = sigel * (r1 - sigel / (Rt * r4))
                Echarge = Em * (r1 - sigel / (Rt * r2))
        else
                teps = epsel - epsut - Rt / edscb
                edsteps = edscb * teps
                if (teps. le. r0) then
                        sigcharge = - edsteps * (edsteps / (r2 * Rt) + r1)
                                + Rt / r2
                        Echarge = - edscb * (edsteps / Rt + r1)
                        else if (teps. le. (Rt / edscb)) then
                                sigcharge = edsteps * (edsteps / (r2 * Rt) - r1)
                                        + Rt / r2
                                Echarge = edscb * (edsteps / Rt - r1)
                else
                go to 2
                endif
        endif

        sigdech = epsel * etra
        Edech = etra

        if (sigdech. lt. sigcharge) then
                Et = Edech
                sigma = sigdech
```

```
        else
                Et = Echarge
                sigma = sigcharge
        endif
        endif

        epstr1 = epstr
endif

continue

parahot(i11,ntot) = epstr1
parahot(idimpara-i5,ntot) = Et
parahot(idimpara-i2,ntot) = sigma
```

11.4 The Routine MATER3

```
else if (cmat.eq.'ATCM') then

if (t. le. (20.d0 + precision))    Rccold = parahot(i1,ntot)

alpha = - parahot(idimpara-i2,ntot) / Rccold
if (alpha. lt. r0) alpha = r0
        parahot(i7,ntot) = alpha
        alpha = parahot(i7,ntot)

epstr1 = parahot(i11,ntot)
epstr  = parahot(idimpara-i4,ntot)

dfy = parahot(idimpara-i8,ntot)

Em = parahot(i9,ntot)

if (epstr1. lt. epstr) then
        epstr = epstr1
        parahot(idimpara-i4,ntot) = epstr
endif

Eo = parahot(i8,ntot)
epssig = epsmec - epstr
if (sigma. lt. r0) then
        epspl1 = epssig - sigma / Eo
        epspl = parahot(idimpara-i1,ntot)
        if (epspl1. lt. epspl) then
                epspl = epspl1
                parahot(idimpara-i1,ntot) = epspl
        endif
else
                epspl = parahot(idimpara-i1,ntot)
                etra = sigma / (epssig - epspl)
```

```
                parahot(i9,ntot) = etra
endif

parahot(i10,ntot) = sigma

phi = parahot(i5,ntot)

if (sigma. le. 0.) then
        epsel = Sigma / Eo
        epsel0 = Sigma / Em
        depsel = epsel - epsel0
        parahot(i12,ntot) = depsel
        epstr = phi * Sigma / Em - epspl - depsel
        parahot(i6,ntot) = epstr
else
        parahot(i6,ntot) = r0
endif
```

11.5 The Routine MATER4

```
else if (ATCM) then

if (tmax.le.t) then
        if (ATCM) then
                rlambda = r2+t*(-0.002d0+0.012*t/14400.d0)
        else
                rlambda = 1.6d0+t*(-0.16d0/120d0+0.008*t/14400.d0)
        endif
else
        if (ATCM) then
                rlambda = r2+tmax*(-0.002d0+0.012*tmax/14400.d0)
        else
                rlambda = 1.6d0+tmax*(-0.16d0/120d0+0.008*tmax/14400.d0)
        endif
endif

rhobeton = 2208d0
rceau = 4180d0
rlateau = 2258800d0

if (dabs(t2-t1).le.precision) t2 = t2+precision
        rcbeton = (ENTHALPYB(t2)-ENTHALPYB(t1))
        rhoeau = (ENTHALPYE(t2,tmax)-ENTHALPYE(t1,tmax))
        qevap = (ENTHALPEV(t2,tmax)-ENTHALPEV(t1,tmax))
        rcrho = ( rhobeton*rcbeton
                +eaulibre*rhoeau*rceau
+eaulibre*rlateau*qevap)/(t2-t1)
```